From Biomass to Bioeconomy: Engineering Biocatalytic Phosphorus Mobilization from Plant Residues Prior to Animal Feeding

Vom Promotionsausschuss der
Technischen Universität Hamburg
zur Erlangung des akademischen Grades
Doktor-Ingenieur (Dr.-Ing.)
genehmigte Dissertation (Monographie)

von
Niklas Johannes Heinrich Widderich

aus
Darmstadt

2025

1. Examiner:	Prof. Dr. rer. nat. Andreas Liese
2. Examiner:	Prof. Dr.-Ing. Martin Kaltschmitt
Chairman of the Audit Committee:	Prof. Dr. Anna-Lena Heins
Date of oral examination:	27.03.2025

This work was carried out at the Institute of Technical Biocatalysis at Hamburg University of Technology between April 2020 and August 2024.

For my family

ABSTRACT

In this work, the technical applicability of biocatalytic phosphorus (P)-mobilization from plant residues and the subsequent conversion of mobilized P into fertilizer has been investigated. Initially, P organically bound to phytate, is liberated by intrinsic and exogenous phytase enzymes. By conditioning plant residues prior to feeding, the enzymatic P-mobilization aims to generate high value feed material and promote a sustainable P-management. Rye bran, a by-product of the milling industry known for its high phytate content, is used as a model substrate in this research.

To monitor and evaluate the P-mobilization rate, an inline process analysis based on Fourier-Transform-Infrared spectroscopy was established. The developed inline analytical approach experienced a root mean squared error of prediction of 81 $mg_P \cdot 100g_{bran}^{-1}$, corresponding to a deviation of about 8% with respect to the total phytate content in rye bran. Using this approach, it is shown that metabolically induced germination activates intrinsic phytate hydrolyzing enzymes. Maximum intrinsic activity was identified at 43 °C, pH 5.3, and a bran to water ratio of 1 to 7 (w/v). Under these conditions, most of the phytate present was degraded within 30 min at a rate of 5565 $U \cdot kg_{bran}^{-1}$. For maximum P-mobilization, an exogenously applied phytase blend consisting of rPhyXT52 phytase and the phytase from *D. castelli* was used. Kinetic studies on the phytase blend demonstrated its suitability for batch operation. The P-mobilization process achieved complete elimination of phytate, resulting in a 90% reduction of the total P-content across different scales up to 400 L reactions. Supportive ultrasound as well as enzymatic treatment of the cellular matrix substantially increased the P-mobilization rate by over 90%. Among the enzyme formulations tested, xylanases showed the most pronounced effect. Struvite precipitation from the process wastewater containing the mobilized P achieved 99% P-recovery with over 90% purity at pH 9, 20 °C, and an equimolar input ratio of constitution ions. The results and observations indicate a very robust process and underline the feasibility and applicability of enzymatic P-mobilization and struvite precipitation for P-recovery on a larger scale. The production of value-added feed material through phytate depletion and utilization of phytate bound P in renewable resources contributes to a more resilient P-bioeconomy.

Keywords: Phosphorus mobilization, phytate, plant residues, phosphorus reduced animal feed, phosphorus recovery, struvite

1 Introduction

Due to the continuous growth of the human population, the worldwide food demand and thus the request for crops and livestock have increased [1,2]. To cover this demand, fertilizers and especially, phosphorus (P) are increasingly gaining more importance [3]. Unlike nitrogen, P cannot be captured from the atmosphere but is almost exclusively gained by P rock mining [4]. With the rise in fertilizer production, the depletion of mineral P reservoirs is expected to occur within a few centuries [3]. Consequently, the EU framework has identified P rocks as a critical and "non-renewable" raw material [5].

However, the increased concentration of livestock production systems and the strongly growing human consumption of livestock products continuously influence the distribution of P across the global landscape [6]. Losses that occur during the human-made P alteration are leading to eutrophication [7]. It is the process in which excessive nutrient inputs to aquatic ecosystems result in algae blooms, oxygen depletion, and declined water quality, adversely affecting aquatic life and ecosystem health. Hence, valid resource management concepts within the framework of a circular bioeconomy are mandatory for the shift towards an economy based on renewable resources and recycling strategies achieved by the sustainable use of resources. [8]

Especially in the case of intensive livestock farming, a significant P oversupply as a result of limited utilization of P in the animal and the subsequent release into the natural environment through the manure pathway is becoming progressively challenging [3,9]. Here, phytic acid (inositol-hexakisdihydrogen phosphate, $InsP_6$) and its corresponding salt phytate play a crucial role. $InsP_6$ is the principal storage form of P in seeds and grains. However, monogastric species, such as swine and poultry, cannot digest phytate present in plant-based feeds due to the limited activity of endogenous intestinal $InsP_6$-hydrolysing enzymes [10] As a result, the insufficient use of phytate-bound P not only impacts agricultural productivity but also poses a threat to water quality due to losses of excess P into water bodies [11]. Moreover, additional P sources are needed to meet the nutritional requirements, which are, in turn, derived from P rock mining [12].

To counteract the environmental impact of $InsP_6$, strategies such as crop rotation, precision agriculture, and phytase enzyme application in monogastric animal diets are already used in grain processing and livestock systems. Nevertheless, it is apparent that there is hidden potential for more sustainable use of resources, particularly in the conditioning of feedstuff [8]. Implementing a P circular bioeconomy aligns with several UN Sustainable Development Goals (SDGs). Recovering and recycling $InsP_6$-bound P prior to feeding, supports SDG 12 (Responsible Consumption and Production) and SDG 14 (Life Below Water) by reducing pollution and conserving resources. Additionally, innovation in P-management fosters SDG 9 (Industry, Innovation, and Infrastructure), promoting sustainable agricultural practices and a greener future.

Parts of this chapter are published in: Widderich *et al.*. Conditioning of Feed Material Prior to Feeding: Approaches for a Sustainable Phosphorus Utilization. *Sustainability* **2022** [8].

1.1 Phosphorus- and "Human"-Phosphorus Cycle

The P-cycle is a crucial process on Earth. P is required by all living organisms for growth and metabolism and is therefore present in all aspects of life [13]. The three main sources of P are rocks; e.g. apatite (about 1013 Mt), soils (about 200,000 Mt), and the ocean (about 100,000 Mt) [14]. Between these three reservoirs, P cycles within the inorganic P-cycle in geological time frames, Figure 1.1 [15]. During these processes, P that is chemically bound in rocks is released through the process of rock weathering and enters soils in the form of phosphates [16]. Subsequently, this P is incorporated into the terrestrial inorganic P-cycle [15]. Erosion facilitates the transfer of P from the soil to aquatic ecosystems, including rivers, lakes, and oceans, where apatite minerals are formed. Through sedimentation, P-enriched rocks accumulate on the seafloor. Over a period of millions of years, tectonic uplift mechanisms transport these P-rich rocks back to the earth's surface, initiating a new iteration of the inorganic P cycle [16].

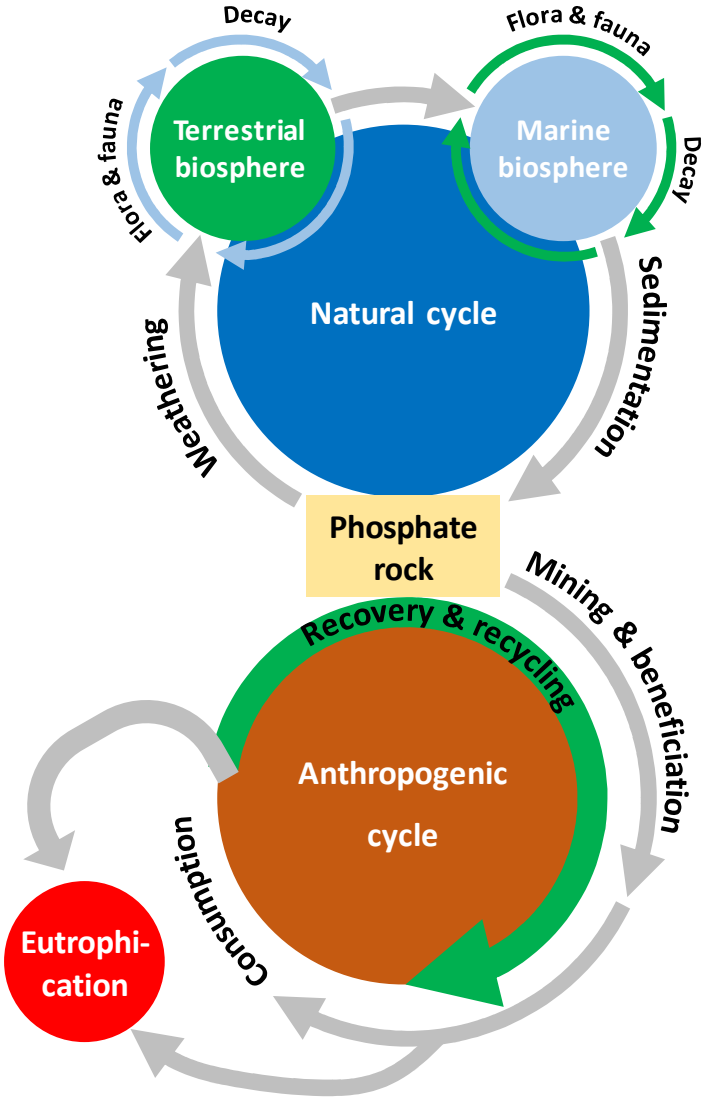

Figure 1.1: Schematic representation of the natural and anthropogenic P-Cycle. Modified according to Jupp *et al.* [17].

The organic P-cycle elucidates the terrestrial P recycling process. Within this cycle, the turnover of P occurs on an annual basis [15]. By extracting P from the soil matrix and assimilating it into their cellular structures, plants act as a crucial link between the inorganic and organic P-cycles. Through the trophic cascade, in which plants provide food for animals, the nutritional demand for P is met. The return of P to the soil transpires through two mechanisms. Firstly, a proportion of P is reintroduced to the soil through excrement deposition. Secondly, the decomposition of dead organic matter contributes to the reabsorption of P, Figure 1.1. In both scenarios, the P-cycle reaches a state of closure and equilibrium [16]. Blume *et al.* state the phosphate mass stored in terrestrial biomass are 3000 Mt [14].

Since P only regenerates within geological timeframes in the form of minerals, it is a resource limited to mining. However, to safeguard the worldwide food demand, humans have been altering the P-cycle by intensifying the releases of P from the lithosphere to ecosystems; referred to as the "Human"-Phosphorus Cycle. Approximately 20 Mt P are extracted from the Earth annually [8]; 87% is used for fertilizer production, most of which is finally diluted from cropland [18].

Apatite minerals are the primary source of P for the production of fertilizers. Since in its original state apatite is not water-soluble and, therefore, unavailable as a plant P source, harsh chemical processing is necessary for its conversion into phosphoric acid (expressed as phosphoric anhydride, P_2O_5). As a side-product, gypsum ($CaSO_4$) is formed and removed by filtration. Generally, four to five times more gypsum is formed compared to P_2O_5 relative to the mass. Besides the intensive resource consumption (1.3 t H_2SO_4, 83 t H_2O/t P_2O_5), the value chain is coupled with heavy metal impurities, pollution in the mining region, geopolitical dependencies, and monopolistic economy to name but a few. [8]

Although the amount of fertilizers and manure applied in agriculture is high, only a small portion of the P is taken up by the plants. Therefore, a significant amount enters freshwater systems and is transported by rivers to coastal areas. When excess P enters aquatic ecosystems, excessive growth and accumulation of algae and other aquatic plants follow in response to increased nutrient input, i.e. eutrophication. Impairment of water quality and loss of biodiversity are observed. Additional P input originating from domestic wastewater further aggravates eutrophication. Therefore, in many developed countries P must be removed in wastewater treatment plants and can be recovered for use in the fertilizer industry. [8]

Parts of this chapter are published in: Widderich *et al.*. Conditioning of Feed Material Prior to Feeding: Approaches for a Sustainable Phosphorus Utilization. *Sustainability* **2022** [8].

1.2 Challenges in Agriculture and Animal Nutrition

Phosphorus is an essential nutrient for all living organisms and one of the most limiting in agricultural production. The total amount of P in the soil of agricultural land might be high but is often present in unavailable chemical-bound forms or in forms that are only available outside the rhizosphere. Additionally, the high chemical fixation rate and slow diffusion in soil (10^{-12} to 10^{-15} m^2/s) make it one of the least available nutrients for plants. [8]
Most of the P acquired by plants is taken up as inorganic P (P_I) in the form of orthophosphate, generally, however, the term is used to refer to any hydrated or substituted form of the ion (e.g. HPO_4^{2-}, $H_2PO_4^-$, H_3PO_4, $CaPO_4^-$). The ideal pH for the P_I uptake is around 4 to 7, it is more likely at lower pH, and is often supported by arbuscular mycorrhiza fungi. After uptake, P_I circulates through the vascular network and enables complex control mechanisms to coordinate the distribution in the plant. A part of the P_I is used to sequentially phosphorylate inositol phosphates. The biosynthesis involves several protein clusters to finally synthesize phytic acid ($InsP_6$), which is the major storage form of P in cereals as well as grains and serves as a significant P source during germination. Therefore, in the main cereal-based feed components such as bran or extraction meal, the majority of P is organically bound to phytic acid or its salt phytate, Table 1.1. [8]

Table 1.1: Total P, Phytate-P, and intrinsic Phytase activity in feed ingredients [8].

	Total P [%]	Phytate-P [%]	(Phytate-P/ total P) · 100	Intrinsic phytase activity [$U \cdot kg^{-1}$]
cereals	0.23-0.31	0.17-0.23	59-78	86-5147
legume seeds	0.33-0.73	0.08-0.33	21-56	32-258
oilseeds	0.60-1.05	0.34-0.76	57-72	79-295
cereal by-products (bran)	0.83-1.16	0.68-0.88	76-82	25-7339

Phytate is a strong chelating agent forming complexes with essential divalent cations, which decreases the bioavailability of these minerals and is therefore an undesirable element in animals' diet [19]. In addition, the limited activity of intestinal $InsP_6$-hydrolyzing enzymes in monogastric animals, results in incomplete phytate digestion [10]. As a result, feeding plant material that is rich in phytate leads to overfertilization, as the unutilized P accumulates in agricultural land through the manure pathway. The P is then leached into water bodies, resulting in eutrophication. In consideration of progressively stringent environmental and German fertilizer legislation (DüV, StoffBilV, NEC Directive, TA-Luft) [20], nitrogen and P-reduced feeding is becoming increasingly important in modern livestock nutrition [21–23].

Parts of this chapter are published in: Widderich *et al.*. Conditioning of Feed Material Prior to Feeding: Approaches for a Sustainable Phosphorus Utilization. *Sustainability* **2022** [8].

Two strategies for providing P according to animal needs are pursued in livestock production. Firstly, ‘phase feeding’ involves providing feed with a lower P-content, supporting growth, and reducing overfeeding and subsequent P-excretion [24]. In the production of compound feed for animal nutrition, the composition of the raw materials can be adjusted to a P-content that is adapted to the animals' needs and reduces oversupply with the resulting environmental impact. However, feedstuffs with high nutritional profiles such as wheat and rye bran, generated as side streams from the milling industry, can only be used in limited proportions as the $InsP_6$-content often exceeds 80% of the total P-content. Secondly, phytase enzymes are routinely added in monogastric animal diets; catalyzing the release of P from phytate in a stepwise hydrolysis reaction [8]. The major challenge concerning phytases in feed application is the rapid and complete hydrolysis of $InsP_6$. The structural conformation of phytases often prevents complete hydrolysis to *myo*-inositol. Although some phytases are able to further hydrolyze to inositol monophosphate (InsP), accumulation of $insP_3$/$InsP_4$ in the intestinal tract is observed [8]. In addition, due to unfavorable conditions in the intestinal tract, the efficiency of supplemented phytase is low, resulting in up to half of the phytate being excreted [25].

1.3 Rye Bran

Globally, cereals are grown on 555 million hectares. This corresponds to a grain volume of 2.8 billion tons (2022) [26]. The most important cereals in Germany are wheat with 3.2 million hectares, barley with 1.6 million hectares and rye with 0.6 million hectares [27]. The structure of these single-seeded cereals is similar, Figure 1.2. The grain has an outer fruit and seed husk. These make up 5% of the grain mass. The aleurone layer, which encloses the endosperm, makes up 7 to 9% of the grain, depending on the grain type. The inner part of the grain consists of the germ (4%) and the endosperm (82%) [28].

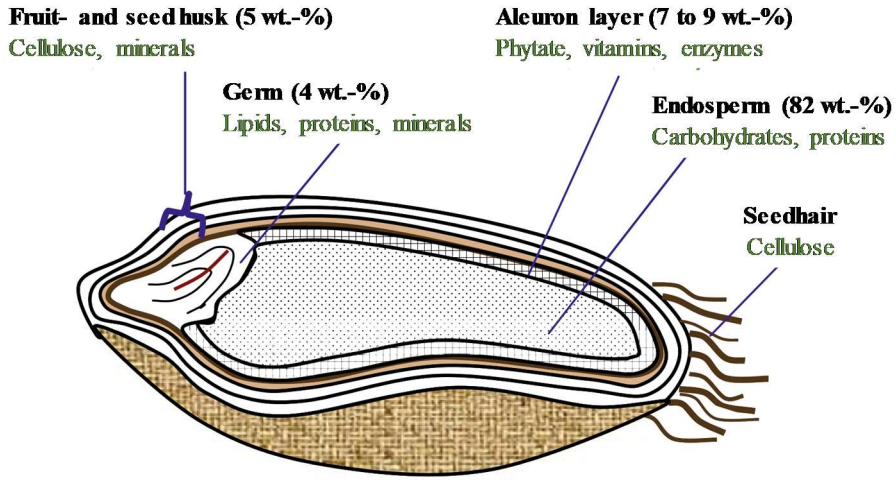

Figure 1.2: Structure of cereal grains. Nutrients such as carbohydrates and proteins are primarily in the endosperm and germ, while the outer layer consist mainly of cellulose and contains most of the phyate. Representation modified according to Rimbach *et al.* [28].

Cereal grains are mostly used in the food industry, accounting for 54%. Animal feed accounts for a further 35%. The remaining shares include industrial use, use as seed and losses during harvesting or storage of the grain. In food industry, cereals are mainly used for the production of flour. Therefore, only the carbohydrate-rich endosperm is used. The hull and germ are removed and accumulate as bran as a by-product of flour production. This makes up 17% of the total grain mass. Bran components include vitamins, minerals, dietary fibre and 50-75% of the phytate, which is stored in the bran fraction and is located in the aleuron layer [28]. However, there are differences in composition depending on harvest location, harvest year (e.g. weather condition) and rye type [29]. Nevertheless, the high nutritional profile makes the by-product bran a suitable component in feedstuffs.

Due to the high cellulose content of the outer layers of the grain, the fibre content of rye bran is 40.6 ± 0.6 g·100g^{-1}_{DM}. This includes, for example, arabinoxylan (24.7 ± 0.4 g·100 g^{-1}_{DM}), cellulose (6.7 ± 0.1 g·100 g^{-1}_{DM}) and β-glucan (1.9 ± 0.1 g·100 g^{-1}_{DM}). Other components of rye bran are starch (24.9 ± 0.2 g·100 g^{-1}_{DM}), proteins (12.8 ± 0.1 g·100 g^{-1}_{DM}) and lipids (3.0 ± 0.1 g·100 g^{-1}_{DM}). The ash content is 4.1 ± 0.1 g·100 g^{-1}_{DM} [30]. Similar proportions were also found by Nordlund *et al.* and Roye *et al*. [31,32]. The remaining components include phenolic acids, vitamins, essential amino acids, minerals and plant pigments [33–36].

The phytic acid content is given by Fretzdorff and Weipert as 3.6 g·100 g^{-1}_{DM} from 1983. For rye from 1984, Fretzdorff and Weipert give a phytic acid content of 4.3 g·100 g^{-1}_{DM} [37]. These deviations are based on biological variations, e.g. due to changing growth conditions in the year of harvest, as well as on the composition of the bran, since the content is related to the bran mass [29,37]. Thus, the expected inositol phosphorus content is 0.83 g·100 g^{-1}_{DM}.

1.4 Phytic Acid

Phytic acid ($InsP_6$), is the hexaphosphate ester of inositol (cyclohexane hexol). The salts of phytic acid (phytates - often in the form of a calcium, magnesium or sodium salt) are considered to be the primary storage form of both phosphate and inositol in plant seeds and grains, and are most abundant in cereals and legumes [25,38]. The molecular mass is 660.04 g·mol^{-1} depending on the counter ion. Figure 1.3 shows the structural composition of $InsP_6$.

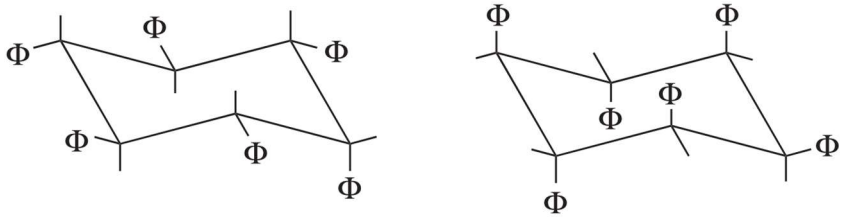

$InsP_6$, $C_6H_{18}O_{24}P_6$, $\Phi = OP(O)(OH)_2$

Figure 1.3: Conformational isomers of phytic acid. Left, $1_{ax}/\text{-}5_{eq}$ conformer; right, $5_{ax}/\text{-}1_{eq}$ conformer. In both cases the substituent is at C2.

In solid state, the conformation of calcium phytate is $1_{ax}/-5_{eq}$. However, sodium phytate has the inverted $5_{ax}/-1_{eq}$ conformation. In aqueous solution, sodium phytate has the $1_{ax}/-5_{eq}$ conformation at low pH and the $5_{ax}/-1_{eq}$ conformation at high pH. The inversion occurs at pH 9.4. Other salts such as tetra-*n*-butylammonium salt exhibit three inversions from $5_{ax}/-1_{eq}$ to $1_{ax}/-5_{eq}$ at pH 2 and at pH 5 from $5_{ax}/-1_{eq}$ to $1_{ax}/-5_{eq}$ at pH 12. Therefore, the preferred conformation depends on the type of counterion and the degree of protonation [38]. Moreover, $InsP_6$ is soluble in water and acetone and slightly soluble in methanol and ethanol. The pK_S values range from -0.15 ($InsP_2$) to 11.76 ($InsP_{1,3}$ and $InsP_{4,6}$). In addition, $InsP_6$ has six reactive phosphate groups and is strongly negatively charged over a wide pH range, giving it a large potential to bind positively charged molecules such as cations or proteins below the isoelectric point. At the same time, $InsP_6$ has a high chelating capacity with these (divalent metal cations and positively charged proteins) [3,38,39]. Furthermore, Mikulski and Klosowski report that phytate can bind starch. The binding occurs either directly via hydrogen bonds or indirectly via starch-associated proteins [40]. Hydrolytic cleavage of the phosphate is achieved by phosphatases [3,10,41].

1.5 Biocatalysis

Biotransformation, achieved through either enzymatic reactions or whole-cell processes, is recognized in organic synthesis for clean and environmentally friendly production [42]. Biocatalysis enables difficult reactions unattainable by traditional organic chemistry and streamlines processes by replacing multiple chemical steps [43]. Compared to traditional chemical catalysis, reactions can be carried out under mild conditions (ambient temperature and pressure, no extreme pH, without toxic solvents, and without heavy metal catalysts) and the catalyst itself is or originates from renewable resources. Furthermore, chemo-, regio-, and stereoselective biotransformations simplify processes, enhance economic viability, and align with the *UN's Sustainable Development Goals* for cleaner production [44].

Isolated enzymes do not necessarily require complex fermenters, aeration, agitation and sterility, and produce fewer by-products than whole cell biocatalysis. Additionally, the substrate conversion does not result in the formation of a *de novo* cellular biomass, simplifying downstream processing [43]. Furthermore, isolated enzymes often lead to higher catalytic efficiency and productivity, as well as simplified scalability, and ensure consistent performance by operating independently of cellular metabolic constrains and complex growth conditions.

According to the recommendations of the International Union of Biochemistry and Molecular Biology (IUBMB), enzymes are divided into seven classes. Each enzyme is given a four-digit classification number beginning with EC (Enzyme Commission): EC A.B.C.D, where the first digit A represents the type of reaction catalyzed by the enzyme, Table 1.2. The classification covers around 5000 enzymes whereas about 60% of biotransformations are catalyzed by hydrolases (EC 3), including phosphatases [45].

Table 1.2: Classification of enzymes. Extended and modified from [45].

Enzyme class	Reaction catalyzed	Examples
oxidoreductases EC 1	reductions/oxidations at –CH-OH, -C=O,-C=C-	dehydrogenase, oxidase, oxygenase, catalase
transferases EC 2	transfer of a functional group e.g. C_1, aldehyde, keto, acyl, glycosyl	transaminase, glycosyltransferase, transaldolase
hydrolases EC 3	hydrolysis/condensation of esters, glycosides, ethers, peptides, amides	esterase, lipase, glycosidase, protease, cellulase, xylanase phosphatase,
lyases EC 4	additions/eliminations, cleavage of C-C, C-O, C-N-bonds	decarboxidase, oxinitrilase, hydratase, dehydratase
isomerases EC 5	racemization, *cis-trans* isomerization, epimerisation	racemase, mutase, epimerase
ligases EC 6	energy consuming formation of C-O-, C-S-, C-N-, C-C-bonds	synthetase, DNA-Ligase
translocases EC 7	transport reactions, usually across a cell membrane	TOM-complex

1.5.1 Biocatalysis in Farm Animal Nutrition

In animal nutrition, enzymatic processes play a vital role in the digestion of feed. These enzymes are either *in vivo* synthesized by the animal or produced by indigenous gut microbes. However, the efficiency of the animal´s digestive system is not absolute. Certain feed components contain indigestible anti-nutritional factors that hinder the digestive process, resulting in pigs and poultry being unable to digest 15-25% of the feed [46]. This inefficiency is due to the low activity or absence of specific enzymes that are essential for the digestion of certain feed components. The addition of targeted enzymes to the animal´s diet has been shown to improve the nutritional value of feed ingredients and increase the digestive efficiency by degrading anti-nutritional factors (e.g. phytate, Chapter 1.2). Moreover, the availability of macro nutrients and essential minerals such as P and Ca is improved [8].

Growing global population and increasing disposable income, especially in developing countries, rising meat consumption, ban on antibiotics as growth promoters, and added health benefits are the major drivers of the feed enzyme market [46–48]. Enzymes that digest dietary fiber, proteins, starch and phytate, namely proteases (EC 3.4.21.x), carbohydrases (EC 3.2.x.x) and phytases (EC 3.1.3.x), all belonging to the class of hydrolases (Chapter 1.3), are most frequently used in animal nutrition [49].

1.5.2 Phytases as Feed Additive

To mitigate the negative impacts of $InsP_6$ on animal feeding, phytase enzymes are routinely used in monogastric diets (Chapter 1.2). First commercialized phytases were derived from the fungi *Aspergillus niger*, *Peniophora lycii* and *Penicillium funiculosum* which were approved in 1991 as feed additive. Given that phytases are not naturally designed for feed application, varieties of phytases have been discovered and engineered in the last 30 years to increase pH stability and protease resistance as well as to withstand pelleting of animal feed; i.e. increased thermal stability. In production, expression hosts are often fungal, even for bacterial phytases, to take advantage of post-translational modifications and high titers. Enzymes from the Enterobacteriaceae family, e.g., *E. coli* or *Y. mollaretii* with specific activities above 1000 $U \cdot mg^{-1}$ lead to commercial bacterial phytase products. Thereby, *E. coli* phytase AppA is one of the most studied and used enzymes due to its high specific activity. [8]

All phytases catalyze the release of P from phytate in a stepwise hydrolysis reaction, Equation 1.1. However, the enzymes do not act directly on the feed but rather become active in the digestive tract [11]. In general, phytases have a monomeric structure with molecular masses of 40 to 70 kDa and are assigned to phosphatases (subclass of hydrolases, Chapter 1.4). Depending on the type of catalytic mechanism, they are known as histidine acid, ß-propeller, cysteine or violet acid phytases [25].

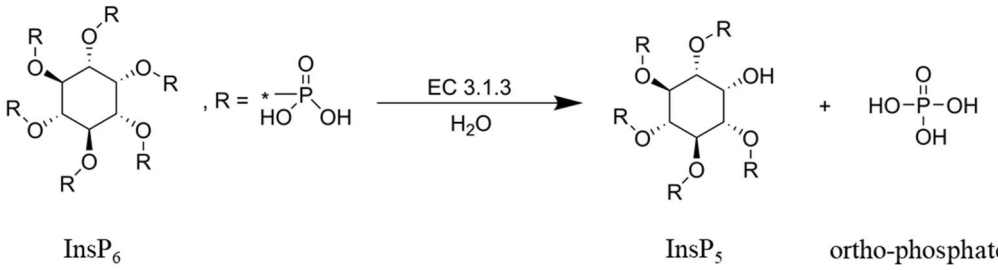

(Eq. 1.1)

Phytases are classified according to their pH maximum as acidic (pH 3.5 to 6.0) or alkaline (pH 7.0 to 8.0) phytases and according to their stereospecificity as 3-phytases (E.C. 3.1.3.8), 6-phytases (E.C 3.1.3.26) and 5-phytases (E.C. 3.1.372). From Figure 1.4 it can be seen that all acid phosphatases (mostly bacterial phytases) hydrolyze five of the six phosphate groups, the end product being inositol-monophosphate (InsP). It was concluded that they have a preference for equatorial phosphate groups and are virtually unable to cleave the axial phosphate group, Figure 1.3. Furthermore, the sequential hydrolysis of $InsP_6$ proved an accumulation of inositol-triphosphate ($InsP_3$). A full hydrolysis to *myo*-inositol is not achieved, due to the structural conformation of these phytases. Even if some phytases are able to further hydrolyze to InsP, an accumulation of $InsP_3$ was observed. Thereby the hydrolysis pattern is influenced by the enzyme dose and the substrate concentration.

Parts of this chapter are published in: Widderich *et al.*. Conditioning of Feed Material Prior to Feeding: Approaches for a Sustainable Phosphorus Utilization. *Sustainability* **2022** [8].

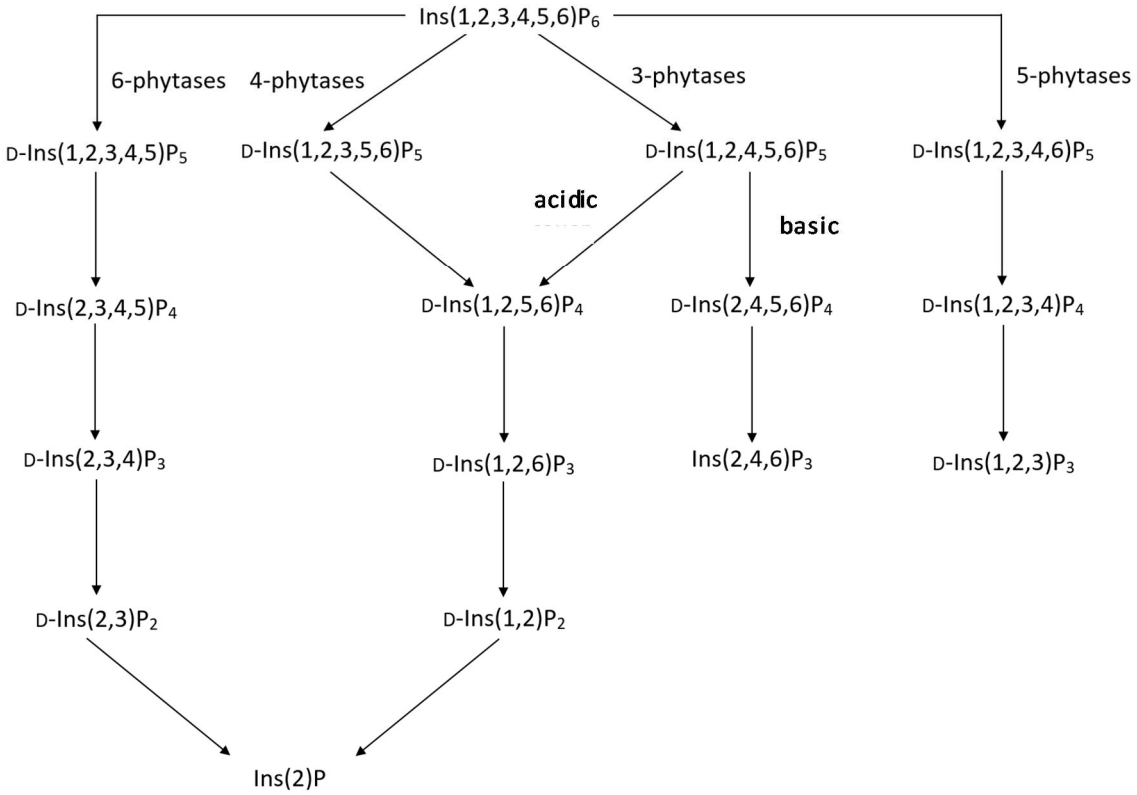

Figure 1.4: Pathways of stepwise dephosphorylation of phytic acid of the four phytase groups 3-, 4-, 5- and 6-phytases.

In vivo, phytases are able to further hydrolyze inositol-tetraphosphate ($InsP_4$). Reports show that in the small intestine of piglets, $InsP_3$ was detectable; meanwhile, hydrolysis *in vitro* ended with $InsP_4$. Indeed, a remaining challenge is that only up to 50% of phytate is degraded in the animal's intestinal tract, releasing considerable amounts of lower inositol-P (< $InsP_4$) (Chapter 1.2). Although phytase from metagenomic analysis like for example rPhyXT52 and phytase blends of a 3- and a 6-phytase were reported *in vitro* to degrade $InsP_6$ to $InsP_1$, an accumulation of $InsP_4$ *in vivo* was measured. [8]

1.5.3 Plant Native Phytase

Besides the application of phytases as feed additive, soaking in water reduces the phytate content of cereal seeds through the action of endogenous enzymes. It remains unclear whether the increase in phytase activity is the result of activation of pre-existing enzymes or based on *de novo* synthesis of the protein. However, it has been shown that phytate hydrolysis during wet-treatment is influenced by temperature and pH. Thus, wet-treatment can effectively reduce phytate under conditions that maximize enzymatic activity, although it is a process that may take several days to reach sufficient phytate reduction. This reduction is also favored by mass transfer, as phytate is water soluble, but loss of minerals, water extractable proteins and vitamins also occurs. [8]

The efficacy of phytate reduction varies across species according to their endogenous enzyme activity, Table 1.1. In the case of lentils, a phytate reduction of up to 60% was observed after 12 hours of pre-steeping and 48 hours of germination under a wet muslin cloth [50]. Greiner *et al.* demonstrated a reduction of over 50% in rye grains within two days, reaching more than 80% reduction after 10 days [51]. Pakfetrat *et al.* investigated the reduction of plant native substances, including phytate, in wheat grains during germination. After 14 days, the phytate content was reduced by 63% [52]. Reddy *et al.* studied phytate degradation in various cereal species, showing complete reduction in rye after five days, followed by 66% reduction in barley, 52% in wheat, and 66% in maize [53].

1.5.4 Biotechnological Phosphorus Mobilization from Plant Biomass

The low hydrolytic efficiency of phytases in the intestinal tract of monogastric animals and the associated negative environmental aspects of $InsP_6$ excretion leave a high potential for more sustainable use of P in animal nutrition, as described in the previous chapters. Biotechnological phosphate production from biomass has emerged as a new strategy to recover phytate bound P and produce P-reduced feed material. Thereby, the conditioning of feed material *prior* to feeding allows to operate under maximum enzyme conditions, resulting in higher efficiencies and, thus, adjustment of the specific nutrient content, valorizing the feed material. The two-step process consists of the enzymatic P-mobilization from biomass to hydrolyze $InsP_6$, which is initially contained in the plant material (e.g. bran, Chapter 1.3). At the same time, the hydrolysis product orthophosphate is solubilized in the aqueous phase. Followed by the recovery of liberated phosphate by converting it into a usable form.
Herrmann *et al.* published initial results on phytase-based phosphate release from plant biomass on a laboratory scale [3]. In this study, the processing of 20 different press cakes and extraction meals from soybean, rapeseed, and sunflower seed demonstrates the broad applicability of enzyme assisted P-mobilization. For this, Herrmann *et al.* used a codon optimized *E. Coli* AppA phytase expressed in *P. pastoris* [3]. A further advance was made by Infanzón *et al.*, who blended the 6-phytase rPhyXT52 from metagenomics with the 3-phytase from *Debaryomyces castellii* to achieve full conversion of $InsP_6$ while reducing the process times [54]. The combined effects of both phytases are shown in another study by Herrmann *et al.* on broader substrate scope including different press cakes and bran of wheat, rice and rye [55]. In conclusion, the phytase blend was proven efficient to obtain $InsP_6$ depleted plant material which has its potential application in animal feeding and is concomitant with the production of green P from renewable resources. The green P-production, thereby, provides a sustainable substitute for P gained by rock mining (Chapter 1.1) and has the advantage of an environmental friendly process [54,55]. Since the production of $InsP_6$-rich plant side streams is prevalent (Chapter 1.3), significant amounts of P could be recovered by enzymatic P-mobilization, leading to a self-sufficient P-cycle, Figure 1.5.

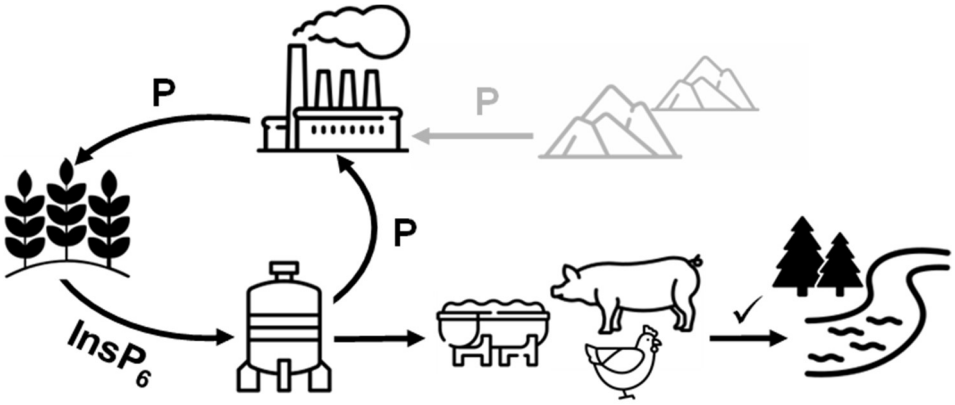

Figure 1.5: Schematic representation of the circular P-bioeconomy achieved through biotechnological phosphate production from biomass to recover phytate bound P while producing valorized feed material.

1.6 Phosphorus Recovery

The concept of enzyme-assisted P-mobilization from biomass is described in the previous chapter. However, to not only split of the organically bound P to increase bioavailability and reduce the P-content in manure but also to enable a circular P-bioeconomy, the solubilized phosphate has to be recovered. There are various technologies, both established and under development, that can be employed for the removal and recovery of P from wastewater. Some of them may also be transferable to the hydrolysate (i.e. the P-containing process wastewater) of enzymatic P-mobilization. In principle, the main P-recovery techniques used in wastewater treatment include biological removal [56], treating sewage sludge [57], and precipitation [58]. In particular, the concept of chemical precipitation is a promising approach, which can be a viable option for P-recovery in enzymatic P-mobilization due to its technical feasibility and applicability.

The widespread use of precipitation for P-removal in wastewater treatment started in Switzerland in the 1950s as a response to the growing issue of eutrophication and is now firmly established in many countries worldwide. The technique involves a physio-chemical process in which wastewater is treated with mono-, di- or trivalent metal salts, leading to the formation of metal phosphate precipitates [58]. It is a straightforward technology based on the addition of iron or aluminum salts in the form of chlorides or sulfates [59]. However, recent research is focused on exploring ways to convert P contained in wastewater into a more sustainable and economical alternative. Struvite [$MgNH_4PO_4 \cdot 6H_2O$] is a mineral that consists of magnesium, ammonium, and phosphate in a 1:1:1 molar ratio that can be used as an eco-fertilizer due to its slow-release properties. It has the potential to reduce nutrient run-off and subsequent water body pollution, making it ideal for use in agriculture [60]. Although only a few struvite precipitation plants in wastewater treatment have been established on an industrial scale, the concept highlights the importance of sustainable circular use and recovery of P. However, the extensive use of P in agriculture features the potential for recycling P also from plant byproducts.

2 Motivation and Objectives

A key challenge in livestock production is the reduction of P inputs into the environment from manure and slurry, to prevent eutrophication of water bodies. The P-content of animal feeds is therefore a quality criterion by which animal feeds are optimized. However, due to the high indigestible phytate content, nutrient-rich by-products from the milling industry such as bran are not used as animal feed. Instead, these valuable by-products are often thermally utilized, missing their potential nutritional contribution to the diet of livestock. At the same time, imported feeds with low P-content are displacing domestic alternatives. To address the challenge of limited phytate digestibility, phytase enzymes are added to monogastric animal diets. However, their hydrolytic efficiency is limited under the intestinal conditions, leaving high potential for a more sustainable use of P. Another approach to reducing P input into the environment is to remove and recover P from manure or wastewater (so called 'End-of-Pipe' approach). Although this has been widely studied, an integrated approach where P is optimized in the feed material prior to feeding is a more sustainable strategy, lowering the P-content in animal excretions from the outset. Therefore, the aim of this thesis is the investigation on the technical realization of the biotechnological P-mobilization from plant biomass for animal feed and the conversion of liberated P into a usable form, targeting a circular P-bioeconomy. Rye bran, a classical by-product of the milling industry with a high phytate content, is used as a model substrate to investigate and optimize the process. However, the process of enzymatic P-mobilization prior to feeding has only been demonstrated on a laboratory scale. In addition, although phytate is the major P store in plant material and intrinsic enzymes release P from phytate during germination, the maximum process conditions under which this degradation occurs have not been demonstrated. Furthermore, due to the lack of monitoring capabilities, it is not possible to adequately respond to biological fluctuations during the ongoing process, which could affect the efficiency and consistency of P-mobilization. For a circular economy, the mobilized P must be recovered. The concept of struvite precipitation from wastewater treatment is a potential approach, but it has not yet been transferred to the process of enzymatic P-mobilization.

The following objectives are outlined for this thesis:

- Establishment of process analytical technologies for real-time monitoring to react to fluctuations caused by the biological origin of the substrate.
- Evaluation of the potential of intrinsic inositol phosphate hydrolyzing enzymes in rye bran and the identification of suitable process conditions for their activation.
- Investigation of the biocatalytic efficiency of exogenously added phytases on the P-mobilization rate as well as reaction engineering (optimization and scaling).
- Determination of the feed properties of enzymatically treated rye bran.
- Transfer of the concept of struvite precipitation from wastewater treatment to the P-containing process wastewater from enzymatic P-mobilization.
- Recovery of additional recyclables from the process wastewater for waste stream minimization and an improved overall process economics.

3 Theoretical Background

This chapter provides the theoretical framework essential to comprehend the underlying principles of this thesis. The order in which the theory is presented aligns with its sequential presentation throughout the course of the manuscript. Less extensive theoretical principles are presented directly in the corresponding chapters.

3.1 Chemometrics

Chemometrics is the application of mathematical and statistical methods to chemical data for extracting valuable information from complex datasets. Modern software such as *The Unscrambler X* (CAMO Software, Norway) is commonly used for analysis. In analytical chemistry, chemometrics is widely applied to process multi-component data from spectroscopic analyses, predicting chemical species concentrations. The process involves developing predictive models from recorded spectra, with the data expressed in a matrix A, Equation 3.1:

$$A = \begin{bmatrix} A_{11} & \cdots & A_{1m} \\ \vdots & \ddots & \vdots \\ A_{n1} & \cdots & A_{nm} \end{bmatrix} \quad \text{(Eq. 3.1)}$$

The conversion of matrix A into concentration data involves multiplication with a vector containing model parameters, determined through calibration of spectral data. The choice between univariate and multivariate regression depends on the data structure. In multivariate analysis, Principal Component Analysis (PCA) and Partial Least Squares Regression (PLSR) are prominent techniques, condensing extensive datasets into significant components for deducing concentration data [61].

3.1.1 Principal Component Analysis (PCA)

PCA is a statistical technique to reduce the dimensionality of high-dimensional data while retaining its essential features. This is done by the transformation of the original variables into a new set of uncorrelated variables called principal components. These components are linear combinations of the original variables, arranged in descending order of variance. The first principal component captures the maximum variance present in the data, and each subsequent component captures as much of the remaining variance as possible [62].

3.1.2 Partial Least Squares Regression (PLSR)

In PLSR the relation between a set of independent variables (X) and a set of dependent variables (Y) is modeled by minimizing the sum of squares of deviations in the dependent variable $\left(\sum |Y_i^* - Y_i|^2\right)$. In the case of complex data sets (e.g. spectroscopic data) the regression model is multi-dimensional and mathematically expressed as shown in Equation 3.2:

$$Y_i^* = \beta_0 + \beta_1 \cdot X_i + \beta_2 \cdot X_2 + \ldots + \beta_m \cdot X_m \qquad \text{(Eq. 3.3)}$$

For "n" number of spectra, a linear equation system is built and can be represented in matrix notation [61]:

$$\begin{pmatrix} Y_1^* \\ \vdots \\ Y_n^* \end{pmatrix} = \begin{pmatrix} \beta_0 \\ \beta_1 \\ \vdots \\ \beta_m \end{pmatrix} \begin{pmatrix} X_{11} & X_{12} & \cdots & X_{1m} \\ X_{21} & X_{22} & \cdots & X_{2m} \\ X_{31} & X_{32} & \cdots & X_{3m} \\ \vdots & \vdots & \ddots & \vdots \\ X_{n1} & X_{n2} & \cdots & X_{nm} \end{pmatrix} + \varepsilon \rightarrow Y^* = \beta \cdot X + \varepsilon \qquad \text{(Eq. 3.4)}$$

Least square regression leads to the determination of model parameter "β" from "n" spectra, by minimizing the residual vector "ε", which defines the deviation between predicted and calibrated data [63]. Partial least square models are based on the principal components (Chapter 3.1.1) derived from both the independent variable (e.g. concentration), as well as the depended variable (e.g. signal). The concept involves the separate calculation of the main components for the matrices X and Y. Then, a regression model is constructed between the score matrices of the main variables [64].

An important part of multivariate data analysis is to decide how many principal components are necessary to describe the data without overfitting the model and the selection of appropriate training (calibration) and validation [61,65]. The number of principal components is often chosen at the lowest root mean square error of cross validation (RMSECV), Equation 3.5. For a full cross validation, each spectrum is omitted and predicted once. However, the prediction accuracy of the final model is given by the root mean square error of prediction (RMSEP), Equation 3.5. To further evaluate the performance of the model, the coefficient of determination R^2 can also be used. An RMSE(-P/-CV) close to zero and a R^2 close to one shows a good agreement with the data. [66]

$$\text{RMSE(-P/-CV)} = \sqrt{\frac{\sum_{i=1}^{n} (y_i - \hat{y}_i)^2}{n}} \qquad \text{(Eq. 3.5)}$$

- y_i = concentration determined by the reference method
- $\hat{y}$ = concentration determined by the PLSR model
- n = total number of samples

3.2 Statistical Design of Experiments (DoE)

Statistical experimental design is a method developed in the 1920s for the efficient design and analysis of experiments. In contrast to the common approach of varying only one factor at a time, it allows the study of interactions between different factors. This is achieved by varying the factors simultaneously. In this way, the effect of a factor can be tested under different conditions, and the entire factor space can be explored uniformly. The principle is often used to reduce experimental effort without compromising the reliability of the predicted data [67,68]. Various programs, including MatLab®, Statgraphics®, JMP®, Statistica®, Stavex®, or Design Expert®, are available for planning and analyzing such experiments. The underlying mathematical model is based on polynomial regression. A distinction is made between linear, quardratic and higher order polynomials. In Equation 3.6, a quadratic regression approach for the target variable (y) is represented by the model constants (k) with two input factors (u_1, u_2).

$$y = k_0 + k_1u_1 + k_2u_2 + k_{1,1}u_1^2 + k_{1,2}u_1u_2 + k_{2,2}u_2^2 \qquad \text{(Eq. 3.6)}$$

The mathematical model consists of the linear terms of the input variables, terms for the interaction of the input variables, and quadratic terms of the input variables. Depending on the chosen model approach and the number of input variables, additional terms are added to the polynomial model.

The choice of the experimental design depends on the number of factors, the form of the model, and the objectives of the experiments. Screening experiments primarily aim to identify, from the multitude of possible factors, those that have a significant influence on the system. In these experiments, only the effects of the influencing factors are considered, while their interactions with each other are not taken into account. Modeling experiments pursue the same goal as screening experiments, but in contrast, they also consider the interactions between factors. Optimization experiments aim to find the minimum or maximum of the target variable depending on the factors [69].

As an example of a design space, the Central-Composite-Design (CCD) is explained. It is based on a two-stage experimental design, which can be divided into two parts: the "cube" and the "star", Figure 3.1. The "cube" corresponds to a two-stage, typically factorial experimental design. The "star" is designed by varying individual factors starting from the center point. In a CCD, these points are located either inside, outside, or directly on the boarders of the factor space, allowing for the investigation of nonlinear relationships [70].

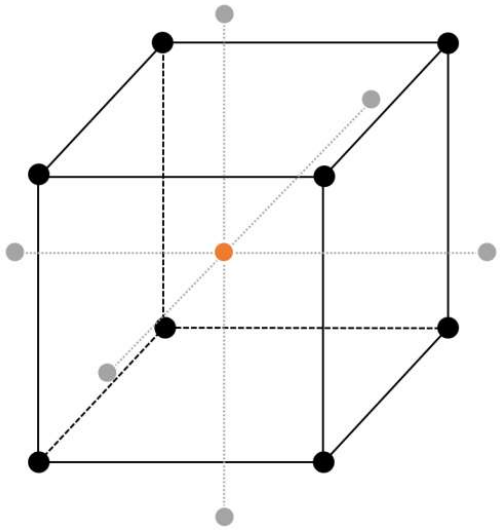

Figure 3.1: Central composite design. Based on a two-stage experimental design ("cube"), additional experiments outside the factor space ("star") offer the possibility of investigating non-linear relationships [67].

In some cases, it may be advisable to deviate from preconfigured designs to create an optimized design for the specific problem; commonly D-Optimal or I-Optimal. This may occur when factors cannot be used in arbitrary combinations, or when a factor is difficult to vary freely ("hard to change"). For this, an optimization criterion focusing on the coefficient matrix X derived from the experimental design and description model is used. A general description is given in Equation 3.7, where y represents the outcome vector of the target variable, X describes the coefficient matrix of the input variables including the transformed input variables, k represents the model constants, and ε denotes the residual error [71].

$$y = Xk + \varepsilon \qquad \text{(Eq. 3.7)}$$

The goal of statistical experimental design is to determine the model constants, and the equation to solve is:

$$c = (X'X)^{-1}X'y \qquad \text{(Eq. 3.8)}$$

In D-Optimal Design, the determinant of the term $(X'X)^{-1}$ is minimized, or the information matrix $X'X$ is maximized, aiming to calculate the model constants stably and minimize the volume of the common confidence region of the vector k [71]. In I-Optimal Design, the focus is on optimizing the average predictive ability within the factor space. This is particularly relevant for optimization experiments in a Response Surface Design [72].

3.3 Enzyme Kinetics

Enzyme kinetics are crucial to optimizing operating conditions and reactor selection. These conditions include concentrations of reactants, enzyme type, temperature, pressure, and pH, which affect space-time yield and enzyme usage. In addition, inhibitory effects that may occur during the reaction can be detected and classified. The simplest case for an enzymatic system is a substrate (S) forming an enzyme-substrate-complex (ES). The ES is stabilized by the enzyme (E), which leads to a decisive reduction in the activation energy necessary to run the reaction, resulting in the conversion to a product (P), Equation 3.9.

$$E + S \underset{k_{-1}}{\overset{k_1}{\rightleftharpoons}} ES \xrightarrow{k_2} E + P \qquad \text{(Eq. 3.9)}$$

The reaction rate (v) depends on the concentration of ES and the rate constant (k_2). The Michaelis-Menten model relates the reaction rate (v) to the substrate concentration (c_S) and shows a hyperbolic curve, Equation 3.10.

$$v = \frac{v_{max} \cdot c_S}{K_M + c_S} \qquad \text{and} \qquad K_M = \frac{k_{-1} + k_2}{k_1} \qquad \text{(Eq. 3.10)}$$

At [S] << K_M, the reaction rate increases linearly (first order kinetics) and reaches a maximum rate (v_{max}) at saturation (zero order kinetics). The Michaelis-Menten constant (K_M) represents substrate affinity; lower K_M indicates higher affinity, Figure 3.2. Enzyme activity is measured in units (U = µmol·min^{-1}), indicating the substrate converted per time unit.

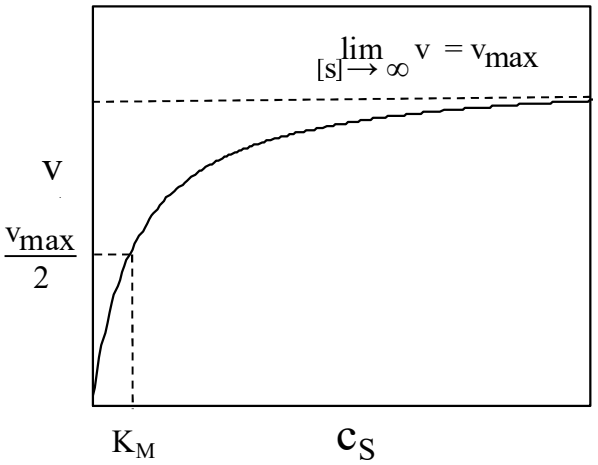

Figure 3.2: Graphical representation of Michaelis-Menten kinetics. K_M (mM): Michaelis-Menten constant; v_{max} (µmol·min^{-1}): maximum rate.

To determine the reaction rates, it is crucial to measure the initial rate ($v_0 \leq 10\%$), as v_0 exhibits hyperbolic behavior with increasing substrate concentration [45].

3.4 Struvite Precipitation

Struvite is a mineral with a crystalline structure that naturally precipitates when the combined concentrations of the involved ions in solution exceed their solubility limit, Equation 3.11.

$$Mg^{2+} + NH_4^+ + PO_4^{3-} + 6\,H_2O \rightleftharpoons MgNH_4PO_4 \cdot 6\,H_2O \qquad \text{(Eq. 3.11)}$$

As can be seen in Equation 3.11, struvite consists of equimolar ratios of Mg^{2+}, NH_4^+ and PO_4^{3-} and contains six crystal water molecules. The molecular weight is 245.43 $g \cdot mol^{-1}$. Due to the low solubility product, even low ion concentrations in solution lead to the formation of struvite crystals [73]. Furthermore, the density of 1711 $kg \cdot m^{-3}$ leads to the sedimentation in aqueous solution. In addition, struvite remains stable when exposed to the atmosphere and appears as a colorless or white to brown powder depending on the structure and type of contamination [74]. The crystallographic system of struvite is orthorhombic [75]. Figure 3.3 shows the corresponding cells as well as the spatial arrangement of the atoms in 2D and 3D. The crystal structure is determined by PO_4^{3-} tetrahedra, $Mg(H_2O)_6^{2+}$-octahedra and NH_4^+-groups. These individual molecules are linked together by hydrogen bonds [76]. While the ammonium group has four hydrogen atoms, it forms a hydrogen bond with only one oxygen atom of the phosphate tetrahedron. As a result, the ammonium group is less strongly bound within the crystal compared to the other two building blocks [77].

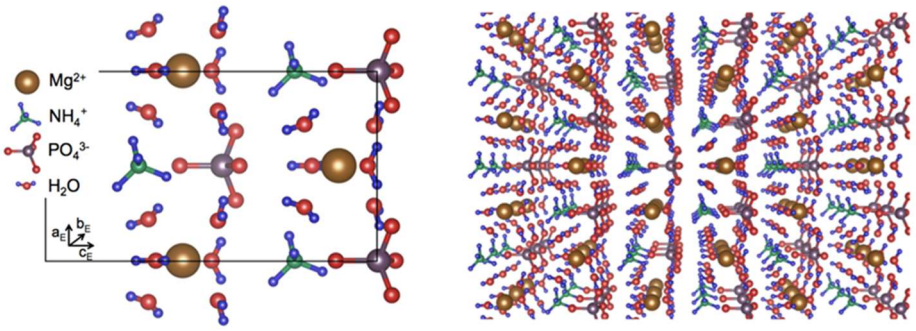

Figure 3.3: Structure and spatial arrangement of a struvite crystal [78]

Although struvite has a uniform lattice structure, the crystals exhibit different appearances depending on the crystallization conditions [78], Figure 3.4.

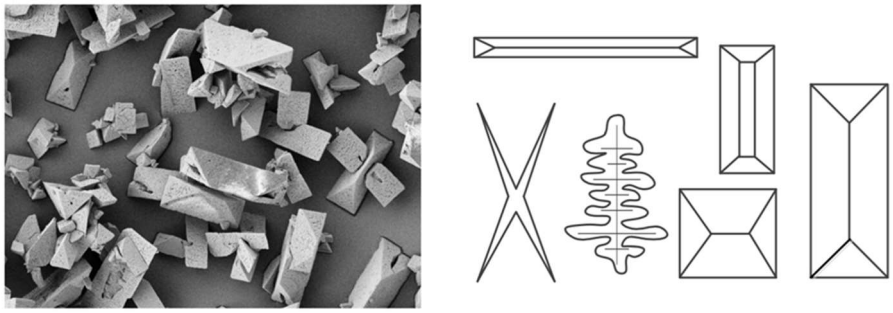

Figure 3.4: Appearance of struvite crystals. Depending on the precipitation conditions, coffin lids, needle-shaped or trapezoidal crystals as well as dendrites and twins are formed [78].

3.5 Solubility Product

The solubility product (K_{sp}) describes the maximum concentration of ions in a saturated solution and is therefore a measure of the solubility of a particular salt in a solvent. Thereby, the influence of the ionic strength of the medium is decisive. If a solution contains an ion that is a constituent ion of the corresponding salt, the solubility is lower. Conversely, solubility may be increased if ions are present in the solution that do not belong to the constituent ions of the salt [79]. Depending on the conditions the K_{sp} values of struvite in aqueous solution range from $4.3 \cdot 10^{-14}$ [80] to $1.2 \cdot 10^{-10}$ [81]. Struvite precipitation occurs when the product of the ion activity of the contained ions exceeds the solubility product, Equation 3.12.

$$K_{sp} = \gamma_{Mg^{2+}} \cdot c_{Mg^{2+}} \cdot \gamma_{NH_4^+} \cdot c_{NH_4^+} \cdot \gamma_{PO_4^{3-}} \cdot c_{PO_4^{3-}} \quad \text{(Eq. 3.12)}$$

The activity coefficients γ_i are determined by the law of mass action. However, in more concentrated solutions, intermolecular interactions must be considered, which lead to a reduction in the thermodynamically effective ion concentration. These effects can be included by determining the activity coefficients according to the Debye-Hückel theory [82], Equation 3.13.

$$\log(\gamma_i) = -A_{DH} Z_i^2 \sqrt{I} \quad \text{(Eq. 3.13)}$$

The Debye-Hückel equation consists of the Debye-Hückel constant (A_{DH}), the ionic strength (I), and the charges of the ions (Z). However, in Equation 3.13 additional interaction among the ions in solution at increasing concentrations are not considered. These interactions can be described using the Güntelberg approximation [82], Equation 3.14.

$$\log(\gamma_i) = -\frac{A_{DH} Z_i^2 \sqrt{I}}{1 + \sqrt{I}} \quad \text{(Eq. 3.14)}$$

With this approximation, the activity coefficients of the ions can be determined as a function of the ionic strength and the charges z_+ and z_-. The ionic strength can be determined according to Equation 3.15, taking into account all ions present in the solution, where c_i represents the molar concentration of each ion. The Debye-Hückel constant (A_{DH}) can be determined using Equation 3.16, where ε is the dielectric constant (water in this case) and T is the temperature in Kelvin [82].

$$I = 0.5 \sum c_i z_i^2 \quad \text{(Eq. 3.15)}$$

$$A_{DH} = 1.82 \cdot 10^6 \cdot [\varepsilon \cdot T]^{-1.5} \quad \text{(Eq. 3.16)}$$

Bube *et al.* calculated the ionic strength taking into account the ions involved in struvite precipitation (Mg^{2+}, NH_4^+, PO_4^{3-}), which can be in equilibrium with other ion species [83]. The following ion species are considered: $H_2PO_4^-$, HPO_4^{2-}, PO_4^{3-}, NH_4^+, Mg^{2+}, MgOH, $MgPO_4^-$. The thermodynamic constants of the equilibrium reactions are listed in Table 3.1

Table 3.1: Thermodynamic equilibrium constants of the considered ion species for the determination of the struvite solubility products [82].

Equilibrium reaction			Log K
H_3PO_4	⇌	$H_2PO_4^- + H^+$	2.15
$H_2PO_4^-$	⇌	$HPO_4^{2-} + H^+$	7.20
HPO_4^{2-}	⇌	$PO_4^{3-} + H^+$	12.38
NH_4^+	⇌	$NH_3 + H^+$	9.24
$MgPO_4^-$	⇌	$Mg^{2+} + PO_4^{3-}$	4.80
$MgHPO_4$	⇌	$Mg^{2+} + HPO_4^{2-}$	2.80
$MgOH^-$	⇌	$Mg^{2+} + OH^-$	2.60
$MgCl^+$	⇌	$Mg^{2+} + Cl^-$	0.60

For phosphoric acid, the dissociation at the respective pH values are taken into account. Phosphoric acid has three protons that are successively donated to water molecules, depending on the pH. Oxonium ions (H_3O^+) are released and dihydrogen phosphate, hydrogen phosphate and phosphate ions are formed, respectively. The corresponding pK_S values are pK_{S1} = 2.16, pK_{S2} = 7.21 and pK_{S3} = 12.32. The first proton is released at low pH values, the second proton at medium pH values and the third proton at high pH values, Figure 3.5.

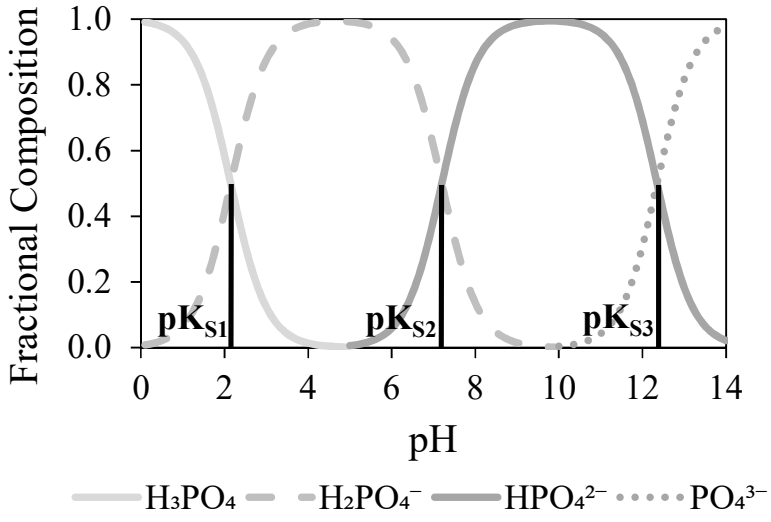

Figure 3.5: Dissociation diagram of phosphoric acid. Modified according to Zeitoun and Biswis [84].

4 Establishment of Analytics

According to the Guidelines for Safeguarding 'Good Scientific Practice', research must, among other things, be conducted objectively and reliably [85]. Thus, proper analysis serves as the backbone for extracting meaningful insights, guiding decision making, facilitating effective problem solving, maintaining scientific validity, and thereby enhancing the credibility of the research conducted. Therefore, the establishment of key analytical procedures that are critical to this work are presented and discussed in the following.

4.1 Offline Analytics

The offline analysis is characterized by manual sampling, sample preparation and analysis by conventional methods. For this thesis, this includes the colorimetric detection of orthophosphate and the associated determination of phytase activity, as well as the extraction and capture of inositol phosphates from rye bran and their quantification by high performance liquid chromatography (HPLC).

4.1.1 Inorganic Phosphorus Quantification and Enzyme Activity Assay

Colorimetric phosphate detections for phosphatase activity determination are mostly based on the method developed by Fiske and Subbarow [86]. In this method, phosphates are detected using an acidic ammonium heptamolybdate solution. Together with orthophosphate, the heptamolybdate, which is in equilibrium with molybdate in water, forms ammonium dodecamolybdate phosphate (molybdenum yellow), Equation 4.1.

$$\begin{gathered} Mo_7O_{24}^{6-} + 4\ H_2O \rightleftharpoons 7\ MoO_4^{2-} + 8\ H^+ \\ PO_4^{3-} + 12\ MoO_4^{2-} + 24\ H^+ + 3\ NH_4^+ \longrightarrow \left(NH_4^+\right)_3\left[P(Mo_3O_{10})_4^{3-}\right] + 12\ H_2O \end{gathered} \qquad \text{(Eq. 4.1)}$$

Reduction of the molybdenum yellow results in the formation of the molybdenum blue complex. Fiske and Subbarow used 1-amino-2-hydroxynaphthalene-4-sulphonic acid for this purpose. Due to its toxic properties, alternative methods are either the absorbance measurement of the molybdenum yellow color complex [87] or the use of a reducing agent. In this thesis, ferrous(II)-sulphate heptahydrate, as described by Eeckhout and Paepe [88], is used. However, when using this method for enzymatic activity on a biological matrix, the released phosphates may not be exclusively derived from $InsP_6$, but may also be hydrolytic products of lower phosphorylated inositols or other sources of P. Therefore, the hydrolytic activity of various endogenous phosphatases must be considered when defining activity with respect to $InsP_6$-hydrolysis on a biological matrix.

To validate this method, the absorbance spectrum of the molybdenum blue complex was recorded at different pH values. In addition to the complex formation with orthophosphate (in the form of dissociated KH_2PO_4), a possible interference with phytic acid was tested, Figure 4.1.

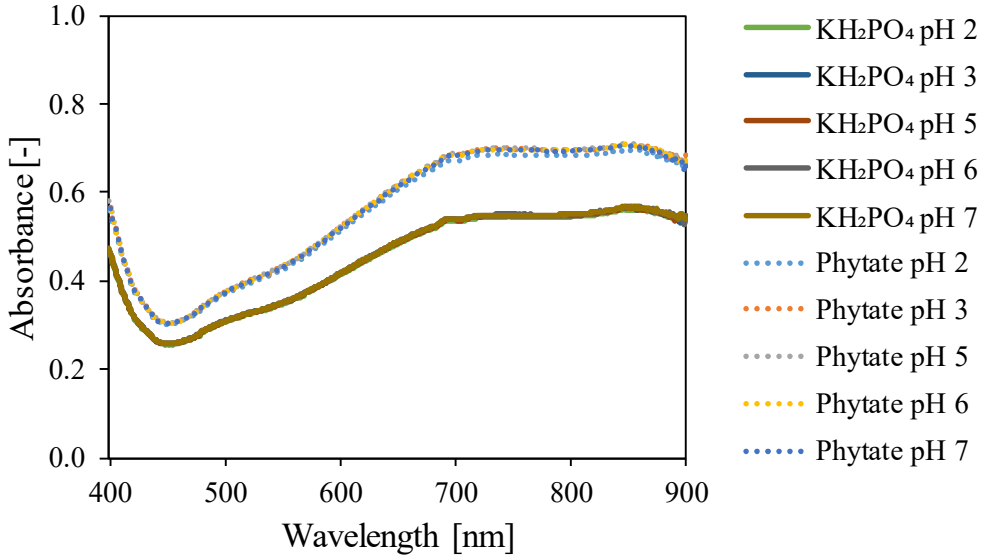

Figure 4.1: Effect of pH on absorbance behavior of the molybdenum blue color complex formation. Wavelength scan in the range of 400 to 900 nm. Reaction conditions: 1 mM KH_2PO_4 or phytic acid diluted with 10% trichloroacetic acid (TCA) to 0.5 mM. pH adjusted with H_2SO_4 or KOH. Measurements performed at room temperature.

As shown in Figure 4.1, the pH has no effect on the absorbance at wavelengths between 400 nm and 900 nm. For all samples, a maximum signal intensity is observed between 700 nm and 850 nm. Furthermore, it can be seen that phytic acid also forms a color complex with ammonium heptamolybdate and, thus, interferes with the colorimetric determination of free inorganic P. Therefore, blank sampling is essential. In addition, the absorbance difference between the color complexes formed with inorganic P and phytic acid is greatest in the range of 700 nm to 850 nm, with a maximum difference at 700 nm.

Figure 4.2 on the left displays the variation in absorbance over time for samples containing an inorganic P concentration of 0.1 mM to 0.5 mM. At higher concentrations, the amount of ammonium heptamolybdate is insufficient, resulting in a constant absorbance. Dilution is therefore necessary for higher concentrations. However, as expected, the time to develop the color complex is influenced by the concentration (up to 0.5 mM) and, thus, the higher amount of substances to be converted. Therefore, at higher concentrations, a longer time is required to reach a constant absorbance, Figure 4.2 on the right. For the concentration range considered, a delay of 2 min between sample preparation and measurement is sufficient to avoid erroneous measurements due to incomplete formation of the color complex.

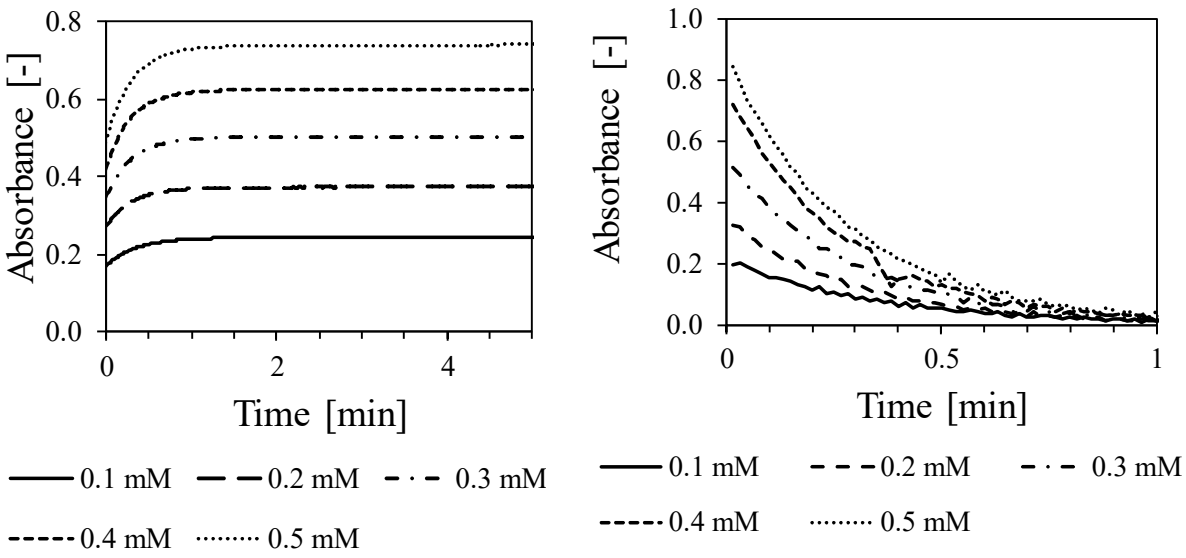

Figure 4.2: Effect of time on the formation of the color complex: 1 mM KH_2PO_4 stock solution diluted with 10% TCA to 0.2 mM, 0.4 mM, 0.6 mM, 0.8 mM and 1 mM. Measured at 700 nm at room temperature.

In Figure 4.3, the effect of temperature on the absorbance for inorganic P concentrations of 0.1 mM to 0.5 mM is given. At temperatures between 25 °C to 40 °C, no change in absorbance is observed. The colorimetric detection is not temperature sensitive and can therefore be used in the temperature range under consideration to detect orthophosphate and ultimately to quantify enzymatic activity related to phytic acid hydrolyzing enzymes.

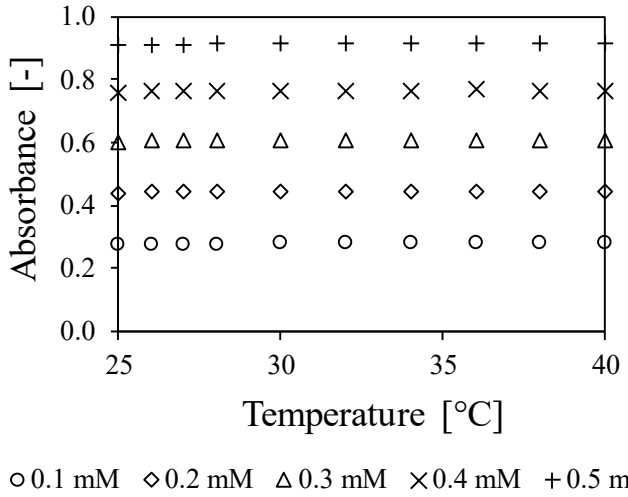

Figure 4.3: Effect of temperature on the absorbance of the color complex: 1 mM KH_2PO_4 stock solution diluted with 10% TCA to 0.2 mM, 0.4 mM, 0.6 mM, 0.8 mM and 1 mM. Measured at 700 nm at room temperature.

In conclusion, the colorimetric orthophosphate quantification by the molybdenum blue color complex formation is a robust and versatile method. However, for the determination of enzymatic activity, blank sampling is essential due to interference from phytic acid. In addition, the methods covers only a narrow concentration range.

4.1.2 Quantification of Inositol-Phosphates in Rye Bran

The quantification of inositol phosphates contained in plant material is a three-step process: extraction, capturing, and analytical detection. The establishment of each step is described below. For comparability reasons, results are expressed in inositol phosphorus (inositol-P), which refers to the amount of P bound to inositol phosphate in relation to a given amount of plant material (100 g in this work). Conversion factors ($C_{f,i}$) are obtained according to the degree of phosphorylation:

$$C_{f,i} = \frac{n \cdot M_P}{M_{phytic\ acid}} \qquad \text{(Eq. 4.2)}$$

Equation 4.2 takes into account the molar mass of P (M_P, 30.97 g·mol^{-1}), the molar mass of phytic acid ($M_{phytic\ acid}$, 660.04 g·mol^{-1}) and the number of P atoms (n). This gives conversion factors of 0.14, 0.19, 0.23, and 0.28 for $InsP_3$, $InsP_4$, $InsP_5$, and $InsP_6$, respectively.

Extraction of Inositol Phosphates

Extraction of inositol phosphates from the biological matrix was performed according to a modified method of Herrmann *et al.* [3]. The extraction is carried out in 0.5 M HCl as extracting agent over a period of 16 h. It is investigated whether mechanical pretreatment increases the extraction efficiency by increasing the specific surface area, Figure 4.4.

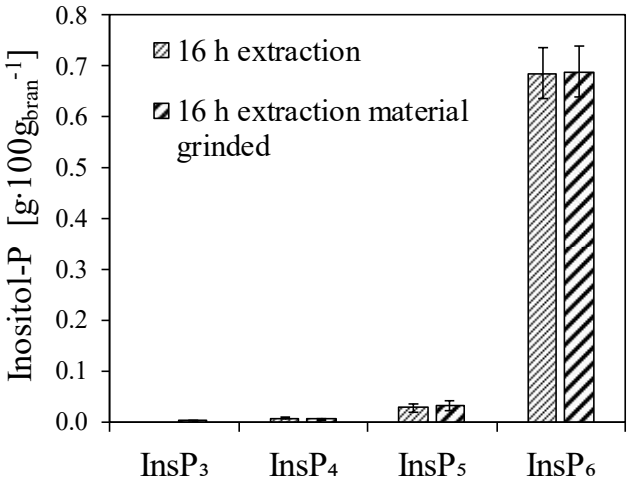

Figure 4.4: Comparison of mechanical pre-treatment on extraction. Grinding conditions: Ball mill, 250 mL grinding bowl, five grinding bowls r = 20 mm, 360 rpm, 3 min grinding time. Measurements in triplicates.

For the untreated sample, an inositol-P content of 0.72 ± 0.06 g·100g$^{-1}_{bran}$ and for the grinded sample 0.69 ± 0.06 g·100g$^{-1}_{bran}$ is determined. Both values are in agreement with literature (Chapter 1.3). Thus, chemical hydrolysis of the inositol phosphates can be excluded. Moreover, within the measuring uncertainty, the same inositol-P content is detected. Thus, the inositol phosphates can be completely extracted from the bran matrix without mechanical pretreatment. To shorten the extraction process, an alternative extraction method is investigated. Lehrfeld was able to achieve complete extraction in 1 h using an ultrasonic homogenizer [89]. A comparison of the two methods is given in Figure 4.5.

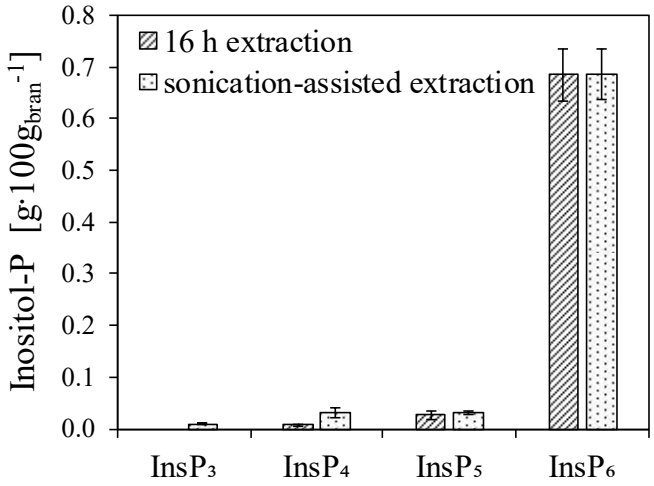

Figure 4.5: Comparison of 16 h extraction and sonication-assisted extraction. 16 h extraction: 5 g bran incubated in 35 mL 0.5 M HCl at 37 °C and 120 rpm. Ultrasonic-assisted extraction: 0.5 g bran incubated in 10 mL 0.5 M HCl, treatment with ultrasonic homogenizer at 70% power for 6 x 30 s in 6 cycles, incubation at 37 °C and 120 rpm for 1 h. Measurements in triplicates.

Inositol-P contents of 0.72 ± 0.06 g·100g$^{-1}_{bran}$ and 0.76 ± 0.06 g·100g$^{-1}_{bran}$ for 16 h extraction and ultrasonic extraction, respectively, are determined. As the deviations are within the measuring accuracy of the triplicates, the ultrasonic treatment achieves comparable results. In view of time savings, the ultrasonic extraction is therefore preferable.
For further validation, the effect of time and power by ultrasonic treatment on the extraction is investigated. In Figure 4.6 on the left, the measured inositol-P content is shown as a function of the duration of ultrasound treatment at 70% power. The graph on the right shows the effect of ultrasound power at a constant treatment duration of 3 minutes.

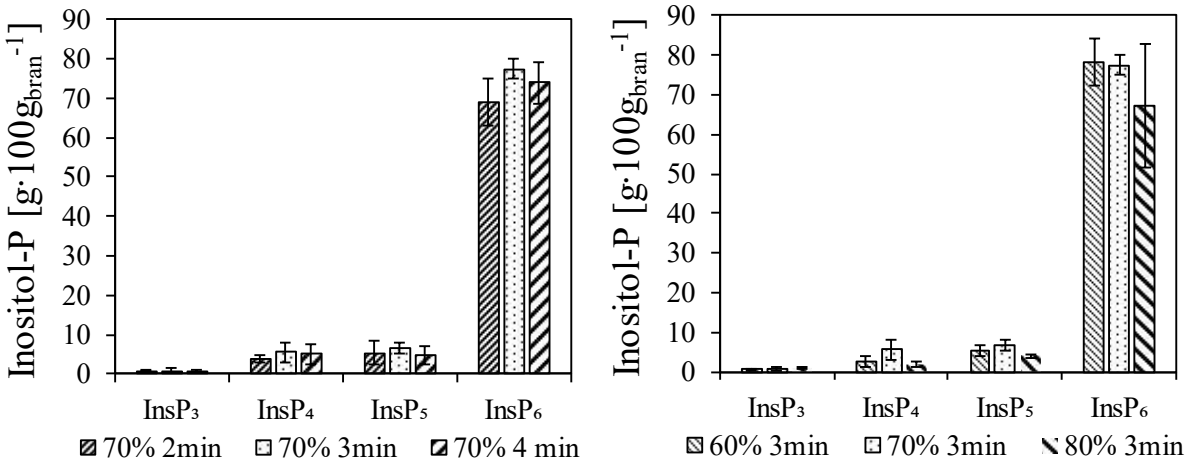

Figure 4.6: Effect of ultrasonic-treatment duration and sonication power. 0.5 g bran in 10 mL 0.5 M HCl. *Left:* Effect of duration on extraction. Power 70% for 4 x 30 s, 6 x 30 s, and 8 x 30 s in 6 cycles. *Right:* Effect of power on extraction. 60%, 70%, and 80% power for 6 x 30 s in 6 cycles for 3 min each. Followed by incubation at 37 °C and 120 rpm for 1 h. Measurements in triplicates.

For a duration of 4 min, 3 min, and 2 min the inositol-P contents are 0.77 ± 0.08 g·100g$^{-1}_{bran}$, 0.83 ± 0.05 g·100g$^{-1}_{bran}$, and 0.73 ± 0.09 g·100g$^{-1}_{bran}$, respectively. All variations are within the standard deviation. Hence, no effect of treatment time on extraction efficiency is observed in the 2 to 4 min time interval. Reducing or increasing the power to 60% or 80% also shows no clear effect on extraction efficiency, Figure 4.6 on the right. At 60% power the inositol-P content is 0.81 ± 0.07 g·100 g$^{-1}_{bran}$ and at 80% power 0.69 ± 0.16 g·100 g$^{-1}_{bran}$.
The effect of acid concentration during extraction is shown in Figure 4.7. For this, the inositol-P content is compared to a sample extracted with 10 mL of 1.0 M HCl instead of 0.5 M, using the method described above. The purification steps were adapted. The extract dissolved in 1.0 M HCl is diluted 1 to 10 instead of 1 to 5 and loaded to the ion exchange column (HyperSep SAX cartridge, Thermo Fisher) for further separation.

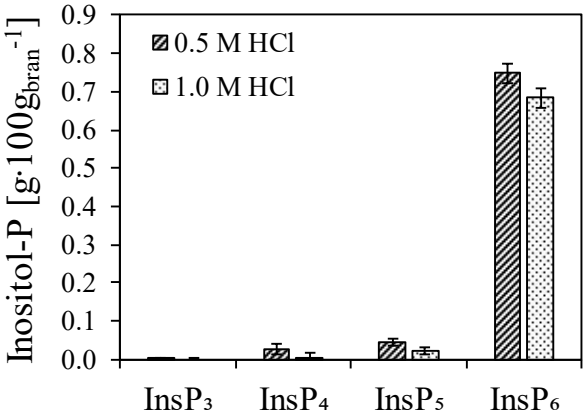

Figure 4.7: Effect of hydrochloric acid concentration on extraction. 0.5 g bran in either 10 mL of 0.5 M HCl or 1.0 M HCl. Ultrasonic treatment at 70% power for 6 x 30 s in 6 cycles, followed by incubation at 37 °C and 120 rpm for 1 h. Measurements in triplicates.

Using 1 M HCl, inositol-P content results in 0.64 ± 0.04 g·100 g^{-1}_{bran}, a loss of 23%. This loss may be due to biological variation, the higher dilution together with the nature of ion exchange chromatography, hydrolysis of phytic acid by the extractant, or a combination of these factors. At 95 °C and pH 4, the rate of chemical hydrolysis of phytic acid is $8.74 \cdot 10^{-4}$ min^{-1} [90]. Due to the chemical stability of phytic acid, chemical hydrolysis is unlikely at an extraction temperature of 37 °C. Based on this result, extraction in 0.5 M HCl is preferable.

Capturing of Inositol Phosphates

Capturing of inositol phosphates is performed by ion exchange chromatography (IEX). Two different resins are investigated for their separation efficiency. On the one hand, the HyperSep SAX cartridge (Thermo Fisher Scientific, Bremen, Germany) with a bed weight of 2 g is studied [3]. This ion exchanger has an aminopropyl resin with a capacity of 0.244 meq/g. The second ion exchange resin is the Roti®Change 1x8 resin (Carl Roth GmbH & Co. KG, Karlsruhe, Germany) according to Graf and Dintzis [91], which consists of a polystyrene resin cross-linked with 8% divinylbenzene and quaternary amines as active groups. The capacity is given as 1.2 eq/L [92]. To ensure comparability, the volume of the Roti®Change resin is adjusted to match the capacity of the HyperSep SAX cartridge. To circumvent biological variations, a mixture of commercially available inositol phosphates (PLD Pharm) was used in aqueous solution. In Figure 4.8 both ion exchange resins are compared with respect to inositol phosphate recovery.

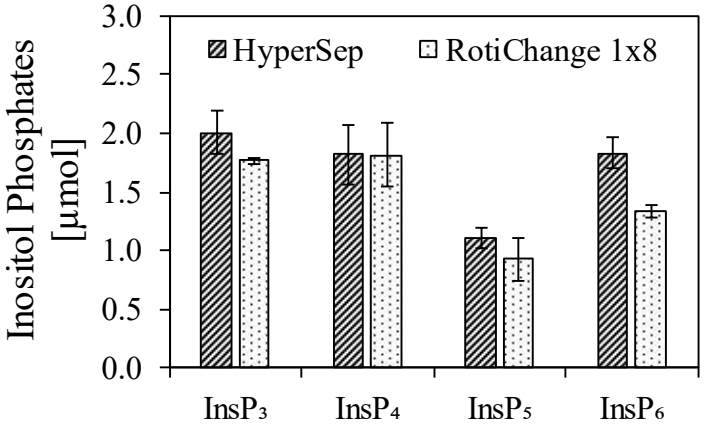

Figure 4.8: Comparison of HyperSep SAX cartridges and Roti®Change 1x8 resin. HyperSep SAX: 2 g bed volume, material: quaternary amines. Roti®Change 1x8: 1.5 mL bed volume, material: polysterene with quaternary amines. Both loaded with 7 µmol differently phosphorylated inositols. Eluted with 4 mL 2 M HCL, evaporated and dissolved in 1 mL of 50 mM NaOAc.

From Figure 4.8 it can be seen that the use of HyperSep SAX results in higher inositol phosphates recovery, especially for $InsP_6$. From the 7 µmol inositol phosphates, 6.78 µmol is detected. Using the Roti®Change 1x8 resin, the detectable amount of substance after elution is only 5.82 µmol, a 16.9% loss. Thus, HyperSep SAX is more suitable to capture inositol phosphates from the extraction solution.

A potential source of error in the capturing of inositol phosphates by IEX is an insufficient elution. Therefore, the amount of eluent required for maximum elution of bound inositol phosphates after extraction, equilibration and loading, is determined , Figure 4.9.

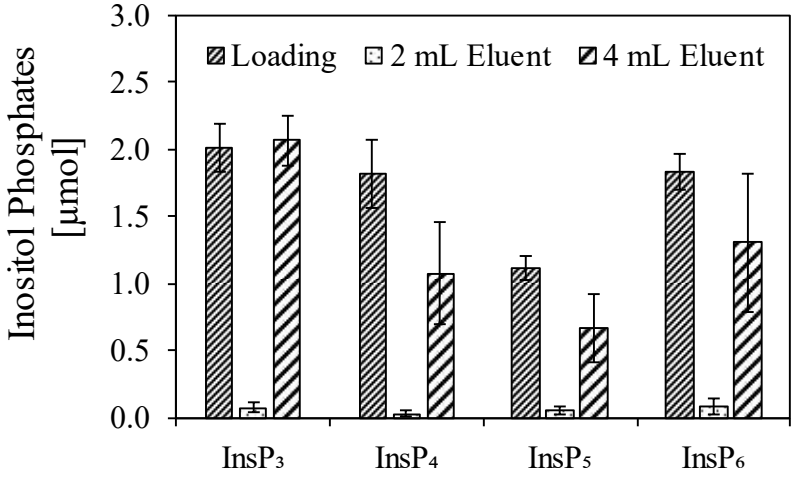

Figure 4.9: Effect of the elution volume on the elution of inositol phosphates from the HyperSep SAX ion exchange chromatography column. Loaded with 7 µmol differently phosphorylated inositols. Error bars are based on triplicates.

At an elution volume of 2 mL, only 4 to 6% (0.25 ± 0.15 µmol) of the bound inositol phosphates are eluted. However, an elution volume of 4 mL results in 75% to 100% (5.11 ± 1.34 µmol) recovery. This shows that, contrary to the expectations, the majority of the bound inositol phosphates were found in fractions eluting at a later stage. In addition, washing with 0.05 M HCl prior to elution removed impurities such as anthocyanins, which are thought to be responsible for the red color of the extract, Figure B.1. Nevertheless, $InsP_3$ and $InsP_4$ are also washed out, Figure 4.10, for this reason, the washing step should be omitted.

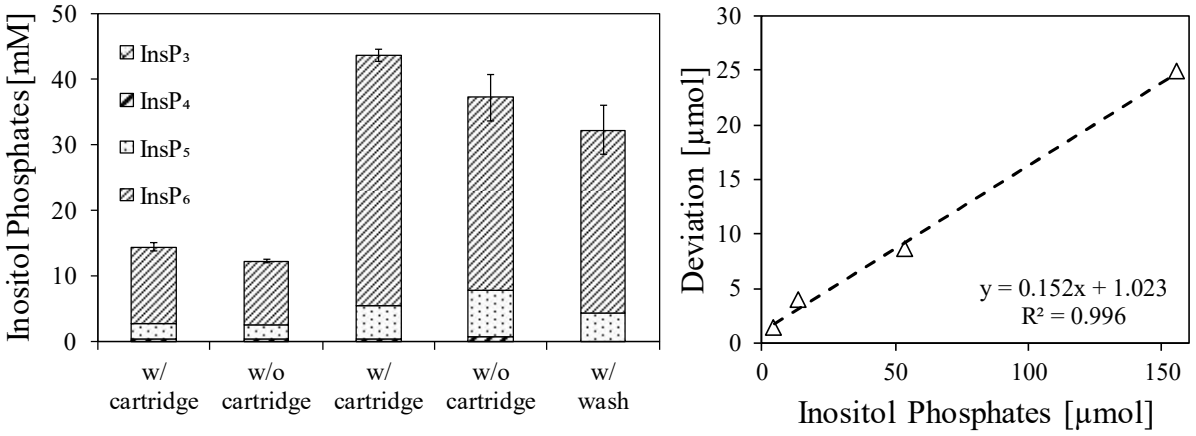

Figure 4.10: Recovery and loss of inositol phosphates as function of the applied inositol phosphate concentration. *Left*: 28 µmol and 80 µmol phytate (P1880, Sigma Aldrich, Darmstadt, Germany), with (w/) and without (w/o) application of IEX, and including a washing step (8 mL of 5 mM HCl). *Right:* Deviation of the detected substance quantity as a function of the applied quantity after IEX. Measurements in triplicates.

Figure 4.10 also illustrates that the extend of losses depends on the amount of inositol phosphates loaded onto the column. At a concentration of 28 µmol the loss is 4.42 µmol, whereas at 80 µmol the loss is 12.92 µmol. To investigate this behavior, columns were loaded with amounts of substances ranging from 5 µmol to 155 µmol and inositol phosphates were subsequently eluted, Figure 4.10 on the right.
A linear relation between the concentration of the stock solution and the losses is observed. At the maximum amount of substance tested, 155 µmol, the loss is 24.84 µmol. At an amount of 5 µmol a loss of 1.39 µmol is detected. Taking into account the applied volumes, the expected inositol phosphate concentration in the extract is 20 mM. Therefore, a loss of 2.3 mM can be expected and is considered in further evaluations. Furthermore, it can be seen, that the capacity of the ion exchanger is higher than the expected concentration in the extract.

Quantification of Inositol Phosphates by HPLC

Chromatography improves accuracy by separating individual inositol phosphates, allowing for precise determination of phytic acid ($InsP_6$). In contrast, precipitation (e.g. using iron(III)) can yield less accurate results due to complex formation with lower phosphorylated inositols ($InsP_1$ to $InsP_6$) [93]. Common HPLC methods for the separation of inositol phosphates are reversed-phase. Columns with a polymer base (PRP columns) [89] and C18 columns [94] can be used as stationary phase. While the C18 columns are not as robust as the PRP column, they allow a more distinct separation due to a higher number of theoretical plates [89].
The first HPLC methods for quantification of inositol phosphates in the early 80´s overlapped the peak of the eluent and of phytic acid [91,95,96]. However, through addition of tetrabutylammonium hydroxide (TBAH) to the mobile phase, peak resolution was achieved [97]. Furthermore, a low pH favors the separation of the inositol phosphates. The combination of an ion pair reagent (TBAH), a low pH, and a methanol content in the mobile phase increased the retention time, enabling the separation of $InsP_3$ to $InsP_6$. However, peak tailing is always observed. Since phytic acid is not UV-active or fluorescent, detection is often carried out using a refractive index (RI) detector [93].
For separation and quantification of various inositol phosphates ($InsP_3$, $InsP_4$, $InsP_5$, $InsP_6$) a reversed phase C18 HPLC method based on Sandberg and Adherrine was established [94]. Details of the stationary as well as mobile phase used can be found in Chapter A.2.2. In the following, it is investigated whether the inositol phosphate content of the bran samples after IEX capturing is within the linear measuring range, Figure 4.11.

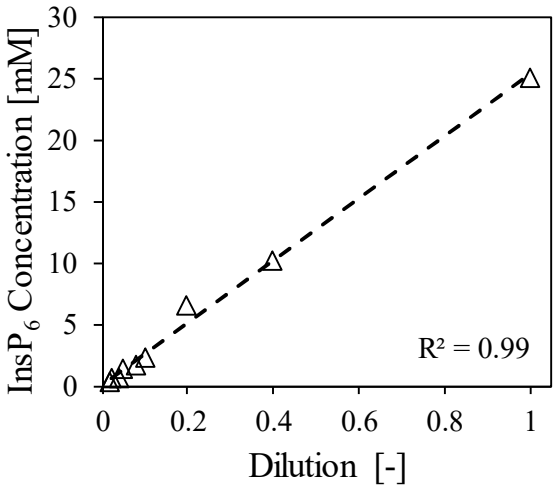

Figure 4.11: Investigation of the linear measuring range. Inositol phosphates extracted from a bran sample. The distilled samples were dissolved in 0.5 mL of 50 mM NaOAc and diluted successively; dilutions: 1:1, 1:2.5, 1:5, 1:10, 1:12.5, 1:20, 1:25, 1:40, 1:50.

In Figure 4.11, the $InsP_6$ concentration as function of the dilution is given. The indicated dilutions refer to an initial volume of 0.5 mL of 50 mM sodium acetate buffer in which the extracted inositol phosphates were dissolved after vacuum distillation. At higher dilution factors (>5), lower phosphorylated inositols are not detected due to their low concentration. Therefore, only the $InsP_6$ peak is considered. However, $InsP_6$ accounts for 90% of the inositol phosphate content in rye bran. Therefore, this simplification is assumed to be a reasonable approximation. The correlation coefficient R^2 of 0.99 confirms the linearity. Consequently, the linear measuring range of the detector is not exceeded for the concentrated rye bran extracts. In addition, the RI detector has been confirmed as a suitable detector for the detection of inositol phosphates.

Calibration represents the major challenge in quantification of inositol phosphates. Most commercially available chemicals contain impurities and are usually a mixture of differently phosphorylated inositol [98]. As pure components are almost non-existent on the market, most calibrations are based on in-house synthesis of the substances or have already been existed for generation. From Figure 4.12 it can be seen that typical retention times of $InsP_3$, $InsP_4$, $InsP_5$, and $InsP_6$ are, 9 min, 12 min, 16 min, and 22 min, respectively. Figure 4.12 also illustrates that neither chemical is a pure substance. Both chemicals contain inositol phosphates with at least 3, 4, 5, and 6 phosphate groups. Additionally, the ratio of these differs. For the dipotassium phytate from BLD Pharm (Shanghai, China), the manufacturer gives a purity of 91.5% and a molecular weight of 738.23 $g \cdot mol^{-1}$, Appendix B. For phytic acid sodium salt hydrate (*myo*-inositol hexakis-dihydrogen phosphate) P8810 from Sigma Aldrich (Darmstadt, Germany), no purity or molecular weight is given neither by the distributor, nor by the manufacturer. However, these values are determined from the certificate of analysis considering the crystal water and sodium ions, Appendix B.

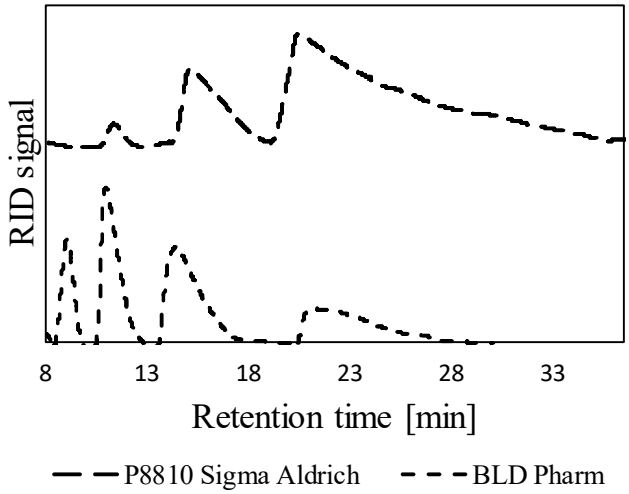

Figure 4.12: Chromatograms of two different commercially available phytic acid chemicals. 25 mM each in 50 mM NaOAc. Peak areas from left to right: $InsP_3$, $InsP_4$, $InsP_5$, and $InsP_6$.

Based on ICP-OES measurement by Sigma Aldrich, 12 sodium ions and two water molecules are bound to phytic acid [99]. Consequently, the molar mass of P8810 phytic acid standard is 971.96 $g \cdot mol^{-1}$. However, it is the average molar mass of phytic acid ($InsP_6$) in the chemical that accounts for only 77.3% of the peak areas. Taking these into account, a defined concentration can be applied. Furthermore, P8810 closely reflects the distribution of inositol phosphates in rye bran. It contains 0.4% $InsP_3$, 2.6% $InsP_4$, 19.7% $InsP_5$, and 77.3% $insP_6$. Whereas in rye bran the percentage in composition is 0.4% $InsP_3$, 1.2% $InsP_4$, 5.3% $InsP_5$, and 93.2% $InsP_6$. Consequently, P8810 was used for calibration. From three different stock solutions, dilution series from 2 to 20 mM were measured in triplicates. In order to determine the concentration (c_i) from the peak area integrals of the different inositol phosphates, the proportion of the individual peak areas (A_i) from the sum of all peak areas (A_{total}) is correlated with the respective concentration used (c_{input}, 2 to 20 mM) (Equation 4.3). The same refractive index is assumed for different phosphorylated inositols.

$$c_i = \frac{A_i}{A_{total}} \cdot c_{input} \qquad \text{(Eq. 4.3)}$$

In Figure 4.13 the resulting calibrations for different phosphorylated inositols ($InsP_3$ to $InsP_6$) are given.

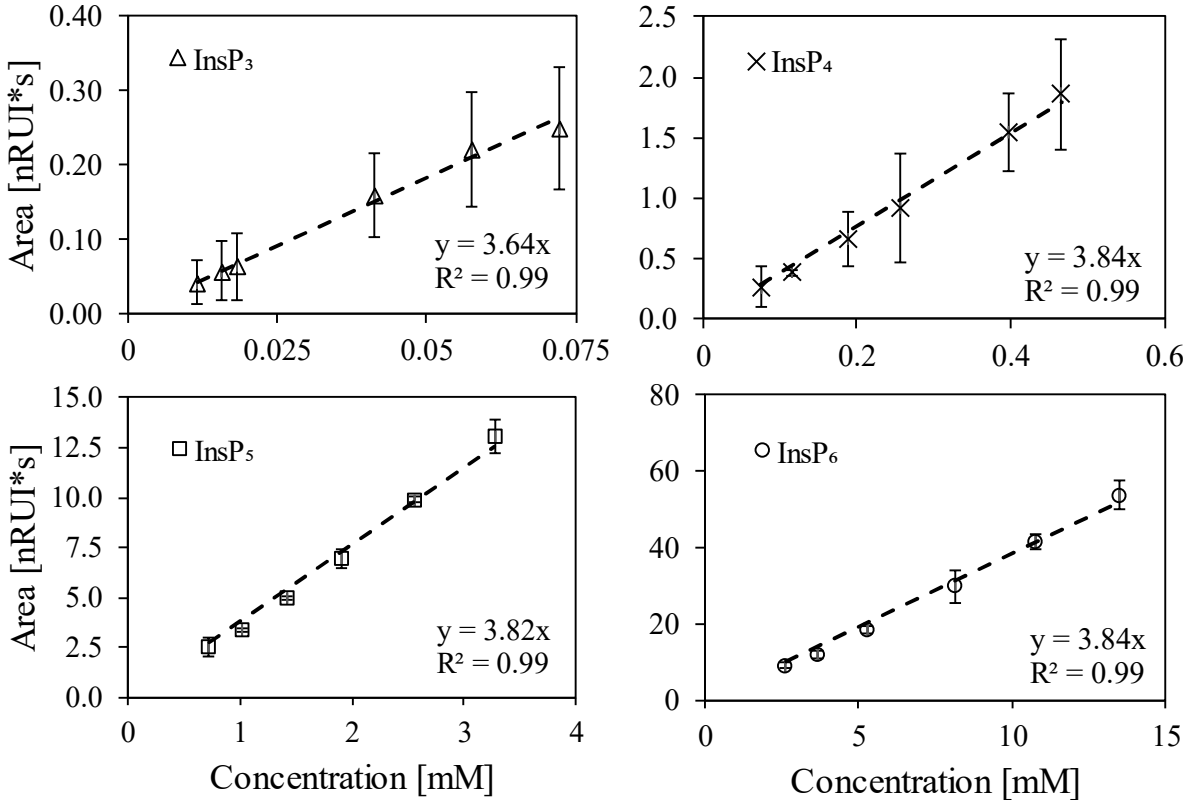

Figure 4.13: HPLC calibration series for different inositol phosphates ($InsP_3$ to $InsP_6$) using the phytic acid salt P1880 (Sigma Aldrich). Concentrations range: 2 to 20 mM. Each data point represents the average of three physical samples as well as measurement triplicates.

Each individual calibration curve results in a correlation coefficient R^2 of over 0.99, allowing for precise quantification of $InsP_3$ to $InsP_6$. Furthermore, the assumption of same refractive indexes is reflected in the almost identical slopes for the $InsP_3$-, $InsP_4$-, $InsP_5$-, and $InsP_6$-calibration curves in Figure 4.13, respectively. While this is a simplification, it is considered a valid approximation due to similarity in structure and associated physical properties. In addition, Figure 4.13 shows that due to the low concentration of inositols with a low degree of phosphorylation in P1880 (in some cases up to the limit of detection; especially for $InsP_3$), the deviation of individual data points for calibration is greater. Moreover, it is noted, when using HPLC methods for quantification of inositol phosphates, only four different phosphorylation states ($InsP_3$ to $InsP_6$) can be detected. For higher resolution, High Performance Ion Chromatography using post column derivatization or 2D Nuclear Magnetic Resonance Spectroscopy (^{31}P and ^{1}H) is required.

For further validation, a comparative analysis was carried out at the Department of Biotechnology (RWTH Aachen University) and the Institute of Environmental Technology and Energy Economics (Hamburg University of Technology). Inositol phosphates were extracted from bran samples of the same batch following the same extraction protocol. For quantification, at the Department of Biotechnology, an HPLC method was already established, while at the Institute of Environmental Technology and Energy Economics, the quantification of phytic acid is based on a commercially available analysis kit K-PHY T (Megazyme) based on enzymatic hydrolysis followed by colorimetric quantification. In direct comparison with HPLC quantification, a deviation in the range of 10^{-3} $g_P \cdot 100g_{bran}^{-1}$ was found, while the deviation from the enzyme kit is in the range of 10^{-1} $g_p \cdot 100g_{bran}^{-1}$. Due to the small deviation from the comparative HPLC analysis, the established analysis is considered valid.

Comprehensive Analysis

For further evaluation and examination of the consistency of data obtained between colorimetry and HPLC analysis (including extraction and capturing), the intrinsic phytase activity in rye bran was determined using both methods, Figure 4.14. Both analytical methods yielded accurate and comparable results, as evidenced by the determination of intrinsic enzyme activity, with colorimetry provided a value of 6299 ± 388 $U \cdot kg_{bran}^{-1}$ and HPLC analysis yield 5613 ± 161 $U \cdot kg_{bran}^{-1}$. The consistency between these measurements suggests that both methods are reliable, thus affirming the validity of their application.

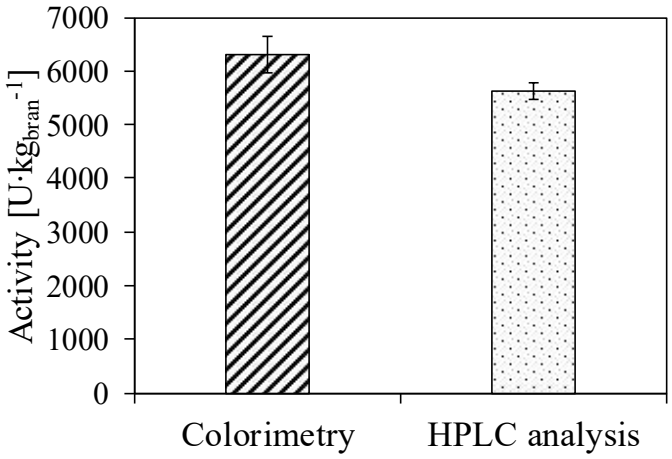

Figure 4.14: Comparison of colorimetrically determined enzyme activity with HPLC analysis.

4.1.3 Error Discussion

The sources of error of the previously shown offline analytical methods for the enzyme activity assay as well as the extraction, capturing and quantification of inositol phosphates are presented. In addition, the effect on the results is discussed.

Enzyme Activity Assay

The major sources of error in the determination of native enzyme activity are the error of the weight balance used, but the greatest error originates from variations in the composition of the biological material caused by inhomogeneity. However, using fine chemicals as substrate for kinetic investigation, the error mostly depends on weighing and standard deviation of the measurement triplicates. The balance used belongs to accuracy class I and has a measuring error of 1 mg. Considering an average sample weight of 0.15 g rye bran for native enzyme activity determination, resulting in an error of 0.7%. Based on an average intrinsic enzyme activity of 5000 $U \cdot kg^{-1}$, the error is 35 $U \cdot kg^{-1}$. Taking into account the standard deviation of all intrinsic enzyme activity measurements performed, the variation in biological material is 349 $U \cdot kg^{-1}$. Thus, the error due to biological inhomogeneity is ten times higher than the weighing error. Accordingly, the total error of the method results from the addition of both errors and is 384 $U \cdot kg^{-1}$. Consequently, the produced data are within a 92% confidence level. However, the error is within biological variation due to crop growth conditions and is, therefore, expected (Chapter 1.3). Thus, the established method has a high accuracy. However, ammonium heptamolybdate solution has a limited storage capacity. Therefore, prior to quantification a new solution has to be prepared. In order to avoid fluctuations in the composition, and associated variations in the extinction coefficient, a calibration series was recorded for each quantification.

Quantification of Inositol Phosphates by HPLC

The error of inositol phosphate quantification depends on the error of the calibration series, the capturing by IEX, and the inhomogeneity of the biological material. Calibration was performed using a mixed spectrum (Chapter 4.1.2), assuming the same refractive index for differently phosphorylated inositols. Second, an averaged molar mass was used to calculate the concentration of the calibration series, resulting in a slightly error-prone starting concentration. From this, the averaged percent area fractions were calculated, leading to slightly error-prone inositol phosphate concentrations. However, the major error is caused by the averaged peak area percentages, Table 4.1.

Table 4.1: Averaged percentage area fractions of the inositol phosphates in P8810 at different concentrations. The calibration series were determined from the mixed spectra. The mean values of the measurement triplicates are shown.

Concentration [mM]	IP_3 [%]	IP_4 [%]	IP_5 [%]	IP_6 [%]
3.45	0.46	2.19	21.05	76.30
4.83	0.38	2.43	21.30	75.89
6.90	0.17	2.74	20.54	76.55
10.35	0.70	2.48	18.36	78.46
13.80	0.42	2.88	18.60	78.11
17.25	0.24	2.70	18.96	78.10
Average	0.4 ± 0.2	2.6 ± 0.3	19.7 ± 1.3	77.3 ± 1.1

The percentage in deviation of the certain peak area fraction are 0.2%, 0.3%, 1.3%, and 1.1% for $InsP_3$, $InsP_4$, $InsP_5$, and $InsP_6$, respectively. These deviations effect the calculated concentrations. Figure 4.15 illustrates the deviation in concentration.

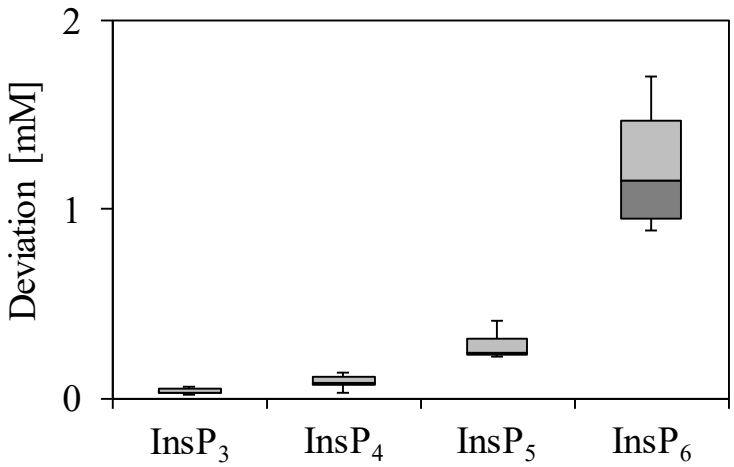

Figure 4.15: Box plots for the distribution of discrepancies in HPLC analysis. The deviations from triplicate measurements are depicted, with the tolerance range covering 75% of the data.

In the box plot shown, 50% of the data points are inside the box. The mean standard deviations are 0.04 mM, 0.09 mM, 0.29 mM, and 1.12 mM for $InsP_3$, $InsP_4$, $InsP_5$, and $InsP_6$, respectively. The standard error (SE) is calculated from the standard deviation (σ) and the number of samples (n), Equation 4.4.

$$SE = \frac{\sigma}{\sqrt{n}} \qquad \text{(Eq. 4.4)}$$

For three stock solutions and six measurements each, the number of samples is 18, resulting in standard errors of 0.009 mM, 0.021 mM, 0.068 mM, and 0.285 mM for $InsP_3$, $InsP_4$, $InsP_5$, and $InsP_6$, respectively. An overview is given in Table 4.2.

To assess the accuracy of capturing by IEX, the inositol phosphate content was quantified with and without employing IEX (Chapter 4.1.2). Taking into account the error due to HPLC calibration, the standard error is calculated according to Equation 4.4. The standard errors caused by IEX capturing are 0.003 mM, 0.109 mM, 0.277 mM, and 0.54 mM for $InsP_3$, $InsP_4$, $InsP_5$, and $InsP_6$, respectively. Furthermore, for the determination of biological variations, the standard error is determined from nine bran samples, resulting in 0.203 mM, 0.445 mM, 0.232 mM, and 1.354 mM for $InsP_3$, $InsP_4$, $InsP_5$, and $InsP_6$, respectively, Table 4.2. It also becomes evident that the error caused by biological inhomogeneity has the greatest impact on the result.

Taking into account the errors described above, the total error (ΔE_{total}) is calculated according to Equation 4.5. Thereby, the defect size originating from IEX (ΔE_{IEX}) and inhomogeneity of the biological material (ΔE_{bio}) contribute additively and is, therefore, summarized as provision of the sample, whereas the total error also takes into account the error caused by calibration (ΔE_{cal}), Equation 4.5.

$$\Delta E_{total} = \sqrt{(\Delta E_{IEX} + \Delta E_{bio})^2 + \Delta E_{cal}^2} \qquad \text{(Eq. 4.5)}$$

Table 4.2 shows the resulting error including defect size for $InsP_3$ through $InsP_6$. As expected, the largest error is attributed to fluctuations in inositol phosphate levels within rye bran, i.e. inhomogeneity, while only small errors are caused by calibration, i.e. HPLC analysis.

Table 4.2: Sources of error in quantification of inositol phosphates. The error of inositol phosphate content is caused by fluctuations, i.e. inhomogeneity, in the biological material (ΔE_{Bio}), by losses during ion exchange chromatography (ΔE_{IEX}), and during HPLC quantification (ΔE_{cal}).

	ΔE_{cal} [mM]	ΔE_{IEX} [mM]	ΔE_{Bio} [mM]	ΔE_{total} [mM]
$InsP_3$	0.009	0.003	0.203	0.207
$InsP_4$	0.021	0.109	0.445	0.555
$InsP_5$	0.068	0.277	0.232	0.513
$InsP_6$	0.285	0.540	1.354	1.916
$\sum$	0.383	0.929	2.234	3.191

The overall methodological error is quantified at 3.2 mM, equivalent to a 16% deviation relative to an expected sample concentration of 20 mM (Chapter 4.1.2). Within this error, 4% arises from ion exchange chromatography (IEX), and only 1% is attributed to HPLC analysis. An additional 11% is caused by biological variation, which can be mitigated through repeated measurements, given its stochastic nature fluctuating around the true value. Nonetheless, for the quantification of phytic acid ($InsP_6$), the overall error percentage remains below 10%. Comparable studies have reported a total error of up to 10% while employing smaller sample sizes [94,100]. Consequently, the observed error falls within the expected range, affirming the method's reasonable accuracy in determining inositol phosphate content.

4.2 Online Analytics

The interest in online monitoring of bioprocesses arises from its ability to reduce time delays due to sample preparations and analysis as well as to provide direct control over reactions. This approach is in particular attractive for industrial applications, with techniques such as infrared-, fluorescence-, nuclear magnetic resonance-, and (UV)-Vis spectroscopy being applied for real-time monitoring [64]. In this chapter, the development of an online analytical method for the quantification of residual phytate content during biocatalytic P-mobilization is presented.

4.2.1 Online Monitoring of Phytate Content in Biological Matrices

Since the beginning of the 19th century, much effort has been made to detect and quantify $InsP_6$ present in plant material [93]. However, most of the methods developed are based on protracted extraction procedures and quantification by chromatography (Chapter 4.1.2). Limitations are often the large sample volumes required and tedious preparation steps that render these methods slow, expensive, and sometimes environmentally unfriendly [101].
Nuclear magnetic resonance (NMR) spectroscopy offers the possibility of real-time data acquisition through inline analysis and has been applied to the analysis of biological samples and to study the hydrolysis pattern of inositol phosphates [102]. The first application of ^{31}P-NMR for inositol phosphate analysis was described by O'Neil *et al.* in 1980 [103]. However, the quantitative determination of phytate in whole grains is until now limited by the complex sample matrix and still requires extraction procedures [104,105]. Although NMR analysis, especially 2D (^{31}P and ^{1}H) NMR, can be used to infer the stereoisomerism of $InsP_1$ to $InsP_6$, it is not the method of choice for online analysis of inositol phosphates in a biological matrix due to the required extraction steps, the high investment cost, and the rather complicated signals to be processed [38].
Other spectroscopic methods such as Fourier-Transform-Infrared (FT-IR) spectroscopy do not necessarily require preceding extraction procedures as well as provide minor complicated spectra and are therefore more suitable for online monitoring of inositol-phosphates in biological matrices. It has been shown that quantification of phytic acid in a biological matrix using near infrared radiation (NIR, 13,000 - 4,000 cm^{-1}) is possible [106,107]. Nevertheless, the precision of quantification is limited, indicated by a low coefficient of determination. This lack of accuracy may be attributed to potential interference arising from the overlapping absorbance patterns of other substances within the biological matrix.

Parts of this Chapter are published in: Widderich, N.; Bubenheim, P.; Liese, A. Online monitoring of phytate content in plant residuals during wet-treatment. *Scientific Reports* **2024** [66].

Infrared light in the mid-infrared region (MIR, 4,000 – 400 cm^{-1}) of the electromagnetic spectrum has the advantage of molecular characteristic absorbance patterns. It contains a series of intricate and closely spaced bands resulting from bond vibrations in molecules. Just as a fingerprint is characteristic of an individual, the spectra in the *fingerprint* region (1400 to 600 cm^{-1}) are characteristic of an individual molecule. Furthermore, mid infrared radiation is extensively used in the determination of plant constituents; e.g. to determine compositions of lignocellulose materials, quality of milling fractions in wheat and compositional changes during seed germination [108–110].

Recent findings reported in $InsP_6$-analysis include the characterization of different metal phytate compounds by He *et al.*, who suggested that some spectral features of metal phytates could be used to distinguish phytate compounds from metal phosphate compounds [111]. Guan *et al.* investigated the complexation behavior of phytate with aluminum hydroxide using FT-MIR. The results revealed that three out of six phosphate groups bound to aluminum hydroxide [112]. Recently, a method for rapid nutritional profiling of pea seeds was developed [101]. However, all investigations were done using solid and dry material. Greater challenges arise when measuring in aqueous systems, as large parts of the IR-spectrum are covered by OH-bands. Attenuated total reflection Fourier-Transform-Infrared (ATR-FTIR) spectroscopy is a highly versatile, label-free, and non-invasive imaging method. The major advantage of ATR-FT-MIR is the opportunity to measure samples that absorb strongly in the IR-spectrum [113]. Morisset *et al.* used ATR-FT-MIR to quantify orthophosphate in aqueous solution during microalgae cultivation. A partial least squares regression (PLSR) algorithm relates the spectral intensities to the concentrations (Chapter 3.1.2). The model was calibrated with KH_2PO_4 in the range of 1771 to 1001 cm^{-1} [114].

4.2.2 Differentiation Between Orthophosphate and Inositol-Phosphates

KH_2PO_4 was used for quantitative analysis of inorganic P (Chapter A.2.4). As shown in Figure 4.16, KH_2PO_4 and phytic acid show similar MIR-absorption behavior in aqueous solution, with the only difference being, that according to the degree of phosphorylation of phytic acid, the absorbance proportionally increases. According to Guan *et al.,* the two most dominant peaks at 1172 and 1065 cm^{-1} are assigned to the asymmetric and symmetric stretching vibrations of P-O in HPO_3^- [112], respectively, both of which are present in KH_2PO_4 (dissociated) and phytic acid. Karunakaran *et al.* studied the IR-absorption behavior of phytic acid and further classified the characteristic peak in the range of 1100 to 1060 cm^{-1} as O=P-O vibration [101]. Nevertheless, this vibration pattern is also found in both substances, making it challenging to distinguish them.

Parts of this Chapter are published in: Widderich, N.; Bubenheim, P.; Liese, A. Online monitoring of phytate content in plant residuals during wet-treatment. *Scientific Reports* **2024** [66].

Further peak assignments in the region below 1000 cm^{-1} were made by Guan *et al.* [112]. However, these peaks are superimposed by water absorption, as is the OH-band at 3500 cm^{-1}, and, therefore, are not considered. Both KH_2PO_4 and phytic acid show a very similar IR-absorption pattern in aqueous solution. Moreover, KH_2PO_4 can be obtained in much higher purity than phytic acid [98], making it suitable to quantify P-O and P=O-P species, including phytic acid, in solution.

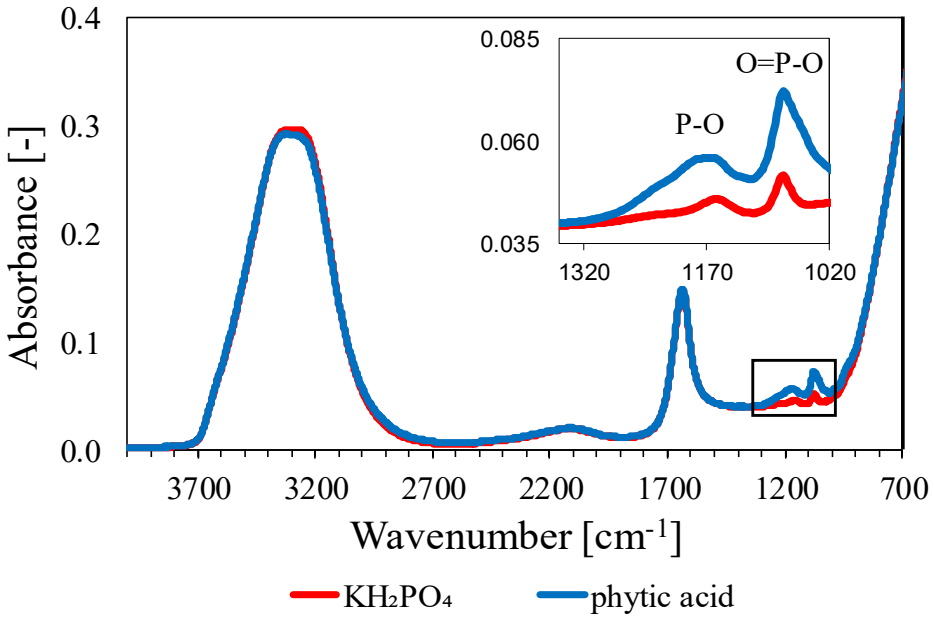

Figure 4.16: Absorbance pattern of 25 mM KH_2PO_4 and 25 mM phytic acid in aqueous solution at room temperature and pH 6.5. The image within the figure shows the calibration range for the PLSR model [66].

For quantification of P-O and O=P-O species in aqueous solution, the frequency range of 1350 to 1020 cm^{-1} was chosen, as it covers all relevant valence vibrations that are not superimposed by OH-bands. Morisset *et al.* chose a frequency range of 17771 to 1001 cm^{-1}. The large integration range was set for quantification of several components such as carbonate and bicarbonate, whereas only the absorbance in the range of 1116 to 1001 cm^{-1} is caused by orthophosphate (HPO_4^{2-}) [114]. In this study, however, the best predictions were obtained for an extended frequency range up to 1350 cm^{-1}, as shown in Figure 4.16.

4.2.3 Continuous ATR-FTIR Measurement in Bran Water Suspension

In the application, the P species are continuously quantified in the aqueous phase of the bran water suspension. In order to prevent particle deposition on the ATR-crystal and thus blindness of the optical fibre, a nylon membrane (mesh size < 10 µm) was used, Figure 4.17. The membrane allows convection and diffusion of all substances in solution while retaining the bran particles. To avoid contact of the membrane with the ATR crystal, a module (protective cage) was made of polyoxymethylene (POM), and is enclosed by the membrane, Figure 4.18. [66]

Figure 4.17: Original image of the optical fibre enclosed by the membrane module.

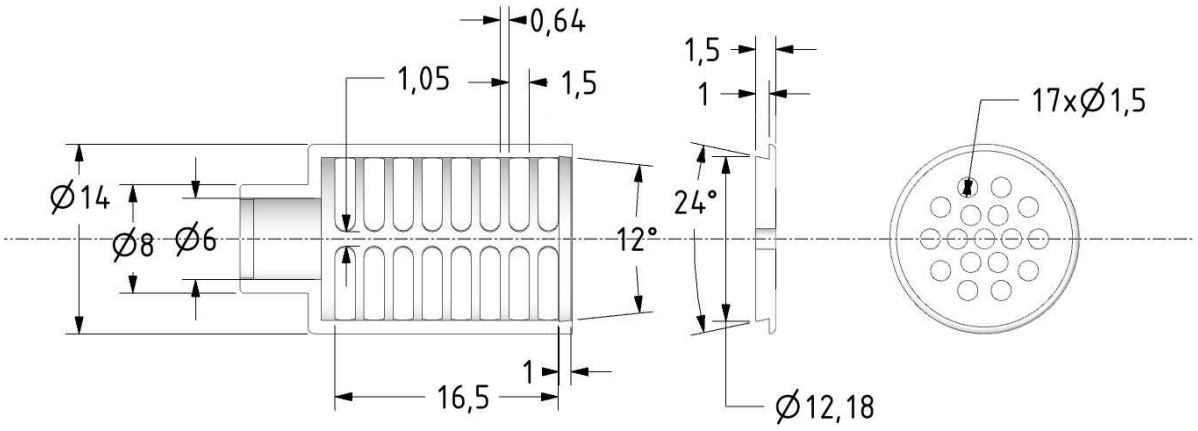

Figure 4.18: Membrane module to retain bran particles, made out of POM (polyoxymethylene) and covered by a nylon membrane (mesh size <10 µm. Length specifications in mm). [66]

4.2.4 Chemometrics

PLSR modeling is used to relate IR-absorption patterns to the concentrations of total P-O and O=P-O species in aqueous solution (Chapter 3.1.2). The training data set with KH_2PO_4 experienced a RMSECV of 2.15 mM KH_2PO_4, equaling 0.36 mM $InsP_6$, with a coefficient of determination R^2 of 0.99. It shows that the calibration data is of high agreement with the model prediction, resulting in reliable results. In addition, best predictions were achieved using two factors that already cover 100% of the spectral variance. However, the lowest RMSECV is given by four factors, resulting in an RMSECV of 1.08 mM KH_2PO_4. Nevertheless, more than two factors lead to overfitting, and noise in the data is described by the PLSR model, resulting in an overestimation of concentrations. This behavior is also reflected by the regression coefficients, Figure 4.19 [63].

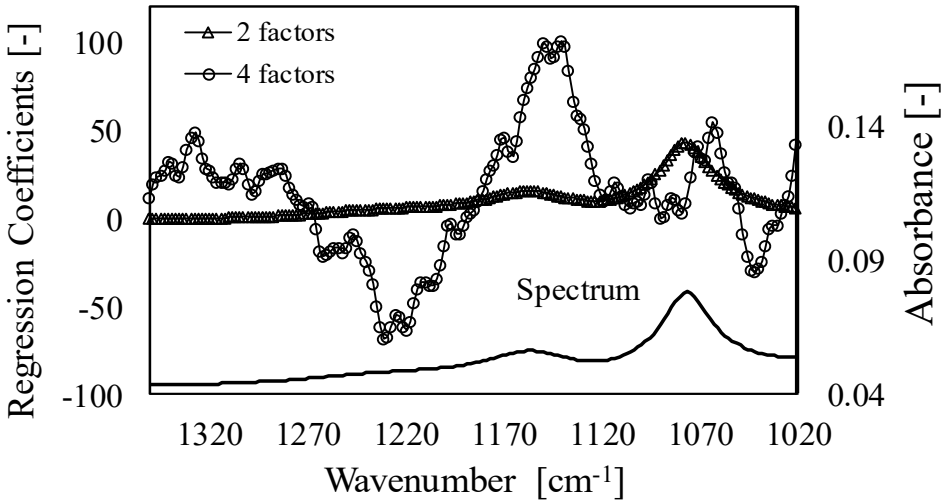

Figure 4.19: PLSR regression coefficients for two factors (RMSECV of 2.15 mM) and four factors (RMSECV of 1.05 mM) [66].

The emergence of noise in the regression coefficients is manifested by reductions in the structure and the existence of sharp peaks with a high degree of directional oscillation [115]. Figure 4.19 shows that when two factors are employed, the course of the regression coefficients has an unambiguous and smooth structure, aligning with the spectra. In contrast, more than two or even four factors lead to the described behavior and noise is included, leading to overfitting and erroneous predictions.

Parts of this Chapter are published in: Widderich, N.; Bubenheim, P.; Liese, A. Online monitoring of phytate content in plant residuals during wet-treatment. *Scientific Reports* **2024** [66].

The predicted values are compared to colorimetrically determined inorganic P concentrations in the liquid phase after different times of wet-treatment (1 h, 2 h, 4 h, 8 h, and 16 h), resulting in a RMSEP of 6.32 mM KH_2PO_4 and the coefficient of determination R^2 of 0.87. Thus, the chemometric and colorimetric data have a high degree of agreement. The lower RMSECV (2.15 mM) of the calibration data set compared to the RMSEP (6.32 mM) shows, that the model is reliable, and also indicates that the model is not over-fitted. Furthermore, the R^2 reflects a high model certainty. Thus, the model is suitable for predicting P-O and O=P-O species in the aqueous phase of the bran-water suspension.
Based on the PLSR model, the lower limit of quantification is 10 mM KH_2PO_4, equaling 1.67 mM $InsP_6$, which corresponds to standard RP-18 chromatography (as presented in Chapter 4.1.2). Morisset *et al.* also determined PO_4^{3-} (KH_2PO_4) concentrations in aqueous solution using ATR-FT-MIR with a similar limit of quantification [114]. Thus, the membrane covering the ATR-probe does not affect the concentration of P species at the ATR-crystal after an equilibrium is reached (Chapter A.2.3). Furthermore, the probe response time at a stirrer speed of 300 rpm is 216 s. The acquisition of the 200 spectra takes 56 s and is already included in the response time of the probe. Compared to sampling, sample preparation, and offline quantification, this represents a significant reduction in the usage of chemicals and time.

4.2.5 Prediction of Residual Phytate Content

Since the training data set only maps the P-O and O=P-O vibration patterns in the liquid phase, the phytate concentration in rye bran during wet-treatment was determined via a mass balance, Equation 4.6.1-2. It was assumed that all P-O and O=P-O absorption patterns in the liquid phase are either attributed to phytic acid or orthophosphate (PO_4^{3-}, hydrolysis product). Due to different phosphorylation states of phytic acid ($InsP_1$ to $InsP_6$) in rye bran, the mass balance is normalized to P (31 $g \cdot mol^{-1}$) and refers to P bound to inositol phosphate (Chapter 4.1.2). In addition, the compression of the aqueous phase due to the water absorption of bran particles is included in the mass balance.

$$\frac{dm_P}{dt} = 0 = m_{InsP,bran}(t_0) - m_{InsP,bran}(t) - m_{P,liquid\ phase}(t) \qquad \text{(Eq. 4.6.1)}$$

$$m_{P,liquid\ phase}(t) = \frac{c_{measured}(t) \cdot V(m_{bran})_{water} \cdot M_P}{m_{bran}} \cdot 100 \qquad \text{(Eq. 4.6.2)}$$

Parts of this Chapter are published in: Widderich, N.; Bubenheim, P.; Liese, A. Online monitoring of phytate content in plant residuals during wet-treatment. *Scientific Reports* **2024** [66].

- $m_{InsP,bran}(t_0)$ = amount of inositol-P present in starting material ($g_P \cdot 100g_{bran}^{-1}$)
- $m_{InsP,bran}(t)$ = amount of inositol-P present at time point t ($g_P \cdot 100g_{bran}^{-1}$)
- $m_{P,liquid\ phase}(t)$ = amount of P in liquid phase at time point t ($g_P \cdot 100g_{bran}^{-1}$)

Where $c_{measured}(t)$ is the feedback variable. It is the concentration of P-O and O=P-O valence vibrations in the aqueous phase, which is determined from the MIR data via the PLS model. $V(m)_{liquid}$ is the volume of the liquid phase. Due to water absorption of the bran particles, it is a factor depending on the amount of bran. Consequently, the actual volume of the liquid phase is lower than the liquid volume introduced to the system at the beginning.

4.2.6 Water Uptake

Water uptake of the bran bulk is mathematically derived from the dry and soaked particle size distributions, Figure 4.20. The factor F_{swell}, Equation 4.7, on average reflects the volume increase of the bran bulk after soaking. No change in particle size distribution could be observed after 15 min of treatment. Due to this, a time-independent value for the water absorption is derived from the average volume increase due to swelling, resulting in a factor F_{swell} of 1.164. Soaked Particles < 150 µm were neglected due to uncertainties of the measurement, resulting in a deviation in the range of 10^{-3}.

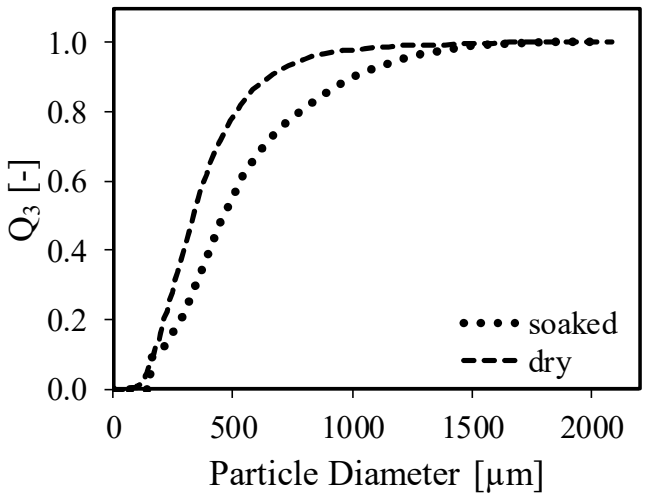

Figure 4.20: Cumulative and volume-specific particle size distributions of dry and soaked bran particles. Distributions are used to calculate an average swelling factor and to derive particle properties. $Q_{3,dry}$ is determined by imaging, whereas $Q_{3,soaked}$ is measured in suspension by laser diffraction applying the Fraunhofer optical model [66,116].

Parts of this Chapter are published in: Widderich, N.; Bubenheim, P.; Liese, A. Online monitoring of phytate content in plant residuals during wet-treatment. *Scientific Reports* **2024** [66].

The sphericity Ψ and the volume-specific surface area S_V are used to calculate the Sauter mean diameter $d_{2,3\ dry}$, Equation 4.8, of dry particles. By applying the Sauter mean diameter (509 µm) the mean volume of dry particles $V_{2,3\ dry}$, Equation 4.9, is determined. The volume ratio of dry to soaked particles is described by F_{swell} and thus $V_{2,3\ soaked}$ is derived, Equation 4.10. The difference between $V_{2,3\ soaked}$ and $V_{2,3\ dry}$ corresponds to the average water volume absorbed V_{H_2O}, Equation 4.11. By correlation of the density of the bulk particles ρ_{bran} 1.49 $g \cdot cm^{-3}$ and $V_{2,3\ soaked}$, the amount of water absorbed is derived and expressed in mass-specific terms, resulting in 0.39 $mL_{water} \cdot g_{bran}^{-1}$.

$$F_{swell} = \frac{\int Q_3(x)_{dry}}{\int Q_3(x)_{soaked}} \quad \text{(Eq. 4.7)}$$

$$d_{2,3\ dry} = \frac{6}{\Psi \cdot S_V} \quad \text{(Eq. 4.8)}$$

$$V_{2,3\ dry} = \frac{6}{\pi} d_{2,3\ dry}^3 \quad \text{(Eq. 4.9)}$$

$$V_{2,3\ soaked} = \frac{6}{\pi} d_{2,3,dry}^3 \cdot F_{swell} \quad \text{(Eq. 4.10)}$$

$$V_{H_2O} = V_{2,3\ soaked} - V_{2,3\ dry} \quad \text{(Eq. 4.11)}$$

4.2.7 Validation and Error Discussion

For the prediction of residual phytate content in rye bran, time-dependent P concentrations in the liquid phase resulting from FT-MIR measurements and chemometrics are used. These concentrations act as a feedback variable in a mass balance, Equation 4.6.1, to infer the residual phytate content in the bran matrix. The results are compared to extraction and HPLC analysis, Figure 4.21, resulting in an RMSEP of 81 $mg_P \cdot 100g_{bran}^{-1}$ and a coefficient of determination R^2 of 0.78. This corresponds to a deviation of about 8% related to the total inositol-P content present in the biological starting material. Taking into account the molecular weight of phytic acid (660 $g \cdot mol^{-1}$), the RMSEP related to phytate is 0.28 $g_{phytate} \cdot 100g_{bran}^{-1}$. In Figure 4.21, it can be seen that the deviation of the data sets is in the range of the measurement uncertainties. Small deviations such as the higher residual phytate content after 8 h compared to the measurement after 4 h of wet-treatment determined by HPLC are thermodynamically impossible and can be explained by the biological origin of the substrate, since a new batch was prepared for each experiment. This is also reflected by the apparently low coefficient of determination R^2 of 0.78.

Parts of this Chapter are published in: Widderich, N.; Bubenheim, P.; Liese, A. Online monitoring of phytate content in plant residuals during wet-treatment. *Scientific Reports* **2024** [66].

In contrast, the result of the mass balance using chemometric as well as colorimetric analysis shows the expected trend, also suggesting that the HPLC data for this time point is slightly erroneous.

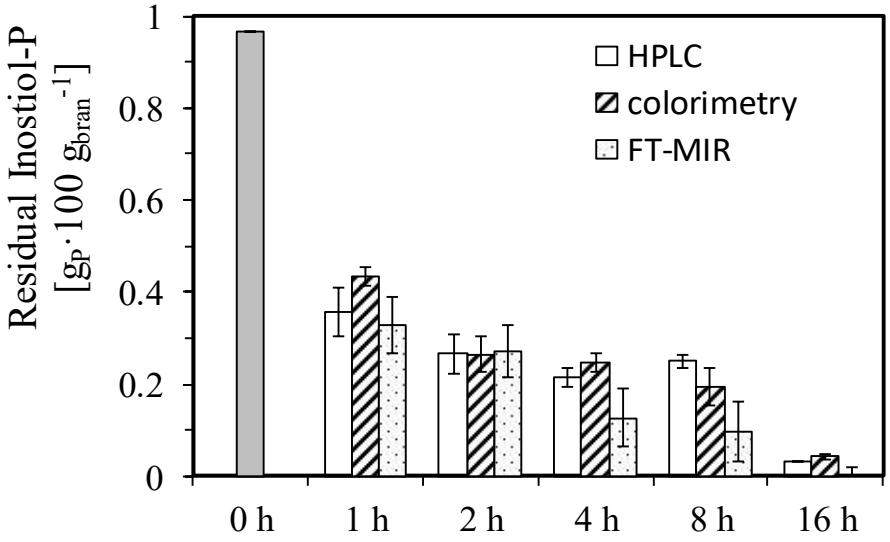

Figure 4.21: Comparison of chemometric data including the mass balance, Equation 4.6.1, for quantification of residual phytate content with wet chemical analytical methods. Wet chemical analytical methods include the colorimetrically determined P-content in the aqueous phase (Chapter 4.1.1) and extraction and HPLC analysis for the residual phytate content (Chapter 4.1.2). The colorimetric data is also used as feedback for the mass balance and compared to the mass balance results using FT-MIR data [66].

Comparison of the results from the colorimetric measurements with the chemometric data, both including the mass balance, give a similar RMSEP of 86 $mg_P \cdot 100g_{bran}^{-1}$ and accordingly 0.30 $g_{phytate} \cdot 100g_{bran}^{-1}$, with a coefficient of determination R^2 of 0.86, demonstrating the robustness of the developed methodology. Based on all data sets, it is concluded that the mass balance is valid. As a conclusion one can state that the developed method for the prediction of the residual phytate content provides as accurate results as the most commonly used methods for inorganic P and inositol phosphate quantification, and is significantly faster, less laborious, and non-invasive in comparison.

Neglecting water absorption by bran particles, the RMSEP is 145 $mg_P \cdot 100g_{bran}^{-1}$ and accordingly 0.512 $g_{phytate} \cdot 100g_{bran}^{-1}$, leading to significant deviations without applicability. Therefore, the consideration of water absorption in the mass balance is of particular importance for the accuracy of the results. Furthermore, the precision of results also confirms the mathematical derivation of the water absorption, which can in principle be applied to various particle distributions of biological origin with similar swelling behavior. It is also evident from this data set that the phytate contained in bran is already partially degraded in the plant matrix and confirms the assumption that all P-species passed to the liquid phase can be assigned to orthophosphate.

4.3 Interim Summary

- Colorimetric quantification of orthophosphate using molybdenum blue complex formation is both robust and versatile. When assessing enzymatic activity, it is essential to include blank samples to reduce interference from phytic acid.

- HPLC analysis allows for quantification of four out of six different phosphorylation states of inositol phosphates, specifically $InsP_3$ to $InsP_6$. However, it is shown that over 90% of the organically bound P is concentrated in $InsP_6$, with the remaining P distributed among the lower phosphorylated inositols in descending order. The total error of inositol phosphate quantification in rye bran by HPLC is 3.2 mM corresponding to 0.46 $gP \cdot 100g_{bran}^{-1}$, including capture by IEX, biological variability, and calibration error, with the primary source of error being biological variability.

- By applying a mass balance for P and considering the effect of water compression, the amount of residual phytate content in the plant material can be determined on the basis of MIR spectra. The approach involves measuring the P-content in the liquid phase of the water bran suspension and using PLSR modelling to predict the time-dependent P concentration. Compared to wet chemical methods, i.e. HPLC quantification, the inline analysis has an error of 0.28 $g_P \cdot 100g_{bran}^{-1}$.

- The established analytical methods are robust and provide reliable and sufficiently precise results. With these validated techniques in place, the next step is to comprehensively characterize the raw material, focusing on its composition and intrinsic properties. This fundamental understanding is essential for optimizing process conditions and improving the overall efficiency of enzymatic P-mobilization in subsequent research phases.

5 Investigation of the Raw Material

This Chapter constitutes an examination of the distribution of P as well as inositol-P and enzymatic inositol phosphate hydrolyzing activity in rye bran, nutrient properties, and storage capacity. Special emphasis is placed on the activation and technical utilization of phosphatases naturally present in rye bran.

5.1 Distribution of Inositol-Phosphorus, Intrinsic Phytase Activity, and Total Phosphorus Across the Rye Grain

The following results refer to a grain cross-section between 0% at the outermost layers and 100% in the grain center. Grain cross section is defined equally from all sides of the grain towards the center so that whole grains are represented by 100% grain cross section. For debranning, a stepwise removal of the outer layers was performed at the Institute of Environmental Technology and Energy Economics (Natalie Mayer, Hamburg University of Technology) according to a simplified pearling process via friction and abrasion [117]. The distribution in Figure 5.1 shows low amounts of P in the outermost layers up to 5% grain cross section, this increases to a peak in the cell layers up to 12%. The inositol-P maximum is at 6% and the total P maximum is at 9%. It can be seen that, across all cross sections, the predominant form of P is inositol phosphate. For the outer layers, up to 30% of the cross section, approximately 80% of the total P is organically bound to inositol phosphates [117].

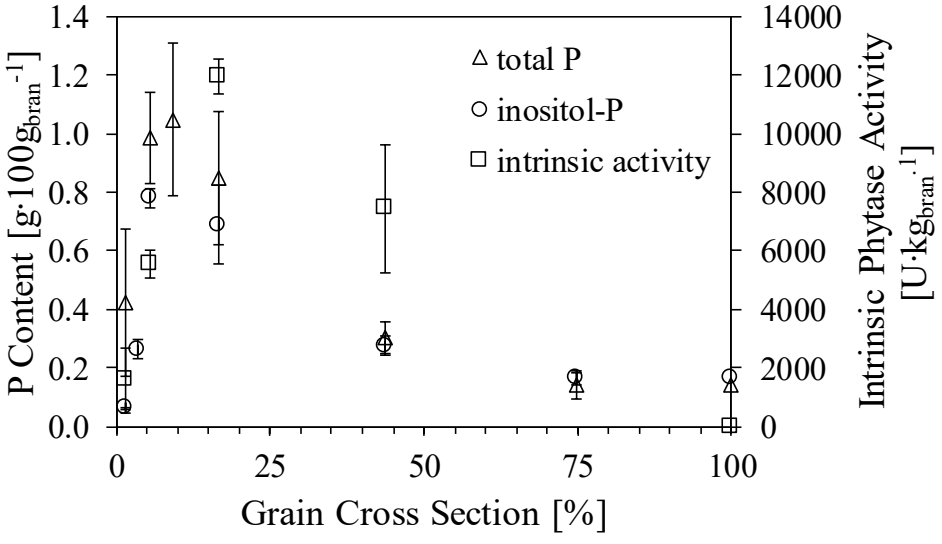

Figure 5.1: Distribution of total P, inositol-P and intrinsic inositol phosphate hydrolyzing enzyme activity over the rye grain cross section [117].

Parts of this chapter are published in: Mayer, N.; Widderich, N.; Scherzinger, M.; Bubenheim, P.; Kaltschmitt, M. Comparison of Phosphorus and Phytase Activity Distribution in Wheat, Rye, Barley and Oats and Their Impact on a Potential Phytate Separation. *Food Bioprocess Technology* **2023** [117].

Intrinsic phytase activity is also highest in the outer layers of the grain, with local maxima corresponding to regions similarly exhibiting elevated P-content. The maximum phytase activity detected is 12,000 $U \cdot kg^{-1}$ at 17% cross section, presumably representing the aleuron cell layer (Chapter 1.3). As expected, the bran fraction, made from the outer layers of the grain, contains the highest P, inositol-P as well as intrinsic phytase activity (Chapter 1.3). In addition, a further activity peak at 45% cross section is detected. In fact, according to the literature, endosperm contains up to one third of the total phytase amount [118].

5.2 Nutrient Properties of Rye bran

In this study, two different preparations of rye bran were investigated. Variations in their composition, particularly in nutrient content, could occur due to different growth conditions of the rye (Chapter 1.3). To ensure comparability, a comprehensive analysis of the composition of both preparations was performed, Table 5.1. In subsequent chapters, reference is given regarding the preparation of bran utilized in the experiments, and accordingly to which the results refer.

Table 5.1: Compositional analysis of the two preparations of rye bran investigated in this work.

	Unit	Preparation I	Preparation II
Dry matter (DM)	%	91.2	90.2
Crude ash	$g \cdot kg_{DM}^{-1}$	60.8	63.6
Crude protein	$g \cdot kg_{DM}^{-1}$	172.2	168.0
Crude lipids	$g \cdot kg_{DM}^{-1}$	34.7	35.4
Crude fiber	$g \cdot kg_{DM}^{-1}$	66.7	66.9
Starch	$g \cdot kg_{DM}^{-1}$	136.0	158.2
Total phosphorus	$g \cdot kg_{DM}^{-1}$	10.1	13.7
Inositol phosphorus	$g \cdot kg_{DM}^{-1}$	7.9	9.7
Intrinsic enzyme activity	$U \cdot kg_{DM}^{-1}$	≈ 5000	≈ 6100

With respect to Table 5.1, minimal variations between the two preparations were found in crude ash, protein, lipid, and fiber, aligning with literature on the nutritional composition [32], indicating consistency between the two preparations. However, a difference of about 15% in starch content was observed, suggesting variability in the carbohydrate fraction and most likely due to the higher residual flour content found in Preparation II, showing a variation in the processing. Notably, pronounced differences in total P, inositol-P and intrinsic phytate hydrolyzing enzyme activity levels were identified, highlighting potential influences from sourcing [119]. Preparation II showed an approximately 30% higher total P-content, a 20% higher inositol-P content, as well as 20% higher intrinsic enzyme activity. The latter can be attributed to the elevated presence of substrate (inositol phosphate) within the cellular matrix.

On the other hand, the congruence in the magnitude of increase for both parameters aligns logically with biological principles. In addition, these biological variations can also be attributed to different growing seasons and regions. A comparison of the two harvest years 1983 and 1984 by Fretzdorff and Weipert shows a difference in inositol phosphate content of 0.15 $g \cdot kg_{bran}^{-1}$ [37]. When comparing different rye varieties from different locations, the difference in chemical composition is even greater [29]. However, the ratio of inositol-P to total P for both preparations is in line with the literature value of 70% to 80% [120]. Therefore, the measured values are within the expected range despite the differences observed.
Table 5.2 shows the distribution of differently phosphorylated inositols in both preparations. The distribution refers to $InsP_3$ to $InsP_6$, as only these can be detected by HPLC analysis (Chapter 4.1.2)

Table 5.2: Distribution of different phosphorylated inositols.

	Preparation I	Preparation II
$InsP_3$	0.6%	0.1%
$InsP_4$	1.2%	1.0%
$InsP_5$	6.7%	3.2%
$InsP_6$	91.6%	95.7%

As can be seen from Table 5.2, both preparations show a high degree of agreement in the distribution of the differently phosphorylated inositol phosphates. However, Preparation II has a slightly higher proportion of $InsP_6$ but a correspondingly lower proportion of $InsP_5$. Nevertheless, with more than 90%, $InsP_6$ is the predominant inositol phosphate in both preparations. This aligns with expectations, given that $InsP_6$ contains P in the most condensed form, making it the most biologically suitable P storage form (Chapter 1.4).

5.3 Storage Capacity of Rye Bran

Rye bran is a biological product. Therefore, changes in composition or native enzyme activity due to storage are possible. Storage stability is essential for reproducible and comparable results. However, changes in composition can be caused by native enzyme activity, microbial or fungal infestation, or inherence, and are attributed to fat, oil and especially moisture content. Hence, storage stability was investigated for Preparation I in terms of intrinsic phytate-degrading enzyme activity, total P-content, and inositol-P content over a period of 20 weeks. Rye bran was stored in tightly closed glass bottles at room temperature, 4 °C, and -20 °C. The specific intrinsic enzyme activities at different storage conditions are shown in Figure 5.2.

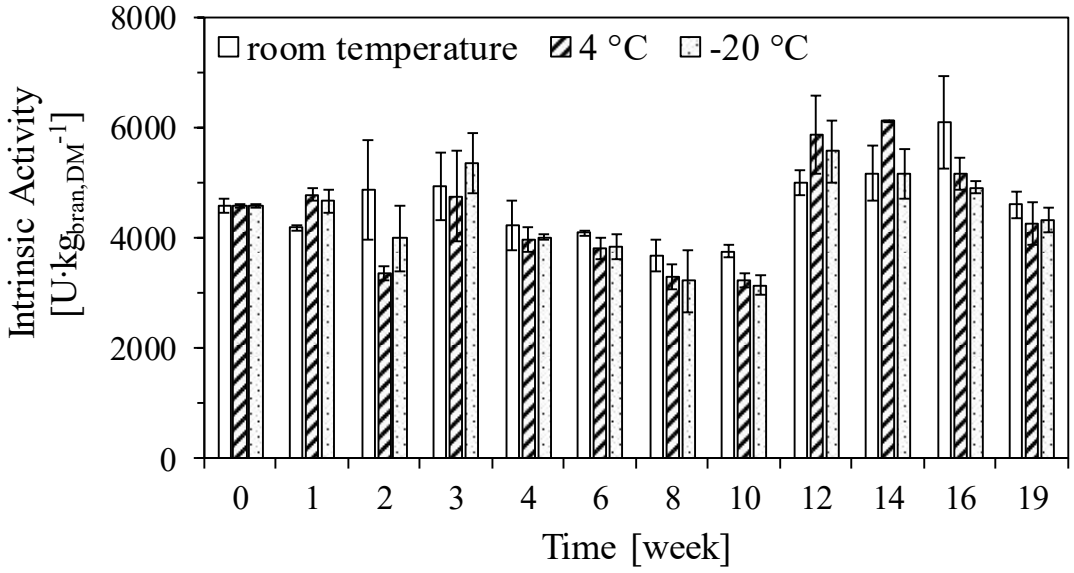

Figure 5.2: Intrinsic inositol phosphate hydrolyzing enzyme activity over a period of 20 weeks. Rye bran (Preparation I) stored in glass bottles at room temperature, 4 °C, and -20°C. Reaction conditions: 37 °C, pH 5.5, 0.1 to 0.2 g bran per 50 mL reaction solution. Reaction solution: 1.5 mM phytic acid, 0.25 M NaOAc.

From Figure 5.2 it can be seen that the specific intrinsic enzyme activity does not decrease over the time period considered. The mean activities over the entire time frame at room temperature is 4730 U·kg$_{bran}^{-1}$, 4431 U·kg$_{bran}^{-1}$ at 4 °C, and 4398 U·kg$_{bran}^{-1}$ at -20 °C. The variations in activity at different storage temperatures are within the analytic error of ± 384 U·kg$_{bran}^{-1}$ (Chapter 4.1.3). Thus, no effect of storage temperature is observed. With a literature value of 5000 to 7500 U·kg$_{bran}^{-1}$ [88,119,120], the values are at the lower level of the expected range, which can be assigned to different processing and growth conditions (Chapter 1.3).

A comparably low activity was detected in the 4th to 10th week. However, this was detected for all storage conditions and can be attributed to the analytical procedure, as the same color reagent was always prepared anew, resulting in batch-to-batch variations. In addition, a noticeable trend of decreasing activity with lower storage temperature is observed. Since for the respective test series no decline in activity over 20 weeks is observed, this trend cannot be explained by a negative impact of the storage temperature on the enzyme activity and is supported by the wide range of typical storage temperatures from 4 °C to 32°C. Depending on the moisture content of the grains, cereals can be stored at these temperatures for several years [121]. Additionally, all three samples are from the same batch and were subsequently stored at different temperatures. The naturally occurring biological fluctuations in activity cannot explain this trend either, since the biological fluctuations are randomly distributed and there is no correlation with time. One possible explanation for the observed trend is the different temperatures of the bran samples at the beginning of the experiment. Experiments were carried out in preheated reaction solution at 37 °C (Chapter A.2.13). Bran samples, stored differently, might not have been at the same temperature during the experiment. Samples stored at -20 °C were colder than those at room temperature. Consequently, individual intrinsic temperatures might have slightly affected the native enzyme activity.

Figure 5.3 shows the total P-content at the different storage temperatures over 20 weeks. The total P-content is expected to remain constant over the entire storage period, as an increase or decrease indicates impurities in the bran sample.

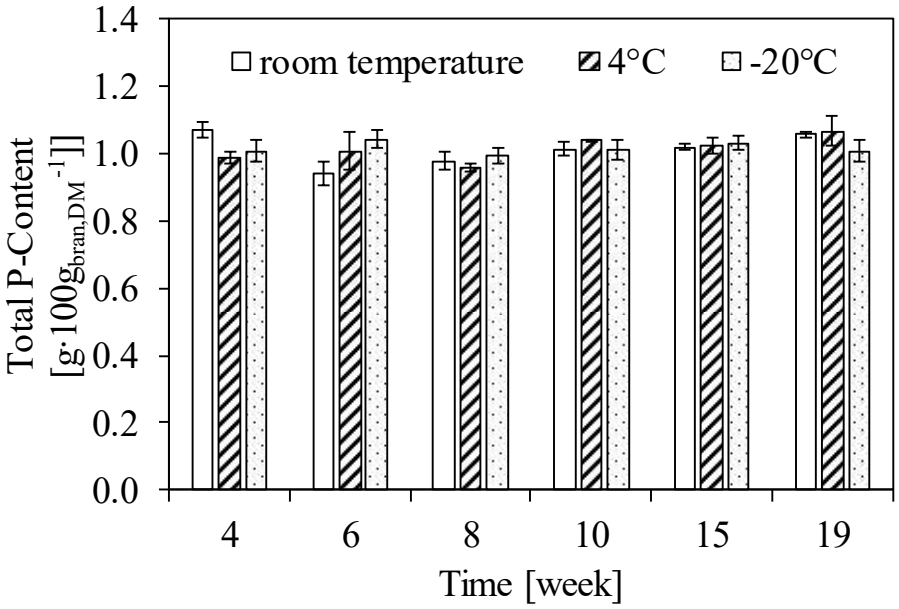

Figure 5.3: Total P-content over a period of 20 weeks. Rye bran (Preparation I) stored in glass bottles at room temperature, 4 °C, and -20°C. Incineration of 1 g bran and 0.5 g zinc oxide. Determination of P-content using molybdenum blue color reaction.

No change in total P-content is observed over the 20-week period. The results fluctuate around a mean value of 1.01 ± 0.02 g·100g$^{-1}_{DM}$. Viveros *et al.* determined a similar total P-content of 0.96 ± 0.01 g·100g$^{-1}_{DM}$ [120].

The inositol-P content in rye bran stored over the time period under consideration at room temperature, 4 °C, and -20 °C was determined, Figure 5.4.

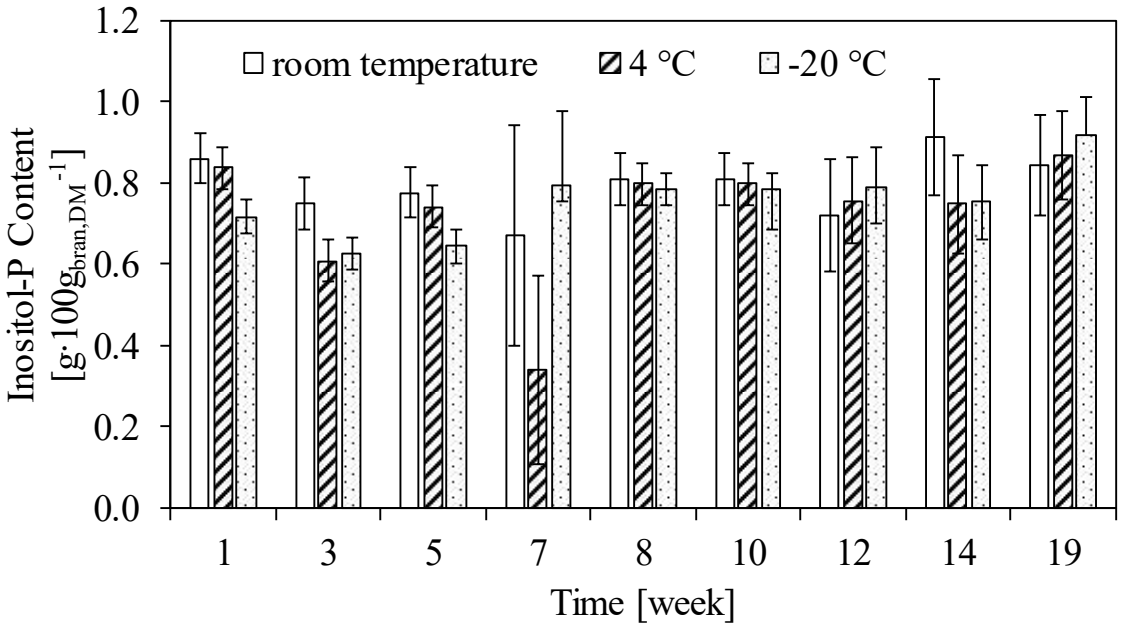

Figure 5.4: Inositol phosphorus content over a period of 20 weeks. Rye bran (Preparation I) stored in glass bottles at room temperature, 4 °C, and -20°C. Extracted from 5 g bran with 0.5 M HCl and ultrasonic treatment and subsequent incubation for 1 h. recovery of inositol phosphates using HyperSep SAX (Thermo Fischer). Obtained fraction distilled at 40 °C and 25 mbar for 40 min. Quantification by HPLC.

For storage at room temperature, 4 °C, and -20 °C the mean inositol-P content is 0.79 g·100g$_{bran}^{-1}$, 0.70 g·100g$_{bran}^{-1}$, and 0.74 g·100g$_{bran}^{-1}$, respectively. According to previous studies, these values are within the expected range of 0.7 g·100g$_{bran}^{-1}$ to 0.8 g·100g$_{bran}^{-1}$ [37,120]. The unexpected difference of 0.1 g·100g$^{-1}_{bran}$ among different storage temperatures is related to the seventh-week measurement, Figure 5.4. Here, clear variations in inositol-P content are observed at all three storage temperatures, notably a value of 0.34 g·100g$_{bran}^{-1}$ at 4 °C, drastically deviating from the expected value. The mean inositol-P contents, excluding this measurement, are 0.80 g·100g$_{bran}^{-1}$, 0.77 g·100g$_{bran}^{-1}$, and 0.75 g·100g$_{bran}^{-1}$ for storage at room temperature, 4 °C, and -20 °C, respectively. These values vary by 0.025 g·100g$_{bran}^{-1}$ around the common mean, corresponding to a percentage variation of 3.2%. The values are therefore within a 95% confidence level, and the seventh-week measurement is considered to be an outlier.

Table 5.3 summarizes the results of the investigation on the storage capacity at different temperatures. In addition to the intrinsic inositol phosphate hydrolyzing enzyme activity, total P content, and inositol-P content, the water content is given.

Table 5.3: Summarized results of the storage stability study.

	Unit	Room temperature	4 °C	-20 °C	Mean
Activity [$U \cdot kg^{-1}_{bran}$]	$U \cdot kg^{-1}_{bran}$	5047	4858	4821	4909
Total P-content	$g \cdot 100^{-1} g_{DM}$	1.1	1.1	1.1	1.1
Inositol-P content	$g \cdot 100^{-1} g_{DM}$	0.79	0.70	0.74	0.74
Inositol P / Total P	%	81	78	76	78
Moisture content	% (w/w)	10.6	10.7	10.8	10.7

Compared to room temperature the inositol-P content for the storage at 4 °C (0.70 $g \cdot 100 g_{DM}^{-1}$) and at -20 °C (0.74 $g \cdot 100 g_{DM}^{-1}$) are 11% and 6% lower, respectively, compared to storage at room temperature. The bran temperature does not influence the inositol-P content due to the prolonged incubation time during extraction. However, the observed differences may be related to the condensation formation during low-temperature storage, potentially activating intrinsic bran enzymes leading to inositol phosphate degradation. Stored cereal grains, including bran, undergo a maintenance metabolism with minimal metabolic rate, releasing moisture. At a moisture content of 22% and 20 °C, this maintenance metabolism results in a mass loss of 1% within 15 days [121].Therefore, the lower inositol-P content might be attributed to degradation by intrinsic phosphatases. Since the variations are within the error of the method determined in Chapter 4.1.3 and the moisture content is very similar for all temperatures investigated, Table 5.3, a definitive statement is not possible. The moisture content has increased slightly under all storage conditions (Chapter 5.2).

Despite of variations in the storage temperature, no clear decline in enzymatic activity is observed over a period of 20 weeks, indicating that rye bran retains its enzymatic inositol phosphate hydrolyzing properties. Furthermore, no clear decrease in total P and inositol-P content is observed as a function of storage temperature and time, resulting in reproducible and comparable results even after long term storage. This also eliminates the possibility of serious fungal contamination and consequent falsification of measurements and was to be expected due to the low water content and the mandatory pre-cleaning of cereal grains before storage in Germany [121].

In conclusion, the results show that rye bran is storage stable at room temperature, 4 °C, and -20 °C. The highest inositol-P content and inositol-P to total P ratio is found for storage at room temperature, suggesting room temperature storage.

5.4 Potential of Intrinsic Enzymes

As shown in Chapter 5.1, rye bran contains a high amount of inositol phosphate in relation to the whole grain. Similarly, the activity of inositol phosphate hydrolyzing enzymes in the bran is at its highest. Inositol phosphate, recognized as a crucial P reservoir in plants, plays a vital role during germination (Chapter 1.5.3). Thus, it is investigated whether the metabolic initiation of the germination process, can be used to dephosphorylate the contained inositol phosphate. For this, the potential of intrinsic inositol phosphate hydrolyzing enzymes is investigated for Preparation I. The aim is to identify the maximum process parameters for hydrolysis and to evaluate whether the intrinsic enzymes can reduce the use of exogenous phytases in the feed conditioning process; i.e. to find an optimum for endogenous and exogenous phytases. With regard to an industrial application for animal feed production, the degradation was studied as a function of temperature, pH, time and water content in the system. Statistical Design of Experiments (DoE) was used to minimize the experimental effort. Appropriate experimental designs were generated using Design Expert® 12 (StatEase) software. Since the temperature could not be changed arbitrarily during the experimental procedure (hard-to-change factor), a split-plot design was chosen (Chapter 3.2). Due to the high prediction quality within the factor space, the split plot was generated using I-optimization [72].
The phytase contained in grains operate over a wide pH range of 3 to 10. They exhibit a maximum activity at pH 5 to 6 [25]. In addition, Greiner *et al.* reported a maximum activity at pH 6 for phytase isolated from rye. No activity was detected outside the pH range of 3 to 8 and the stability range is between pH 4 and 7.5 [122]. Based on these literature values, a pH range of 2 to 8 was investigated. In a study of activity at temperatures ranging from 10-80°C, Greiner *et al.* observed a maximum activity at 45°C for the isolated phytase. Furthermore, during incubation of the enzyme at temperatures of 40°C, 50°C, and 60°C for 90 minutes each, residual activities of 100%, 85%, and 20% were detected, respectively [122]. Hence, temperatures from 15°C to 60°C were studied in this series of experiments. A lower limit of 30%(v/w) was set for the water content, as enzymes contained in bran are activated at this moisture level [123]. An upper limit of 1000%(v/w) is defined. The percentages refer to the quantity of water in relation to the quantity of bran used. Hence, 1000% corresponds to 10 times the amount of water in relation to the mass of bran.

5.4.1 Intrinsic Enzyme Activity as Function of Temperature and pH

A mathematical model is used to find a maximum of the target variable (activity) as a function of the factors in the in the experimental space. In this case, a quadratic model was used, incorporating the two input variables temperature and pH, Equation 6.1.

$$\text{activity} = k_0 + k_1 T + k_2 pH + k_{1,1} T^2 + k_{1,2} T \cdot pH + k_{2,2} pH^2 \qquad \text{(Eq. 6.1)}$$

To provide a suitable description of the data by the model, the measurement data were transformed. The Box-Cox plot exhibits a minimum at λ values ranging from 0.1 to 0.5, Figure B.2. By employing a square root transformation (λ = 0.5), the descriptive model was optimized. In Figure 5.5 (left), the residuals in the probability graph are plotted against the quartiles of a Gaussian normal distribution, showing that the data points are normally distributed. Similarly, in Figure 5.5 (right), the predicted values are given as a function of test results; there are no outliers. Therefore, the model is suitable for the prediction of the activity as a function of pH and temperature.

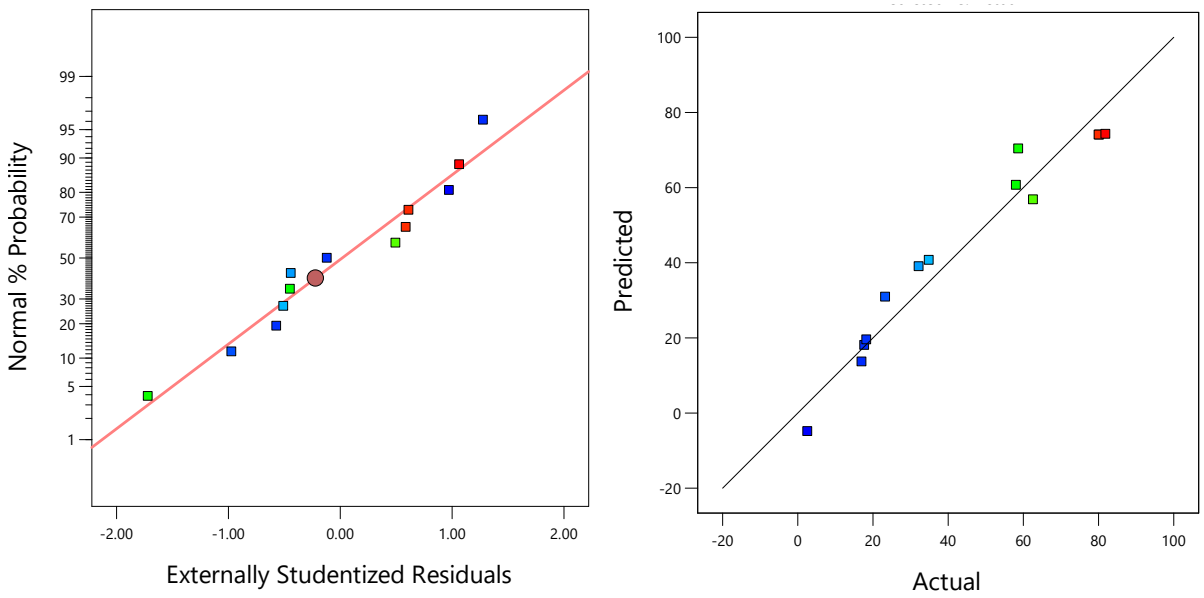

Figure 5.5: *Left:* Normal plot of residues, *right:* Predicted vs. actual. The color of the data points correlates with the response (intrinsic activity). Blue indicates a low response and red a high response.

A block formation of experiments one and two as well as six and seven is observed, Figure B.3. Experiments one and two are center points, conducted at 42.5 °C and pH 5.0, and show minimal differences, indicating low biological fluctuations. Experiments six and seven, carried out at different temperatures but sharing low pH values (2.0 and 3.6), exhibit a block pattern. This block formation is likely due to the enzyme activity of phytase decreasing drastically below a pH of 3.0, as indicated by Greiner *et al.* [122]. No other block formations are observed, suggesting no influence from external disturbance variables. However, experiment nine is an outlier, as the Cook distance is greater than one, Figure B.4. Hence, this experiment might falsify the prediction [67]. Nevertheless, experiment nine is within the tolerance limit, Figure B.5, and has to be taken into account, as it is a corner point of the factor space. The experiment was carried out at 60 °C and pH 2.0, resulting in an activity of 282 $U \cdot kg^{-1}_{bran}$. Due to low pH and the stability range of native phytases, a low activity is anticipated. Thus, no negative impact on the predictive quality of the mathematical model within the factor space is expected and the experiment was used to build the model.

It is noticeable that the identified outlier as well as the experiments, where block formation is observed, were performed at a low pH. In order to analyze the effect of a low pH, the experiments are compared with those below pH 4.0, Table 5.4.

Table 5.4: Comparison of experiments carried out at a pH below 4.0.

Experiment	pH [-]	Temperature [°C]	Activity [U·kg$^{-1}_{bran}$]
6	2.0	43.2	327
7	3.6	25	1211
9	2.0	60	282
12	2.0	25	0

Table 5.4 shows a strong dependence of the activity on the pH. No activity is detected at pH 2.0, taking into account the error of ± 384 U·kg$_{bran}^{-1}$ determined in Chapter 4.1.3. At pH 3.6 and 25 °C, an activity of 1211 U·kg$_{bran}^{-1}$ is determined. The comparison with experiment 13 clearly shows the strong influence of the pH. Experiment 13 was carried out at 25 °C and pH 6.4, Table B.1, resulting in 3914 U·kg$_{bran}^{-1}$. A comparison of experiment nine with experiment 10 also shows that the effect of the pH is greater than that of the temperature. In experiment 10 (60 °C, pH 5.0) the activity is 3365 U·kg$_{bran}^{-1}$. A similar result as in the experiments at pH 2.0 was also observed at pH 8.0. This confirms the pH range of 3 to 8 given by Greiner *et al* [122]. The influence of pH and temperature for the entire factor space can be seen in the response surface graph, Figure 5.6. In a pH range of 5 to 6, an activity of about 3000 U·kg$_{bran}^{-1}$ is predicted even at a low temperature of 25 °C or a high temperature of 60 °C. On the other hand, at a temperature between 39 to 46 °C, only an activity of around 1000 U·kg$_{bran}^{-1}$ is predicted at pH 2 and 8, respectively.

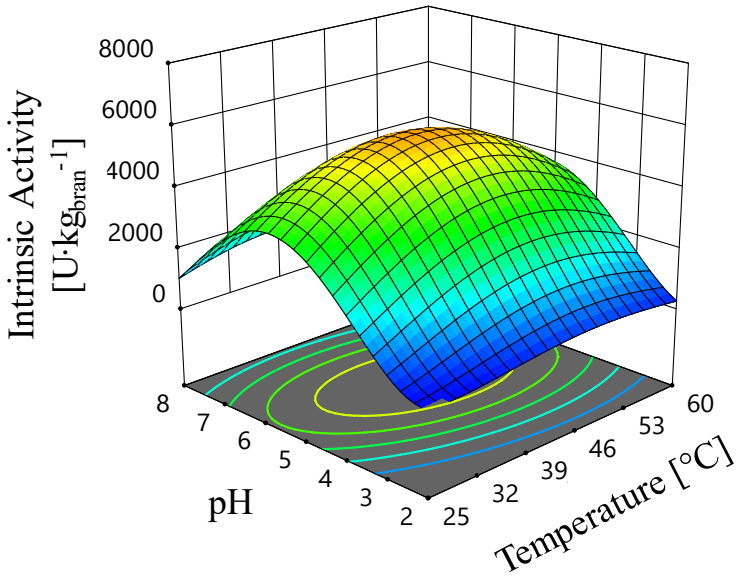

Figure 5.6: Response surface plot of intrinsic inositol phosphate hydrolyzing enzyme activity as function of temperature and pH. The maximum intrinsic activity is at pH 5.3 and 42.8 °C.

In the response surface plot the maximum activity is within the specified factor space. Given that the I-optimization focuses on prediction quality within the factor space, conclusions can be drawn about maximum activity as a function of pH and temperature. A maximum of 5565 $U \cdot kg^{-1}_{bran}$ is predicted at pH 5.33 and 42.8 °C, aligning with literature (pH 5 to 5.5 and 45 °C, [122]). The small difference in temperature is explained by the limitation of the prediction accuracy of temperature as a hard-to-change factor. Nevertheless, the results generated are valid and plausible.

5.4.2 Maximizing the Inositol Phosphate Degradation

Taking into account a maximum activity of 5565 $U \cdot kg_{bran}^{-1}$ (42.8 °C, pH 5.3), the time for complete degradation of inositol phosphate is 43 min. At the minimum activity of 1000 $U \cdot kg_{bran}^{-1}$ (25 °C, pH 8.0), the theoretical duration is 4 h. However, inhibitory effects such as inhibition by orthophosphate are not considered. Similarly, deactivation of enzymes by extreme pH and temperature as well as lower reaction rates during degradation of lower phosphorylated inositols are not considered [122]. Therefore, according to Egli *et al.*, the process duration was set to 6 h, as complete degradation of inositol phosphates in wheat was observed after 6 h [124].

A quadratic regression was chosen for the model description. Due to the insignificance of individual terms, the model was reduced to a more appropriate representation of the measured data. Equation 6.2 shows the resulting model equation with the input factors temperature (A), pH (B), water content of the system (C) and time (D).

$$\text{degradation} = k_0 + k_1A + k_2B + k_3C + k_4D + k_{1,1}A^2 + k_{1,4}AD + k_{2,3}BC + k_{2,4}BD + k_{2,2}B^2 + k_{3,3}C^2 + k_{4,4}D^2 \quad \text{(Eq. 6.2)}$$

Figure 5.7 shows the inositol-P degradation as a function of temperature and pH. It can be seen that the inositol-P degradation has a maximum within the factor space. Thus, the factor frames are reasonable. For a more appropriate description of the data, the measured data were transformed by a square root function. No critical outliers could be identified (Figure B.7 to Figure B.10). Thus, no falsification of the model due to inconsistent measurement results is to be expected. For the validation, inositol phosphate degradation at 42.5 °C and pH 5 was examined. At this point, the model predicted an inositol phosphate degradation of 0.56 ± 0.03 $g_P \cdot 100g_{bran}^{-1}$. The result of the measurement and the predicted values of the model are shown in Table 5.5.

Table 5.5: Validation of the mathematical model. Conditions defined by the Software Design Expert®.

	Inositol-P degradation [$g_P \cdot 100g^{-1}_{bran}$]
Measurement	0.59 ± 0,02
Lower limit	0.53
Predicted value	0.56
Upper limit	0.59

The degradation in the experiment at 42.5 °C and pH 5 was 0.59 ± 0.02 $g_P \cdot 100g_{bran}^{-1}$ (79 %). Thus, the measured value is within the expected range of 0.53 to 0.59 $g_P \cdot 100g_{bran}^{-1}$. Thus, the model proofed to be valid and is used to predict the maximum inositol phosphate degradation. Maximum degradation is determined at 33 °C, pH 5.5, and a water content of 709%(v/w) corresponding to a bran to water ratio of around 1 to 7. At these experimental parameters, a degradation of 1 $g_P \cdot 100g_{bran}^{-1}$ is predicted after 360 min. This value is higher than the inositol-P content at the beginning of the reaction (Preparation I, 0.79 $g \cdot 100g_{bran}^{-1}$) and therefore cannot be achieved. The reason for this is the nature of the mathematical model to describe real data. Real conditions, such as substrate limitation or the maximum achievable conversion, are not taken into account. Furthermore, inhibition, deactivation, and lower reaction rates for the conversion of $InsP_5$ to $InsP_1$ [122,125] are also not considered by the model. Due to the stability range of phytase in rye and a stabilizing effect of the bran matrix [25], the deactivation of the enzyme might have only a minor influence on the incomplete inositol phosphate degradation at 33 °C and pH 5.5. The main influence is expected to be the product inhibition combined with a lower reaction rate for the conversion of lower phosphorylated inositols. Many inositol phosphate hydrolyzing enzymes are inhibited by phytic acid and orthophosphate in addition to metal ions [46]. As inositol phosphate degradation progresses, the concentration of orthophosphate in the reaction medium increases over time, leading to product inhibition, resulting in reduced reaction rates or even termination of the hydrolysis reaction.

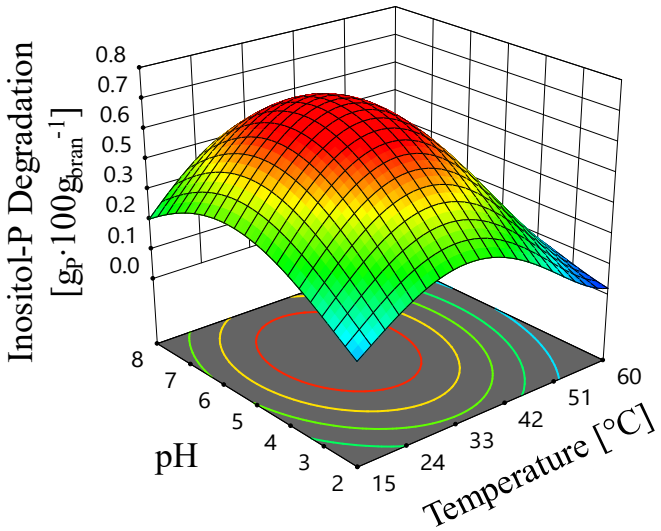

Figure 5.7: Maximum inositol-P degradation as a function of temperature and pH. The maximum degradation occurs at 33 °C, pH 5.5, and a bran to water ratio of 1 to 7.

5.4.3 Comparison of Intrinsic Enzyme Activity and Inositol Phosphate Degradation

The results of the investigation on intrinsic enzyme activity and the inositol phosphate degradation at different process parameters are summarized in Table 5.6:.

Table 5.6: Summarized results of the statistical experimental design.

	max. activity	max. degradation	Validation point (max. degradation)
Temperature [°C]	42.8	33.0	42.5
pH	5.33	5.50	5.00
Water content [% (v/w)]	-	709	515
Time [min]	-	360	195
Activity [$U \cdot kg_{bran}^{-1}$]	5565	-	716[a]

[a]Activity calculated from inositol phosphate degradation at validation point (43.3 °C, pH 5.0, 515%(v/w), and 195 min

A maximum activity of 5565 $U \cdot kg_{bran}^{-1}$ at 42.8 °C and pH 5.33 is predicted. This result is in agreement with the results of the activity determination in Chapter 6.3, where an average activity of 4909 $U \cdot kg_{bran}^{-1}$ at 37.0 °C and pH 5.5 is determined. However, the low activity of 716 $U \cdot kg_{bran}^{-1}$ at the validation point of maximum inositol phosphate degradation is conspicuous. From Table 5.6 it can be seen that temperature (± 0.3 °C) and pH (± 0.33) are approximately the same for the maximum activity and the activity of the validation point, and can therefore be excluded. Possible causes are product inhibition and a limited availability of the substrate. Notably, for the determination of maximum activity, the substrate was present in excess (Chapter A.2.13). In the inositol phosphate degradation experiments, only the inositol phosphates contained in the bran were available as substrate, resulting in lower substrate concentration and availability, leading to a decrease in activity. Furthermore, it is possible that a substantial portion of conversion occurs early in the reaction process. In such instance, the indicated activity of 716 $U \cdot kg_{bran}^{-1}$ represents an apparent activity averaged over the entire reaction duration and is, therefore, artificially reduced by the longer reaction time considered. To validate this, the degradation at the validation point is compared with the predicted degradation after 30 min under the boundary conditions of maximum activity, Table 5.7.

Table 5.7: Comparison of the predicted degradation. Boundary conditions 1) 42.5 °C, pH 5.0, 515%(v/w) water content, 30 min 2) 52.8 °C, pH 5.33, 709%(v/w) water content, 60 min. The degradation of the validation point (195 min) was determined experimentally

Experiment	degradation [$g_P \cdot 100g_{bran}^{-1}$]
Validation point (30 min)	0.70
Maximum activity (60min)	0.70
Validation point (195 min)	0.59

It can be seen that a degradation of 0.7 $g_P \cdot 100g_{bran}^{-1}$ is predicted for the boundary conditions of maximum activity as well as for the validation point after 30 min. Thus, the same conversions are predicted for a reaction duration of 60 min and 30 min. In the context of limited ability to reproduce a real data using a mathematical model, the predictions correspond to the experimentally determined degradation of 0.56 $g_P \cdot 100g_{bran}^{-1}$, resulting in around 80% inositol-P degradation. However, the data suggests that much of the inositol phosphate degradation is completed within the first half hour of reaction. Based on this, the calculated enzymatic activity during inositol phosphate degradation is determined to be 4653 $U \cdot kg^{-1}_{bran}$. Hence, the value aligns with the results obtained from the activity test, confirming the internal consistency and reliability of the results.

The predicted temperature of maximum enzyme activity is 42.8 °C, which is within the expected range (Chapter 6.4). However, the temperature of 33 °C predicted for inositol phosphorus degradation is lower than the literature value of 45 °C [122]. This difference can also be attributed to the reaction time. The activity determination was carried out over a period of 60 min. For inositol-P degradation, the reaction time was 6 h. Taking into account the expected completion of the reaction within the first 30 min, the predicted maximum temperature for inositol-P degradation is 40 °C, Figure B.12. This temperature is within the expected range. In conclusion, the efficiency of native phytase for the degradation of phytic acid in rye bran is demonstrated. Through activation of these enzymes under maximum enzyme activity conditions presented, a substantial reduction in inositol phosphate content is achieved, reducing the need for exogenous phytase for a feed material conditioning prior to feeding. Furthermore, it is apparent that in other biological matrices with similar intrinsic phytase activity, Table 1.1, a similarly high degradation is achieved. However, due to the presence of different types of phytase, Figure 1.4, the maximum process parameters for their activation may differ.

5.4.4 Inositol Phosphate Degradation by Intrinsic Enzymes monitored by ATR-FT-MIR

The previous Chapter (Chapter 5.4.3) showed that the majority of phytate contained in rye bran can be degraded in a short time by the metabolic initiation of intrinsic phytates. The well-established ATR-FT-MIR analysis (Chapter 4.2) was used to a gain deeper insight into inositol-P degradation by intrinsic enzymes. For this, the residual phytate content after certain time points of wet-treatment was used to infer the specific intrinsic inositol phosphate hydrolyzing activity, Figure 5.8.

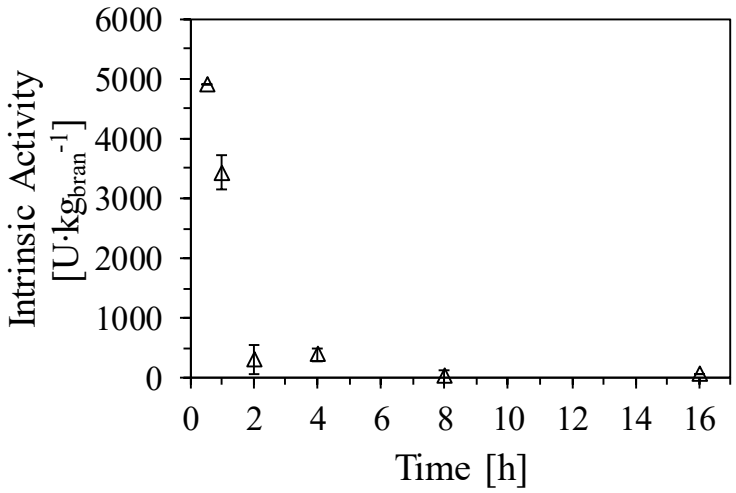

Figure 5.8: Intrinsic phytase activity as function of different wet-treatment times. Activity calculation from inline measurements of residual phytate content. Reaction performed at pH 5, room temperature, and a bran to water ratio of 1 to 5.

It can be seen from Figure 5.8 that the enzymatic activity is highest in the first 30 min of wet treatment and steadily decreases between the subsequent time points aligning with previous findings. The observed trend also aligns with expectations, as the degradation of phytate progresses over time. Consequently, the substrate concentration within the cellular matrix diminishes, leading to a decrease in enzymatic activity, a phenomenon described by the Michaelis-Menten kinetics (Chapter 3.3). The graphical representation in Figure 5.8 clearly indicates, that the degradation of phytate follows neither simple zero-order nor first-order kinetics, since the rate neither remains constant nor decreases proportionally. Therefore, either a limitation of mass transfer or a decrease in enzyme activity during wet-treatment can be concluded. Certainly, a decrease in reaction rate is observed during wet-treatment as the substrate concentration in the biological matrix decreases over time. However, as the decrease in enzyme activity does not follow a linear trend, it is very likely that the degradation is mass transfer limited. Considering 1 h of conditioning the degradation rate is 3263 U·kg$_{bran}^{-1}$. The conventionally determined intrinsic enzyme activity is 5000 U·kg$_{bran}^{-1}$ (Chapter 4.2), resulting in a deviation of 34%.

Parts of this Chapter are published in: Widderich, N.; Bubenheim, P.; Liese, A. Online monitoring of phytate content in plant residuals during wet-treatment. *Scientific Reports* **2024** [66].

This deviation might be within biological fluctuations, but may also be due to the different substrate concentrations and process conditions (pH 5 and room temperature compared to 5.5, and 37 °C). However, the conventional approach only considers the release of inorganic P from extrinsic phytate standards, whereas the chemometric analysis also takes the mass transfer of phytate into account. Thus, this rate does not correspond exactly to the intrinsic enzyme activity. However, this analysis provides more valuable information from a process engineering point of view, showing a more realistic behavior of intrinsic phytate degradation and suggest mass transfer limitation.

The ATR-FT-MIR analysis is real-time analytical method. Therefore, the residual phytate content and the corresponding enzymatic acitivity can be determined during the treatment and not only after treatment, which provides more accurate insights into phytate degradation. In this context, Figure 5.8 also shows that phytate degradation is detected up to 16 h of wet-treatment, whereas even after 16 h small amounts of residual phytate (3.8% remaining) are still detected in the biological substrate. Considering the intrinsic enzyme activity and the amount of substrate, a treatment of more than 16 h is recommended for complete degradation of the contained phytate. Reddy *et al.* showed complete phytate degradation after 5 days of wet-treatment at 25 °C [53]. However, 63% of the contained phytate is initially degraded within the first hour of wet-treatment. Furthermore, one hour of wet-treatment prior to feeding already represents a significant improvement compared to phytase supplementation to animal feed rations, where 50% of phytate still ends up in manure [25].

5.5 Interim Summary

- Total P, inositol-P, and intrinsic inositol phosphate hydrolyzing enzyme activity are primarily contained in the outer layer of the rye gran; i.e. predominantly in bran.
- Rye bran is storage stable regarding total P, inositol-P, and enzymatic activity when stored at -20 °C, 4 °C, 20 °C ensuring reproducibility of results.
- Metabolically triggering germination by wet-treatment leads to activation of intrinsic inositol phosphate hydrolyzing enzymes, resulting in phytate degradation.
- It is shown that maximum intrinsic enzyme activity occurs at 43 °C and pH 5.3 and a bran to water ratio of 1 to 7 (w/v) leads to maximum inositol phosphate degradation.
- Under maximum conditions, most of the phytate is degraded within 30 min at rate of 5565 $U \cdot kg_{bran}^{-1}$.
- One hour of wet-treatment is already more effective in reducing the phytate content in rye bran than the conventional phytase supplementation to animal feed ration.
- The reduction of exogenous phytate for feed material conditioning can be achieved by appropriate process parameters and activation of intrinsic enzymes.

6 Enzymatic Phosphorus Mobilization

In the following, the technical realization of enzymatic P-mobilization from rye bran is investigated and discussed. The principles of this phytase based method have already been described in the literature by RWTH Aachen University, in particular by Herrmann *et al.* and Infanón *et al.* [54,55]. However, this biotechnological process in which phytate in plant material is hydrolyzed by exogeneously added phytases and the liberated orthophosphate is solubilized in an aqueous phase (Chapter 1.5.4) is not yet industrially established. Therefore, this chapter addresses the technical realization. Special emphasis is placed on the biotransformation, the scale-up as well as process limitations and how to overcome them. The experiments and results described were carried out with rye bran Preparation II (Chapter 5.2)

6.1 System Characterization

The characteristics of the bran-water suspension, focusing on pH alteration upon adding rye bran to water and the rheology of the behavior of the suspension are evaluated. The technical implications are discussed with respect to a batch process.

6.1.1 pH-Shift

Upon adding biological material to an aqueous system, a pH shift may occur. When biological material, e.g. bran, is suspended in water, organic acids or bases can be released, thereby altering the pH of the suspension. Furthermore, buffering components, such as weak acids or bases and their conjugate salts, can stabilized the pH [126]. Additionally, the metabolic activity of microorganisms present in the biological material can lead to the production of acids, further influencing the pH. Enzymatic reactions themselves may also contribute to pH changes, as certain enzymatic processes involve the release or consumption of protons, affecting the overall acidity or alkalinity of the system [127]. Knowing the degree of pH change is essential for effectively managing and controlling the pH during the enzymatic conditioning processes, ensuring optimal process performance and thus productivity. The change in pH with the addition of rye bran at different bran to water ratios is shown in Figure 6.1.

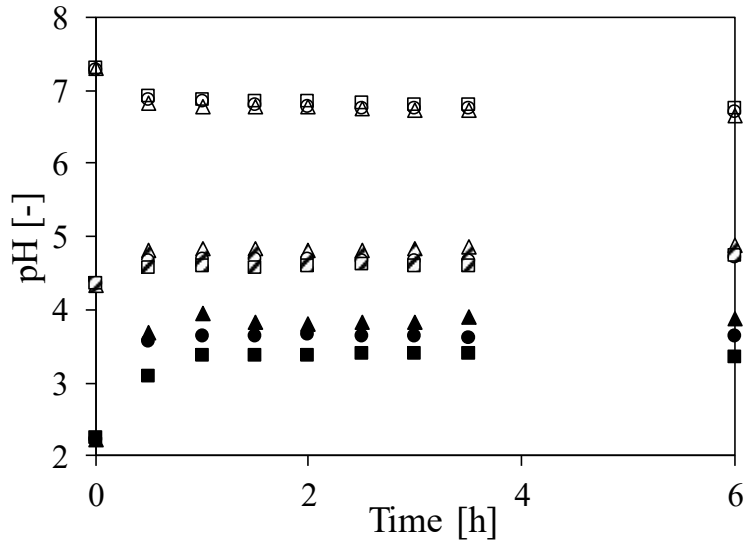

Figure 6.1: Effect on pH upon the addition of bran to water at bran to water ratios of 1 to 5, 1 to 7, 1 to 10 (w/v). The initial pH of 2, 5, and 8 was adjusted for each batch with citric acid and potassium hydroxide.

As illustrated in Figure 6.1, the addition of rye bran to an alkaline solution results in a decrease in pH, whereas the pH increases when added to an acidic solution. In any given case, a stable pH is reached within one hour, suggesting minimal influence of microbial metabolic processes on the pH. Furthermore, a pH shift is observed immediately upon the addition of rye bran, indicating a buffering effect. Notably, only at an initial pH of 2.0 the bran to water ratio clearly affects the final pH of the suspension. At a ratio of 1 to 5 (w/v), the pH shifts from 2.0 to 3.9, while at a ratio of 1 to 10 (w/v), the pH shifts to 3.4, indicating low buffer capacity of rye bran. Additionally, at an initial pH of 5.0, the pH decreases to 4.4 before stabilizing at 4.7. In conjunction with the other pH profiles, it becomes evident that the system buffers around pH 4.5. This suggests the introduction of weak acids and their conjugate bases to the system due to bran addition. However, at high or low pH values, the buffer capacity is quickly exceeded, as depicted in Figure 6.1. Given the pH maximum for intrinsic (Chapter 5.4.1) and exogenously added phytases [54] is around pH 4 to 5 and a bran to water ratio of 1 to 7 (w/v), a weak externally added buffer is sufficient to maintain pH within this range. However, buffering of liberated orthophosphate (mobilized P), originally bound to phytate, is necessary. Considering a bran to water ratio of 1 to 7 (w/v), the maximum released orthophosphate concentration is 45 mM. Therefore, a 50 mM NaOAc buffer is sufficient to buffer the system, as employed by Herrmann *et al.* [3], although works were carried out with different biological material. Alternatively, for large-scale applications, pH titration is a more economically feasible option, particularly for downstream processing (P-recovery).

6.1.2 Rheology of the Bran-Water Suspension

Inspired by the Greek word "*rhein*" meaning flow, rheology refers to the theory of material deformation and flow. It also includes the study of highly viscous fluids and solids with viscoelastic and viscoplastic properties. Newtonian fluids obey Newton's linear law of friction, while non-Newtonian fluids, like most suspensions (e.g. paint) and biological fluids (e.g. blood) deviate from this law [128]. When the objective, as in this study, is to extract a substance from plant material, effective mixing and homogenization of the material are crucial for proper mass transfer and ultimately the development of an effective process. These technical characteristics are influenced by the rheology of the bran-water suspension. Therefore, the flow behavior of the suspension is investigated, Figure 6.2.

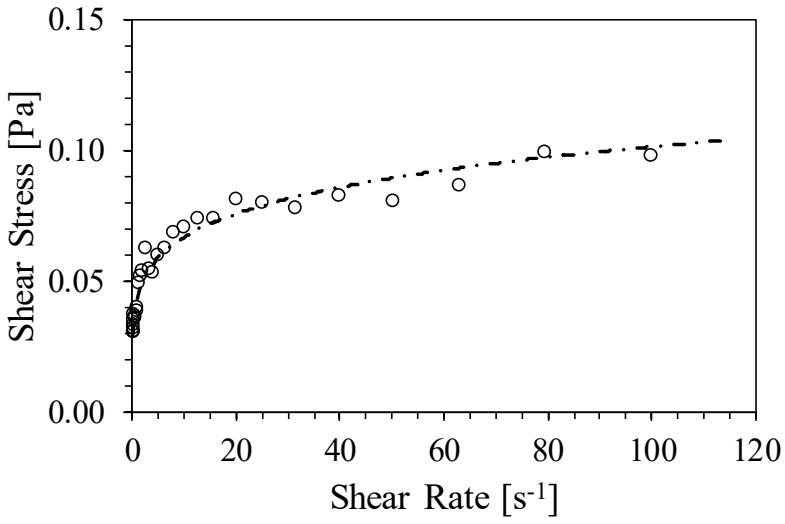

Figure 6.2: Flow behavior of the bran-water suspension at a ratio of 1 to 7 (w/v). Recorded with Kinexus pro rhemoeter (NETZSCH-Gerätebau GmbH, Selb/Bavaria, Germany). A disk was used as geometry [129]. The dashed line is a visual aid.

As shown in Figure 6.2, the bran-water suspension behaves as expected, a shear-thinning fluid. This means that as shear forces increase, the viscosity of the suspension decreases. The decrease in viscosity is caused by a structural change in the fluid, allowing individual particles to slide past each other more easily. This structural change is due to weakened cellular integrity [116]. The higher the shear forces, the greater the abrasive effect on the cell walls. From a process engineering perspective, this is a desired effect, as it not only enhances mass transfer from the bran matrix into the aqueous phase [130] but also reduces the required energy input for homogenous mixing. This ensures that the extraction process is uniform, resulting in all areas of the plant material being adequately treated. Shear-thinning fluids may exhibit reduced sedimentation resistance due to their lower viscosity under shear [131]. Therefore, homogeneous mixing is essential. Nevertheless, beyond a certain threshold, increased energy input provides little additional benefit. Furthermore, the suitability of the resulting material as animal feed has to be considered in terms of its structural properties.

In addition to shear thinning, the material also exhibits Bingham pseudoplastic flow behavior. A certain shear stress is required to initiate flow in the fluid. This phenomenon is particularly relevant in fibrous suspension, where fibers (polymers or sugar chains such as cellulose) must align themselves before the fluid can start moving. This characteristic impacts the energy input required to start and maintain fluid motion. Therefore, ribbon blender or anchor stirrer are particularly advantageous to ensure homogenous mixing. The stirrer should be operated at speeds, i.e. energy input, sufficient for the initiation of fluid flow and to provide the necessary shear rate to maintain homogeneity in the fluid.

6.2 Biotransformation

A phytase blend consisting of rPhyXT52 phytase [132] and *Debaryomyces castellii* phytase (GenBank accession number KM873028, EF121003) [133] both expressed in *P. pastoris* was used for enzymatic dephosphorylation. The blend is optimized for complete dephosphorylation [54] and was kindly provided by Dr. Anna-Joelle Ruff (Lehrstuhl für Biotechnologie, RWTH Aachen University). Both enzymes exhibit maximum activity at 37 °C and pH 4.4, with ideal performance at a bran to water ratio of 1 to 7 (w/v) [134], similar to findings for plant native enzymes (Chapter 5.4.1). Despite prior investigation [54], no kinetic investigation was conducted. Hence, the kinetics are shown in Figure 6.3.

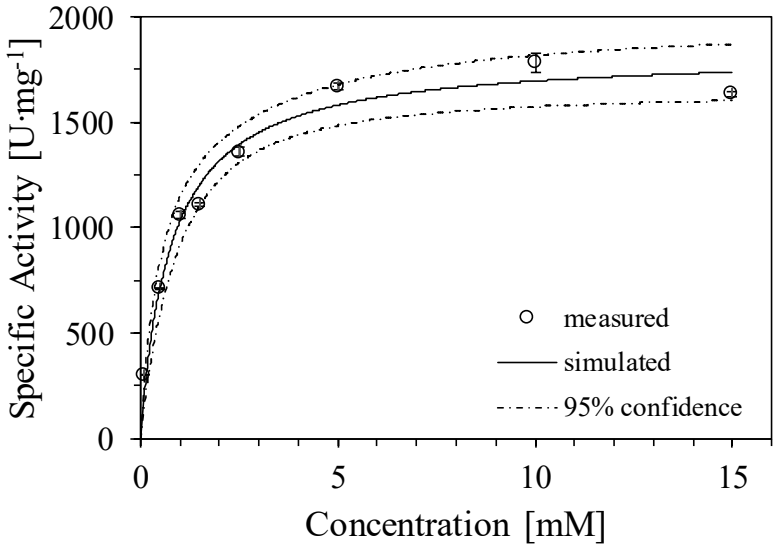

Figure 6.3: Kinetics of rPhyXT52 and *D. castelli* phytase cell-free extract blend at 37 °C in 50 mM NaOAc buffer pH 4.4 on a phytate model solution. Both enzymes are individually expressed in *P. pastoris* [135].

Parts of this chapter are published in: Widderich, N.; Stotz, J.; Lohkamp, F.; Visscher, C.; Schwaneberg, U.; Liese, A.; Bubenheim, P.; Ruff, A.J. An up-scaled biotechnological approach for phosphorus-depleted rye bran as animal feed. *Bioresources and. Bioprocessing* **2024** [135].

From Figure 6.3 no inhibition by substrate or products (orthophosphate, partially phosphorylated inositols, *myo*-inositol) in the concentration range considered (up to 15 mM) can be concluded. For *D. castelii* phytase, however, inhibition by phosphates has been demonstrated at substrate concentrations lower than 8 mM [133]. Nevertheless, there is a slight reduction in activity at a substrate concentration of 15 mM, as shown in Figure 6.3. However, this is considered to be an outlier. In addition, the concentration of inositol-phosphates that are transferred to the liquid phase is always at a low level due to the ongoing hydrolysis. Only the accumulating orthophosphate could led to a small inhibitory effect. The hydrolysis is a double substrate kinetics. However, since H_2O is present in excess and, therefore, can be neglected, the phytase blend follows simple Michaelis Menten kinetics as expected (Figure 6.3, and Chapter 3.3). Simulation to the measured data has a correlation coefficient R^2 of 0.97, with all measured data within the 95% confidence level. The concentration range investigated was chosen to cover the maximum possible concentration of inositol phosphates in the aqueous phase. Therefore, the phytase blend is suitable for batch operation at a given bran to liquid ratio of 1 to 7 (w/v). Curve fitting to the measurement data gives a Michaelis-Menten constant K_M of 0.78 ± 0.12 mM and a maximum specific reaction rate v_{max} of 1828 ± 68 U/mg. Compared to literature data for the individual enzymes (*D. castellii*, expressed in *P. pastoris*, 182 U·mg^{-1} (in 200 mM NaOAc, pH 4, 37 °C, 8 mM sodium phytate) [133] rPhyXT52 phytase *fungus garden metagenome*, expressed in *E. coli*, 3102 U·mg^{-1} (in 200 mM acetate buffer, pH 3.9, 37 °C, 1 to 5 mM phytate) [132]), the v_{max} value lies in the arithmetic mean. Whereas the K_M value (*D. castellii* [133]) is slightly elevated but can be attributed to differences in pH, salt concentration, substrate range, and the substrate itself. In this study, a mixture of differently phosphorylated inositol-phosphates was used, similar to the distribution in rye bran (Chapter 4.1.2).

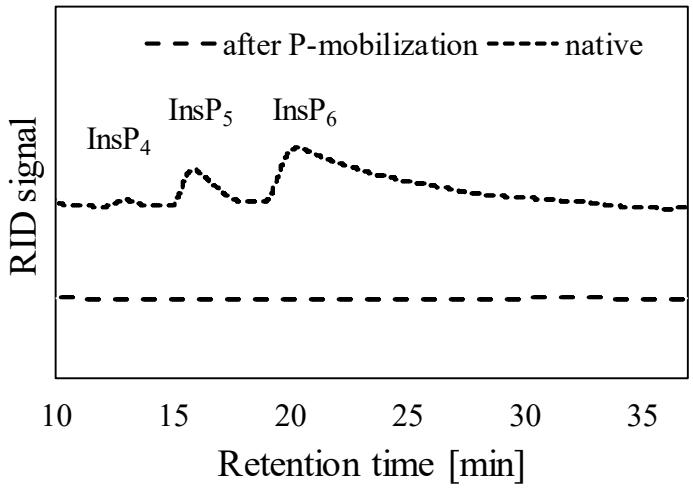

Figure 6.4: Qualitative overlay of chromatograms from HPLC analysis showing inositol phosphates present in the native rye bran and after16 h of enzymatic P-mobilization.

The efficacy of the phytase blend may differ from a phytate solution and a biological matrix due to the simplified conditions and composition compared to a complex biological matrix such as rye bran. In a phytate solution, there may be no other substances present that could affect the enzyme activity, whereas in rye bran, there are a variety of components that could potentially interact with the phytase blend and its activity, including other enzymes, ions, proteins, or fibers. The investigation on the biological substrate shows that after 16 h of phytase treatment, the phytate contained in the biological matrix is eliminated, Figure 6.4. Since the P-mobilization process reaches complete hydrolysis of $InsP_6$ to $InsP_3$, the obtained treated rye bran is a valorized feed material.

Despite the successful elimination of the contained phytate, the treatment with the exogenous applied phytase blend is only slightly more effective than the activation of intrinsic enzymes; i.e. simple wet-treatment (4% residual phytate content after 16 h, Chapter 5.4.4). Even increasing the phytase blend dosage does not lead to an increased dephosphorylation rate and thus to a shorter process time. This phenomenon is attributed to the cellular structure of grains and, consequently, the localization of phytate within the cellular network, particularly in the aleuron cells (Chapter 1.3). The phytases added exogenously to the process are present in the aqueous phase. In contrast, intrinsic phytases are already present in the aleuron cells (Chapter 5.1). Therefore, phytate has to solubilize in the aqueous phase in order to become hydrolyzed by exogenous phytases. Consistent with the findings from Chapter 5.4.4, this means that mass transfer from the bran matrix to the aqueous phase must occur prior to hydrolysis, which is the limiting factor. In this case, mass transfer is facilitated solely by the soaking process, which has an impact on the cell wall [116] and ultimately allows phytate mass transfer [130]. In Chapter 6.4 it is discussed how to overcome the mass transfer limitation and thereby reduce the process time.

6.3 Scale-Up of Enzymatic Phosphorus Mobilization

The scalability of a biocatalytic process is decisive to its technical implementation and industrial scale deployment. Various factors, such as reactor design, can influence process parameters (e.g. mixing), leading to fluctuations across different scales, and thereby affecting the process efficiency. Thus, the scalability and applicability of enzymatic P-mobilization is examined. Batch mode investigations were conducted to mobilize P from 100 g to 37.1 kg rye bran in bioreactor vessels of 2.5 L to 400 L. The reaction conditions were adapted from previous findings on the kinetic investigations (Chapter 6.2) and the activation of intrinsic enzymes (Chapter 5.4). The results were obtained in collaboration with the RWTH Aachen University (Dr. Anna-Joelle Ruff, Lehrstuhl für Biotechnologie).

Parts of this chapter are published in: Widderich, N.; Stotz, J.; Lohkamp, F.; Visscher, C.; Schwaneberg, U.; Liese, A.; Bubenheim, P.; Ruff, A.J. An up-scaled biotechnological approach for phosphorus-depleted rye bran as animal feed. *Bioresources and. Bioprocessing* **2024** [135].

Initially, temperature (26 °C, 37 °C), pH (maintained at 4.4), and the reaction medium (buffer, water, tab water) were investigated in a 2.5 L bioreactor using 200 g rye bran. For an economical process design, the conditions were set to water as reaction medium, a temperature of 26 °C (i.e. without temperature control) and pH regulation to pH 4.4. Subsequently, the process was scaled up to 100 L and 400 L reactions in which P was enzymatically mobilized from 8.5 kg and 37.1 kg rye bran respectively. A total of 42 samples were analyzed across the different scales to determine the residual P and inositol phosphate content after conditioning. These results, along with detailed reaction parameters, are summarized in Figure 6.6. Native rye bran without any treatment is given as a reference for comparative analysis. Enzymatic hydrolysis combined with soaking in an aqueous medium reduced the total P-content by an average of 89%, from 1.27 to 0.14 $g_P \cdot 100g_{bran}^{-1}$, Figure 6.6. The most efficient results were obtained under reaction conditions close to the maximum conditions of the added phytases (37 °C, pH 4.4, [54]), resulting in a P depletion of 91%, with a remaining P-content of only 0.11 $g_P \cdot 100g_{bran}^{-1}$. Increasing the temperature from 26 °C to 37 °C and using a buffered reaction medium (50 mM NaOAc) enhanced P-mobilization by 42%, leading to a decrease in total P-content to 0.12 $g_P \cdot 100g_{bran}^{-1}$ compared to 0.17 $g_P \cdot 100g_{bran}^{-1}$. However, as expected no explicit difference is observed at 26 °C or 37 °C when water without pH titration is used as the reaction medium (Chapter 6.1.1). In the 2.5 L scale, a substantial difference in total P-content is observed when comparing tap water, deionized water, and buffered reaction medium at 37 °C with a pH maintained at 4.4 (tap water: 0.27 $g_P \cdot 100g_{bran}^{-1}$, deionized water: 0.11 $g_P \cdot 100g_{bran}^{-1}$, buffered: 0.12 $g_P \cdot 100g_{bran}^{-1}$). The higher residual P-content when using tap water is attributed to local water supply. In addition, it is concluded that the variations in P-reduction (0.14 ± 0.03 $g_P \cdot 100g_{bran}^{-1}$) result from the natural occurring variations in phosphate content in the starting material (Chapter 4.1.3). Furthermore, results from the 400 L scale at 26 °C with tap water titrated to pH 4.4 are comparable in efficiency to the 100 L scale, achieving a total P-reduction of 90% (1.3 to 0.13 $g_P \cdot 100g_{bran}^{-1}$).

Figure 6.5: Images of A) 400 L bioreactor setup, B) solid-liquid separation by centrifugal forces (separator), and C) P-reduced rye bran.

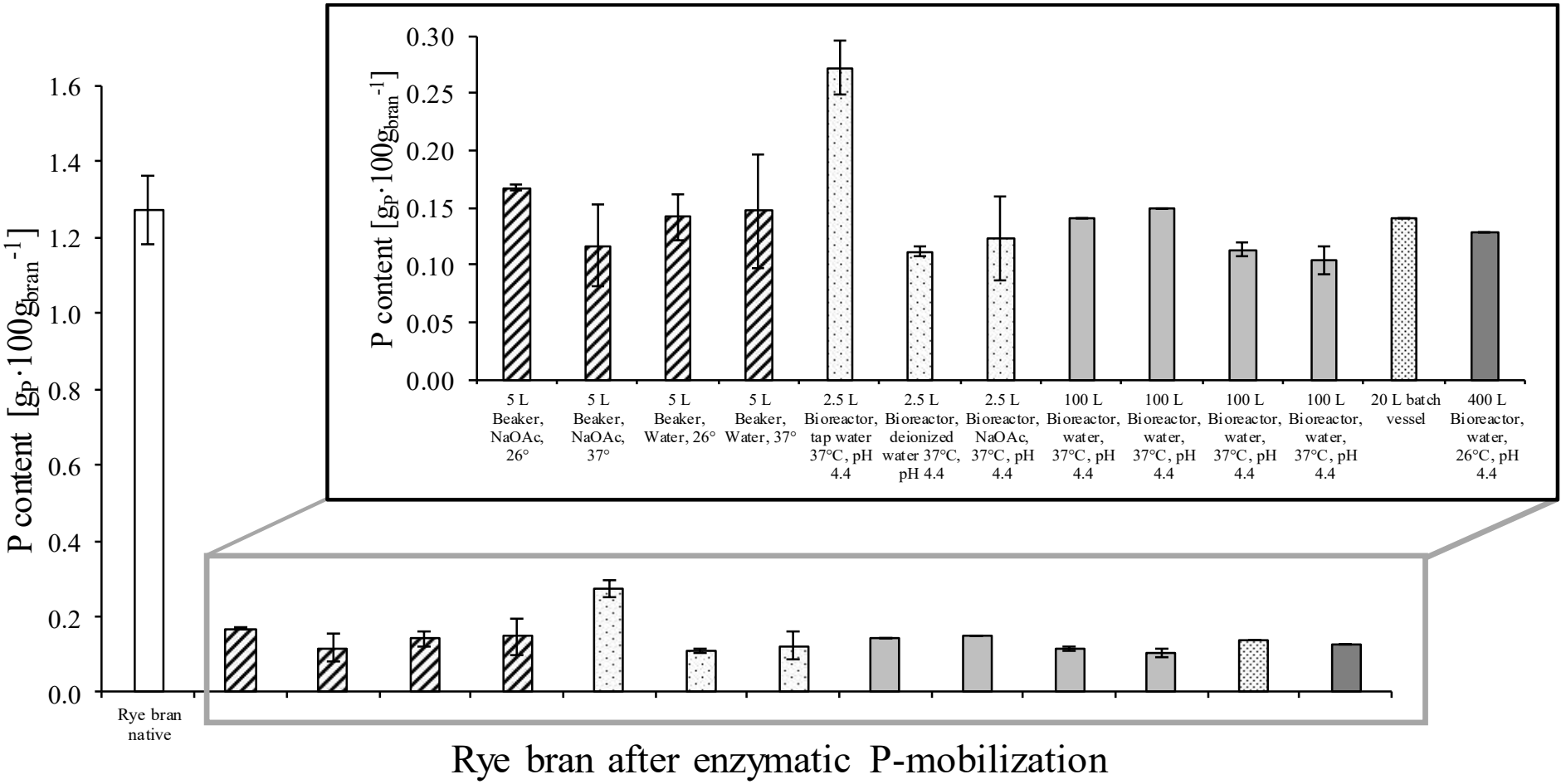

Figure 6.6: Total P-content of native rye bran and rye bran after enzymatic P-mobilization in different reaction scales and conditions. In each reaction 4000 $U \cdot kg_{bran}^{-1}$ of phytase blend used [135].

In fact, differences between the beaker and bioreactor setups include variations in mixing efficiency, pH control, and shear stress. The mixing efficiency of the beaker relies on orbital shaking, which may result in less homogenous mixing compared to the controlled agitation of the bioreactor, affecting substrate availability. The bioreactor´s automated pH control provides a consistent environment, whereas in a shaken beaker, pH may drift over time (in case of tap water). These differences could potentially affect enzyme activity. However, in Figure 6.7 it can be seen that the reaction volume, i.e. vessel size and geometry, does not impact the process, indicating that mixing in the shaken beaker was sufficient for effective P-mobilization. Successful scale-up from 100 g to 37 kg of rye bran, with reaction volumes ranging from 2.5 L to 400 L, achieved substantial P-reduction of 89% to 92% (from 1.27 $g_{P}{\cdot}100g_{bran}^{-1}$ to 0.14 – 0.13 $g_{P}{\cdot}100g_{bran}^{-1}$). Comparable reductions in P-content have been reported for rapeseed and sunflower meal (82% to 90%), which have only been performed at laboratory scale [54,55].

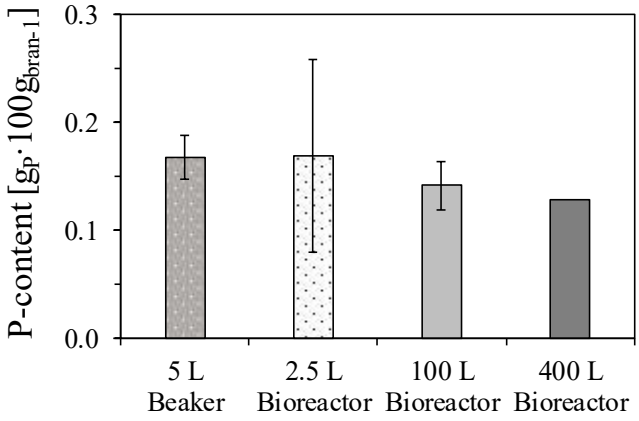

Figure 6.7: Rye bran after enzymatic P-mobilization. Comparison of reactor size in mobilization reaction. Reaction conditions: 4000 $U{\cdot}kg_{bran}^{-1}$ of phytase blend, pH titration to 4.4 with NaOH and HCl, 2.5 L scale: 50 mM NaOAc buffer, stirred at 700 rpm; 100 L scale: deoinized water and pH titration, stirred at 500 rpm; 400 L scale: tab water and pH titration, stirred at 910 rpm [135].

Due to the limitation to quantify the residual inositol phosphate content by HPLC (Chapter 4.1.2), a High Performance Ion Chromatography (HPIC) analysis was performed at RWTH Aachen University according to Widderich *et al.* [135], allowing the determination of all inositol phosphates ($InsP_1$ to $InsP_6$) including isomeric forms. The experiments prove that stirring is essential to enhance mass transfer during the process (Chapter 6.1.2). In an unstirred system (20 L batch reaction, Figure 6.6), incomplete $InsP_6$ hydrolysis is observed. This results in a residual $InsP_6$ content of about 8%, along with small amounts of $InsP_5$ as detected by HPIC analysis, Figure 6.8. However, in all stirred systems, regardless of the bioreactor design and reaction volume, inositol phosphates fully converted to phosphate. The consistent P-reduction by complete inositol phosphate hydrolysis across the process scales shows that enzymatic P-mobilization exhibits adaptability to various reaction parameters, which allows flexibility in its practical implementation.

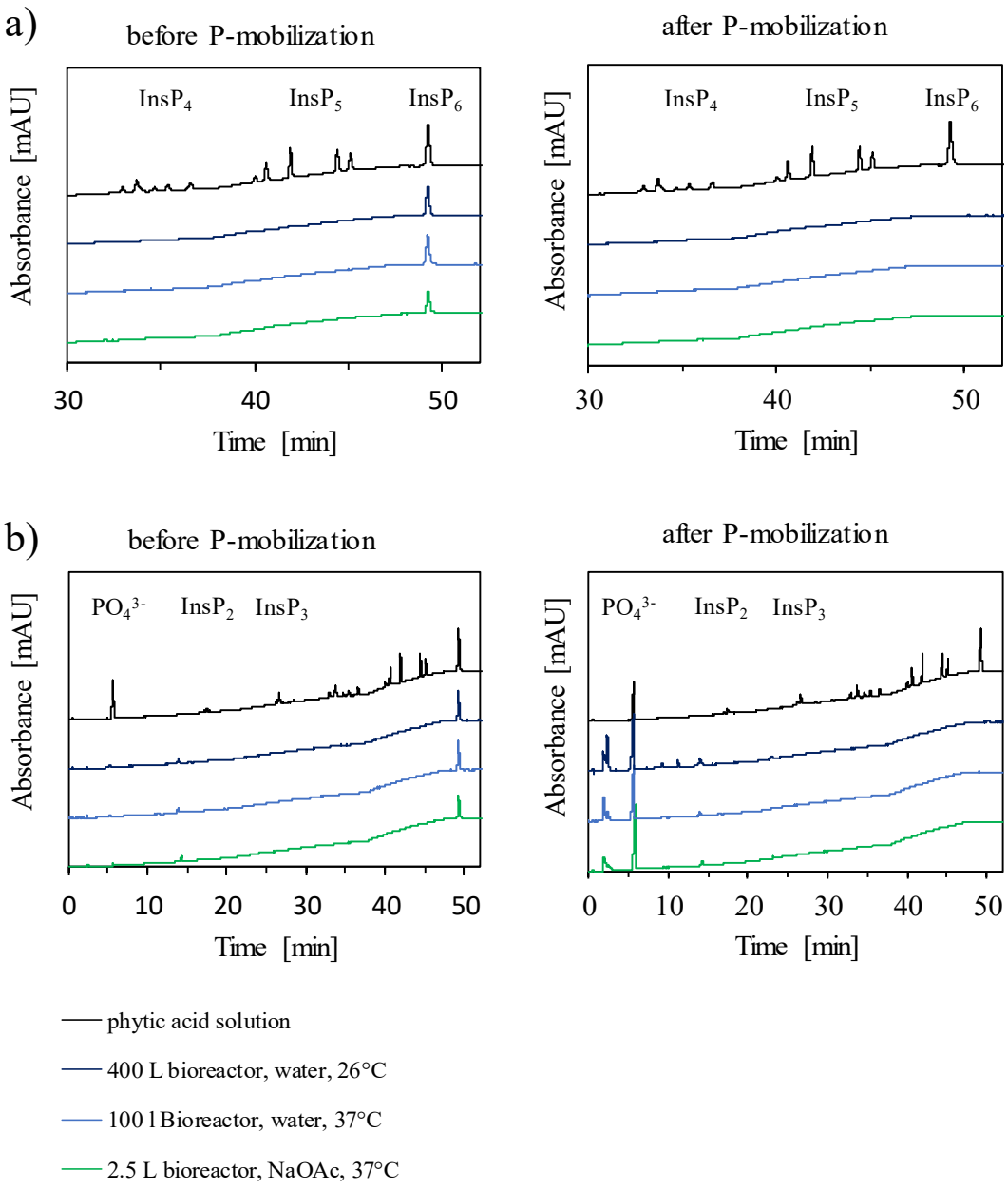

Figure 6.8: Qualitative overlay of chromatograms from HPIC analysis of inositol phosphates in HCl-extracts before and after enzymatic P-mobilization. a) HPIC chromatogram from 30 to 50 min. b) HPIC chromatogram from 0 to 50 min. Retention time of $InsP_6$ at 50 min after injection. The phytic acid solution is shown as a reference. [135]

6.4 Overcoming Process Limitations

Phytate hydrolysis by exogenous phytases relies on its solubilization in the aqueous phase, a process facilitated by mass transfer from the biological matrix. However, in the previous investigations, this transfer is primarily limited by the efficiency of the soaking process and the abrasive effective of the stirrer. These factors weaken the cellular structure, ultimately enhancing mass transfer from the biological matrix (Chapter 6.2 and Chapter 6.3). Figure 6.9 shows the time course of P bound to inositol phosphate (inositol-P) contained in the bran matrix as well as the liberated P during enzymatic P-mobilization. For this, the liberated P was monitored over time. For modeling the inositol-P content, it was assumed that the released P was originally bound to inositol phosphates (Chapter 4.2).

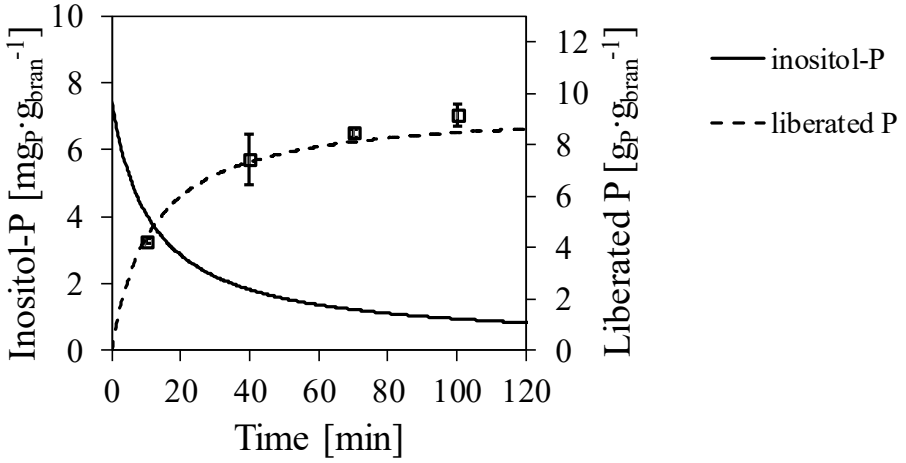

Figure 6.9: Inositol-P content in rye bran and the liberated P during enzymatic P-mobilization. Kinetic simulation to measured data using Michealis-Menten model (Chapter 3.3) resulting in R^2 of 0.97. Curve fitting to eight measuring points up to 240 min. Conditions: 4000 $U \cdot kg_{bran}^{-1}$ rPhyXT52 and *D. castellii* phytase blend, pH 4.4, 37 °C.

A time-dependent decrease in the substrate concentration (inositol-P) is observed with a simultaneous increase in product concentration (liberated P). Therefore, the typical course of a batch reaction can be seen in Figure 6.9 [45]. In line with previous findings on the activation of intrinsic phytases (Chapter 5.4), a rapid decrease in substrate concentration is observed at the beginning of the reaction. This decrease flattens over time as expected. However, the decrease occurs well before the substrate is nearly depleted, indicating a limitation. In fact, the reduction of inositol phosphates within the cellular matrix is induced by diffusion into the surrounding medium. In this case, inositol phosphate hydrolysis by intrinsic phytases is the main mechanism involved in P release [136], as lixiviation of P is more likely than that of inositol phosphate due to steric hindrance and the location within the cellular network [137]. Also in line with previous findings (Chapter 5.4, Chapter 6.2, Chapter 6.3), a period of more than 120 min is required to hydrolyze the inositol phosphate contained in rye bran, although the added phytase activity is in excess and is therefore sufficient to hydrolyze the substrate within this time frame.

Calson and Poulsen showed for barley and wheat that with intact endogeneous phytase, phytate was degraded to almost the same extent as when exogenous phytase was added. Despite the fact that exogeous phytase resulted in higher total phytase activity, any extra phytase activity did not contribute to considerable additional degradation of phytate [137]. Hence, methods for increasing the mass transfer and thus the hydrolytic efficiency of exogenous phytases are described and compared below.

6.4.1 Sonication

Ultrasonic technology has various applications in the food industry, including anti-foaming actions, cell disruption, dispersion of aggregates, inactivation of microorganisms and enzymes, and viscosity modification [130]. Besides that, Ertas *et al.* showed that sonication can accelerate water absorption, reducing soaking time by up to 75%, and reduce phytic acid content in grains and legumes [138]. In addition, it was shown that ultrasonic treatment increases the extraction rate of phytic acid from rice bran by disrupting its surface integrity [139]. The latter has already been examined and confirmed in Chapter 4.1.2. Thus, the effect of ultrasonic treatment on the process of enzymatic P-mobilization is investigated. Figure 6.10 shows the inositol-P content in the biological matrix as well as the liberated P as a function of time during enzymatic P-mobilization combined with ultrasonic treatment. As a reference the courses without ultrasonic treatment, Figure 6.9, are given.

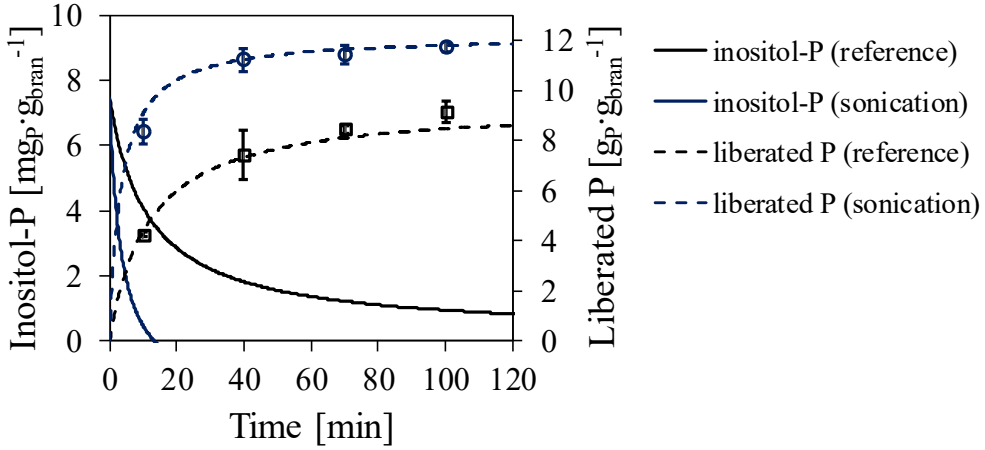

Figure 6.10: Inositol-P content in rye bran and the liberated P during the combined P-mobilization and ultrasonic treatment. Kinetic simulation to measured data using Michealis-Menten model (Chapter 3.3) resulting in R^2 of 0.98. Curve fitting to eight measuring points up to 240 min. Conditions: 4000 U·kg$_{bran}^{-1}$ rPhyXT52 and *D. castellii* phytase blend, pH 4.4, 37 °C, sonication for 10 x 30 s cycles at 70% performance.

Ten cycles of ultrasonication for 30 s at 70% power in combination with exogenously added phytases show a substantial increase in efficiency, resulting in a reduction of the processing time to less than 20 min, Figure 6.10. However, it is apparent that more P is liberated than is bound in inositol-P.

A possible explanation for this is that P bound to other organic molecules, such as phospholipids, adenosine phosphates, and nucleic acids, or in other organic forms as well as inorganic P present in the biological matrix, is also released by the treatment as the cell integrity is attacked. This could lead to a slightly distorted course of inositol-P degradation. However, inositol-P accounts for the majority of total P-content (Chapter 5.2), hence the influence is minimal. Furthermore, no clear effect of the ultrasonic treatment on the enzymatic activity is observed. However, exogenously added phytases were present in excess. Therefore, the effect of ultrasound treatment on exogenously added phytase activity cannot be clearly determined. Conceivably, at least intrinsic phytases may be stabilized by the cellular matrix. Nevertheless, the method proves to be effective in treating the cellular matrix, thus increasing the mass transfer of phytate and its solubilization rate in the liquid phase, which ultimately increases the rate of hydrolysis. However, the implementation of this treatment on an industrial scale poses challenges due to the implementation in the reaction system, the inhomogeneity and the substantial costs involved. Therefore, the following chapter presents a different treatment method using enzymes to disrubt cellular surface integrity.

6.4.2 Enzymatic Treatment of the Cellular Matrix

The plant cell wall consists mainly of carbohydrate-based polymers, i.e. cellulose, hemicelluloses and pectins. Bran is rich in non-cellulosic polysaccharides, with heteroxylans (56 % dry matter arabinoxylan) accounting for the majority [140]. In terms of dry weight, rye bran contains around 14% xylose, 7% arabinose, 26% glucose and 1% galactose as polimeric structural carbohydrates [141]. Therefore, a synergistic effect of several enzymes is required for the degradation of the cell wall and bran structures [31], while endo-1,4-xylanases play a key role in the degradation of arabinoxylan [142]. Nyström *et al.* have shown that xylanase has a significant influence on the degradation of the cell wall structure [33].
Phytic acid is mainly found in aleurone cells (Chapter 1.3, Chapter 5.1). Therefore, enzyme formulations that hydrolyze aleurone cell wall components were screened. The enzyme formulation Depol 761 P (high xylanase activity) effectively degrades arabinoxylan in rye bran [116,143]. The results of Petersson *et al.* clearly show degradation of the aleurone cell wall by Depol 761 P [116]. However, other enzyme formulations such as Viscoferm (high xylanase and ß-glucanase activity), Viscozyme L (high polygalacturonase and endogluconase activity as well as proteolytic side activity) and Depol 740 L (endoxylanase, ß-glucanase, endoglucanase and ferulic esterase activity) also showed considerable degradation of cell wall arabinoxylan [116,143].

It is also apparent that selective degradation of the aleurone cell wall is not possible. Therefore, the goal is to find an enzyme formulation that primarily degrades the components of the aleurone cell wall. Another challenge is that non-starch polysaccharides are the major dietary fiber component in rye bran [140]. This results in a trade-off between the mobilization rate of phytate bound P and the solubilization of the crude fiber components. However, the latter can be converted into high-value components such as antioxidants (ferulic, protocatechuic, sinapinic, vanillic, hydroxybenzoic acids) [33,35,116,143] and thus contribute to the economic establishment of the overall process. Table 6.1 lists the enzyme formulations screened for cell matrix treatment. To ensure comparability, the activities on either cellulose or xylose at pH 4.4 and 37 °C (maximum phytase activity, Chapter 5.4) of the different enzyme formulations were determined using 3,5-dinitrosalicylic acid (DNS) assay.

Table 6.1: Enzyme formulation for the treatment of the cellular matrix for supportive release of inositol phosphates. Activity on xylane and cellulose determined at 37 °C and pH 4.4.

Ezyme formulation	Enzymatic activity	Manufacturer/ supplier	Spezific activity	Substrate used
Depol 761 P	Xylanase	Biocatalysits	160 ± 10 $U \cdot mg^{-1}$	Xylane
Depol 740 L	Endoxylanase-, ß-glucanase-, endoglucanase, ferulic acid esterase	Biocatalysits	131 ± 12 $U \cdot mL^{-1}$ 100 ± 21 $U \cdot mL^{-1}$	Xylane Cellulose
Pentopan Mono BG	Xylanase from *Aspergillus oryzae*	Sigma Aldrich	283 ± 82 $U \cdot mg^{-1}$	Xylane
Viscozyme L	Polygalacturonase, endogluconase, proteolytic side activity	Novozymes	470 ± 46 $U \cdot mL^{-1}$	Cellulose
Cellic CTec2	Cellulase, proteolytic side activity	Sigma Aldrich	566 ± 30 $U \cdot mL^{-1}$	Cellulose
Celluclast	Cellulase from *Trichoderma reesei*	Sigma Aldrich	392 ± 21 $U \cdot mL^{-1}$	Cellulose
Hemicellulase	Hemicellulase from *Aspergillus niger,* α-amylase, ß-galactosidase, pectinase, protease, xylanase	US Biological	402 ± 38 $U \cdot mg^{-1}$ 75 ± 5 $U \cdot mg^{-1}$	Xylane Cellulose
Pektinex Ultra SP-L	Pectinase, hemicellulase, ß-glucanase	Novozymes	653 ± 17 $U \cdot mL^{-1}$	Cellulose

In Figure 6.11, the stability of the respective enzyme formulations from Table 6.1 is depicted over a period of 4 h at 37 °C and pH 4.4. All enzyme formulations remain active over 4 h under the reaction conditions investigated, redering them suitable for use. However, the enzyme formulation Pectinex exhibits a decrease in activity to approximately half of its initial level. In contrast, no loss in activity is observed in any of the other enzyme formulations. Furthermore, the increased activity of Celluclast at 1 h appears as an outlier.

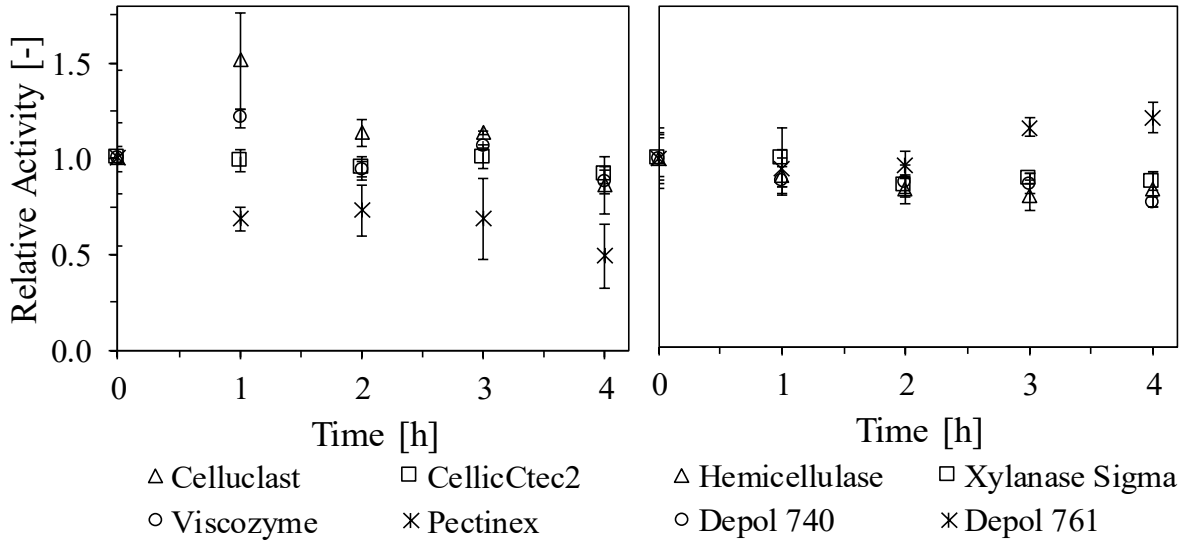

Figure 6.11: Stability of enzyme formulations for the treatment of the cellular matrix at pH 4.4 and 37°C (maximum phytase activity). *Left*: activity on cellulose, *right:* activity on xylane.

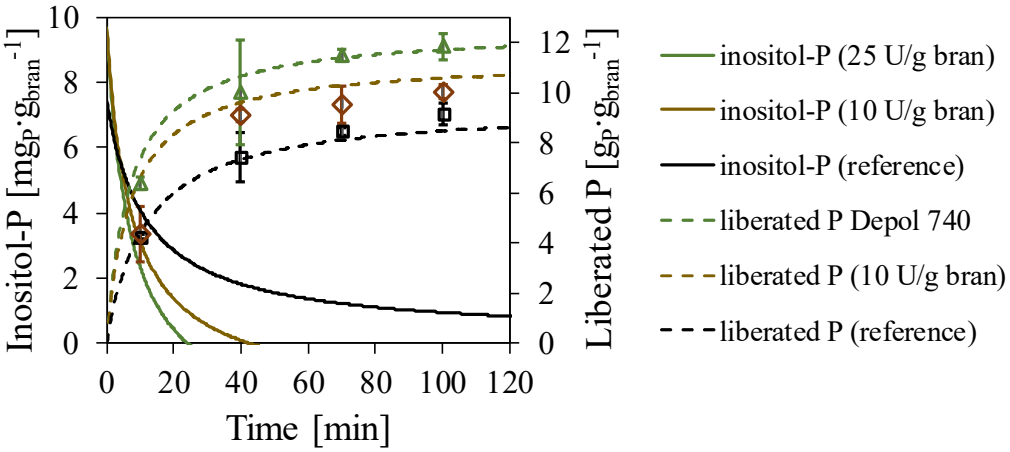

Figure 6.12: Inositol-P content in rye bran and the liberated P during the combined enzymatic P-mobilization. Addition of 10 and 25 U·g$_{bran}^{-1}$. Kinetic simulation to measured data using Michaelis-Menten model (Chapter 3.3) resulting in R^2 of 0.91 and 0.99, respectively. Curve fitting to eight measuring points up to 240 min Conditions: 4000 U·kg$_{bran}^{-1}$ rPhyXT52 and *D. castellii* phytase blend, pH 4.4, 37 °C.

The screening of the enzymatic treatment of the cellular matrix with different enzyme formulations, Table 6.1, combined with enzymatic P-mobilization, confirmes that fomulations based on xylanase activity exhibit the most pronounced effect on the mobilization of P, Figure B.13. However, as expected, formulations based solely on xylanase activity are less effective than those based on the synergy of multiple enzymatic activities. In particular, formulation Depol 740 most effectively increased the P-mobilization, Figure 6.12. Nevertheless, a positive effect on P-mobilization is also observed for formulations based on cellulase activity. Furthermore, except for the formulations Celic Ctec2 and Hemicellulase, the increased enzyme activity (from 10 $U \cdot g_{bran}^{-1}$ to 25 $U \cdot g_{bran}^{-1}$) further enhances P-mobilization. Treatment with 25 $U \cdot g_{bran}^{-1}$ Depol 740 during enzymatic P-mobilization reduces the process time to about 20 min and is therefore comparable in efficiency with ultrasound treatment (10 cycles of 30 s at 70% performance). However, this formulation has the lowest specific activity, Table 6.1, which results in a higher amount of enzyme required compared to the other formulations.

6.4.3 Comparison of Mass Transfer Enhancing Treatments

As shown in the previous chapter, treatment with 25 $U \cdot g_{bran}^{-1}$ Depol 740 is similarly effective as ultrasonic treatment. However, Figure 6.13 shows that the ultrasonic treatment has a greater influence on the P-mobilization rate, especially at the beginning of the treatment (slope of the curves). A possible explanation for this is the penetration depth of the treatment and the distribution of the enzymes in the substrate, which affect the effectiveness of the two methods differently. As with ultrasound treatment, for enzymatically treated samples more P is released than is bound in inositol-P. The release of other organic and inorganic P compounds is suggested to be the cause (Chapter 6.4.1). Nevertheless, it could be shown that both methods are suitable for supportive treatment of the cellular matrix and thus for increasing the P-mobilization rate.

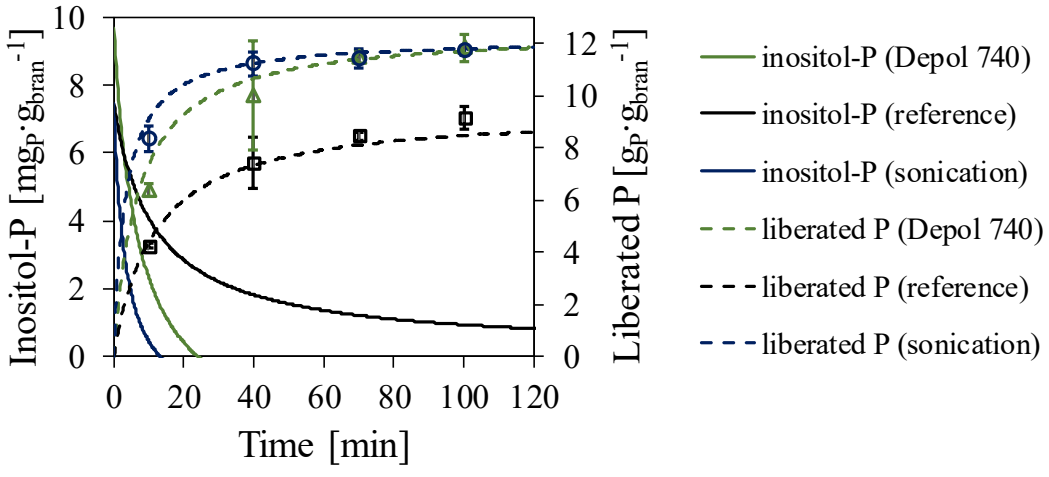

Figure 6.13: Comparison of mass transfer enhancing treatments. Conditions: 4000 $U \cdot kg_{bran}^{-1}$ rPhyXT52 and *D. castellii* phytase blend, pH 4.4, 37 °C.

Figure 6.14 shows fluorescence microscopic images of A) native rye bran, B) enzymatic P-mobilization for 16 h, and enzymatic P-mobilization for 1 h in combination with C) Depol 740 treatment and D) ultrasonic treatment. Blue staining indicates ß-glucans (cell wall component), while red staining indicates proteins. As observed, the most intense blue staining is originating from untreated rye bran (serving as a reference). For all treatments, a substantial decrease in blue staining can be seen, attributed to the desired weakening of the cell wall structure induced by each treatment. The lowest blue staining is found for the 16 h enzymatic P-mobilization, due to the prolonged soaking process. Consistent with previous findings, the blue staining is nearly identical for the ultrasonic and Depol 740 treatments. In addition to the desired increase in P-mobilization rate, both treatments weaken the cell wall integrity to a lesser extent compared to the 16 h wet-treatment. As a result, additional enzymatic as well as ultrasonic treatment is not only shortening processing times, but also alter the structural properties to a lesser extent, providing a more suitable product for further processing in feed formulations.

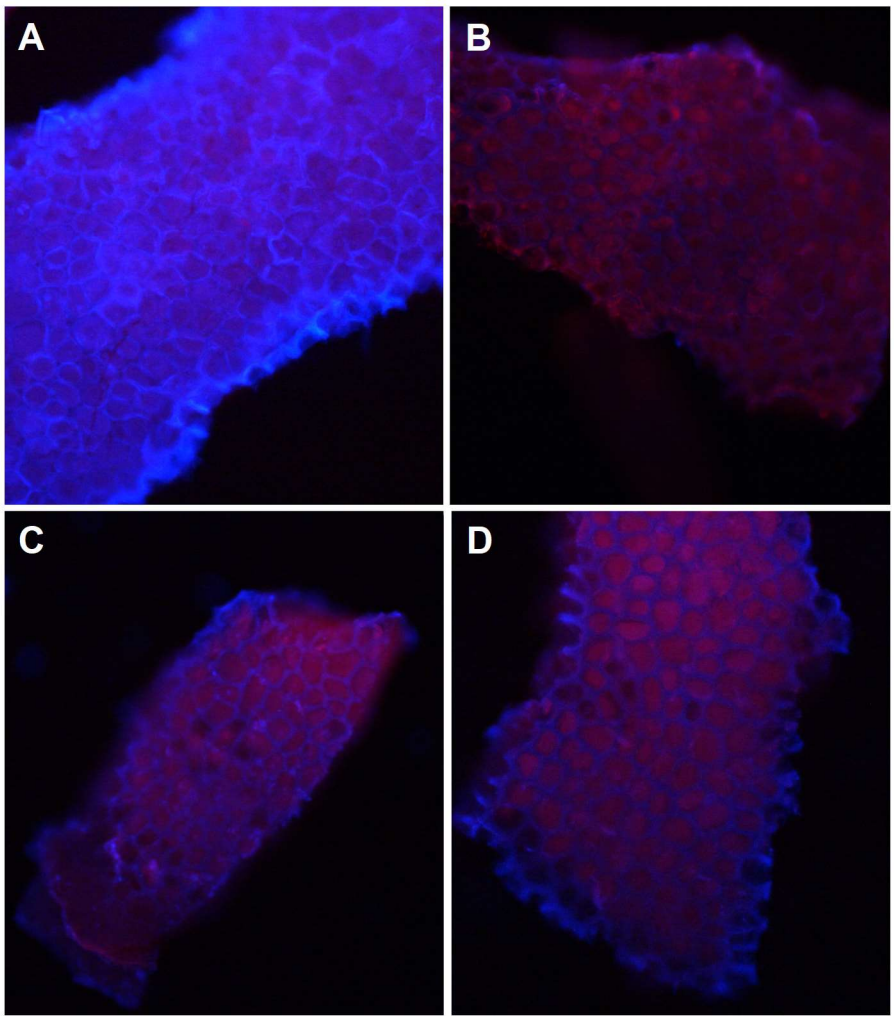

Figure 6.14: Fluorescence microscopic images of A) native rye bran, B) after 16 h enzymatic P-mobilization, C) 1 h enzymatic P-mobilization and Depol 740 treatment, D) 1 h enzymatic P-mobilization and ultrasound treatment. Proteins are stained red with acid fuchsin, ß-glycans are stained blue with calcoflour white.

6.5 Interim Summary

- When rye bran is added to water, a pH shift occurs. A buffering effect is observed at about pH 4 to pH 5. pH titration or a weak buffer (50 mM NaOAc) is sufficient to maintain pH 4.4 during enzymatic P-mobilization.

- Kinetic study of blended rPhyXT52 phytase and *D. castelli* phytase showed no inhibition by substrate or products. The phytase blend is suitable for batch operation at a bran to water ratio of 1 to 7 (w/v).

- P mobilization using the phytase blend on rye bran results in complete hydrolysis of inositol phosphates and a 90% reduction in total P-content.

- Process conditions of exogenously added phytase blend are close to the maximum intrinsic enzyme activity.

- Process of enzymatic P-mobilization is straightforward scalable and adaptable to various reaction parameters.

- Additional ultrasonic as well as enzymatic treatment of the cellular matrix leads to a substantial reduction of the process time. With respect to additional enzymatic treatment, enzyme formulations based on xylanase activity are most effective and in particular the formulation Depol 740 due to the synergistic effect of different activities.

7 Properties of Enzymatically Treated Rye Bran as Animal Feed

Enzymatic P-mobilization substantially reduces the P-content in rye bran by eliminating the contained phytate (Chapter 6). However, whether the P-depleted rye bran is a valorized feed component depends on both its nutrient and physiochemical properties after P-mobilization. After solid-liquid separation under centrifugal forces, the rye bran was either lyophilized or dried at 60 °C. No significant differences in physiochemical and nutritional properties were observed between differently treated batches. Therefore, both drying methods are valid for processing. However, micronutrients (e.g. vitamins) were not analyzed. Nevertheless, the physiochemical properties of rye bran are influenced by process conditions such as reactor design and in particular the stirrer geometry and speed, i.e. the power input. Therefore, the following section presents and discusses the physiochemical properties of the P-depleted rye bran after various production scales (Chapter 6.3). Most importantly, its suitability as a feed component depends strongly on its nutritional properties after enzymatic P-mobilization as well as the combined enzymatic treatment (Chapter 6.4.2), which are discussed below. The results relate to rye bran Preparation II.

7.1 Nutrient Properties

The results of the feed analysis of native and treated rye brans are presented in Table 7.1. The nutritional profile was analyzed at the University of Veterinary Medicine Hannover (Institute of Animal Nutrition). The analytical procedure is published in Widderich *et al.* [135]. As it can be seen in Table 7.1, lower crude ash and crude protein contents and higher crude lipids and crude fiber contents were found in the 16 h treated rye bran compared to the native rye bran. The same was found for the combined enzymatic P-mobilization for 2 h, with the exception that the fiber content remains at the same level. The amounts of carbohydrates starch and sugar were also lower for the 16 h P-mobilization. However, for the combined enzymatic P-mobilization these values were not determined. In both cases, the treatments reduced the total P-content by 89% to 91%. Furthermore, the P-mobilization does not affect the calculated energy value, but this value could not be determined for the combined process as the data for carbohydrate fractions were not determined.

Parts of this chapter are published in: Widderich, N.; Stotz, J.; Lohkamp, F.; Visscher, C.; Schwaneberg, U.; Liese, A.; Bubenheim, P.; Ruff, A.J. An up-scaled biotechnological approach for phosphorus-depleted rye bran as animal feed. *Bioresources and. Bioprocessing* **2024** [135].

Table 7.1: Comparison of nutrient properties between native and enzymatically treated rye bran.

	Unit	Native	16 h P-mobilisation	2 h combined P-mobilization and Depol 740 treatment
Dry matter	%	90.2	97.5	93.8
Crude ash	$g \cdot kg_{DM}^{-1}$	64	7	36
Crude protein	$g \cdot kg_{DM}^{-1}$	168	111	146
Crude lipids	$g \cdot kg_{DM}^{-1}$	35	49	32
Crude fiber	$g \cdot kg_{DM}^{-1}$	67	125	69
Starch	$g \cdot kg_{DM}^{-1}$	158	82	ND
Sugar	$g \cdot kg_{DM}^{-1}$	108	8	ND
Total P	$g \cdot kg_{DM}^{-1}$	13.7	1.3	1.5
ME_{pig}	$MJ \cdot kg_{DM}^{-1}$	11	11	ND

ND: not determined

Treatment of native rye bran resulted in changes in nutrient composition that can be explained by the P-mobilization process. The process not only increases the solubilization of P, but also of other nutrients. Mainly due to the loss of crude ash, starch, water soluble proteins and other soluble polysaccharides during washing, the fiber and lipid content increased. Similar results were observed by Nyombaire and Ng [144]. This also explains that more P is released from the biological material than is bound to inositol phosphate (Chapter 6.4). In addition, it is known from other studies that native rye grain contains both endogenous enzymes and indigenous microbes in the outer layers of the grain, which also can lead to hydrolytic enzyme activities and to an altered grain composition after fermentative processes [145–147]. However, as expected, the crude fiber content of the combined treatment is lower than that of the phytase treatment alone, due to the degradation of the cell wall by Depol 740, which leads to the solubilization of crude fiber components (Chapter 6.4.2). The extraction of protein from bran depends on the conditions during treatment (pH, time, temperature, solvent, and particle size) [148]. The addition of water for 16 h without enzyme addition increases the soluble organic nitrogen content of wheat bran from 14% to 43% [143]. Roberts *et al.* extracted 66% of the protein from wheat bran at pH 4.5 followed by three washes at neutral pH. However, the temperature was 60 °C and the highest extraction rates were obtained under alkaline conditions [148].

Washing the biomass not only increases the extraction of proteins but also decreases the P-content after P-mobilization, as it influences the concentration of inorganic P in the supernatant. This concentration determines the adherent P-content after drying, thus affecting the total P-content of produced feed material. At a biomass-to-liquid ratio of 1 to 7 (w/v), the P-content in the supernatant is on average 1.70 $g_P \cdot L^{-1}$. Nevertheless, after sedimentation and a single wash with water, the P-content is reduced by 47% to 0.90 $g_P \cdot L^{-1}$. Subsequent washes lead to further reductions. After two and three washes the P-content decreases to 0.55 $g_P \cdot L^{-1}$ and 0.16 $g_P \cdot L^{-1}$, respectively, resulting in a 92% reduction of inorganic P-content in the supernatant. However, since the animals require P for their metabolism and the remaining P in the supernatant is bioavailable, washing the biomass to further reduce the P-content is not necessarily required. If P levels in the diet are too low, additional sources of P must be added to the diet.

The calculated values of the metabolizable energy according to the formula of the GfE [149] are based on analyzed results and table values on nutrient digestibility of rye bran [150]. The latter may differ from the samples analyzed. Nevertheless, the energy values found in the treated rye bran seem quite conceivable due to the low crude ash content and the associated high amount of organic residue. In addition, the substantial P-reduction and high nutritional profile make the produced feed suitable for animal consumption and therefore a valorized feed material.

7.2 Physicochemical Properties

The physiochemical properties of the feed material to which bran has been added, influence the sensory food quality. This dependence extends to factors such as water holding capacity (WHC), whereby a higher WHC is associated with an increased swelling capacity. In particular, the particle size is an important parameter, as studies indicate its influence on the WHC [116]. Additionally, the adherent P-content is investigated, as it contributes to the total P-content of the final product. Table 7.2 presents a comparison of the equivalent corcle diameters X_{10}, X_{50}, X_{90} (10^{th}, 50^{th}, 90^{th} percentile respectively), the WHC, and the adherent P-content after P-mobilization.

The alteration in particle size distribution is evident in the equivalent circle diameters, indicating a shift towards larger particle sizes post P-mobilization. This trend is observed across all production scales, with the exception of the 400 L scale. The shift primarily results from the wash out of smaller particles during solid-liquid separation, and is reflected by the X_{10} values, which are consistently lower for all production scales compared to the native rye bran. However, the X_{90} values are increased due to agglomeration formation after drying, with not all agglomerates being appropriately dispersed by the measurement device.

Parts of this chapter are published in: Widderich, N.; Stotz, J.; Lohkamp, F.; Visscher, C.; Schwaneberg, U.; Liese, A.; Bubenheim, P.; Ruff, A.J. An up-scaled biotechnological approach for phosphorus-depleted rye bran as animal feed. *Bioresources and. Bioprocessing* **2024** [135].

Table 7.2: Comparison of physiochemical properties of rye bran post P-mobilization at different production scales.

	Unit	Native	After enzymatic P-mobilization			
Reaction volume	L		2.5 (1)	2.5 (2)	100 (3)	400 (4)
X_{10}	µm	432.7 ± 9.3	357.6 ± 21.9	353.2 ± 51.1	401.7 ± 11.2	271.5 ± 3.7
X_{50}	µm	788.8 ± 36.7	915 ± 102.1	931 ±68.9	807.6 ± 12.8	572.2 ± 7.0
X_{90}	µm	1448.0 ± 223.0	2126.2 ± 119.0	1970.8 ± 52.8	1716.8 ± 15.3	1417 ± 50.1
WHC	$mL \cdot g_{DM}^{-1}$	2.8 ± 0.1	5.1 ± 0.3	5.0 ± 0.2	5.1 ± 0.1	5.3 ± 0.4
Adherent-P	$g_P \cdot kg_{DM}^{-1}$	-	0.7 ± 0.1	1.0 ± 0.1	0.5 ± 0.1	0.4 ± 0.0

(1) deonized water and pH titration, 700 rpm; (2) 50 mM NaOAc buffer, 700 rpm; (3) deonized water and pH titration, 500 rpm; (4) tab water and pH titration, 910 rpm.

The average particle size X_{50} does not seem to be clearly influenced by the P-mobilization processes. This is explained by the fact that, in addition to washout and agglomerate formation, the stirrer and the soaking in liquid also affect particle distribution. The soaking, in particular, has an impact on the cell wall [116], which also enables phytate mass transfer [130]. However, there is no difference between water or buffer as a reaction medium. In addition, the stirrer has an abrasive effect on the cell wall, which has been weakened by the soaking process. Due to the higher energy input and the stirrer geometry (propeller impeller; high shear force) in the 400 L reaction, the particle distribution after P-mobilization is shifted towards smaller particles. As expected, the stirring has the greatest influence on the resulting particle distribution.

WHC of the initial substrate was found to be 2.8 $mL \cdot g_{bran}^{-1}$, which is in agreement with others [116,151]. However, after P-mobilization WHC increased by a factor of 1.7 to 1.8. Consequently, the conditioned rye bran has a higher capacity to swell compared to the native substrate. This is a desirable effect and is correlated with the fiber content, Table 7.1. The higher the fiber content, the more material is available for network formation, resulting in an increased WHC [151].

The adherent P-content varies from 0.4 to 1.0 $g_P \cdot kg_{DM}^{-1}$. It is noteworthy that the adherent P-content is lower in the large scale than in the small scale. After sedimentation, larger wash volumes were used in relation to biomass. Considering the adherent P-content, Table 7.2, and the total P-content after P mobilization, Table 7.1, half of the P adheres to the final product. For maximum P-reduction, washing of the biomass is required. However, in order to minimize process wastewater, washing of the biomass may not be necessary.

7.3 Interim Summary

- WHC is about 2-fold increased post P-mobilization, correlating with fiber content.
- P-mobilization alters nutrient composition of rye bran, resulting in higher fiber and lipid content due to the loss of crude ash, starch, water soluble protein, and other soluble polysaccharides.
- Combined enzymatic P-mobilization for enhanced process performance (Chapter 6.4.2) leads to the solubilization of crude fiber components.
- About half of the P adheres to the final product.
- Enzymatically treated rye bran has a high nutritional profile suitable for animal consumption. Substantial P-reduction makes the treated rye bran a valorized feed component.

8 Process Wastewater: Characterization and Valorization

The concept of enzymatic P-mobilization facilitates the depletion of P contained in phytate from residual streams of flour processing (Chapter 6). Subsequently, the valorized plant material can be used as feedstuff (Chapter 7). Thus, the process of enzymatic P-mobilization prior to feeding minimizes the issue of excessive P inputs into the environment through manure and the associated eutrophication of surface waters. In this chapter, the P containing process wastewater is characterized. Based on this, the concept of struvite precipitation for P-recovery is examined for its applicability. In addition, the recovery of mobilized phenols from the process wastewater is investigated and the residual process wastewater is evaluated for its potential use as a medium for industrial bioconversions. The following results refer to rye bran Preparation II.

8.1 Characterization

The P containing process wastewater was separated from the conditioned feed material to enable efficient P-recovery and drying of the feed material. Figure 8.1 shows the flow characteristics of the process wastewater after solid-liquid separation. As can be seen, the shear stress is proportional to the shear rate. Accordingly, the process wastewater behaves as expected as a Newtonian fluid [128]. The proportionality is expressed by the dynamic viscosity and is 1 mPa·s. Furthermore, the gravimetric density determination at 20 °C, Figure B.14 resulted in a density of 1017 kg·m^{-3}. Consequently, the dynamic viscosity and the density correspond to those of water (0.001 Pa·s, 998 kg·m^{-3}).

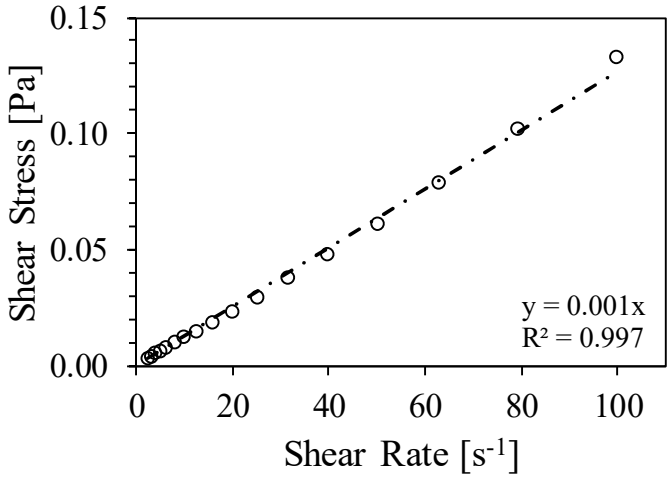

Figure 8.1: Flow behavior of the process wastewater after enzymatic P-mobilization. Recorded with Kinexus pro rhemoeter (NETZSCH-Gerätebau GmbH, Selb/Bavaria, Germany). A cone was used as geometry [129]. The line is a visual aid.

Table 8.1 shows the ion content in the process wastewater that is decisive for the recovery of P, including interfering ions (Chapter 3.4). In addition to P (approx. 50 mM), K^+ is most abundant with a concentration twice that of P. The high concentration is presumably due to the hydrolysis of phytate, as potassium phytate is often present in the plant material (Chapter 1.4). In addition, K^+ is associated with other cellular constituents, such as polysaccharides in the plant cell structure. Mg^{2+} is present at about half the concentration of P, followed by low concentrations of Ca^{2+} and NH_4^+, with NH_4^+ just above the detection limit.

Table 8.1: Ion content in the process wastewater after enzymatic P-mobilization.

	Concentration [mmol·L^{-1}]	Ratio to P
$H_2PO_4^-$ (pH 4.4)	49.5	1
Ca^{2+}	3.3	0.07
Mg^{2+}	19.8	0.40
K^+	104.9	2.12
NH_4^+	< 0.1	< 0.01

Carbohydrate analysis, Table 8.2, shows that phytase treatment alone or in combination with sonication resulted in predominantly monomeric sugars, as expected (Chapter 7.1). Consequently, there is an increased risk of microbial proliferation, requiring either storage at low temperature, microbial inactivation or immediate processing. However, additional treatment with Depol 740 resulted in increased concentrations of oligomeric sugars, also increasing the risk of microbial contamination. Hydrolytic cleavage resulted in increased levels of arabinose and xylose, in line with expectations (Chapter 6.4.1, Chapter 7.1).

Table 8.2: Carbohydrate analysis of the process wastewater after A) 16 h enzymatic P-mobilization, enzymatic P-mobilization for 1 h in combination with B) 25 U·g_{bran}^{-1} Depol 740 treatment and C) ultrasonic treatment

	Component	Concentration [g·L^{-1}]			Oligosaccharides [g·L^{-1}]		
		A)	B)	C)	A)	B)	C)
Raw	Cellobiose	1.14	0.57	0.96			
	Glucose	5.78	7.69	5.55			
	Xylose	6.05	8.04	4.93			
Hydrolysed	Cellobiose	1.95	1.62	1.50			
	Glucose	7.84	12.71	9.51	2.25	5.01	3.92
	Xylose	4.59	8.49	3.93	-	1.71	-
	Arabinose	1.69	7.74	1.78	-	5.39	0.24

8.2 Phosphorus Recovery

This chapter deals with the recovery of P from the process wastewater. The recovered P is intended for use in agriculture, thereby facilitating the use of P in a closed-loop system. To achieve this, P was precipitated as struvite due to its eco-friendly fertilizer properties (Chapter 3.4). It is investigated whether the recovery of P in the form of struvite from wastewater treatment is applicable to the enzymatic P-mobilization process. The ideal process conditions to achieve maximum yield and purity will be determined, and subsequent purification steps to increase the purity will be explored. In addition, the scalability of struvite precipitation from the process wastewater is evaluated.

Drying of struvite can lead to thermal decomposition, which causes ammonium, water of hydration, and water of constitution to enter the gas phase. As a result, struvite loses mass and dissociates into another crystal or amorphous state [152]. Hence, the drying temperature was investigated. In agreement with the results of Bayuseno *et al.*, it is confirmed that struvite transforms into an amorphous state at a drying temperature of 60 °C, Figure B.15 [152]. A drying temperature of 40 °C was chosen in order to be able to detect struvite by X-ray diffraction patterns and to not affect the gravimetrically determination of purity. In addition, the degree of dissociation of P in solution was taken into account in all calculations, Figure 3.5. The solubility product was calculated for each of the experiments according to Chapter 3.4.1 and is expected to be in the range of 10^{-10} [153] to 10^{-14} [81].

8.2.1 Determination of P-Recovery and Struvite Purity

Colorimetric P analysis (Chapter A.2.1) was used to determine the amount of P in the hydrolysate at the beginning (n_{t0}) and after precipitation in the filtrate (n_{t1}). The latter takes into account the increase in volume due to the titration volume. P-recovery from struvite precipitation was calculated according to Equation 8.1.

$$\text{P-recovery [\%]} = \left(1 - \frac{n_{t1}}{n_{to}}\right) \cdot 100\% \qquad \text{(Eq. 8.1)}$$

To calculate the purity of the precipitate after struvite precipitation, the gravimetrically determined mass of the precipitate ($m_{grav,dry}$), considering the dry weight, was related to the theoretically possible mass of the precipitate ($m_{theoretic}$), Equation 8.2.

$$\text{purity [\%]} = \frac{m_{grav,dry}}{m_{theoretic}} \cdot 100\% \qquad \text{(Eq. 8.2)}$$

The maximum possible theoretical mass of the precipitate was calculated according to Equation 8.3. c_{t1} is the substance concentration of the quantity n_{t1}.

$$m_{theoretic} = \left(c_{t0} \cdot V_{t0} \cdot M_{struvite,\,adj.}\right) \cdot \frac{\text{P-recovery}}{100} \qquad \text{(Eq. 8.3)}$$

Struvite is hygroscopic. Therefore, the precipitate may still contain some residual moisture after drying. In order to account for this, the dry mass was determined. A defined amount of the precipitate was heated to 105 °C until weight constancy. The weight loss corresponds to the water content. $M_{struvite,adj.}$ includes the evaporation of crystal water caused by the measurement.

8.2.2 Investigation of Maximum Process Conditions for Struvite Precipitation

To investigate maximum process conditions for struvite precipitation from the process wastewater, the pH, the temperature, the stoichiometric Mg^{2+} precipitant input ratio, dilution of the process wastewater and the molarity of the precipitation agent were varied, Figure 8.2 to Figure 8.9. In addition, the influence of stirring on struvite precipitation was investigated, Figure 8.10 to Figure 8.13. A list of all solubility products under the respective process conditions can be found in Table B.2 to Table B.7. As can be seen from Figure 8.2, Figure 8.4, Figure 8.6, Figure 8.8, Figure 8.10, and Figure 8.12, a P-recovery of over 95% was observed under all process conditions tested. Furthermore, struvite was detected by X-ray diffraction for all conditions, Figure 8.3, Figure 8.5, Figure 8.7, Figure 8.9, Figure 8.11, Figure 8.13. Both observations indicate a very robust process, which is adaptable to various conditions, and highlight the feasibility and reliability of the process for industrial-scale P-recovery. However, it is also evident that under certain process conditions, the purity of the precipitated struvite is superior. Therefore, the following sections will delve into the results of varying the different process parameters, thereby establishing a basis for enhancing the quality of the struvite and the efficiency of its precipitation from the P-mobilization process wastewater.

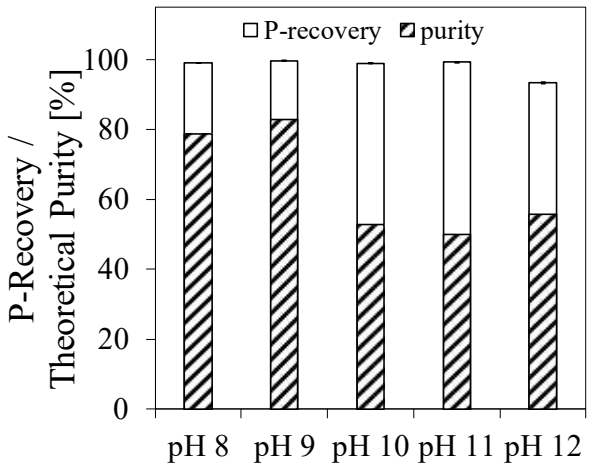

Figure 8.2: P-recovery at different pH, and 20 °C.

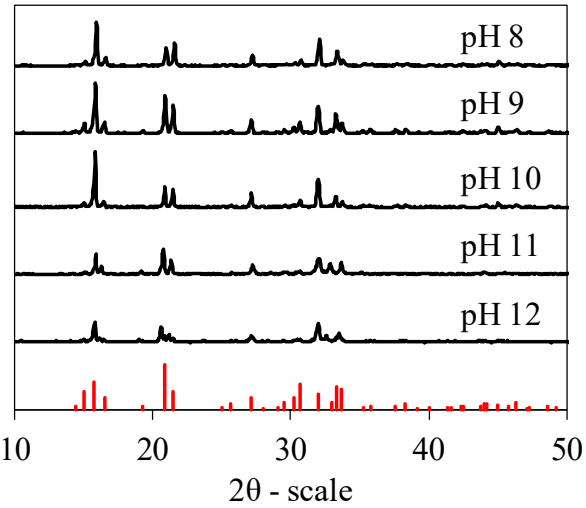

Figure 8.3: Diffractograms of precipitates at different pH, and 20 °C.

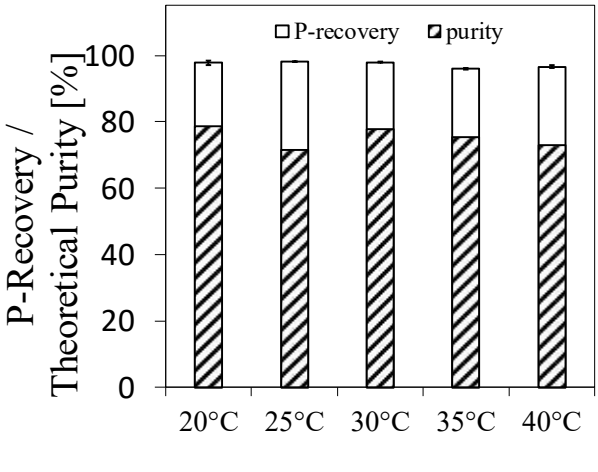

Figure 8.4: P-recovery at different temperatures, and pH 9.

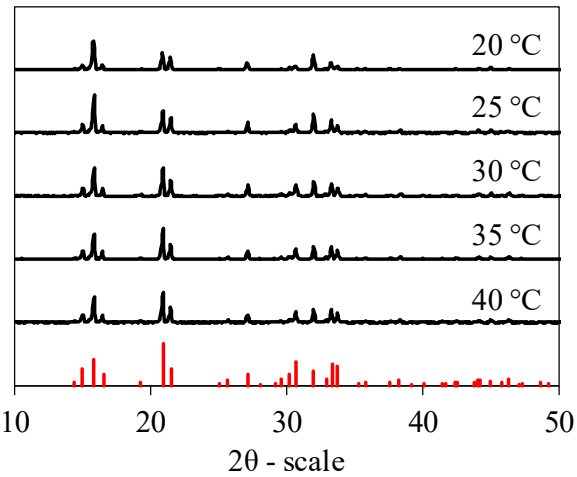

Figure 8.5: Diffractograms of precipitates at different temperatures, and pH 9.

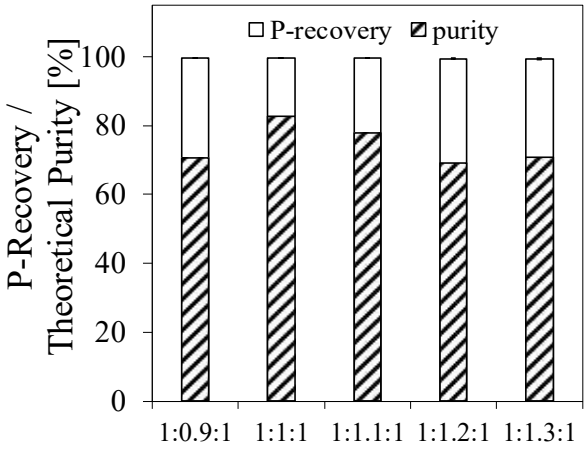

Figure 8.6: P-recovery at different Mg^{2+}-input ratio, 20 °C, and pH 9.

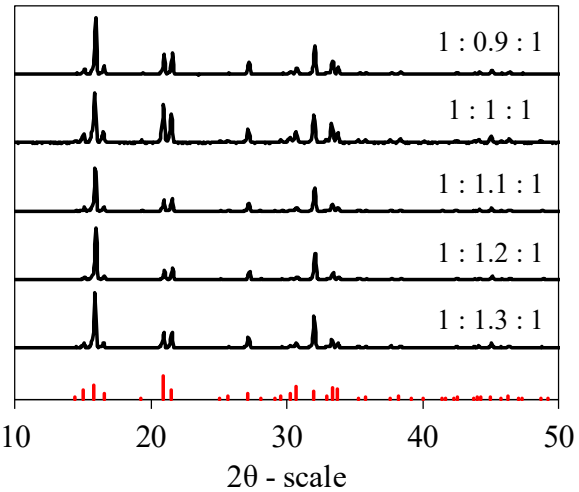

Figure 8.7: Diffractograms of precipitates at different Mg^{2+}-input ratio, 20 °C, and pH 9.

Struvite precipitation is achieved under moderately alkaline conditions. Consequently, reagents such as NaOH, MgO, KOH, NH_3, or CO_2 stripping are effective in adjusting the pH to the desired level [154,155]. The limitations of these approaches include the limited solubility of MgO and KOH, the energy-intense nature of the CO_2 stripping method, and potential ammonia losses due to aeration [156]. NaOH is a widely used and chemically available. The use of NaOH typically has minimal impact on the quality of the formed struvite [157]. Compared to other pH regulators, such as NH_3, the use of NaOH is less likely to lead to undesirable contaminants or byproducts [158]. Thus, NaOH was used as the precipitation agent. Several studies indicate that struvite precipitation is most favorable around pH 9. Tünay *et al.* identified pH values between 8.5 and 9.3 as optimal for precipitation using tannery wastewater [159]. Hao *et al.* conducted elemental analyses of precipitation products from synthetic wastewater at various pH levels, showing that a pH range of 9.0 to 9.5 is most favorable, with the purity of the recovered precipitate exceeding 90% [160]. Huang *et al.* observed a rapid increase in the reaction rate of struvite formation in response to a pH increase from 8.6 to 9.1 [161]. Quintana *et al.* found that pH 9 is optimal for the precipitation from the filtrate of digested sludge from the dewatering process at the Madrid (Spain) wastewater treatment plant [162].

In this study, a maximum P-recovery of over 99% and a maximum purity of 83% were achieved at pH 9, Figure 8.2. In addition, X-ray diffraction analysis showed the highest match with the struvite reference at this pH, Figure 8.3. Furthermore, the solubility product is lowest at pH 9 with a K_{sp} of $3.9 \cdot 10^{-12}$, indicating that struvite precipitation from the process water of enzymatic P-mobilization is most efficient at pH 9. However, other research indicates that higher pH values are ideal for struvite precipitation. Ohlinger *et al.* reported maximum precipitation at pH 10.3 [73], and Shin and Lee observed maximum struvite precipitation when the pH was increased to 10.5 [163]. The differences in the maximum pH values for struvite precipitation can be attributed to the variability in the composition of the treated wastewater in the different studies. Changes in the chemical composition of the wastewater lead to variations in ionic strength and ionic activity, which affect the precipitation potential [75]. In addition, the type of ionic species present in the wastewater affects the formation of struvite crystals and the struvite solubility product, Table 8.1. However, in order to further increase the struvite precipitation efficiency from P-mobilization wastewater and to identify maximum pH conditions, the pH range can be narrowed since the pH was studied in single unit intervals.

Temperature has a major influence on the solubility and morphology of struvite crystals and their formation. The higher the temperature, the higher the solubility of struvite and *vice versa* [164]. A higher temperature can increase the reaction rate and allow faster precipitation of struvite. However, it can also result in smaller crystals due to greater particle movement. At lower temperatures, the ions tend to move more slowly, which can result in larger and more defined crystals [165]. Considering the ratio of volume to surface area and the nutrient releasing properties of struvite, the morphology is of utmost relevance. In numerous studies, the temperatures between 25 °C and 35 °C are commonly regarded as maximal for struvite precipitation. Crutchik and Garrido demonstrated that elevating the temperature from 25 °C to 30 °C and 35 °C results in an increase in the solubility product of struvite, promoting the presence of lower purity crystals and their dissolution [82]. Consistent with the findings of Crutchik and Garrido, the determined purity decreases with increased precipitation temperature, Figure 8.4. Also depicted in Figure 8.4, the highest P-recovery of 98% and highest purity of 79% were achieved at 20 °C. At the same time, depending on the ambient temperature, 20 °C requires the least amount of energy to heat and is therefore the most economical. The purity recorded at 25 °C is considered an outlier. Furthermore, the solubility products rise from $1.4 \cdot 10^{-10}$ at 20 °C to $5.5 \cdot 10^{-7}$ at 40 °C as expected. Aage *et al.* similarly observed an increase in the solubility product up to 50 °C, with a subsequent decline only upon further temperature increase [166]. According to Moussa *et al.*, the ionic activities and the saturation coefficient increase with increasing temperature, which reduces the efficiency of crystal formation [167]. The degree of saturation also affects the crystallization process, as it leads to a shortening of the nucleation time and growth [167,168].

Struvite consists of an equimolar proportion of NH_4^+, Mg^{2+} and PO_4^{3-}, therefore incomplete precipitation or the formation of additional phases can occur if the ratios of the constituent ions in solution deviate [169]. Hence, controlling and adjusting the ions in solution according to stoichiometry can help ensure maximum precipitation of struvite and minimize unwanted by-products. Kim *et al.* showed that struvite formation is also influenced by the order in which precipitants are added. In particular, high struvite yields are obtained in NH_4^+ removal when the Mg^{2+} and PO_4^{3-} ions in solution dissociate prior to pH adjustment [170], but only low NH_4^+ concentrations (< 0.1 mM, Table 8.1) are present in the P-mobilization process wastewater. However, Siciliano *et al.* confirm that pH adjustment after addition of Mg^{2+} and PO_4^{3-} reduces precipitation of compounds other than struvite, such as calcium phosphates (3.3 mM Ca^{2+}, Table 8.1) [169,170]. Therefore, the precipitation reagents ($MgCl_2$, NH_4Cl) were added analogously before the pH adjustment with NaOH. Furthermore, ion species already present in the process wastewater were considered.

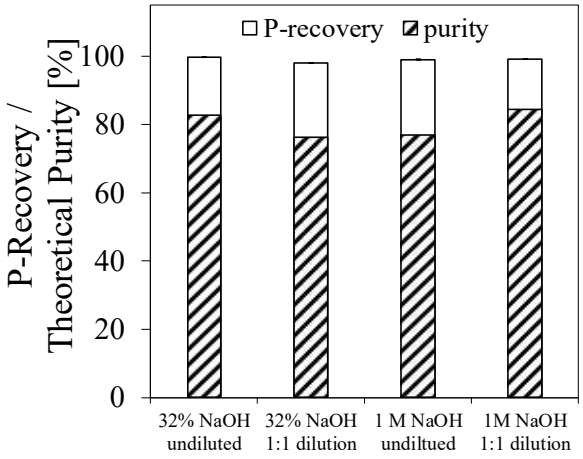

Figure 8.8: P-recovery at different NaOH concentrations, and dilutions, pH 9, and 20 °C.

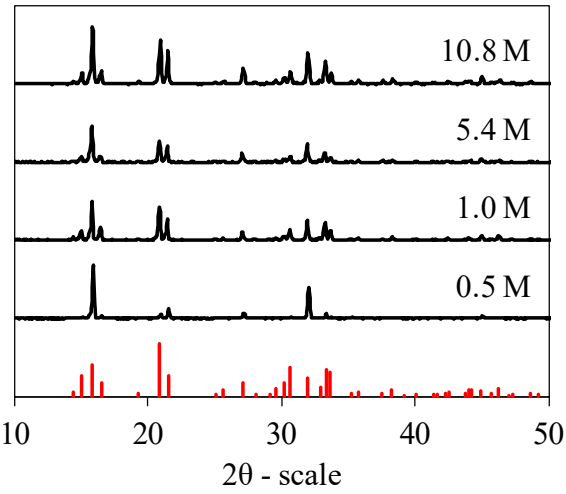

Figure 8.9: Diffractograms of precipitates at different NaOH conc., dilutions, pH 9, and 20 °C

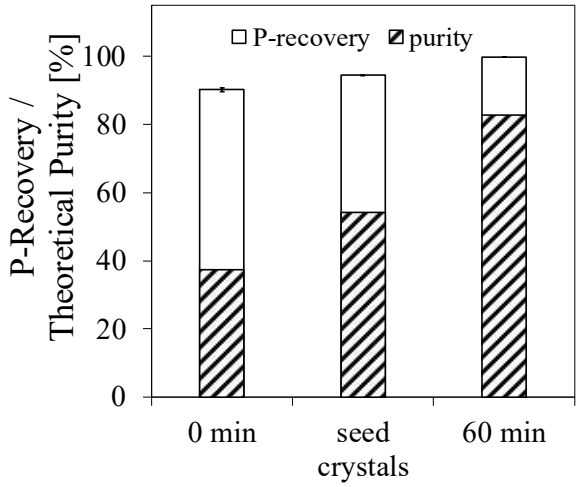

Figure 8.10: P-recovery at different nucleation conditions, pH 9, and 20 °C.

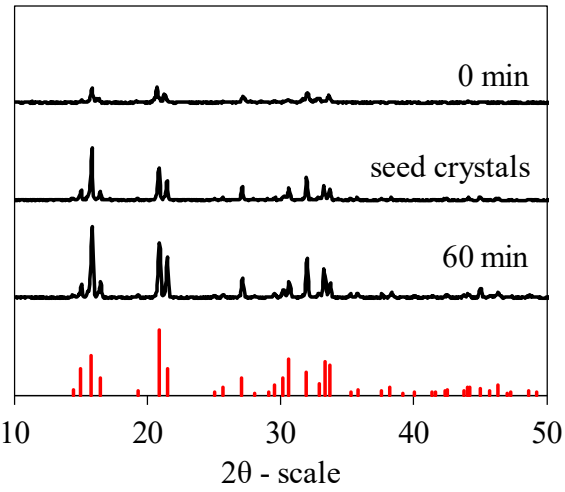

Figure 8.11: Diffractograms of precipitates at different nucleation conditions, pH 9, and 20 °C.

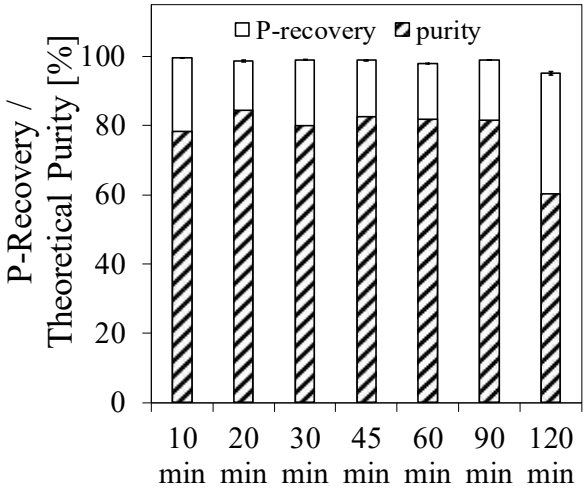

Figure 8.12: P-recovery after different stirring times ,pH 9, and 20 °C.

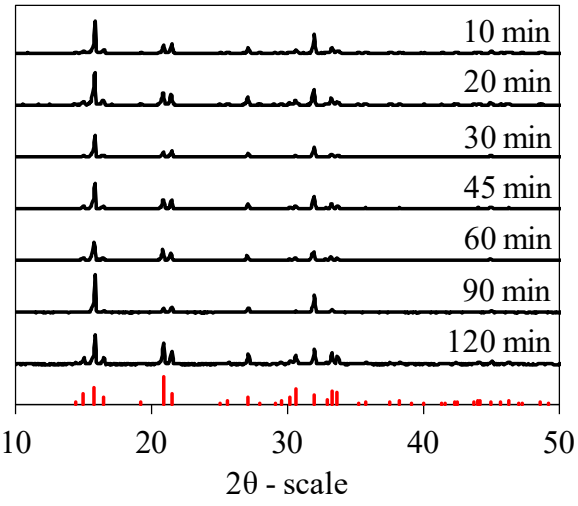

Figure 8.13: Diffractograms of precipitates after different stirring times ,pH 9, and 20 °.

According to the studies of Hutnik *et al.* the equilibrium of the precipitation reaction shifts towards struvite when an excess of Mg^{2+} ions is present [171]. However, as shown in Figure 8.6, a maximum P-recovery of more than 99% and a purity of 83% were observed at an equimolar ratio. A possible explanation for this contradiction is that the process wastewater differs from the wastewater in the aforementioned study, particularly with respect to the ions contained. The lower purity with a sub-stoichiometric (1:0.9:1) Mg^{2+} input ratio is in line with expectations, as struvite consists of an equimolar ratio. The ratio of P-recovery to purity indicates that there are other ionic species in solution that complex P, such as high K^{+} (104.9 mM, Table 8.1) and even low Ca^{2+} (3.3 mM, Table 8.1) concentrations. However, the X-ray diffraction patterns show that mainly struvite was formed, Figure 8.7. Contrary to expectations, the solubility of struvite increased from $3.9 \cdot 10^{-12}$ at an equimolar input ratio to $1.4 \cdot 10^{-11}$ at 1.3 times over-stoichiometric input ratio. Possible explanations are further complexation reactions, or ion pairing, effectively reducing the concentration of free Mg^{2+} ions and shifting the equilibrium towards more dissolved struvite. At higher stoichiometric input ratios, however, incomplete precipitation or formation of additional phases may occur, leading to reduced purity at over-stoichiometric Mg^{2+} input ratio, Figure 8.7.

Both the concentration of the precipitating reagent and the ion concentration in the process wastewater can affect P-recovery and purity. Therefore, the use of a 1 M NaOH solution and a 32% (10.8 M) NaOH solution were compared with respect to 1:1 diluted and undiluted process wastewater. The highest P-recovery of over 99% was observed using a 32% NaOH solution in undiluted process wastewater and a 1 M NaOH solution in diluted wastewater, Figure 8.8. Both experiments also achieved the highest struvite purity, 83% and 84%, respectively. This is reflected in the solubility products, with the lowest values within this series of experiments being in the range of 10^{-12}, Table B. 5 From a process engineering and economic perspective, the undiluted state of the substrate is advantageous, as it results in lower volumes to be processed and minimizes the wastewater stream. For similar reasons, a more concentrated alkali solution is preferable. Using a 1 M NaOH solution requires approximately ten times the volume compared to a 32% NaOH solution (10.8 M) to achieve the desired pH level. Additionally, the target pH is reached faster at the same titration rate, accelerating the reaction and reducing undesirable side reactions. Furthermore, the X-ray diffraction patterns show the greatest alignment when using undiluted process wastewater and the concentrated NaOH solution, Figure 8.9.

The crystallization process generally includes supersaturation by the addition of a precipitating agent, nucleation, and growth. Nucleation refers to the formation of crystal embryos and is mainly a reaction-controlled process [157]. At higher supersaturation, larger concentrations of ionic constituents are available, which shortens the lag time for nucleation [73]. Nucleation can occur both homogeneously and heterogeneously through the addition of existing surfaces. Growth refers to the incorporation of ionic components into an existing crystal lattice structure and follows nucleation. It is mainly a transport-limited process.

Thus, the mixing energy has a significant influence on the nucleation and growth of struvite crystals. By manipulating the mixing conditions, crystal growth can be controlled and a desired accumulation can be favored [156]. To investigate the influence of mixing on struvite formation in the process wastewater, mixing was stopped after adjusting the pH to 9, and seed crystals were added, or convection (Re = 10326, turbulent) was added to the system for 60 min after pH 9 was reached. As shown in Figure 8.10, the highest P-recovery of over 99% and the highest purity of 83% were determined for the system under convection. The solubility product of $3.9 \cdot 10^{-12}$ is also considerably lower compared to the other two experiments. Here the solubility product is in the range of 10^{-8}, Table B.6. It is also noted that the P-recovery and struvite purity are higher with the use of seed crystals than without the use of seed crystals and without convection. Ohlinger *et al.* showed that the lowest growth rates during struvite formation occur in rest zones, while the highest rates are always found in zones with high convection [73]. In addition, Ohlinger *et al.* found that preferential accumulation occurs in locations with high mixing energy [157]. Furthermore, it was shown that the mixing energy has the greatest influence on overcoming transport limitations during crystal growth [78]. However, based on Figure 8.10, convection in the system has also a clear influence on the nucleation. Convection leads to a homogeneous distribution of ions in solution, which increases the probability of collisions, causing them to react and form struvite crystals. In addition, the X-ray diffraction patterns of precipitates formed without convection show different phases, Figure 8.11, indicating a higher degree of impurities or a lower homogeneity of the crystals, correlating with the calculated purities.

Since convection is crucial for struvite formation, it was investigated whether the time of convection input after pH adjustment has an effect on struvite formation. Longer convection input may result in better crystallization and more uniform particles [74,172]. Figure 8.12 shows that the maximum purity of 84% is achieved after 20 min of stirring (40 mL, 900 rpm). P-recovery is greater than 99% for almost all stirring times except 120 min. Stirring times of 45, 60 and 90 min show only slight differences in purity (82% to 83%). However, after 120 min of stirring, the purity decreased to 60%. The maximum process parameters for precipitation from previous experiments were used, which improved the reaction kinetics and increased the precipitation efficiency. However, sufficient stirring time is required to ensure a uniform distribution of the constitution ions (NH_4^+, Mg^{2+}, and PO_4^{3-}) in solution. Thus, after 20 min, struvite formation is complete. A long stirring time of more than 90 min can lead to excessive growth of the struvite crystals, resulting in impurities, Figure 8.12 and Figure 8.13 [74,172]. It is also noticed that the solubility product increases with increasing stirring time ($9.5 \cdot 10^{-12}$ at 10 min to $1.3 \cdot 10^{-9}$ at 120 min). Accordingly, supersaturation was achieved within a shorter stirring time and a longer energy input leads to dissolution of the struvite constitution ions.

8.2.3 Scalability of Struvite Precipitation

The scale-up of struvite precipitation, expanding from 40 mL to 1.7 L, was conducted under the optimized process conditions previously identified (pH 9, 20 °C, 32% NaOH solution, and a stoichiometric ratio of precipitants as outlined in Chapter 8.2.2). Convection in the system was shown to be decisive for precipitation. Thus, a constant volumetric power input was chosen as the scale-up criterion. The power input for the stirrer was calculated according to Equation 8.4.

$$P = Ne \cdot \rho \cdot n^3 \cdot d^3 \qquad \text{(Eq. 8.4)}$$

P is the power input of the impeller [W], Ne is the Newton number [-] and depends on the type of impeller, ρ is the density [kg·m^{-3}], n is the impeller speed [s^{-1}] and d is the outer diameter of the impeller [m]. The Newton number Ne has been determined empirically for different stirrer types as a function of the Reynolds number (Re) and can be found graphically in the literature [173]. In the laminar flow regime, Ne is directly proportional to Re, while in the turbulent flow regime it is independent of Re. The Reynolds number can be calculated using Equation 8.5. The value ν represents the kinematic viscosity [m^2·s^{-1}].

$$Re = \frac{n \cdot d^2}{\nu} \qquad \text{(Eq. 8.5)}$$

Taking into account the density and dynamic viscosity of the process wastewater (Chapter 8.1), a volumetric power input of 419 W·m^{-3}· was set. The titration curve for the scale-up experiments is shown in Figure 8.14.

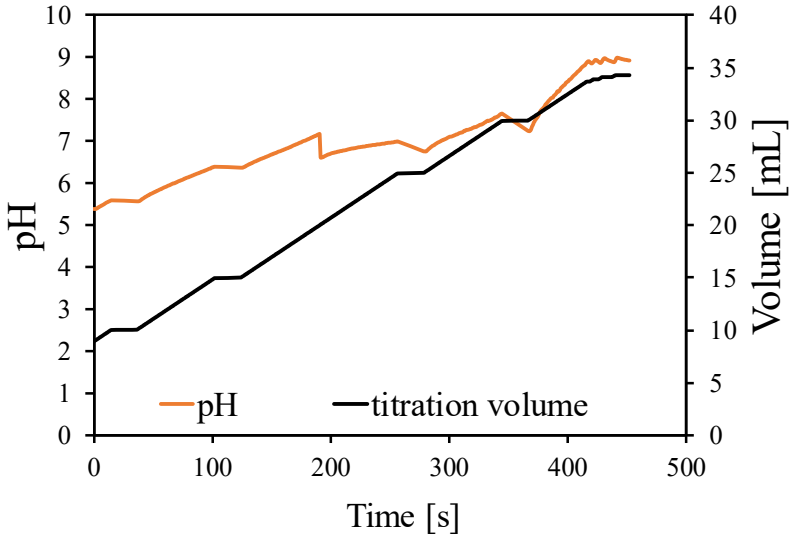

Figure 8.14: Titration curve during the scaling of struvite precipitation at pH 9, 20 °C, and an equimolar input ratio of the constitution ions.

Using a pre-titration volume, the initial pH curve begins slightly above pH 5. The titration curve exhibits a discontinuous pattern due to the 5 mL increment of the titration burette. Compared to the volume curve, the pH curve has a gentler slope, suggesting that impurities such as Ca^{2+} or K^{+} ions, or other ions that bind OH^{-}, may be precipitating. Upon reaching pH 7, a noticeable drop in pH is observed at approximately 180 s, indicating the onset of struvite precipitation. The subsequent pH course also indicates the ongoing precipitation of struvite. The observed fluctuations after reaching the target value of pH 9 at around 420 s are attributed to an inherent delay associated with the supersaturation of struvite, Figure 8.14 [174].

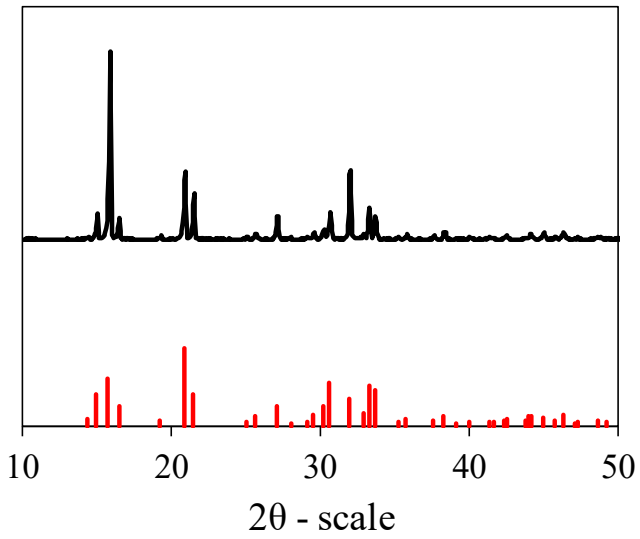

Figure 8.15: Diffractogram of the precipitate produced during scaling at pH 9, 20 °C, and an equimolar input ratio of the constitution ions.

The X-ray diffraction pattern in Figure 8.15 confirms that the precipitate obtained is predominantly struvite. A purity of 80% was determined. However, to determine the nature of the impurities more precisely, a thermogravimetric analysis was performed, Figure 8.16. Based on the mass balances, it is assumed that complete dehydration occurs up to 110 °C (25 °C → 110 °C), contrary to the thermal decomposition described by Paul *et al.* [175]. Alternatively, the mass balance is closed when five of the six crystal water are liberated and deamination occurs. Nonetheless, due to the complexation of NH_3, complete dehydration up to 110 °C is more likely. This is also consistent with the results of the dry substance determination.

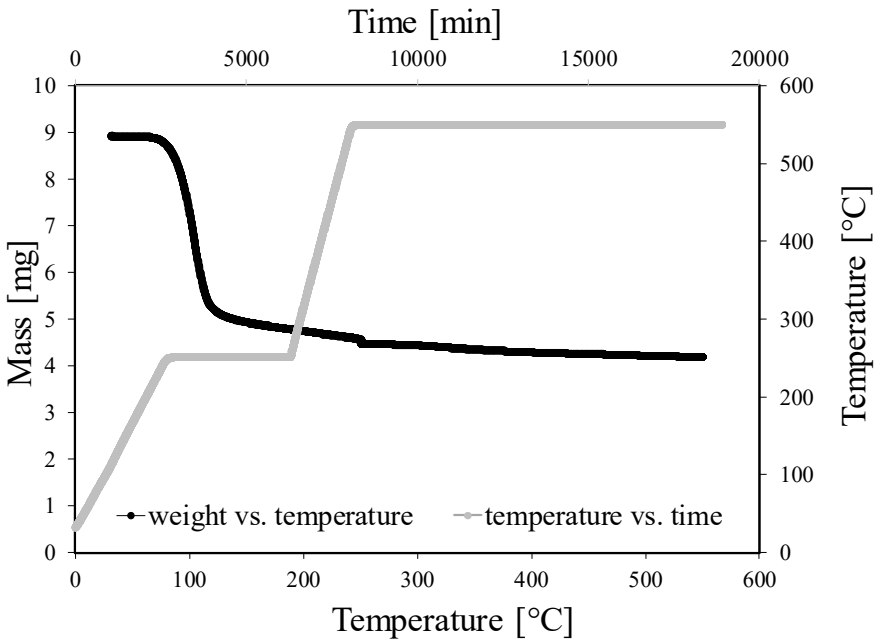

Figure 8.16: Thermogravimetric analysis of the precipitate produced during scaling pH 9, 20 °C, and an equimolar input ratio of the constitution ions.

Accordingly, deamination takes place up to 550 °C and the organic components contained are pyrolyzed (110 °C → 550 °C). Above 550 °C, only inorganic components remain. The following reaction equations are postulated, Equation 8.6 and 8.7.

$$25\ °C \rightarrow 110\ °C: \quad MgNH_4PO_4 \cdot 6\ H_2O \rightarrow MgNH_4PO_4 + 6\ H_2O \qquad \text{(Eq. 8.6)}$$

$$110\ °C \rightarrow 550\ °C \quad 2\ MgNH_4PO_4 \rightarrow Mg_2P_2O_7 + 2\ NH_3 + H_2O \qquad \text{(Eq. 8.7)}$$

To determine the percentages of water, organic and inorganic impurities, the initial amount of struvite ($n_{struvite}$) at 25 °C was used, taking into account the determined purity (R), Equation 8.8.

$$n_{struvit} = \frac{m_{25°C} \cdot R}{M_{Struvit}} \qquad \text{(Eq. 8.8)}$$

Based on the initial amount of struvite and the weight loss due to dehydration, the percentage water content W was calculated, Equation 8.9.

$$W\ [\%] = \frac{m_{25°C} - m_{110°C} - n_{struvite} \cdot 6\ M_{H_2O}}{m_{25°C}} \cdot 100 \qquad \text{(Eq. 8.9)}$$

The percentage of organic matter (O) in struvite is determined according to Equation 8.10, taking into account the deamination and the conversion of two moles of magnesium-ammonium-phosphate to one mole of magnesium-pyrophosphate:

$$O\ [\%] = \frac{m_{110°C} - m_{550°C} - 0.5\ n_{struvite} \cdot (2\ M_{NH_3} + M_{H_2O})}{m_{25°C}} \cdot 100 \qquad \text{(Eq. 8.10)}$$

The total impurity is the sum of the water, organic, and inorganic components. Therefore, Equation 8.11 applies to the percentage fraction of inorganic impurity I:

$$I\,[\%] = 100\,[\%] - R\,[\%] - O\,[\%] - W\,[\%] \qquad \text{(Eq. 8.11)}$$

This results in an impurity composition of 6% water, 4% organics and 11% inorganics for the produced struvite. An elemental analysis revealed that inorganic impurities are mainly potassium, Table B.8, consistent with the observations from the titration curve and Table 8.1. Despite of these impurities, the precipitated struvite remains suitable for use as a fertilizer, as conventional fertilizers typically consist of nitrogen, phosphorus, and potassium, which aligns with the composition of the impure struvite. The minimal organic content of the precipitated struvite does not adversely affect its potential or effectiveness as a fertilizer.
The light microscopic images of the struvite crystals are presented in Figure 8.17. The crystals predominantly exhibit a coffin-like morphology, with an average size of approximately 5 µm. Compared to dendritic or twin-structured crystals, these coffin-shaped crystal have a lower surface-to-volume ratio. This characteristic results in a slower mineral release rate into the soil, facilitating a controlled release of nutrients. The advantages are a more efficient nutrient uptake by plants, reduced risk of over-fertilization and nutrient loss through leaching, which can occur during heavy rainfall. Ultimately, the slow release of nutrients reduces the risk of eutrophication.

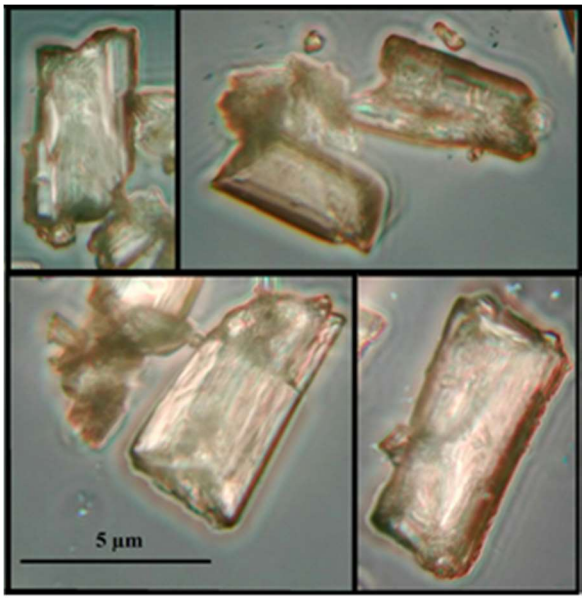

Figure 8.17: Section of the light microscopic images of the struvite precipitates produced during scaling.

Despite the prevalence of coffin-like crystals, some dendritic and twin-structured crystal were also found among the struvite precipitates. Concluding, it could be shown, that the concept of struvite precipitation from wastewater treatment is applicable to the process wastewater from enzymatic P-mobilization and can effectively scaled up.

8.2.4 Purification of Struvite

It was investigated whether the purity of struvite could be increased by subsequent agitation in polar protic (boiling water, methanol, ethanol, isopropanol, 1% HCl, 1% acetic acid), polar aprotic (acetone, acetonitrile), and nonpolar aprotic (ethyl acetate, methyl tert-butly ether, isooctane) solvents as well as by recrystallization. For this, the struvite produced in the scale-up experiment was used. The thermogravimetric and X-ray diffraction analyses after each treatment are shown in Figure B.17. The results clearly show that all treated precipitates can be identified as struvite. However, the diffractograms of the precipitates purified by recrystallization and boiling water show that additional phases are present. Figure 8.18 shows the respective changes of the impurities in the struvite crystal (water, organic and inorganic impurities) in relation to the initial impurity. The calculation was done analogously to Chapter 8.2.3.

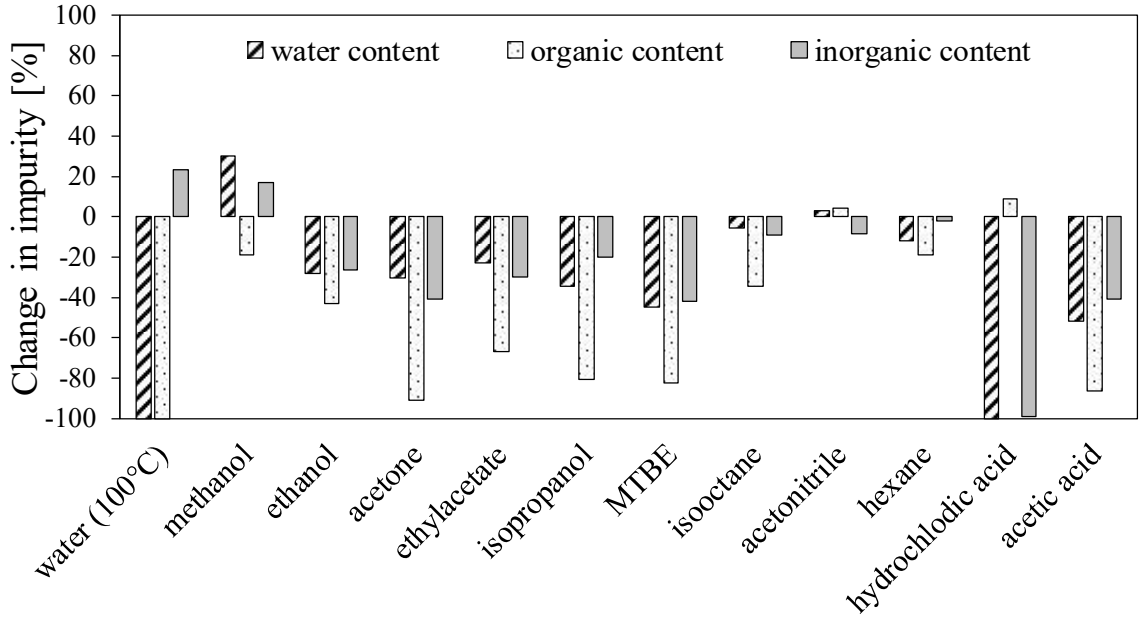

Figure 8.18: Percentage change in impurity compared to the initial impurity after washing in various solvents and subsequent vacuum filtration.

By monitoring the pH during recrystallization (not shown in Figure 8.18), it was observed that the precipitate completely dissolves at pH 2. The titration curve flattens at pH 6, Figure B.16, indicating the onset of struvite precipitation. The percentage composition of the precipitate during purification exceeds 100%, due to the lower mass of the precipitate after treatment, indicating incomplete recrystallization, which is also reflected by the diffractogram, Figure B.17. The percentage of water and organic content increased after purification, while inorganic impurities decrease. The addition of HCl to the system during recrystallization reduces inorganic impurities, probably through the formation and removal of chlorides. However, an increase in organic content is not plausible, as no additional organic matter has been added to the system and is therefore artificially increased due to measurement uncertainties.

Furthermore, recrystallization can change the crystal structure of the precipitate, which can lead to a different distribution of the components and additional water absorption. This increase also causes the clearly greater mass loss over temperature, Figure B.18.

Agitation in isooctane, acetonitrile, and hexane show negligible differences from the untreated sample, indicating that only moderately polar organic contaminants are likely present. Methanol treatment has minimal effect on the precipitate compared to its original state. Ethanol, acetone, ethyl acetate, and methyl tert-butyl ether (MTBE) effectively reduce organic impurities and wash out water, with acetone providing the best reduction. The decrease in the water content is presumably due to the entrainment of water molecules during the evaporation of the respective solvents. According to the elutropic series, acetone is effective in removing a wide range of organic impurities, due to its moderate polarity. Compared to the organic solvents tested, it is central positioned in the elutropic series, indicating sufficient solvent strength and versatility. It can effectively dissolve and elute both polar and some nonpolar compounds. In addition, the high volatility makes it a suitable solvent for purification, and it is widely available at a reasonable cost. It is also less toxic than other solvents tested, making it suitable as purification agent. Moreover, the low efficiency of protic solvents as well as the greater efficiency of aprotic solvents suggests, that organic impurities are most probably present in the form of inclusion bodies.

The highest purification was achieved with 1% HCl, which gave a purity of about 96%, leaving 4% organic impurities. The water content was completely removed and the inorganic impurities were completely reduced, although a slight apparent increase in the organic content was within the measurement error and negligible. The reduction in inorganic impurity is most likely facilitated by ion exchange, the dissolution of monovalent cations such as K^+, increased struvite solubility, or the displacement by a stronger acid. HCl dissociates into H^+ and Cl^- ions in aqueous solution. The H^+ can replace K^+ ions that are associated with the struvite matrix other impurities. In addition, the dissolution of organic impurities helps to separating them from the solid struvite. Furthermore, the acidic environment enhances the solubility, not only of struvite but also of other inorganic compounds, allowing them to be washed out more easily. Moreover, if P is not present as struvite, HCl can also expel phosphate as struvite, as HCl is a stronger acid than phosphoric acid.

Purification with 1% acetic acid showed similar results to MTBE, with a reduction in inorganic impurities and a substantial reduction in organic content of approximately 80% compared to the initial sample. The slight reduction in water content suggests that acetic acid, an organic acid, may bind and remove organic contaminants from the struvite crystals.

In conclusion, protic solvents are suitable for the removal of organic contaminants, while aprotic solvents are suitable for the removal of inorganic contaminants, as expected. However, the fact that not all organic impurities could be removed with any of the solvents used indicates that both polar impurities, such as carbohydrates, and nonpolar organic impurities, such as fatty acids, are present consistent with the findings in Chapter 7.1. Nevertheless, given that the struvite from the process wastewater of the enzymatic P-mobilization already has suitable fertilizer properties, further downstreaming may not be necessary. Nonetheless, if further downstreaming is required due to, for example, changes in regulations, purification with 1% HCl is most efficient but does not remove the organic fraction. The latter could be removed by a subsequent purification step with acetone.

8.3 Phenol Recovery

As shown in the previous chapters, the process of enzymatic P-mobilization depends on the solubilization of inositol phosphate in the aqueous phase. This mass transfer occurs via the penetration of the cell wall and is facilitated by the weakening of the cell wall during the soaking process in the aqueous phase, the abrasive effect of the stirrer as well as by additional treatment steps (Chapter 6.4). The weakening of the cell wall results in the solubilization of cell wall constituents, such as phenolic components (Chapter 7.1). Phenols find application in various industries, including the production of synthetic tannins, tire production, and in the treatment of wood-based materials. Commercially, phenols are predominantly produced by cumene peroxidation (Hock process). As a result, phenols are subject to price fluctuations and the availability of crude oil. Therefore, the demand for phenolic components of biogenic origin is increasing. Consequently, the recovery of these components from the process wastewater after enzymatic P-mobilization can contribute to the economic establishment of the overall process. For the liquid-liquid extraction of phenolic components from the process wastewater after P precipitation, various solvents were tested in a one-to-one volume ratio according to the elutropic series. This screening showed that methyl-tertiary-butyl ether (MTBE) and ethyl-actetate are the most promising solvents tested with extraction efficiencies of around 10% and 7%, respectively, Figure B.19. To improve the extraction efficiency, the process wastewater was acidified, which protonates the phenols, making them more hydrophobic and thus more likely to partition into the organic phase. In addition, salting-out effect according to the chaotropic series was investigated for the two selected solvents by saturating the process wastewater with Na_2SO_4, both individually and in combination with acidification. The combination of both methods increased the extraction efficiency to approximately 25% for both solvents, Figure B.20. However, the low efficiency of the tested liquid-liquid extractions renders this approach uneconomical.

It was investigated whether solid-liquid extraction, where the adsorbates (phenolic compounds) adsorb onto an adsorbent (resin), is a valid method for the extraction. Given the likely broad distribution of molecular weights of phenolic compounds in the process wastewater, various resins were tested. According to the manufacturer's specifications, the resins XAD 4, XAD 16, XAD 1180 (Amberlite®) were examined for the adsorption of low, medium and high molecular weight molecules, respectively. These resins are intended for the removal of organic compounds from aqueous solutions. Additionally, resin XAD 7HP (Amberlite®), specifically designed for the adsorption of phenols and polyphenols, and silica gel 60 (Merck) as a reference material, were tested. In Table 8.3, the resins the physiochemical properties of the resins are given.

Table 8.3: Physiochemical properties of the resins used for phenol recovery from the process wastewater.

	XAD 4	XAD 16	XAD 7HP	XAD 1180	Silica gel
Material	Styrene-divinylbenzene copolymer	Styrene-divinylbenzene copolymer	Polyacrylate	Styrene-divinylbenzene copolymer	Amorphous silicone oxide
Pore size (Å)	90	100	200	90	20 to 1000
specific surface area [$m^2 \cdot g^{-1}$]	750	800	450	700	300 to 800
Polarity	nonpolar	nonpolar	polar	nonpolar	polar
Swelling capacity	low	medium	high	low	none
Chemical stability	high	high	good	high	low stability in strong bases or acids

In addition to the extraction efficiency, it was investigated whether adjusting the pH of the process wastewater has an effect on the adsorption capacity of the different resins, Figure 8.19. It is noted that before use, washing the resins for 30 min in ethanol, followed by vacuum filtration and subsequent repetition of the procedure with 100 mM NaOH, along with drying for 24 h, increased the extraction efficiency. For example, the extraction efficiency of XAD 16 increased from 20% to 52%. Furthermore, a blank has shown that no phenols are degraded by e.g. oxidation through exposure to the atmosphere over the time periods investigated. For an economic process design, incubation was done at room temperature.

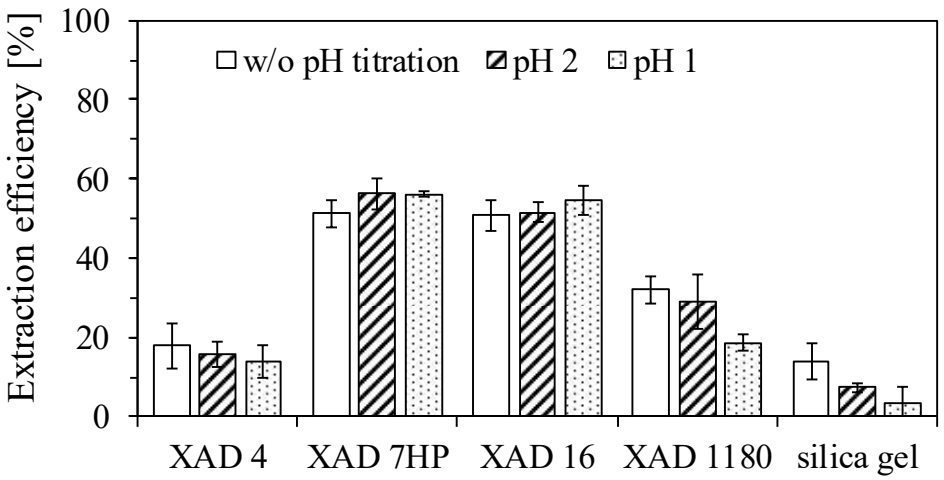

Figure 8.19: Removal efficiency of the tested adsorbents without adjusting the pH of the process wastewater and adjusting to pH 1 and pH 2. 50 mg·mL^{-1} adsorbent, room temperature and shaken overnight.

As depicted in Figure 8.19, only adsorption onto XAD 1180 and silica gel is pH-dependent. However, for both resins, the highest extraction efficiency occurred without pH titration, specifically pH 4.4 (Chapter 6.2). This behavior was to be expected from silica gel due to its poor stability in an acidic environment. Furthermore, silica gel exhibited the lowest overall extraction efficiency, while XAD 7HP and XAD 16 showed the highest efficiency. The distribution of the extraction efficiency of XAD 4, 16, and 1180 indicates a similar molecular weight distribution of adsorbed phenolic compounds. Based on the similarly high extraction efficiency of XAD 7HP and XAD 16 (acrylic and sterene-divinylbenzene functionalization, respectively), it is reasonable that the process wastewater contains a considerable amount of polyphenols. However, based on the collected data quantitative statements about the quantity of polyphenols is not possible.

The amount of adsorbents was varied up to the maximum possible concentration in the liquid phase, Figure 8.20. It can be seen, that adsorbent concentrations above 55 mg·mL^{-1} do not show any reasonable improvement. However, the sum of either XAD 7HP or XAD 16 in combination with XAD 4 and XAD 1880 would achieve full adsorption of the present phenols, which further supports the manufacturer´s specification that phenolic compounds with a certain molecular weight bind to a certain resin.

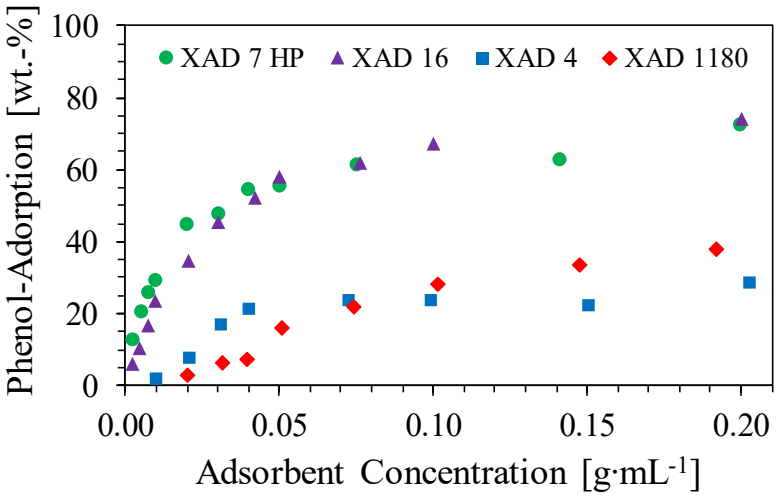

Figure 8.20: Percentage mass fraction of adsorbed phenols as a function of adsorbent concentration for the different resins.

In order to confirm the hypothesis and to recover all phenolic compounds, present in the wastewater, phenols were adsorbed on XAD 16 at a concentration of 55 mg·mL^{-1} (20 °C, overnight) and subsequently from the supernatant using XAD 4 or XAD 1180. A total of 56% of the phenolic compounds were adsorbed onto XAD 16. From the supernatant, adsorption efficiency at various XAD 4 and XAD 1180 concentrations was investigated, Figure 8.21.

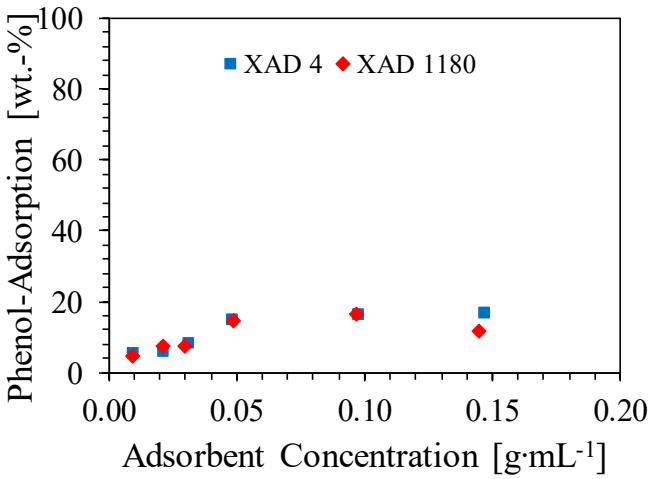

Figure 8.21: Percentage mass fraction of adsorbed phenols on XAD 4 and XAD 1180 after adsorption onto XAD 16 as a function of adsorbent concentration. Shaken overnight at room temperature. 56% of the phenols present in the process wastewater were previously adsorbed onto XAD 16.

As can be seen from Figure 8.21, contrary to expectations, only about 20% of the remaining phenols and thus 9% of the total phenols present in the wastewater were adsorbed. A possible explanation for the unexpected results is that the content of polyphenols determined by the Folin-Ciocalteu assay is overestimated, as described by Geogé *et al.* [176]. Since a large proportion of the phenols primarily present have already been adsorbed by XAD 16 resin, a small fraction of phenols that do not bind to any resins tested or other interfering compounds, lead to uncertainties in the determination. This thesis is supported by the fact that the mass balance is not closed by the values recorded. Nevertheless, a subsequent or combined adsorption process is not suitable for an economic process design.
An adsorption isotherm was recorded for each of the two most efficient resins (XAD 16, XAD 7HP) to determine their suitability. The data obtained was linearized according to the Freundlich model, Equation 8.12.

$$q = K_F \cdot c_{eq}^{n} \qquad \text{(Eq. 8.12)}$$

where q [mg·g^{-1}] corresponds to the load of sorbent, and c_{eq} [mg·mL^{-1}] to the equilibrium concentration of the sorbate in solution. K_F [g·mL^{-1}] is the Freundlich coefficient and n is the Freundlich exponent. The exponent describes the heterogeneity of the adsorbent. For $1 < n < 10$ the adsorption process is favorable.

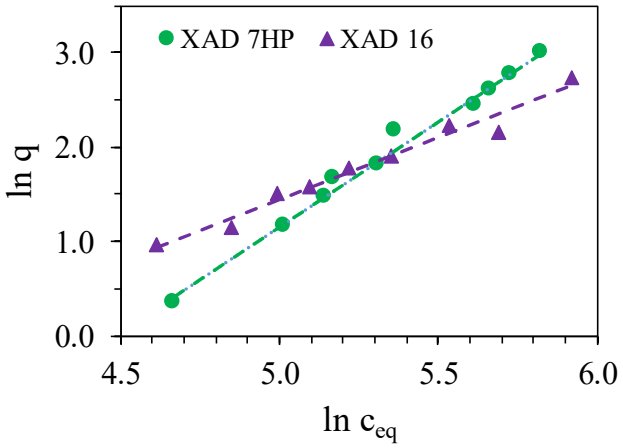

Figure 8.22: Sorption isotherms of XAD 7HP and XAD 16 according to the Freundlich model.

With a coefficient of determination R^2 of 0.99 for XAD 7HP and 0.97 for XAD 16, the adsorption process is satisfactorly described by the Freundlich model. However, with a Freundlich exponent n of 0.45 for XAD 7HP and 0.76 for XAD 16, both resins appear not suitable for the adsorption process, XAD 16 is, however, more suitable than XAD 7HP. Nevertheless, considering the effect of inaccurate determination of phenol concentrations by the Folin-Ciocalteu assay, the performances of the both resins are expected to be higher.

Besides the adsorption process, the desorption is crucial for the recovery of phenolic compounds contained in the process wastewater. The desorption was investigated using a temperature shift, but no clear differences were found, Figure B.21. Therefore, the desorption was carried out with organic and alkaline solution. Desorption of adsorbed phenolic compounds from XAD 16 was achieved by agitation in 0.1 M NaOH followed by agitation in ethanol, Figure 8.23. In addition, the recyclability of XAD 16 was investigated with a view to economic process design. The adsorbates were dried for 24 h between each cycle.

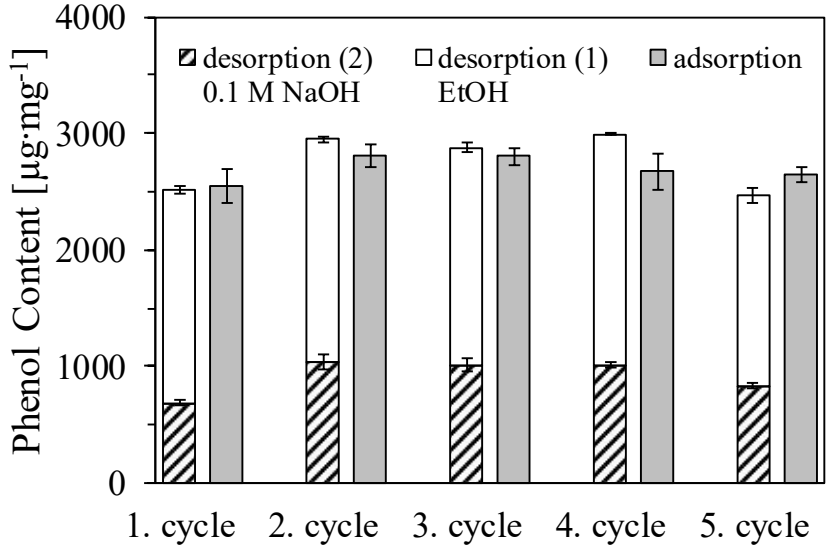

Figure 8.23: Desorption of phenols in 0.1 M NaOH and ethanol as well as recyclability of XAD 16.

As shown in Figure 8.23, the mass balance reveals complete desorption of the adsorbed phenols by the desorption procedure, with deviations within the range of the triplicates. Furthermore, the XAD 16 adsorbates remain stable over at least five cycles without any noticeable reduction in adsorption capacity, making the resin a viable option for multiple uses. The desorption process itself is the same as the regeneration process. Therefore, additional labor is minimized. However, after desorption, recovery from two different phases, one of which is an aqueous phase, is energy intense and requires different distillation operations. A water/ethanol solution is also challenging to separate due to the azeotrope at 96 wt.-% water. Further desorption procedures should therefore be considered in future studies.

In conclusion, the combination of resins only slightly increases the efficiency of phenol adsorption. It has been shown that among the resins used, XAD 16 resin is the most suitable for adsorption of phenols from the process wastewater. Further refinement of the analytical methods, by e.g. liquid chromatography, is required to improve accuracy of phenol determination. If the improved analytics show that utilization of XAD 16 does not lead to complete adsorption of existing phenols, further resins can be investigated. For this, bentonites display an suitable option [177].

8.4 Process Wastewater as 2nd Generation Feedstock for Microbial Fermentation

The second-generation bioconversion industry holds promise by transforming cellulose-based, nonedible biomass and agricultural waste into clean, affordable, high-value fuels or chemicals [178]. This potential is largely dependent on enzymes, such as cellulases and xylanases, which effectively hydrolyze plant cell walls into fermentable sugars [179]. To further establish economic viability and minimize waste streams of the enzymatic P-mobilization process, the process wastewater was used for microbial fermentation. *E. coli* BL21, a commercially relevant strain, was chosen as a model organism. After P-precipitation, the process wastewater was autoclaved with no additional pretreatment. The contained nutrients, particularly carbon sources, are detailed in Chapter 8.1. Figure 8.24 illustrates the growth of *E. coli* BL21 in autoclaved process wastewater over the time period of 10 h in a 250 mL baffled shake flask. The growth phases, including the lag phase, the exponential growth phase, and the stationary phase, are marked by vertical dashed lines.

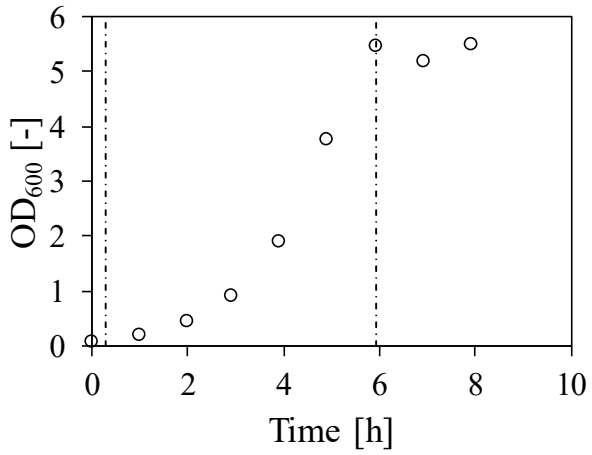

Figure 8.24: Growth curve of E. coli BL21 in baffled shake flask on autoclaved process wastewater after P-recovery. Optical density measured at 600 nm.

Figure 8.24 shows the typical growth behavior of a batch culture. The growth rate was calculated to be 0.71 h^{-1}, with a doubling time of 0.97 h, which is twice as long as expected in LB medium, indicating nutrient limitation. However, the maximum optical density at 600 nm is comparable to that in LB medium. Considering the high sugar content in the process wastewater, Table 8.2, and the final optical density, it is inferred that the previously precipitated nitrogen and phosphorus, or other components crucial for growth are limiting the growth rate. However, the typical growth curve and final optical density suggesting that the process wastewater can be used as second-generation feedstock for fermentation. Nevertheless, for high cell density cultivation, higher carbon source content and the identification and supplementation of limiting nutrients is necessary. In addition, there is a risk of contamination if the process wastewater is stored under non-sterile conditions. Therefore, proper handling and storage protocols have to be established to ensure the viability and safety of using P-mobilization process wastewater in large-scale bioconversions.

8.5 Interim Summary

- 50 mM P, about twice as much K^+ and 20 mM Mg^{2+} were detected in the process wastewater. Small amounts of Ca^{2+} were also detected. The NH_4^+ level is just above the detection limit (< 0.1 mM). Various oligomeric sugars were also found.

- The concept of struvite precipitation from wastewater treatment is applicable to the process wastewater from enzymatic P-mobilization and is straightforward scalable.

- Struvite precipitation from the process wastewater is at its maximum at pH 9, 20 °C, with an equimolar input ratio of constitution ions, and concentrated alkaline solution as precipitant. In addition, convection in the system was shown to be decisive for precipitation. Precipitation is completed 20 min after reaching pH 9.

- Under maximum process conditions, P recoveries of 99% were achieved with a struvite purity of over 90%.

- There are low levels of organic and inorganic impurities. The latter are mainly K^+ and its corresponding precipitates.

- Organic impurities can be removed with acetone, inorganic impurities with 1% HCl solution. However, due to the nature of the impurities, downstream processing does not appear to be necessary.

- Among the resins tested, the resin XAD 16 (Amberlite®) proved to be the most efficient in phenol adsorption and is stable over at least five cycles. However, not all phenols were adsorbed. A reason could be the overestimation by the Folin-Ciocalteu assay as described by Georgé et al. [176].

- The growth of *E. coli* BL21 on the process wastewater proofs that the wastewater is suitable as 2nd generation feedstock due to the carbohydrate fraction present. However, there is a high risk of microbial contamination if stored under non-sterile conditions.

9 Overall Discussion and Outlook

In this chapter, the main results of the investigation of the enzymatic P-mobilization process are presented and implications and limitations are discussed. In addition, recommendations for a possible process design and prospective for future work are given. The results of the individual chapter are discussed within each chapter and in a cross-chapter context.

9.1 Overall Discussion

The current method for the reduction of inositol phosphates in animal feed is the supplementation of phytates to the animal's diet. However, due to unfavorable conditions in the intestinal tract of monogastric animals, the hydrolytic efficiency of phytases is limited, resulting in incomplete digestion and eutrophication through the manure pathway. Thus, the process of biotechnological P-mobilization from feed material prior to feeding is described and investigated in this thesis. The process aims to produce value-added, P-depleted feed, and to recover the mobilized P for use as fertilizer, allowing the valorization of all process fractions.
For any process development, appropriate analytics to detect target molecules in a fast manner is essential. FT-MIR spectroscopy, offers the advantage of reduced sample handling, rendering this technique suitable for inline analysis. However, a distinct differentiation between orthophosphate and inositol phosphates in aqueous solution on the basis of mid-infrared spectra is not possible. Nevertheless, by applying a mass balance for P and considering the effect of water compression due to the addition of rye bran to the system, the residual inositol-P content in the plant material can be determined. The developed inline analytical approach uses PLSR modeling to predict the time-dependent P concentrations in the liquid phase of the bran-water suspension, with an RMSEP of 81 $mg_P \cdot 100g_{bran}^{-1}$ compared to wet chemical methods (Chapter 4). Total P, inositol-P, and intrinsic inositol phosphate hydrolyzing enzyme activity is primarily located in the outer layer of rye grain, predominantly in bran. Metabolic triggering of germination is activating intrinsic inositol phosphate hydrolyzing enzymes and is leading to phytate degradation. Maximum intrinsic enzyme activity was identified at 43°C, pH 5.3, and a bran-to-water ratio of 1 to7 (w/v). Under these conditions, the majority of inositol phosphates contained in rye bran were degraded within 30 min at a rate of 5565 $U \cdot kg_{bran}^{-1}$ (Chapter 5). The kinetic study of the blended rPhyXT52 phytase and phytase from *D. castelli* for enzymatic P-mobilization by exogenous phytases showed no inhibition by substrate nor by product, rendering the phytase blend suitable for batch operation. P-mobilization using the phytase blend on rye bran resulted in complete hydrolysis of inositol phosphates and in combination with biomass washing, a 90% reduction in total P-content that was consistent across different production scales. In addition, process conditions for the exogenously added phytase blend are close to maximum intrinsic enzyme activity (Chapter 6).

The enzymatically treated rye bran had a high nutritional profile, and the substantial reduction in P makes it a valorized ingredient in compound feeds (Chapter 7). Additional ultrasonic as well as enzymatic treatment of the cellular matrix enhanced the P-mobilization rate and, thus, increased the process efficiency. Among the enzyme formulations tested, those based on xylanase activity, particularly Depol 740, experienced the most pronounced effect on the P-mobilization rate (Chapter 6). The resulting process wastewater contained approximately 50 mM mobilized P, which could be recovered by struvite precipitation. Maximum struvite precipitation was achieved at pH 9, 20 °C, an equimolar input ratio of constituent ions, and a concentrated NaOH solution as precipitant. In addition, convection in the system was identified to be crucial for precipitation, which completed 20 min after reaching pH 9. Under maximum conditions, P recoveries of 99% with over 90% struvite purity were obtained. Inorganic impurities were mainly K^+; presumably NH_4^+ substituted by K^+. Organic impurities could be removed with acetone and inorganic impurities with 1% HCl solution (Chapter 8). Phenols were identified as possible recyclables for enhancing the overall process economy. Among the resins tested, XAD 16 (Amberlite®) proved most efficient in phenol adsorption and remained stable over at least five cycles, although not all phenols were adsorbed, possibly due to overestimation by the Folin-Ciocalteu assay. For waste stream reduction, the growth of *E. coli* BL21 on the process wastewater indicates its suitability as a 2nd generation feedstock (Chapter 8).

The developed inline analytical approach is transferable to other plant materials containing phytate, since FT-MIR spectra are merely used to analyze the P-content in the liquid phase. Additionally, the method can be adapted to various real-time analytical techniques such as Near-Infrared (NIR), Nuclear Magnetic Resonance (NMR), or Raman spectroscopy. Its scalability makes the approach suitable for inline process control in feed material conditioning prior to feeding, even on a larger scale. It is also shown that one hour of germination at maximum conditions for intrinsic enzyme activity is more effective in reducing the phytate content in rye bran than conventional phytase supplementation to the animal diet. Under process parameters close to maximum intrinsic enzyme activity, reduction of exogenous phytase addition can be achieved. In addition, further insights into the behavior of inositol phosphate degradation is provided by the developed inline analysis and shows the limitation of mass transfer during enzymatic P-mobilization. The application of additional enzymes to open the cellular matrix and thus enhance the mass transfer substantially decrease processing times. However, these enzymes must be approved as feed additives. Alternatively, ultrasonication proved to be equally efficient, but requires a more complex process design and higher energy demand during processing. Furthermore, it is shown that enzymatic P-mobilization from rye bran can be scaled up to 400 L reaction. The process exhibits adaptability to various reaction parameters, which allows flexibility in its practical implementation and thus rendering the process more economical. The consistent P-reduction and a high nutritional profile of the feed produced across all process scales shows the ability to process larger quantities, enhancing productivity and optimizing the resource utilization.

One of the key advantages of enzymatic P-mobilization is the valorization of biomass side streams generated in milling industry. The process is expected to be transferable to other biological matrices, as has been shown on laboratory scale [3]. Thus, the P-mobilization process paves the way for its increased utilization in animal feed, aligning with regulations by legislation. It is shown, that the concept of struvite precipitation from wastewater treatment is applicable to the process wastewater from enzymatic P-mobilization and is straightforwardly scalable. Struvite can be used as an eco-fertilizer due to its slow release properties. It has the potential to reduce nutrient runoff and subsequent water body pollution, making it ideal for use in agriculture. Compared to the Belgian NuReSys process, the purity was approximately 10% higher [17]. Subsequent downstream processing further increased the purity of the struvite produced, although it does not appear necessary due to the nature of the impurities. Nevertheless, P-recovery from renewable resources is well suited for a better management of natural resources in the framework of a circular bioeconomy. Given that mineral P is mainly utilized in agriculture and subsequently in livestock farming, a considerable proportion of P flows can be recycled, taking a step towards a self-sufficient P-cycle. By producing value-added feed material through depletion of phytate and utilization of phytate bound P in renewable resources, a contribution to a more sustainable and diversified P-management is made.

Given the advantageous implications and positive societal benefits of biocatalytic P-mobilization, there are also limitations, especially in its technical, regulatory, and practical implementation, that need to be considered. The developed inline analysis based in FT-MIR spectra is sensitive to variations in the initial substrate. Bran preparations will be heterogeneous, due to variations in growth conditions. In this thesis, only two different preparations of rye bran were examined. However, both preparations represent a common mixture from different cultivation areas in Germany, enhancing generalizability. Nevertheless, differences in nutritional and physiochemical compositions were observed. Different particle sizes and moisture contents can affect the measurements. Therefore, inline analytics need to be calibrated regularly to ensure accurate and reliable measurement results. Since the residual inositol-P content is determined indirectly by a mass balance, the initial inositol-P content must be determined for each new preparation, e.g. by wet chemical methods. Consequently, the operating costs might be high in addition to the acquisition costs. Furthermore, dust and other contaminants in industrial environments can affect the optical components reducing the system´s performance and accuracy. Thus, the devices require regular maintenance. The reduction of exogenously added enzymes through the activation of intrinsic inositol phosphate hydrolyzing enzymes is given for rye bran. This is also expected for plant materials with high intrinsic enzyme activity such as wheat bran or barley, but not for plant materials such as soybean hulls, sunflower hulls, legume seed or oat bran [120]. Therefore, a considerably higher exogenous phytase addition is expected to be required for P-mobilization from these plant materials.

The use of exogenously added enzymes in animal feed is subject to regulatory approval, which can vary by region and may impose additional requirements and restrictions. In addition, the introduction of exogenous enzymes must be carefully managed to ensure that they do not pose any health risks to animals or humans. Since the phytase blend used in this thesis is neither certified as animal feed nor commercially available, its production must first be established on an industrial scale and also undergo a certification process. The production and disposal of enzymes, as well as the potential environmental impact of enzyme residues, must also be considered. Alternatively, commercially available phytase formulations can be used. However, these must be selected based on their hydrolytic efficiency and stability, as they are primarily optimized for the gastrointestinal conditions of monogastric animals.

Besides technical and regulatory limitations, the practical implementation of the P-mobilization process might be complex and challenging. For its realization, there are two viable options: a centralized or a decentralized process, where the latter involves biotechnological conditioning of the feed material directly at the livestock producer. In contrast to the addition of phytase to the feed rations, the inositol phosphate contained in the feed material is eliminated directly before feeding. The advantages are a considerably higher efficiency of inositol phosphate hydrolysis compared to phytase supplementation and thus better absorption by the animal, resulting in less P in the manure, as well as simplified logistics due to shorter transport routes. In addition, the process design is less complex compared to a centralized process, requiring only a stirred tank reactor (STR) with peripherals, as wet feeding eliminates the need for a separator and a drying process. However, a disadvantage is that there is no P-recovery, except from the animal, and the liberated P remains in the feed, resulting in no P adjustment. Since the P is digestible, the eutrophication potential is reduced. But there is still a risk of eutrophication from manure application if the feed contains more P than the animal can absorb. Thus, the composition of the feed must be adjusted; i.e. feed material with low P-content must still be added to the compound feed. Additionally, it is unclear who will bear the additional costs of implementing such a small-scale system, raising concerns about the financial burden on the consumer. In contrast, a centralized process can be integrated into existing milling industry. Offering nutritionally enhanced feed products that can provide competitive advantages in the market, appealing to livestock producers looking for high-quality and efficient feed. The implementation into the existing milling process is innovative and can help to differentiate a brand in competitive market. In addition, the process can be applied to various plant residues, making it versatile and beneficial across different product lines. However, the incorporation into existing milling processes can be complex. It requires equipment and process modifications that can disrupt established operations and requires extensive planning and coordination. Milling processes are typically optimized for dry processing. Enzymatic P-mobilization requires water, which may not align with water conservation efforts and could increase the environmental footprint of the feed production process.

However, the implementation requires capital investment in new equipment, infrastructure, and enzyme procurement as well as operational costs for maintenance of process conditions, increase in energy consumption, and manpower. The costs can be prohibitive for some companies. Nevertheless, the recovery of P as struvite and other valuable materials such as phenols supports the economic establishment of the integrated process. Another centralized approach is to build an autonomous production facility. Compared to an integrated process, this approach offers advanced automation, custom-designed equipment, built-in regulatory compliance, process scalability and flexibility. However, disadvantages are the high initial capital expenditure as well as investment risk, longer time to become operational, high logistical effort and associated environmental impact due to transport routes. In conclusion, while the centralized concept offers a holistic approach, due to downstream processing, the decentralized concept appears to be the most economical, as the conditioned feed material does not need to be dried, and is also more environmentally friendly due to shorter transportation routes. Figure 9.1 shows a schematic representation of the enzymatic P-mobilization process. While the decentralized concept is limited to the upstream part, the centralized concept refers to the entire process.

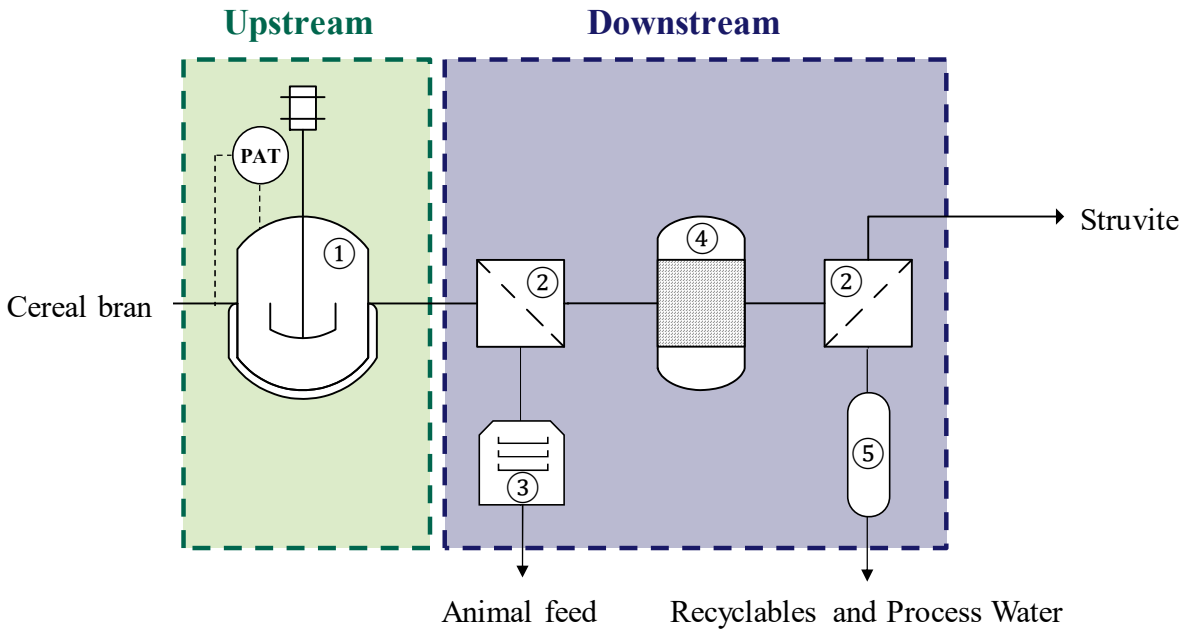

Figure 9.1: Schematic representation of the biocatalytic P-mobilization process. The figure includes the feed material conditioning (upstream), subsequent feed drying as well as recovery of P as struvite and other recyclables (downstream). The process consists of: ① bioreactor with process analytical technology (PAT), ② solid-liquid separation, ③ dryer, ④ struvite precipitation plant, ⑤ capturing of further recyclables.

The schematic representation of the biocatalytic P-mobilization process illustrates a series of integrated unit operations designed for inositol phosphate hydrolysis in the feed material and subsequent recovery of P and other valuable substances such as phenols. The process starts with the introduction of plant residues into a stirred tank bioreactor, equipped with process analytical technology, e.g. the developed FT-IR based inline analysis. Here, the plant material undergoes biocatalytic conditioning. Within the bioreactor, controlled conditions and the application of exogenous phytase facilitate the mobilization of P. Following conditioning in the bioreactor, the bran-water suspension undergoes solid-liquid separation. This stage separates the liquid phase, containing the dissolved P and other valuable substances, from the P reduced feed material. The solid fraction is then directed to a drying unit, where moisture is removed to stabilize the conditioned feed for storage and transportation. Meanwhile, the P-enriched liquid phase proceeds to a precipitation plant, where P is recovered in the form of struvite crystals. The struvite recovery involves a second solid-liquid separation. Lastly, the process includes the capture of additional recyclables, ensuring efficient utilization of resources. In summary, the biocatalytic P-mobilization process eliminates the inositol phosphates contained in the plant material and recovers the liberated P through a sequence of different unit operations. From bioreactor based conditioning to struvite precipitation and recyclable capture, each stage contributes to a sustainable nutrient management and environmental stewardship. This approach not only mitigates the ecological impact of agricultural practices but also drives innovation in P-management. This strategy ensures longterm resource availability and aligns with SDGs focused on responsible production, innovation, and environmental sustainability.

9.2 Outlook

The results achieved in this thesis demonstrate the advancement in the technical applicability of enzymatic P-mobilization from plant biomass and the subsequent P-recovery as struvite. Due to the substantial reduction in P-content, the limits for P in manure can be met, ensuring compliance with environmental regulations. In addition, the improved nutrient efficiency results in the valorization of agricultural by-products. The process provides increased P availability, reducing reliance on inorganic fertilizers and minimizing the environmental impact of P runoff. However, the transition towards a fully integrated circular P-bioeconomy is not yet complete. Recommendations for future research on specific topics related to this field of work are categorized and described below.

Inline Process Control

It was shown that the developed inline process analysis, based on MIR spectra and a mass balance around P, allows the determination of residual inositol phosphate in rye bran during enzymatic P-mobilization. It is assumed that this method is transferable to processes where P is mobilized from different inositol phosphate containing plant materials. However, due to the different biological matrices, different components may be solubilized in the aqueous phase, potentially causing interference in the calibrated measurement range. To investigate the broad applicability, the developed method should be applied during the conditioning of various plant materials. In case of interferences with other plant constituents, it should be investigated whether a calibration to a different wave number range is feasible. Additionally, the inline analysis is sensitive to variations in the initial substrate. Batch heterogeneity arises due to different growth conditions, such as soil composition and climate. As the residual inositol phosphate content is indirectly assessed via a mass balance, determining the initial inositol phosphate content for each new preparation is essential. In view of climate, the development of predictive models that forcast the phytate content resulting from climatic conditions can be advantageous [180]. However, in this thesis, this achieved by wet chemical methods, which are labor intensive and time consuming. Therefore, spectroscopic techniques such as NIR or Raman Spectroscopy on the dry plant material could potentially provide rapid quantification on the initial inositol phosphate content [107]. Raman and NMR spectroscopy, may also be advantageous for distinguishing between orthophosphate and inositol phosphate in the liquid phase. These techniques could provide additional insights on the efficacy of exogenous applied phytases in P-mobilization, especially for plant material with low intrinsic phytase activity. However, no literature could be found on online quantification and differentiation using Raman spectroscopy or other spectroscopic methods, with the exception of NMR. The methods found in the literature use an additional precipitation step [38,93], which is not suitable during inline process control. Furthermoe, the aqueous phase can affect the quality of Raman spectra by altering scattering effects and decreasing the signal-to-noise ratio, thereby reducing measurement sensitivity. Similarly, the complexity of the liquid phase challenges NMR based analysis, even 2D NMR (^{1}H and ^{31}P), due to the presence of other P containing compounds such as phospholipids and nucleic acids. The validity and extent to which these spectroscopic methods are suitable for quantification requires further investigation.

Application of Commercially Available Phytase Formulations

The phytase blend used in this thesis is neither certified for use as animal feed nor commercially available. A certification and the establishment of an industrially viable production process is both time consuming and costly. To reduce the time to marked, commercially available enzyme formulations should be evaluated for their suitability in enzymatic P-mobilization. These formulations have to be screened according to their hydrolytic efficiency and stability, as they are typically optimized to withstand pelleting of animal feed [181].

Effect of Ultrasound Treatment on the Activity of Exogenous Phytases

No effect of ultrasound treatment for the supportive release of inositol phosphates on the activity of the exogenously applied phytase blend was observed. However, the blend was added in excess. For an economical process design, it is necessary to match the activity of the exogenous applied phytases with the solubilization rate of the inositol phosphates. Therefore, quantification of potential effects and identification of optimum process conditions is required. For this, the concept of statistical experimental design of experiments can be used. Relevant factors include treatment time, volumetric power input, applied enzyme activity, biomass concentration, temperature, and pH value. In addition, it is advisable to investigate whether a coupled or decoupled process is more effective. For quantification, the enzyme activity assay established in this thesis, based on the molybdenum blue color reaction, can be used.

Feed Suitability of Conditioned Rye Bran

The calculated energy values in the treated rye bran seem plausible due to the low crude ash content and the resulting high amount of organic residues. In addition, the substantial P reduction of 90% and the high nutritional profile make the produced feed suitable for animal consumption. P-mobilization does not affect the calculated energy value; however, this value could not be determined for the combined phytase and xylanase treatment due to lack of data on carbohydrate fractions. Xylanase treatment is expected to reduce the metabolizable energy value, requiring calculation of metabolizable energy for treated rye bran after the combined enzymatic process. Furthermore, the calculated metabolizable energy values using the GfE formula are based on analytical results and nutrient digestibility tables for rye bran, which may differ from the sample. Future studies should determine the exact digestibility using classical methods on the target species to identify potential deviations from this estimated equation.

Waste Stream Valorization

The recovery of phenols from the process wastewater can contribute to the economic establishment of the overall process. Both liquid-liquid extraction and adsorption onto resins were investigated for recovery, with adsorption proving to be the more efficient among the extraction agents examined. However, since liquid-liquid extraction involves less process engineering complexity, further extractants should be evaluated. In addition, since not all phenols are removed from the process wastewater by adsorption, other adsorbents should also be investigated. The influence of the Folin-Ciocalteu assay on the results is unclear; thus, the establishment of a reference analytical methods, such as HPLC analysis, as well as identification of phenolic compounds is advisable.
The results demonstrate that the process wastewater after P-recovery can effectively support the growth of *E. coli* BL21, providing a viable application in the second generation bioconversion industry. Future research should focus on identifying the growth limiting nutrients. Based on this, the nutrient composition can be optimized through additional enzymatic treatment or the supplementation of missing nutrients. In addition, an appropriate selection of potentially suitable microorganisms should be made in advance. These should be able to grow in environments with limited nutrients, utilize a variety of substrates, and produce high yields of the desired products despite the nutrient poor conditions. Industrially relevant bacteria that fulfill these requirements are *Bacillus subtilis*, *Corynebacterium glutamicum* and *Escherichia coli*. Suitable yeasts are *Pichia pastoris* and some genetically modified strains of *Saccharomyces cervisiae* [182].

Life Cycle Assessment and Techno-Economic Analysis

A Life Cycle Assessment (LCA) provides a comprehensive framework for evaluating environmental impacts, including resource efficiency, emissions, and waste at all stages of the process. Within the LCA, environmental hotspots are identified, allowing process optimization for improved sustainability. Conducting an LCA will help ensure compliance with evolving environmental regulations and support applications for eco-labels and certifications, thereby enhancing marketability and consumer confidence. The LCA can be compared to the traditional ‘End-of-Pipe’ approach of extracting P from manure to provide a clearer understanding of the environmental impact, resource efficiency, and potential for integrating sustainable practices.
Alongside the LCA, a Techno-Economic Analysis (TEA) should be conducted. The TEA will provide insight into the feasibility and economic viability of implementing the process at commercial scale. In a comprehensive TEA covers the costs associated with each stage of the process, including capital investment, operating costs, and revenue from valorized and recovered products. This analysis will help potential stakeholders understand the financial implications and feasibility of adopting these sustainable practices.

In addition, a comparative TEA between the P-mobilization process and the 'End-of-Pipe' approach provide insights into cost effectiveness and competitiveness in the agricultural sector. In conclusion, conducting a TEA along with the LCA allows for a systematic assessment of the feasibility of the process. For a centralized process, this includes modeling the corresponding refineries and comparing conditioned and unconditioned feed, as well as considering the recovery of P and other valuable compounds. This should also be compared to a decentralized process where the feed is conditioned directly at the livestock producer without recovery of P and other valuable substances. Both LCA and TEA are part of the German Environmental Foundation´s PhANG project (34976/01) and a work package of the Institute of Environmental Technology and Energy Economics at the Hamburg University of Technology.

Construction of a Pilot Plant

Following LCA and TEA the construction of a pilot plant is imperative. The scalability of the process has already been demonstrated in this work up to a scale of 400 L. However, in order to generate sufficient feed material to determine the digestibility using classical methods on the target species, large quantities of conditioned feed are required. In addition, possible unidentified effects can be investigated on a larger scale. Although some of these effects have already been investigated in this thesis, additional mixing and mass transfer challenges, as well as challenges in temperature control, may arise due to geometric and operational differences and need to be validated at pilot scale. In larger bioreactors, it becomes increasingly complex to achieve homogeneity in the reaction medium, resulting in gradients in temperature, pH and enzyme concentration. In addition, different stirring rates for the same power input can introduce shear stress that can affect enzyme stability. Moreover, larger bioreactors may require different impeller designs and operating parameters to achieve similar mixing and mass transfer characteristics as in the smaller systems, potentially creating areas of stagnation or insufficient mixing, which slow down the process. Altough recommendations for a suitable stirrer for the two-phase system (bran-water suspension) are given in Chapter 6.1.2, the energy dissipation as a function of different stirrers should be determined. This analysis will allow a more accurate assessment of the most appropriate type of stirrer for the system. Moreover, maintaining a consistent temperature is also challenging, as differences in heat transfer rates can lead to localized hot spots that negatively impact enzyme activity and stability. However, in this thesis it is shown that the process is temperature flexible and therefore temperature control can be omitted at minimal impact on process performance. Nevertheless, the heat input from the agitator has to be considered. Effective process monitoring and control is critical to managing these complexities, but sensors used to monitor key parameters may not provide the same accuracy as in small scale systems.

Therefore, construction of a pilot plant will allow further process optimization prior to commercial scale. In particular, the pilot plant should provide data on process performance, product quality, and resource consumption. This empirical data is crucial for the refinement of the economic model, e.g. the TEA, and the validation of assumptions. The aim is to bring the process to market, serving different value chains while minimizing environmental burden.

10 Summary

In this thesis, the process of biocatalytic P-mobilization from plant residues prior to feeding and the recovery of liberated P, initially organically bound to inositol phosphate, in the form of struvite, is examined. Rye bran serves as the model substrate for investigating and optimizing this process.

The research presents a novel inline analytical methodology using FT-MIR spectroscopy and PLSR modeling for rapid quantification of liberated P during enzymatic treatment. Based on this, the developed approach allows reliable quantification of residual inositol-P content in rye bran with a RMSEP of 81 $mg_P \cdot 100g_{bran}^{-1}$ and a coefficient of determination R^2 of 0.78. The inline nature of this analytical method provides real-time monitoring and control, which is essential for industrial scalability and efficiency.

For process optimization, the concept of statistical experimental design was used to identify the maximum intrinsic inositol phosphate hydrolyzing enzyme activity. It is shown that maximum intrinsic enzyme activity occurs at 43 °C, pH 5.3, and a bran-to-water ratio of 1 to 7 (w/v). At these conditions, most of the inositol phosphate content in rye bran was degraded within 30 min at a rate of 5565 $U \cdot kg_{bran}^{-1}$. The maximum intrinsic enzyme activity is close to the maximum activity of the exogenously applied phytase blend (rPhyXT52 phytase and phytase from *D. castelli,* 37 °C, pH 4.4). This allows for a reduced application of exogenous enzymes under these conditions. Kinetic studies on the exogenous phytase blend proved complete hydrolysis of all phosphorylated inositols and confirmed its suitability for batch operation. In addition, supportive ultrasound as well as enzymatic treatment of the cellular matrix substantially increased P-mobilization rate, with xylanases being the most effective enzymes. The optimized hydrolysis, showcase the advancement and technical feasibility of enzymatic P-mobilization for the processing of agricultural residues.

Scaling the process to up to 400 L reactions in all cases resulted in the complete elimination of inositol phosphates in rye bran and a consistent reduction of the total P-content by 90%. The robust nature of this process and the successful 99% P-recovery by struvite precipitation demonstrate its feasibility for large-scale implementation. P-recovery as struvite helps to prevent nutrient runoff into water bodies, mitigating potential eutrophication and promoting a circular economy.

This research not only presents a technological innovation in agricultural processing but also emphasizes the need for its international adoption to support a circular P-bioeconomy. By integrating this process into industrial practices, it would be possible to reduce environmental pollution and to promote a sustainable agriculture in line with SDG 9, SDG 12, and SDG 14.

A Materials and Methods

A.1 Materials

All chemicals, except dipotassium phytate from BLD Pharmatech Ltd. (Shanghai, China) and phytic acid sodium salt hydrate (P1180) from Sigma-Aldrich (Traufkirchen, Germany), were of analytical grade or higher quality and were purchased from Sigma-Aldrich (Traufkirchen, Germany), Carl Roth (Karlsruhe, Germany), IVA (Meerbusch, Germany), Bernd Kraft (Duisburg, Germany), TCI Deutschland (Eschborn, Germany), Omnilab (Bremen, Germany), LAT (Garbsen, Germany), VWR (Darmstadt, Germany). Rye bran was provided by Aurora Mühlen GmbH (Hamburg, Germany) containing a common mixture from different cultivation areas in Germany.

Table A.1: Device list

Offline Analytics	
HPLC-System Agilent 1100 Series Equipped with (1) two pumps, (2) auto-sampler, (3) diode array, and (4) reflective index detector	Agilent Technologies GmbH, Germany
HPLC-Column LiChrospher®100, 5 µm, 250 mm x 4 mm	Merck KGaA, Germany
UV-1280 UV/Vis spectrophotometer	Shimadzu Scientific, Japan
UVIKON® photometer	Goebel Instrumentelle Analytik GmbH, Germany
Varian Cary 50 Bio UV-Visible (photometer)	Varian, Inc., Netherlands
Infinite M200Pro (photometer)	Tecan Trading AG, Switzerland
Axioskop (light microscope)	Carl Zeiss Microscopy GmbH, Germany
D 500 X-ray (diffractometer)	Siemens AG, Germany
Kinexus pro (rheometer)	NETZSCH-Gerätebau, Germany
Em 120-HR (moisture analyzer)	Precisa Gravimetrics AG, Switzerland
766 Calimatic (pH-meter)	Knick Elektronische Messgeräte GmbH & Co. KG, Germany
FiveGo (pH-meter)	Mettler-Toledo, USA
Camsizer XT (particle imaging)	Microteac Retsch GmbH, Germany
LS 13 320 (laser diffraction analyzer)	Beckman Coulter Life Sciences, USA
AccuPyk II (density analyzer)	Micrometric Instrument Corporation, USA

Online Analytics	
Vertex 70 (FTIR) Equipped with (1) sample compartment, (2) optical fiber, (3) MCT detector, and (4) N_2 purge gas generator	Bruker Optik GmbH, Germany
Fiber Probe In 350-T (FTIR)	Bruker Optik GmbH, Germany
PG 28L (purge gas generator)	Cmc Instruments GmbH, Germany
Titrando 902 (auto titrator)	Metrohm GmbH & Co. KG, Germany
Weight Balances	
Sartorius A1205 (weight balance)	Sartorius GmbH & Co. KG, Germany
Sartorius BCE124I-1S (weight balance)	Sartorius GmbH & Co. KG, Germany
Sartorius LC 2200 P (weight balance)	Sartorius GmbH & Co.KG, Germany
Sartorius R 300 S (weight balance)	Sartorius GmbH & Co.KG, Germany
Thermostats & Incubators	
Incubation shaker model G25	New Brunswick Scientific, USA
SW 23 (water bath)	JULABO GmbH, Germany
IKAMAG®RCT (magnetic stirrer with heating plate)	IKA-Werke GmbH & Co. KG, Germany
IKA ETS-D5 (thermostate)	IKA-Werke GmbH & Co. KG, Germany
T_{S1} Thermoshaker	Biometra GmbH, Germany
Circulation thermostat MA-4	JULABO GmbH, Germany
Ecotron (incubator)	Infors AG, Switzerland
Centrifuges	
Universal 320 R	Andreas Hettich GmbH & Co. KG, Germany
Avanti J-25	Beckman Coulter GmbH, Germany
Minifuge T	Heraeus Sepatech, Germany
Vacuum Devices	
BÜCHI Rotavapor R-200	BÜCHI Labortechnik GmbH, Germany
SPE vacuum chamber	J.T. Baker, Germany
VARIO Chemie-Pumpstand PC 3001	Vacuumbrand GmbH & Co. KG, Germany

Dry Cabinets	
B 50	Memmert GmbH & Co. KG, Germany
WTC	Binder GmbH, Germany
Bioreactors	
KLF 2.4 dm^3 bioreactor	Bioengineering AG, Switzerland
Laboratory Pilot Fermenter LP351	Bioengineering AG, Switzerland
PID 2 media preparation vessel	Bioengineering AG, Switzerland
Other Devices	
Pulverisette 6 (mill)	Fritsch GmbH, Germany
Phoenix (muffle furnance)	CEM GmbH, Germany
Bandelin Sonoplus HD 2070 (ultrasonic homogenizer)	Bandelin electronic GmbH % Co. KG, Germany
Purification Materials	
HyperSep SAX cartridges 2G	Thermo Fisher Scientific, Germany
Amberlite® XAD 4 (adsorbens)	Thermo Fisher Scientific, Germany
Amberlite® XAD 16 (adsorbens)	Thermo Fisher Scientific, Germany
Amberlite® XAD 7HP (adsorbens)	Thermo Fisher Scientific, Germany
Amberlite® XAD 1180 (adsorbens)	Dow Chemical, USA
Silica gel 60	Merck KGaA, Germany
Expandable Materials	
Cellulose Acetate Filter 0.2 µm	Sartorius Stedim Biotech GmbH, Germany
Fisherbrand QL 115 (filter)	Fisher Scientific GmbH, Germany
Ahlstrom 3 hw (filter)	Munktell & Filtrak GmbH, Germany
Syringe filters (0.22 µm)	Agilent Technologies, USA
Automated Microliter Pipettes	Eppendorf AG, Germany
Capped Plastic Tubes (1.5 – 5 mL)	Eppendorf AG, Germany
Capped Plastic Tubes (15 mL and 50 mL)	Greiner AG, Austria
96-Well microtiter plates	Greiner AG, Austria
Glassware (Cap Bottles, Beakers, Measuring Cylinders, Baffled Flasks, etc.)	DURAN Group GmbH, Germany

A.2 Methods

A.2.1 Colorimetric Analyses

Quantification of inorganic phosphate was performed spectrophotometrically in 96-Well microtiter plates using a modified protocol of the molybdenum blue reaction according to Eeckhout and Paepe [88]. Depending on the inorganic P concentration, the sample was diluted with H_2O to a total volume of 100 µL and then 100 µL color reagent was added. The color-developing reagent consisted of four parts of acidic 0.012 M $(NH_4)_6Mo_7O_{24}\cdot 4H_2O$ solution and one part of 0.711 M $FeSO_4\cdot 7H_2O$ solution. After 5 min of incubation, the absorbance of the formed color complex was measured at 700 nm. For quantification of free inorganic P, a standard curve of KH_2PO_4 (from 100 µM to 500 µM) was used on each plate. [135]

3,5-dinitrosalicylic acid (DNS) assay was used to quantify the activities and stabilities of cellulases and xylanases on either cellulose or xylene as substrate. The solutions were prepared according to the protocols outlined in Tables A.2.1 to A.2.3. Enzymes were added to the reaction in appropriate dilutions. The mixtures were incubated in 50 mM NaOAc at 37 °C and pH 4.4. After incubation, the reaction solutions were mixed with DNS solution in a 1 to 1 volumetric ratio and heated in a boiling water bath for 5 min. Subsequently, the mixtures were cooled to room temperature in an ice bath, and the absorbance was measured at 546 nm.

Table A.2.1: DNS solution

DNS	1% (w/v)
NaOH	0.4 M
K-Na-tartrate	30% (w/v)

Table A.2.2: Substrate solution

0.1 M NaOAc	10 mL
H_2O	40 mL
Substrate	0.5 g

Table A.2.3: Reaction solution

Substrate solution	250 µL
NaOAc	50 µL
Enzyme	50 µL
H_2O	150 µL

Phenolic content was quantified in 96-Well microtiter plates using the Folin-Ciocalteu assay as described by Singleton and Rossi [183]. A 20 µL aliquot of the sample was mixed with 100 µL 0.2 N Folin-Ciocalteu reagent and incubated in the dark for 5 min. Following this incubation, 80 µL of a 75 $g\cdot L^{-1}$ sodium carbonate solution was added. The mixture was then incubated at room temperature for 70 min. The absorbance was measured at 760 nm to quantify the phenolic content, using a calibration curve prepared with gallic acid ranging from 0 $\mu g\cdot mL^{-1}$ to 500 $\mu g\cdot mL^{-1}$.

The figures below show typical calibration curves for quantification using the colorimetric methods.

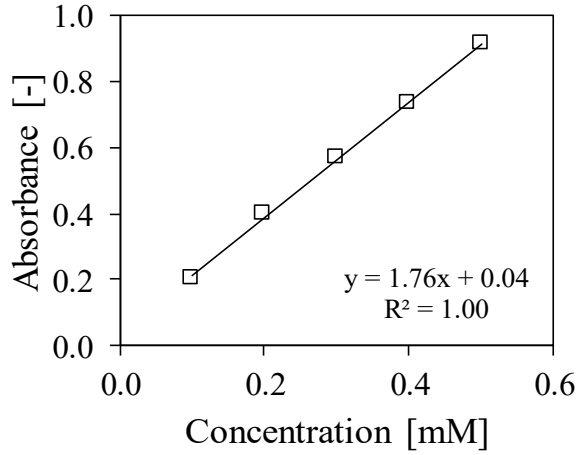

Figure A.2.1: Typical calibration curve for the quantification of inorganic P using molybdenum blue color reaction.

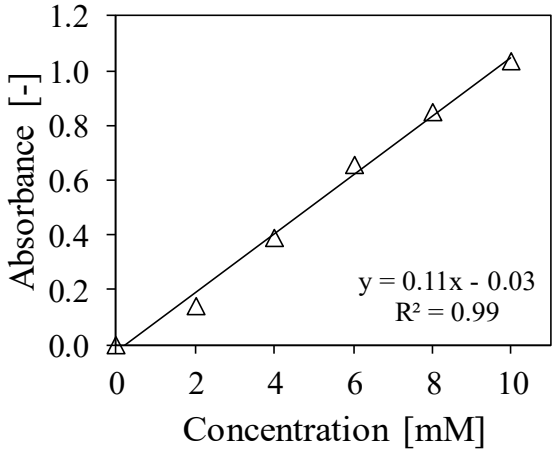

Figure A.2.2: Typical calibration curve for the 3,5-dinitrosalicylic acid (DNS) assay.

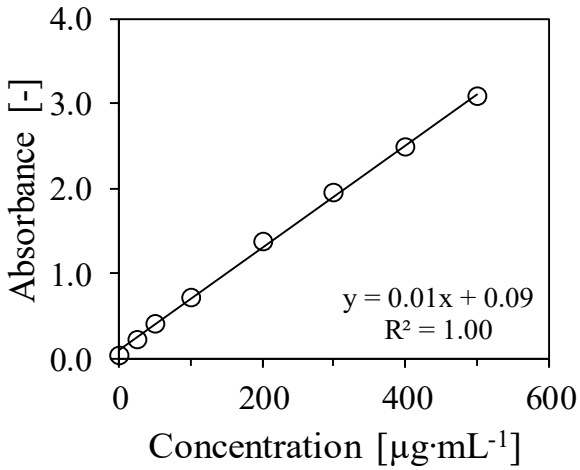

Figure A.2.3: typical calibration curve for the quantification of phenolic compounds using the Folin-Ciocalteu reagent.

A.2.2 Phytate Extraction and Quantification by HPLC

When the residual inositol phosphate content was determined after certain time points, the suspension was transferred to centrifuge tubes and then washed repeatedly to remove the P species in solution. The suspensions were centrifuged three times (3860xg, 5 min), the supernatant was removed, and the bran fraction was dissolved in ultrapure H_2O. Prior to analysis, plant material was resuspended in 0.5 M HCl at a ratio of 1:7 (w/v), sonicated for 2 min at 70% performance, and afterwards incubated for 1 h (at 37 °C, stirred at 250 rpm) for phytate extraction. For purification, a modified protocol from Herrmann *et al.* was used [3]. In brief summary, HCl extracts were diluted 1 to 5 in H_2O and applied to HyperSep SAX cartridges using reduced pressure (800 mbar). Samples were eluted with 2 M HCl, evaporated, and phytate was dissolved in 50 mM NaOAc pH 5 for HPLC analysis. For quantification an HPLC method from Sandberg *et al.* was used in a modified manner [94]. A reversed-phase RP18 analytical column was used with a mobile phase consisting of MeOH, H_2O, formic acid, and tetrabutylammonium hydroxide (40% in H_2O). Inositol phosphates were detected at 39 °C using a refractive index detector. Typical retention times were 8 min ($InsP_3$), 12 min ($InsP_4$), 16 min ($InsP_5$), and 23 min ($InsP_6$). [66]

A.2.3 HPIC Analysis of Inositol Phosphates

HPIC analysis was performed at RWTH Aachen University. Inositol phosphates were extracted from 5 g of biological plant material using 35 mL of 0.5 M HCl. The suspension was incubated and shaken for 16 h. Afterwards, the samples were centrifuged for 40 min at 3220xg. Phosphate and InsP to $InsP_6$ isomers were separated on a Thermo Scientific™ Dionex™ IC-6000 HPIC™ system equipped with a Dionex ACP Auxiliary Pump, Thermo Scientific Dionex EGC carbonate mixer kit, a CarboPac™ PA100 guard (4x50 mm) and CarboPac™ PA100 analytical column (4x250 mm). Separation was achieved using a gradient of 0.5 M HCl followed by a postcolumn reaction in a knitted reaction coil (750 µL) with ferricnitrate (0.1% $Fe(NO_3)_3$ in 0.33 M perchloric acid). A typical retention time for PO_4^{3-} is 5.6 min and for $InsP_6$ 49.3 min. [135]

A.2.4 Online Monitoring using ATR-FT-MIR

Data Collection

ATR-FT-MIR measurements were performed using a Vertex 70 spectrophotometer equipped with an optical fiber. The optical fiber has an ATR cell implemented, consisting of a diamond prism (2 reflections, 45° angle of incidence) as the internal reflection element. For detection, a thermoelectrically cooled MCT (Mercury-Cadmium-Telluride) detector at a scanner velocity of 40 kHz was used.

Spectra were taken at a resolution of 4 cm^{-1} in the wavenumber range of 4000 to 600 cm^{-1}. Each ATR spectrum represents an average of 200 scans and was recorded with the blank ATR configuration as background. To minimize the interference from water vapor and carbon dioxide absorption bands, the device was purged with dry nitrogen. The ATR cell was cleaned after each experiment by washing it with ultrapure water and ethanol until no significant bands due to impurities appeared in the blank ATR configuration. Measurements were always done in the aqueous phase. [66] The experimental setup is shown in Figure A.2.4.

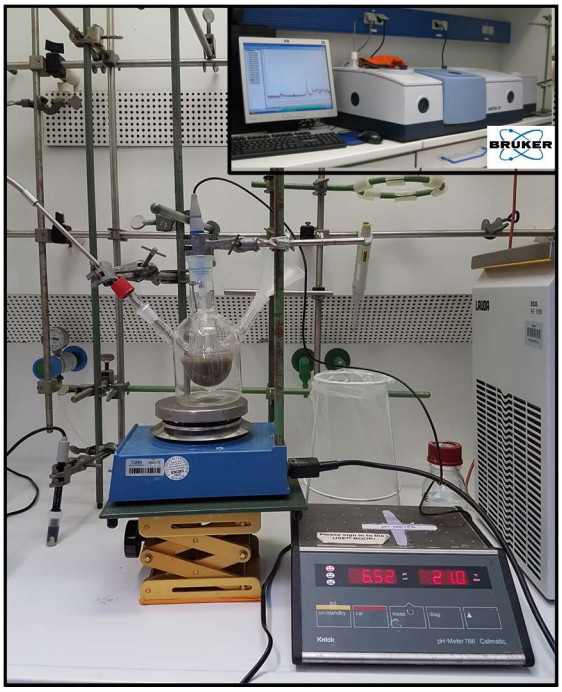

Figure A.2.4: Experimental setup for ATR-FT-MIR inline measurements.

Data Analysis

PLSR was used for quantitative analysis; i.e., to predict the amount of inorganic P in the liquid phase. This method with a calibration series of KH_2PO_4 at 18 different concentrations ranging from 0 to 200 mM was used to develop a calibration model. To increase the model´s accuracy, a spectrum of each concentration was taken twice and the duplicates were averaged for calibration. In addition, KH_2PO_4 was used for the determination of the probe response time and the detection limit. The spectra were cut to the fingerprint region from 1700 to 900 cm^{-1} covering the target molecular vibrations. In addition, the data preprocessing techniques included a baseline offset and a maximum normalization at the water band appearing at 1600 cm^{-1} using The Unscrambler X statistical software (version 10.5.1, Camo Software, Norway). Based on this, the PLSR model was trained in the range of 1350 to 1020 cm^{-1}. The number of factors for the PLSR model was selected for an optimum between error of calibration and error of prediction. Accordingly, the lowest possible RMSECV was aimed for without overfitting the model. A full cross validation was performed, i.e. each averaged spectrum was omitted and predicted once. [66]

A.2.5 Determination of Particle Size Distribution

Particle size distributions were determined in the interval from 0.1 to 2000 µm, in triplicates. The cumulative and volume-specific particle size distribution of the dry plant material was determined by imaging allowing to derive the volume-specific surface area S_V ($\mu m^2\ \mu m^{-3}$) and sphericity Ψ. Particle size distribution of the soaked plant material was measured in suspension by laser diffraction applying the Frauenhofer optical model. The density of the bran bulk was determined by means of gas displacement measurement. [66] Particle size distribution of dried and P-depleted as well as untreated rye bran was studied in the range of 180 µm to 2 mm by imaging. The equivalent circle diameters X_{10}, X_{50}, and X_{90} were derived from the volume specific particle size distribution. [135]

A.2.6 Fluorescence Microscopy

Fluorescence microscopic imaging was performed as described in Arte *et al.* in a modified manner [143]. A spatula tip of the plant material was stained in a 200 µL solution consisting of 100 µL aqueous 0.05%(w/v) calcoflour white solution and 100 µL 0.1% (w/v) acid fuchsin in 1.0% acetic acid solution for 2 min. The supernatant was removed and the sedimented plant material was resuspended in H_2O and placed on the silde. Protein was stained by Acid Fuchsin. ß-Glucan was stained by Calcoflour White. In exciting light (400-410 nm, emission >455 nm) intact cell walls stained with Calcoflour appeared blue and proteins stained with Acid Fuchsin appeared red.

A.2.7 X-Ray Diffraction Analysis

The precipitates were filtered and dried at 40 °C for 48 h before X-ray diffraction (XRD) analysis. The analysis was performed at room temperature using Cu Kα radiation. The XRD patterns were recorded in the 2 θ scanning range from 3° to 63° every 0.05° at a resolution of 1 s per increment.

A.2.8 Analysis of Feed Suitability

The analysis was performed at the University of Veterinary Medicine Hannover. For statements on the suitability as animal feed, common raw nutrients in the P-depleted rye bran as well as in the native rye bran were examined according to the methods of the VDLUFA. Dry matter was determined gravimetrically before and after drying the samples at 103 °C until weight constancy. The crude ash content was calculated via the mass difference after the combustion of the sample materials in a muffle furnace at 600 °C. The fiber content was determined with the Foss Fibertec 2010 Hot Extractor after washing the samples in 1.25% (v/v) H_2SO_4 and 1.25%(v/v) NaOH and the crude fat content was quantified by automated hydrolysis and extraction using the Hydrotherm and SOXTHERM 416 (C. Gerhardt GmbH & Co. KG, Königswinter, Germany). Crude protein contents were analyzed using a MAX N translational nitrogen and protein analyzer (Elementar Analysesysteme GmbH, Langenselbold, Germany). The starch contents of the brans were determined polarimetrically (Schmidt und Haensch GmbH & Co., Berlin, Germany) and sugar contents were tested using the Luff-Schoorl method [184]. Additionally, calcium was analyzed by atomic absorption spectroscopy (ZEEnit 700P, Analytik Jena GmbH, Germany) and the total P-content was determined colorimetrically using a photometer (UV-1900 i, Shimadzu) at 365 nm or at NutriControl BV (Veghel, Netherland). [135]

A.2.9 Ion Content in Process Wastewater and Struvite

The ion content in the process wastewater and in struvite were measured at the Central Laboratory for Chemical Analysis at the Hamburg University of Technology using NCHS and ICP-OES analysis.

NCHS elemental analysis:	Alina Stahl / Heike Frerichs (valid from 2019) M02.00.02 Hamburg University of Technology, Central Laboratory for Chemical Analysis
ICP-OES elemental analysis:	Alina Stahl (valid from 2020) M02.015.03 Hamburg University of Technology, Central Laboratory for Chemical Analysis

A.2.10 Quantification of Monomeric and Oligomeric Sugars

Samples were analyzed for monomeric sugars and cellobiose without performing analytical hydrolysis. The total sugar content, including oligosaccharides, was determined with analytical hydrolysis. For the direct measurement of monomeric sugars and cellobiose, the samples were adjusted to pH 5 to 6 with calcium carbonate, the supernatant was decanted and filtered through a 0.2 µm nylon filter. For the determination of the total sugar content in the samples, a 5 mL aliquot of each sample was transferred into a pressure tube. The pH of each sample was measured to calculate the required amount of H_2SO_4 to achieve a 4 wt.-% solution. Additionally, 5 mL of the sugar recovery standards were added into a pressure tube, and 174 µL H_2SO_4 was added. The pressure tubes were then autoclaved at 121 °C for 60 min and allowed to cool to room temperature. Post-hydrolysis, calcium carbonate was used again to adjust the samples to pH 5 to 6. The liquid was decanted and filtered through a 0.2 µm nylon filter for HPLC analysis. The stationary phase was a Dionex™ CarboPac™ column. The mobile phase consisted of 5 mM H_2SO_4 and 1 vol.-% acetonitrile. Separation was achieved at 0.7 $mL \cdot min^{-1}$ and 60 °C. For detection, a refractive index detector was used.

A.2.11 Rheological Investigations

The viscosity of the bran water suspension and of the process wastewater was determined using a Kinexus pro rotational viscometer. The C52 SW1236 SS cone was used as geometry. Gravimetric determination of the process wastewater density was performed with defined volumes.

A.2.12 Thermogravimetric Analysis

The TGA/DSC 1 was used for the thermogravimetric analysis. The oven temperature was increased in stages according to DIN 18122. Initially, the temperature was increased linearly to 250 °C over a period of 45 min and then kept constant for another 60 min. After a total of 105 min, the temperature was increased linearly to 550 °C for 30 min and finally kept constant at this value for 200 min. During this time, the mass of the sample was automatically determined gravimetrically using the built-in balance.

A.2.13 Experimental Procedures

All experimental procedures that are not explicitly and in detail described in the respective chapters are described below:

Total phosphorus content in rye bran was determined according to a method of the Association of Official Analytical Collaboration (AOAC) [185]. Samples of 1 g plant material were thoroughly dried at 105 °C for at least 4 h. Dried samples were incinerated at 550 °C and extracted in 10 mL of 6 M HCl and heated to the Boiling point. Dissolved inorganic P-content was quantified using the molybdenum blue color reaction as described in Chapter A.2.1. [66]

Intrinsic phytase activity was quantified according to a modified protocol of Eeckhout and Paepe [88]. 0.2 g of rye bran was incubated in 50 mL reaction solution and stirred at 120 rpm. The reaction solution was a 1.5 mM phytic acid solution (P1880, Sigma Aldrich) of 180 mL H_2O and 820 mL of a 0.25 M potassium acetate buffer. The pH was adjusted with H_2SO_4. After 10 min and 70 min 50 µL sample were taken and immediately mixed with 450 µL of 0.612 M TCA and 500 µL of the molybdenum blue color developing reagent (Chapter A.2.1). The difference in liberated inorganic P after 10 min and 70 min was used to determine the activity (expressed in $\mu mol \cdot min^{-1} \cdot kg^{-1}$ of biological material as dry matter). Thereby, the phytase unit is defined as the amount of inorganic P released in one minute from 0.0015 M phytate solution [66].
To determine the activity as function of temperature and pH, KOH and citric acid were used to adjust the pH and the experiments were carried out in a water bath and preheated reaction solution. Design Expert® was used to create the experimental plan. The experimental conditions are listen in Table B.1.

Activity of exogenous phytase was determined in a thermoshaker by varying the concentration of phytate (P8810, Sigma-Aldrich) in 50 mM NaOAc. The reaction was started by the addition of 20 µL cell-free extract in appropriate dilution. Each reaction batch had a total volume of 1 mL. In order to not exceed a conversion of 10%, the added volume of cell-free extract was reduced from 0.01 mL to 0.001 mLThe reaction was stopped after 3 min using 10% (w/v) TCA. The liberated inorganic P was determined by the molybdenum blue color reaction as described in Chapter A2.1. [135]

Debranning of the rye grain was performed at the Institute of Environmental Technology and Energy Economics at the Hamburg University of Technology as described in Mayer *et al.* [117]. In brief summary, a stepwise removal of the outer layers was done according to a simplified pearling process via friction and abrasion. A drill machine with grinding disks was used. During grinding, the temperature did not exceed 40 °C to prevent enzyme denaturation. After the debranning, residual grains were separated from the abrasion by a shaking separation unit with a sieve size of 1 mm.

Phosphorus mobilization from biomass was performed as described in Herrmann *et al.* [3]. In summary, the bran was suspended in either 50 mM NaOAc or H_2O using a ratio of 1 to 7 (w/v). The reaction was started by adding the phytase blend. A total of 4000 U (2000 U rPhyXT52 phytase + 2000 U *D. castelli* phytase) per kg bran were used. After incubation, the P containing supernatant was separated from the biomass by centrifugation (3860xg, 20 min). Afterwards, the obtained bran pallet was dried for further analysis. [135]

Phosporus mobilization on large scale was performed in a 400 L bioreactor (PID 2 media preparation vessel) equipped with a 3-winged propeller impeller (ø 150 mm) filled with 37.1 kg of bran and 248 L tab water as well as in a 100 L bioreactor (Laboratory Pilot Fermenter LP351) filled with 8.6 kg of bran and 65 L of deionized water and in a 2.5 L bioreactor equipped with two stirring blades (KLF bioreactor) filled with 200 g of bran and either 1.2 L of tap water, deionized water or buffer (50 mM NaOAc, pH 5.5). The pH was adjusted to 4.4 with 2 M HCl in case of water. Phytase was added (rPhyXT52 phytase, and *Debaryomyces castellii* phytase; 4000 $U \cdot kg_{bran}^{-1}$) and the reaction was carried out under stirring (1 h at 910 rpm in 400 L scale; 6 h at 500 rpm in 100 L scale; 12 h at 700 rpm in 2.5 L scale). The flow pattern in the bioreactors was comparable, but the speed varied due to different blade configurations and vessel sizes. Due to economic feasibility, the temperature of the largest scale production (400 L reaction) was not controlled. pH control in the bioreactors was done with NaOH and HCl (2 M in 2.5 L and 65 L scale; 5 M in 400 L scale). Supernatant and biomass were separated by sedimentation, biomass was washed three times with tap water in either half or equal volume as reaction volume (122 L, 65 L, or 1.2 L respectively), and separation was performed by sedimentation between each washing step. [135]

Water holding capacity (WHC) was determined using a modified protocol of Petersson *et al.* [116]. 5 g of biological material was incubated in 35 mL H_2O and shaken at 120 rpm. After 30 min of incubation, the bran/water slurries were centrifuged at 3860xg for 20 min. The supernatant was removed and the centrifuge tube containing the pellet and adsorbed water was weighted. The WHC was calculated as g water g^{-1} original dry sample. [135]

Adherent phosphorus content after enzymatic P-mobilization and drying was quantified by the molybdenum blue color reaction as described above. For this, 5 g of conditioned rye bran and 40 mL H_2O were shaken in a centrifuge tube at 200 rpm. After 20 min the suspension was centrifuged at 3860xg for 20 min and the P-content in the supernatant was determined as described in Chapter A.2.1. [135]

Xylanase and cellulase treatment of the cellular matrix was performed in preheated 50 mM NaOAc buffer at pH 4.4 and 37 °C. 1.5 g bran was added to 35 mL of the buffer, and 10 $U \cdot g_{bran}^{-1}$ or 25 $U \cdot g_{bran}^{-1}$ of the respective enzyme formulation as well as 4000 $U \cdot kg_{bran}^{-1}$ of the phytase blend (rPhyXT52 and *D. castellii* phytase) were added. At regular intervals, 500 µL was withdrawn, centrifuged for 1 min at 3860xg, and the P-content in the supernatant was determined using the molybdenum blue color reaction as described in Chapter A.2.1.

Ultrasound treatment of the cellular matrix was performed in 50 mL capped plastic tubes. The treatment was conducted in preheated 50 mM NaOAc buffer at pH 4.4 and 37 °C, with a bran to water ratio of 1 to 7. 4000 $U \cdot kg_{bran}^{-1}$ phytase blend (rPhyXT52 and *D. castellii* phytase) was added. The samples were sonicated for ten cycles of 30 s each at 70% power. After each cycle, the tubes were incubated at 37 °C for 1.5 min. For each time point, a new batch was prepared, and the experiments were performed in triplicates. Following the respective number of cycles, the tubes were centrifuged at 3860xg for 5 min, and the P-content in the supernatant was determined using the molybdenum blue color reaction as described in Chapter A.2.1.

Struvite precipitation was performed from 40 mL of process wastewater in a 100 mL glass beaker, unless otherwise stated. Likewise, the precipitations were carried out at room temperature, an equimolar input ratio of constituent ions and 32% NaOH solution. The Titrando 902 autotitrator was used for dosing. After reaching the target pH, the titration was stopped, the suspension was filtered with a round paper filter and the filter including filter cake was dried at 40 °C in a drying oven for 20 h to 70 h. For temperature studies, the beaker was placed in a water bath. The experimental setup is shown in Figure A.2.6 on the left.

Figure A.2.6: *Left:* Experimental setup for struvite precipitation in glass beaker, and *right:* during scaling of the precipitation (right).

Scaling of the struvite precipitation was realized using the same volumentric power input. The KLF (2.4 dm^3) contains three Rushton stirrers, each with six disks. The total diameter of the stirrer disks is 40 mm, with the respective disks being 11 mm long and 8 mm high. P contained in 1.74 L of the process wastewater was precipitated at 20 °C, and 438 rpm, using an equimolar input ratio of struvite constitution ions. After reaching pH 9, titration with 32% NaOH solution was stopped and the suspension was stirred for further 20 min at 438 rpm. The experimental setup is illustrated in Figure A.2.6 on the right

Struvite purification was investigated using the precipitate produced in the scaling experiment. First, recrystallization was performed. 1 g of precipitate was mixed with 40 mL of H_2O in a 100 mL beaker and dissolved at 900 rpm on a magnetic stirring plate and the dropwise addition of 32% HCl. The pH was recorded with a pH meter. After complete dissolution, struvite was precipitated with 32% NaOH solution. In addition to recrystallization, purification with organic and inorganic solvents was investigated. 1 g of the precipitate was stirred in 10 mL of the corresponding purification solution in a 50 mL glass beaker at room temperature and 900 rpm for 60 min. The purification solutions used were MeOH, EtOH, acetone, ethyl acetate, isopropanol, MTBE, isooctane, acetonitrile and hexane, 1% H_2SO_4, 1% HCl, and 1% acetic acid. Boiling water was also used for purification. Here, 1 g of precipitate was stirred with 40 mL H_2O in a 100 mL beaker at 900 rpm and heated to 100 °C in 10 °C steps. After purification, the suspensions were filtered, the filters including filter cake were dried at 40 °C and the purity was determined both gravimetrically and using thermo gravimetric analysis. For calculation, the purity of the initial precipitate was taken into account.

Phenol recovery from the process wastewater by liquid-liquid extraction was conducted with n-heptane, MTBE, n-xylol, and ethyl acetate in a one to one volume ratio. The emulsions were shaken overnight at room temperature. To improve extraction efficiency, the pH of the process wastewater was adjusted to pH 2 with 32% HCl solution as well as saturated with Na_2SO_4. Prior and after the incubation, the phenolic content in the process wastewater was measured using the DNS assay as outlined in Chapter A.2.1.

For phenol recovery from the process wastewater by solid-liquid extraction, the resins XAD 4, XAD 16 (both styrene-divinylbenze functionalized), XAD 1180 (designed for the recovery of large molecular weight plant extract, crosslinked divinylbenze), XAD 7HP (acrylic), and silica gel were tested. Prior to use, each resin was washed in ethanol for 30 min, followed by vacuum filtration. Subsequently, the resins were washed in 0.1 M NaOH for 30 min and filtered under vaccum. Finally, the resins were rinsed with H_2O during vaccum filtration until the filtrate reached a neutral pH. After each washing step, samples were taken to determine the dry matter gravimetrically at 105 °C until no further weight loss was observed.

Adsorbent testing

The adsorption experiments were initiated with a concentration of 50 mg·mL^{-1} of each adsorbent at varying pH levels: without pH adjustment (pH 4.4), pH 2, pH 1.

Concentration variation and Adsorption efficiency

The concentration of the resins was varied from 0.01 g·mL^{-1} to 0.2 g·mL^{-1} to determine the adsorption efficiency. Data obtained for XAD 4 and XAD 16 were also used to calculate adsorption isotherms.

Sequential adsorption testing

Adsorption studies were performed on 50 mg·mL^{-1} XAD 4 and XAD 1180 after initial adsorption on 50 mg·mL^{-1} XAD 16 to investigate the different molecular weights of phenolic compounds present in the process wastewater.

Desorption and recyclability

The desorption and recyclability of the resins were tested by first determining the load after adsorption. The resins were then agitated in ethanol for 20 min, followed by vaccum filtration. A sample of the filtrate was taken, diluted 1 to 10, and measured using the Folin-Ciocalteu assay as described in Chapter A.2.1. The resins were then agitated in 0.1 M NaOH for 20 min and filtered under vacuum. A sample of the filtrate was also taken, diluted 1 to 10, and measured. Subsequently, the resins were rinsed with deionized water during vaccum viltration until the filtrate reached a neutral pH. Dry matter content was determined, and the procedure was repeated to evaluate the recyclability of the resins.

***E. coli* BL21 growth** was performed on autoclaved process wastewater. Prior to sterilization, the P contained in the process wastewater was precipitated as struvite, resulting in 99% P removal. Two cryo-donuts containing *E. coli* BL21 with kanamycin resistance were inoculated in 20 mL LB medium supplemented with 50 µg·mL^{-1} kanamycin and incubated at 37 °C and 120 rpm in a culture flask with baffles. After 16 h the preculture reached an OD_{600} of 3.9. The preculture was then centrifuged and the cell pellet resuspended in 200 mL of the prepared process wastewater for growth.

B Supplementary Figures, Tables and Certificates

This chapter provides supplementary figures and tables that complement the main findings discussed in this thesis. In addition, the certificates of analysis for both phytic acid chemicals provided by the supplier are shown.

Figure B.1: Coloring of the bran extract by anthocyanins. The eluent of the ion exchange chromatography is shown. Loading of the IEX column with 5 mL bran extract diluted 1 to 5. Elution with 4 mL HCL. *Left:* Washing step with 8 mL 0.05 M HCL and *right:* subsequent elution with 4 mL 2 M HCL.

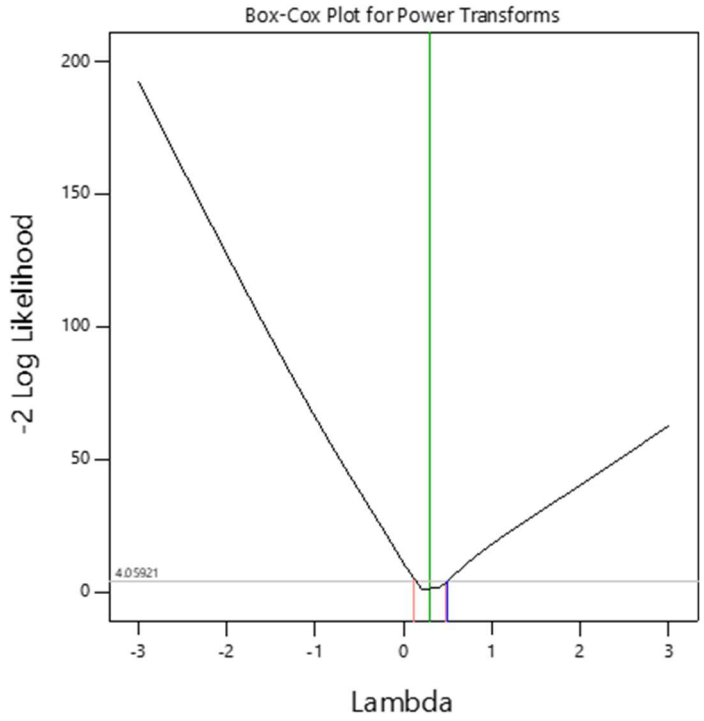

Figure B.2: Box-Cox plot for maximization of intrinsic enzyme activity. Conditions: 0.1 to 0.2 g bran in 50 mL reaction solution. Reaction solution: 0.0015 M phytic acid, 0.25 M NaOAc, 25 to 60 °C, pH 2 to 8. Software: Design Expert ® 12.

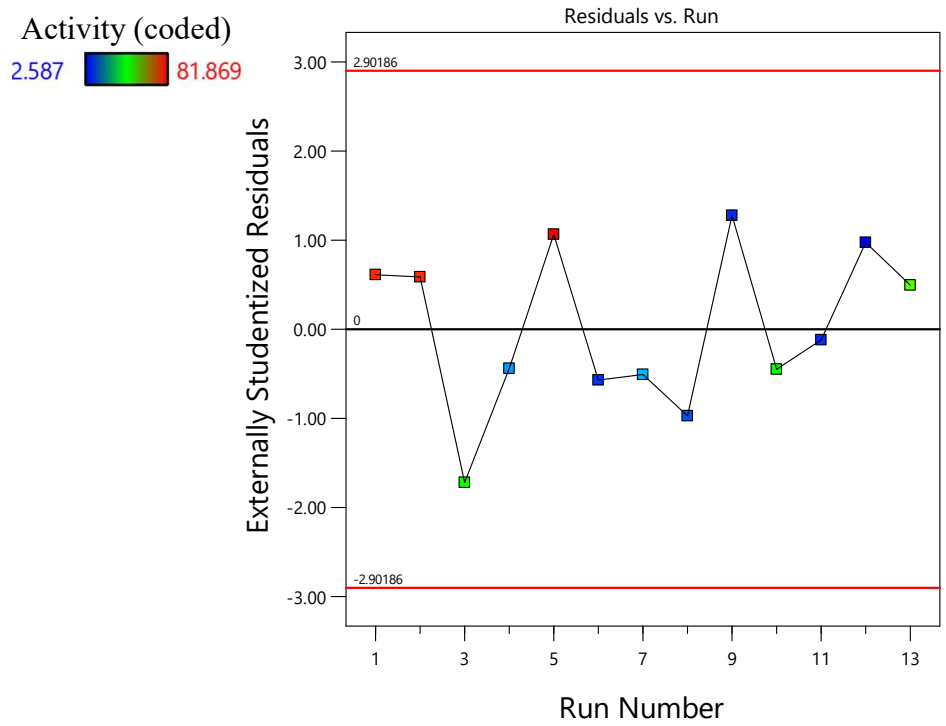

Figure B.3: Residues vs. experimental number for maximization of intrinsic enzyme activity. Conditions: 0.1 to 0.2 g bran in 50 mL reaction solution. Reaction solution: 0.0015 M phytic acid, 0.25 M NaOAc, 25 to 60 °C, pH 2 to 8. Software: Design Expert ® 12.

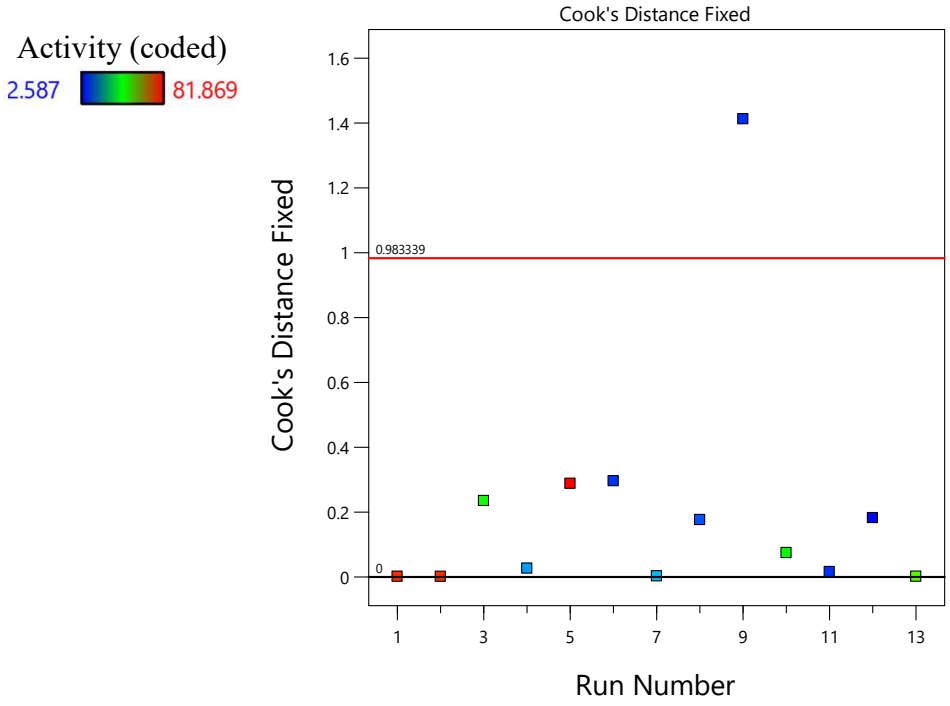

Figure B.4: Cook´s distance vs. experimental number for maximization of intrinsic enzyme activity. Conditions: 0.1 to 0.2 g bran in 50 mL reaction solution. Reaction solution: 0.0015 M phytic acid, 0.25 M NaOAc, 25 to 60 °C, pH 2 to 8. Software: Design Expert ® 12.

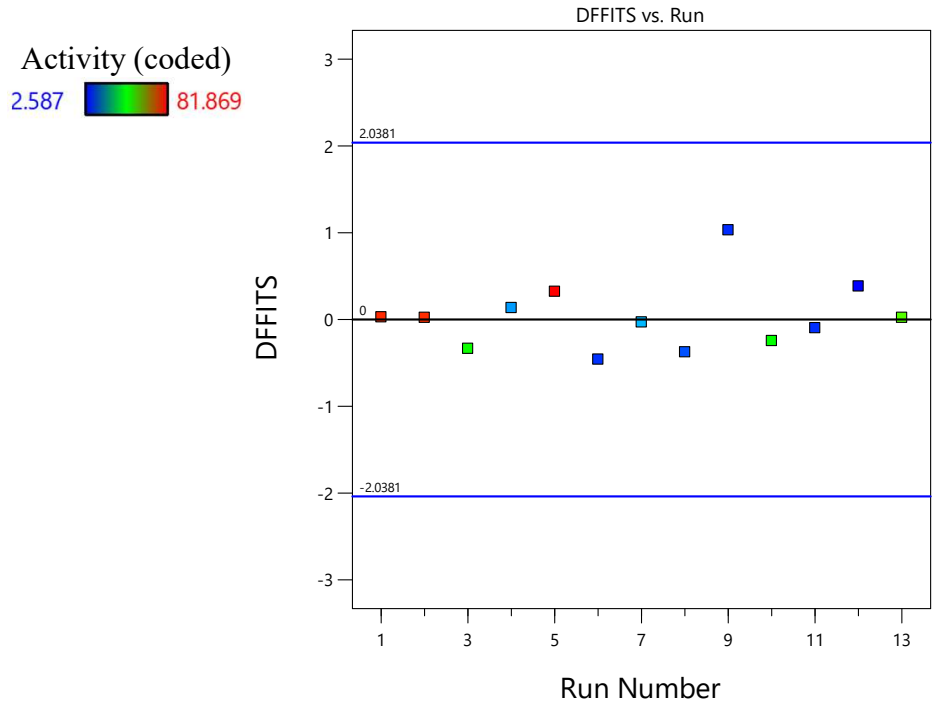

Figure B.5: DFFITS representation for maximization of intrinsic enzyme activity. Conditions: 0.1 to 0.2 g bran in 50 mL reaction solution. Reaction solution: 0.0015 M phytic acid, 0.25 M NaOAc, 25 to 60 °C, pH 2 to 8. Software: Design Expert ® 12.

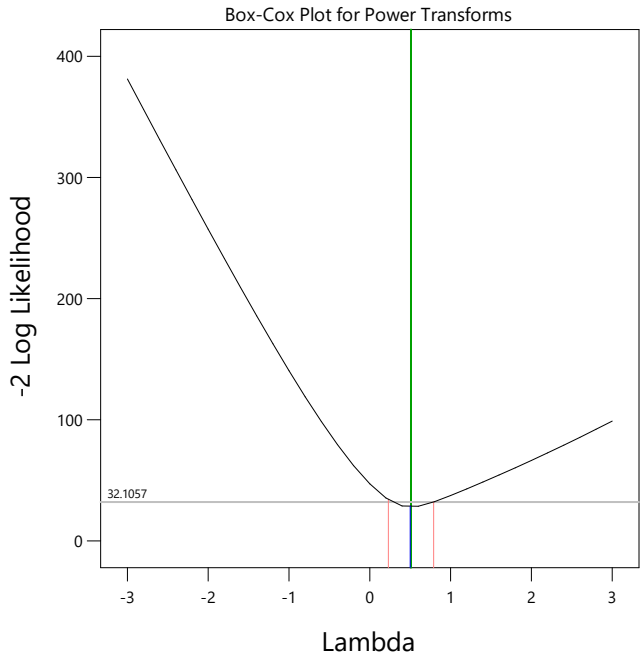

Figure B.6: Box-Cox plot for the maximization of inositol-P degradation by intrinsic enzymes. Conditions: 1.5 g bran, 25 to 60 °C, pH 2 to 8, 30 to 1000% (v/w) water content, 30 to 60 min reaction time. Software Design Expert® 12.

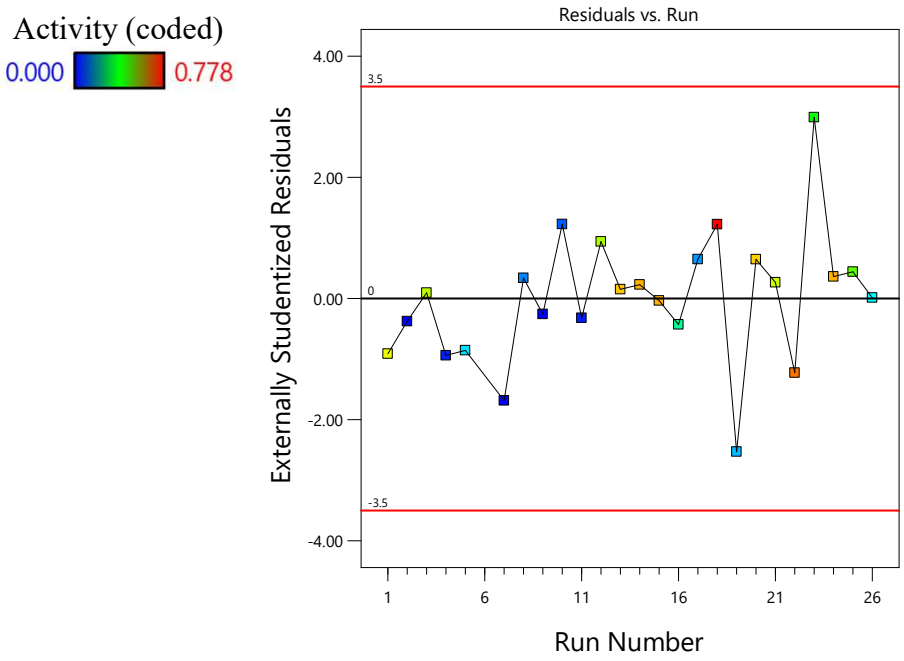

Figure B.7: Residuals vs. experimental run for the maximization of inositol-P degradation by intrinsic enzymes. Conditions: 1.5 g bran, 25 to 60 °C, pH 2 to 8, 30 to 1000% (v/w) water content, 30 to 60 min reaction time. Software Design Expert® 12.

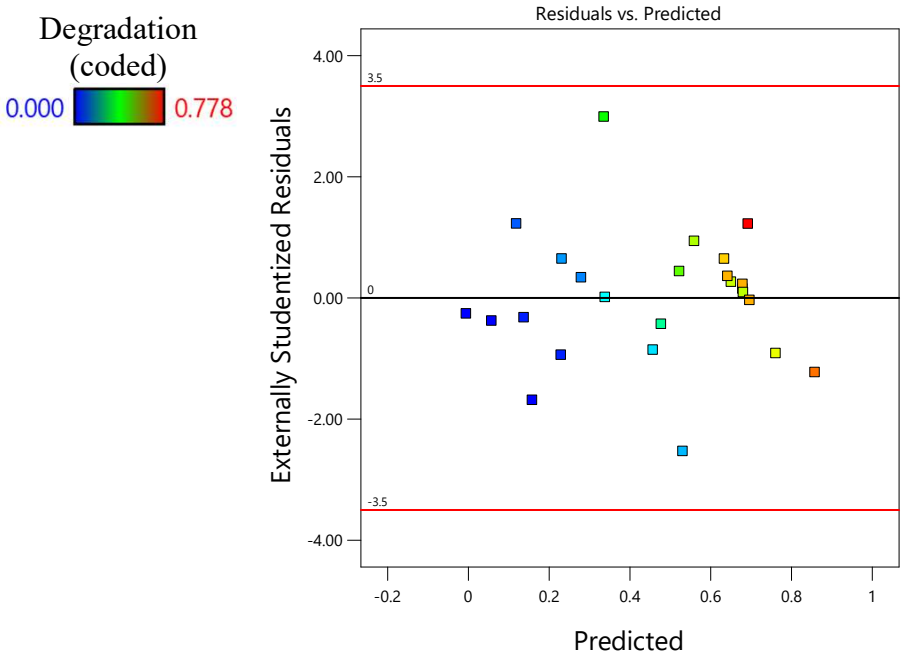

Figure B.8: Residues vs. predicted values for the maximization of inositol-P degradation by intrinsic enzymes. Conditions: 1.5 g bran, 25 to 60 °C, pH 2 to 8, 30 to 1000% (v/w) water content, 30 to 60 min reaction time. Software Design Expert® 12.

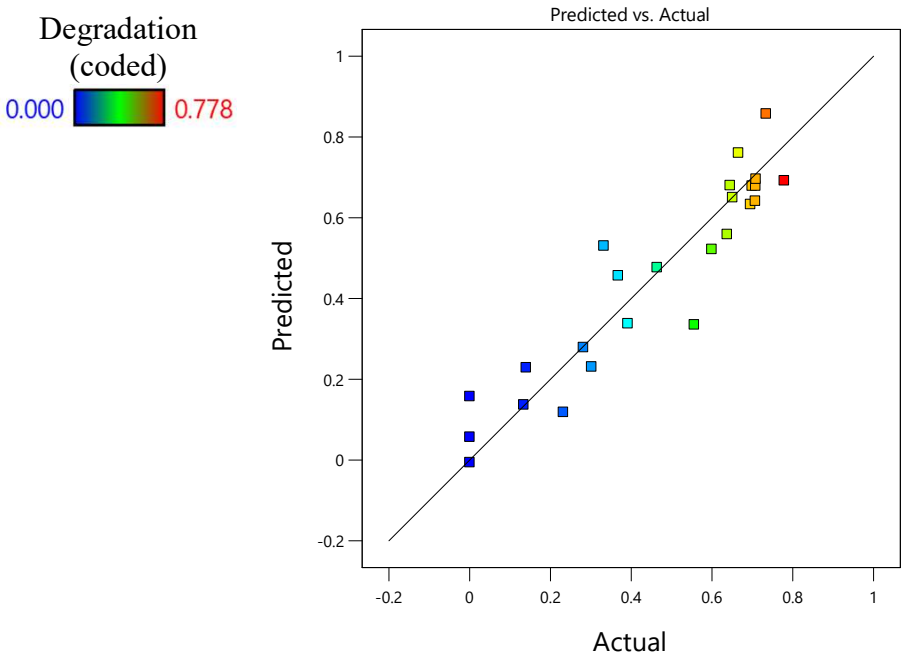

Figure B.9: Precited vs. actual plot for the maximization of inositol-P degradation by intrinsic enzymes. Conditions: 1.5 g bran, 25 to 60 °C, pH 2 to 8, 30 to 1000% (v/w) water content, 30 to 60 min reaction time. Software Design Expert® 12.

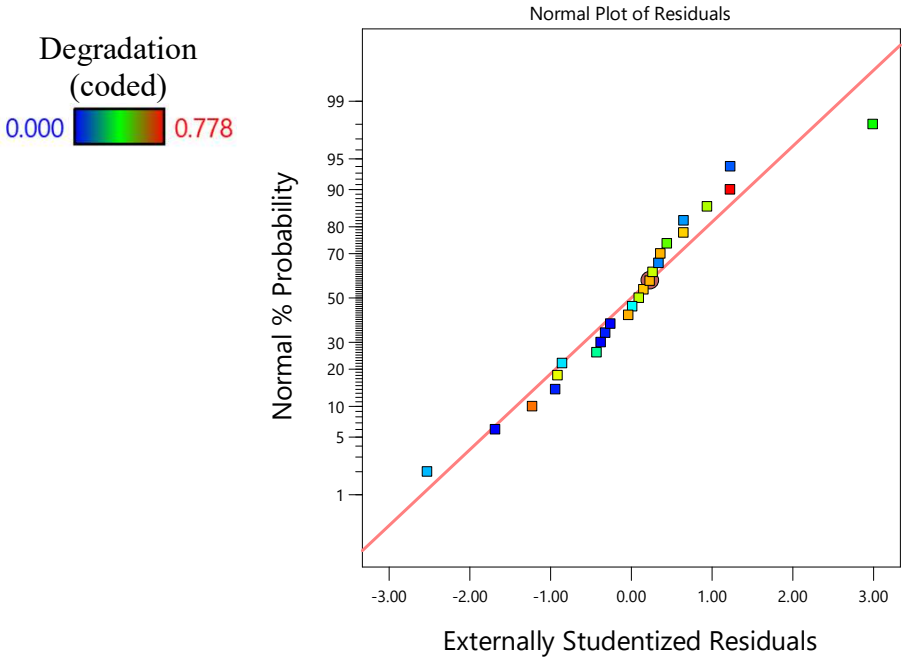

Figure B.10: Probability plot for maximization of inositol-P degradation by intrinsic enzymes. Conditions: 1.5 g bran, 25 to 60 °C, pH 2 to 8, 30 to 1000% (v/w) water content, 30 to 60 min reaction time. Software Design Expert® 12.

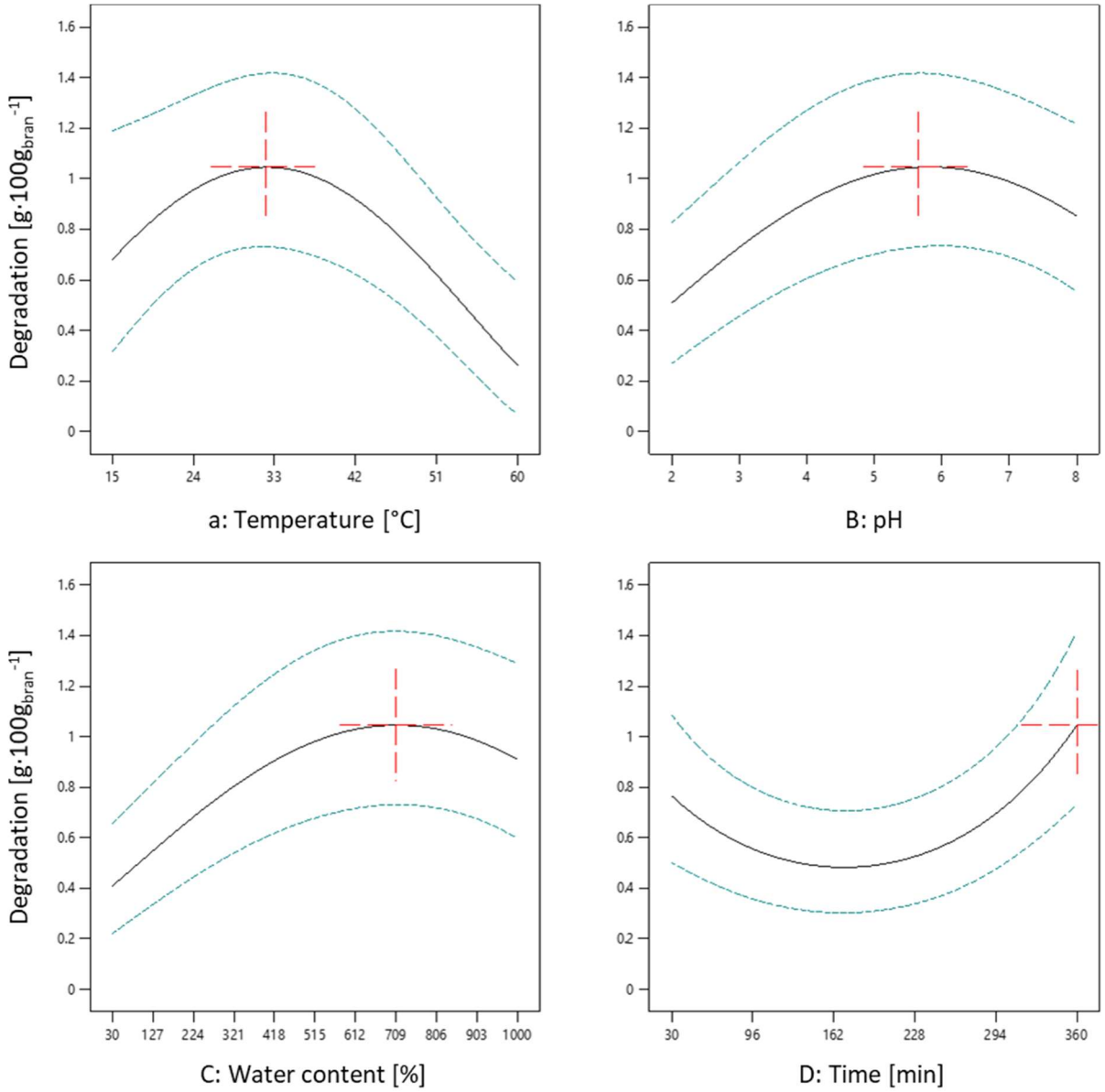

Figure B.11: Influence of temperature, pH, water content and time on inositol-P degradationby intrinsic enzymes. Conditions. 1.5 g bran, 25 to 60 °C, pH 2 to 8, 30 to 10005 /(v/w) water content, 30 to 60 min. Software Design Expert® 12.

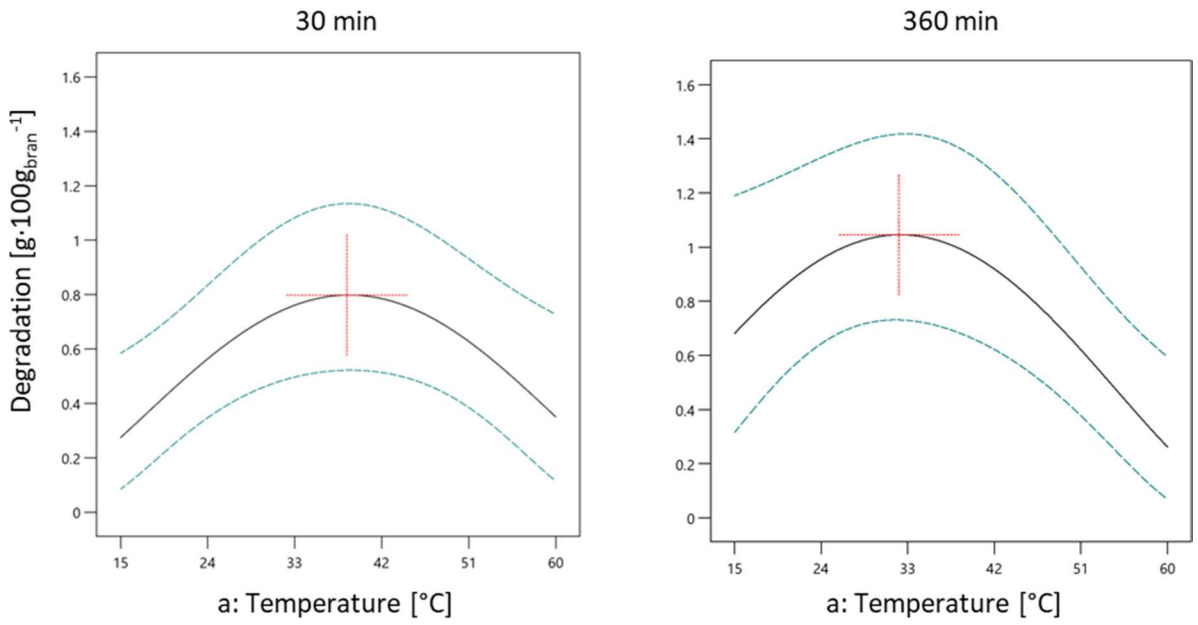

Figure B.12: Temperature influence at 30 min and 360 min reaction time for the maximization of inositol-P degradation by intrinsic enzymes. Software Design Expert® 12.

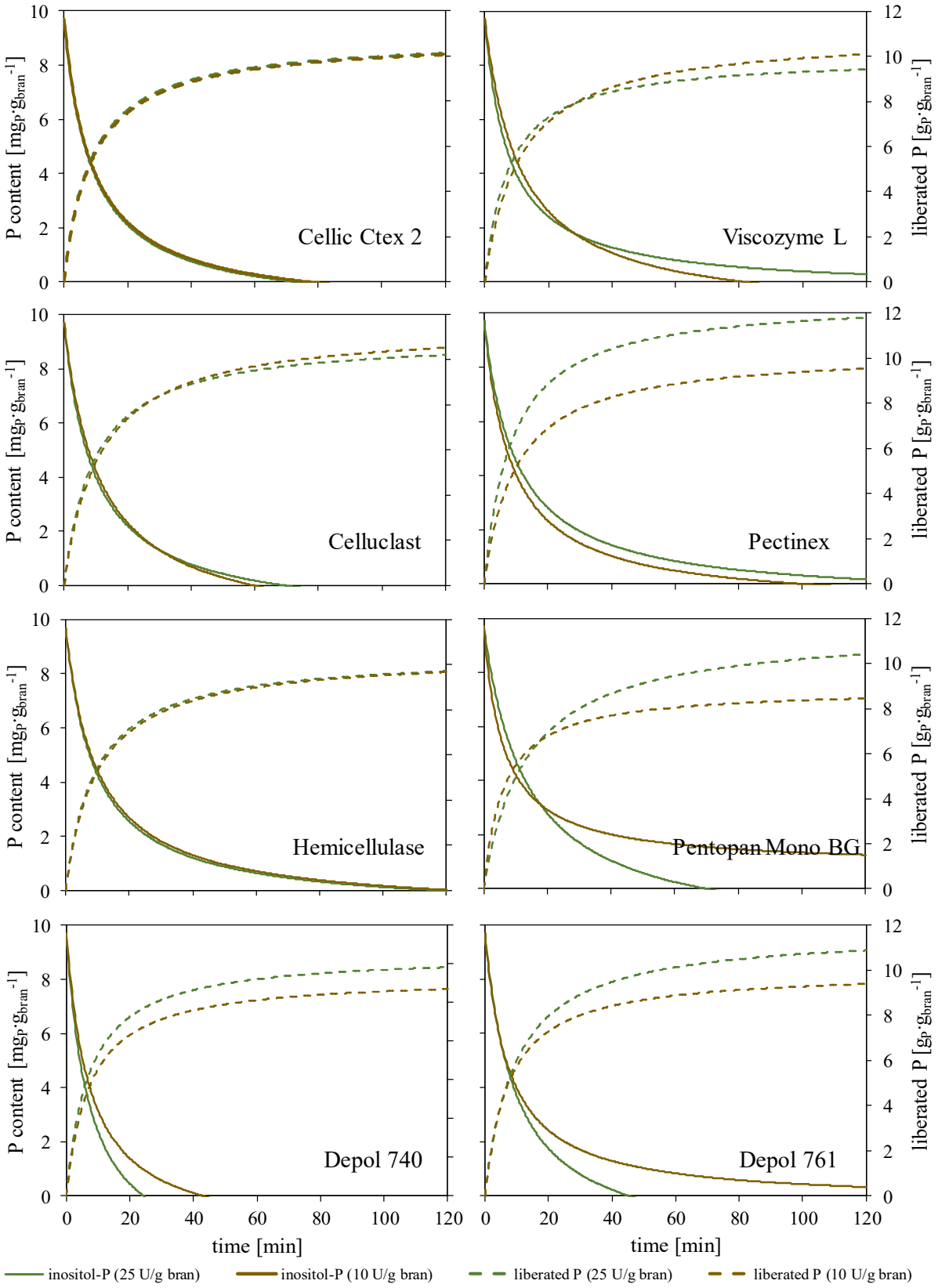

Figure B.13: Inositol-P content in rye bran and the liberated P during the combined enzymatic P-mobilization. Addition of 10 and 25 U·g_{bran}^{-1} of the respective cellulase and xylanase formulations and 4000 U·kg^{bran-1} rPhyXT52 and *D. castellii* phytase blend. Conditions: pH 4.4 and 37 °C. Kinetic simulations to the measured data using Michealis-Menten model.

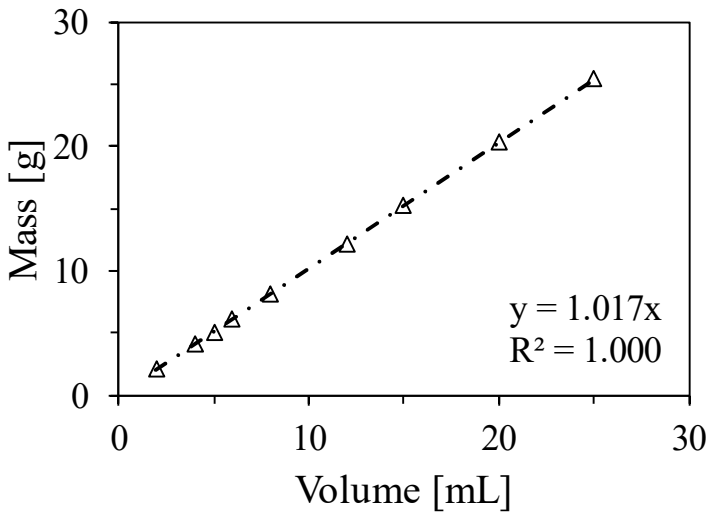

Figure B.14: Density determination of the process wastewater at room temperature.

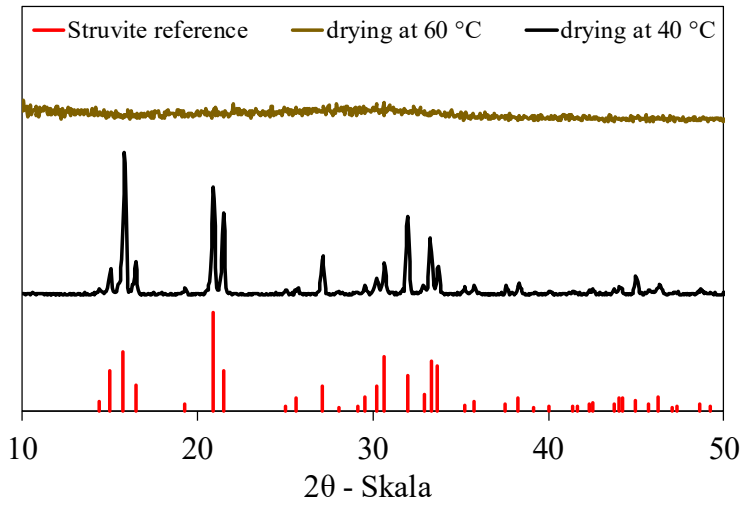

Figure B.15: Diffractograms for the precipitate after drying at 40 °C and 60 °C.

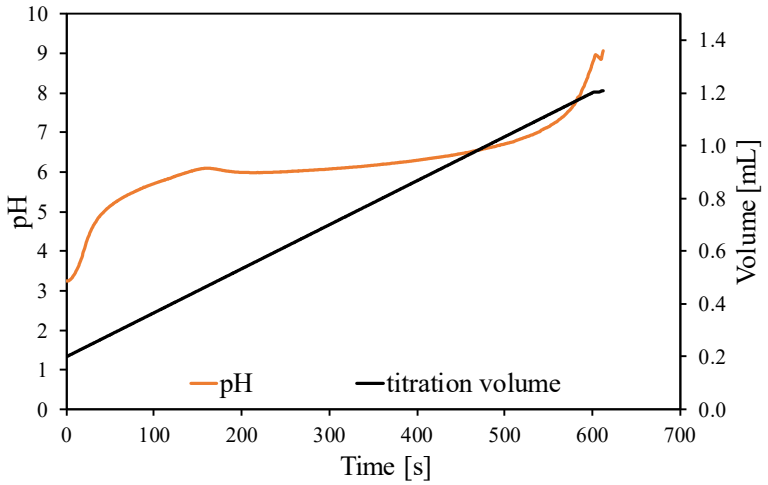

Figure B.16: Titration curve for the recrystallization experiment.

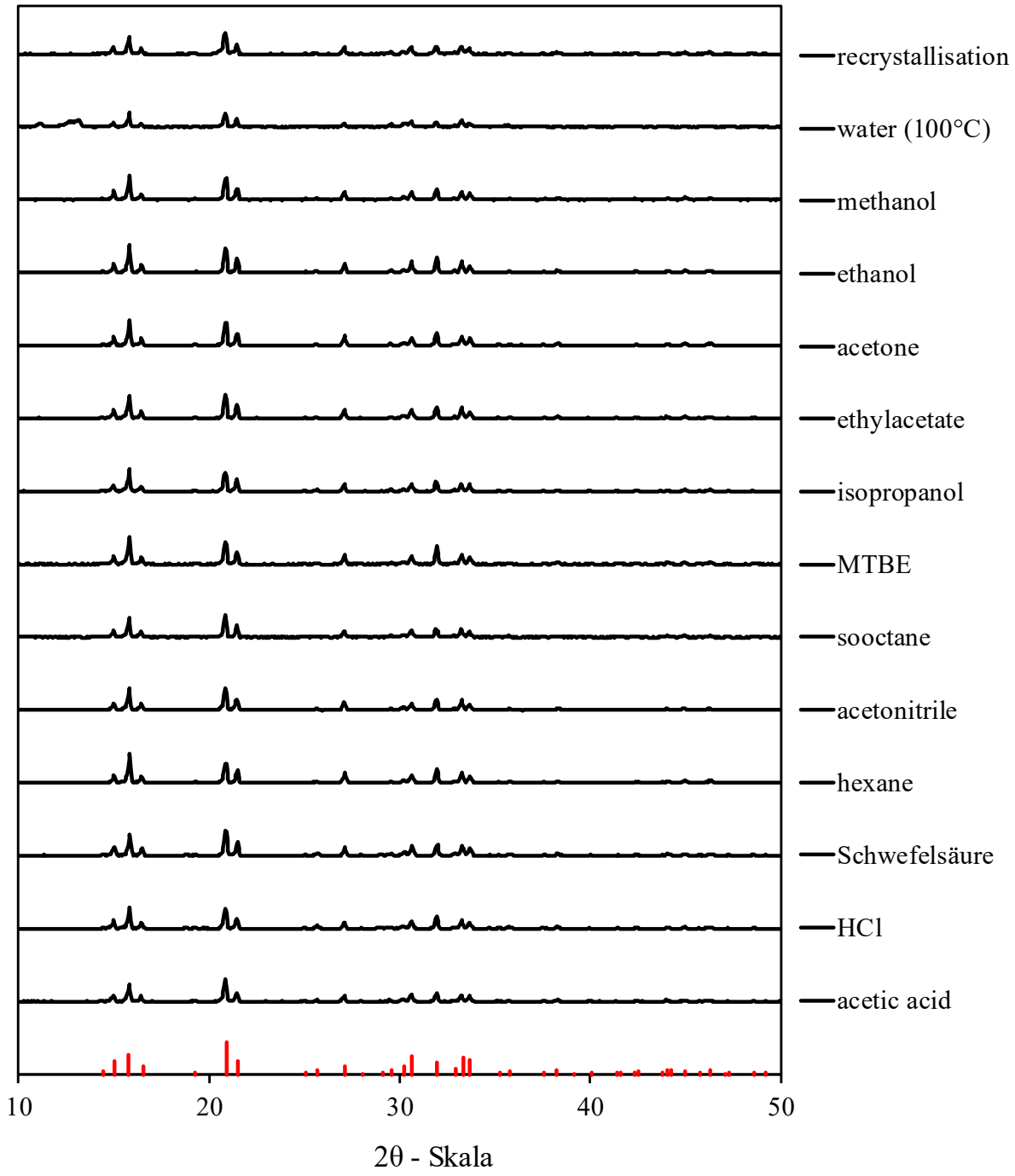

Figure B.17: Diffractograms of the precipitates after different purification treatment.

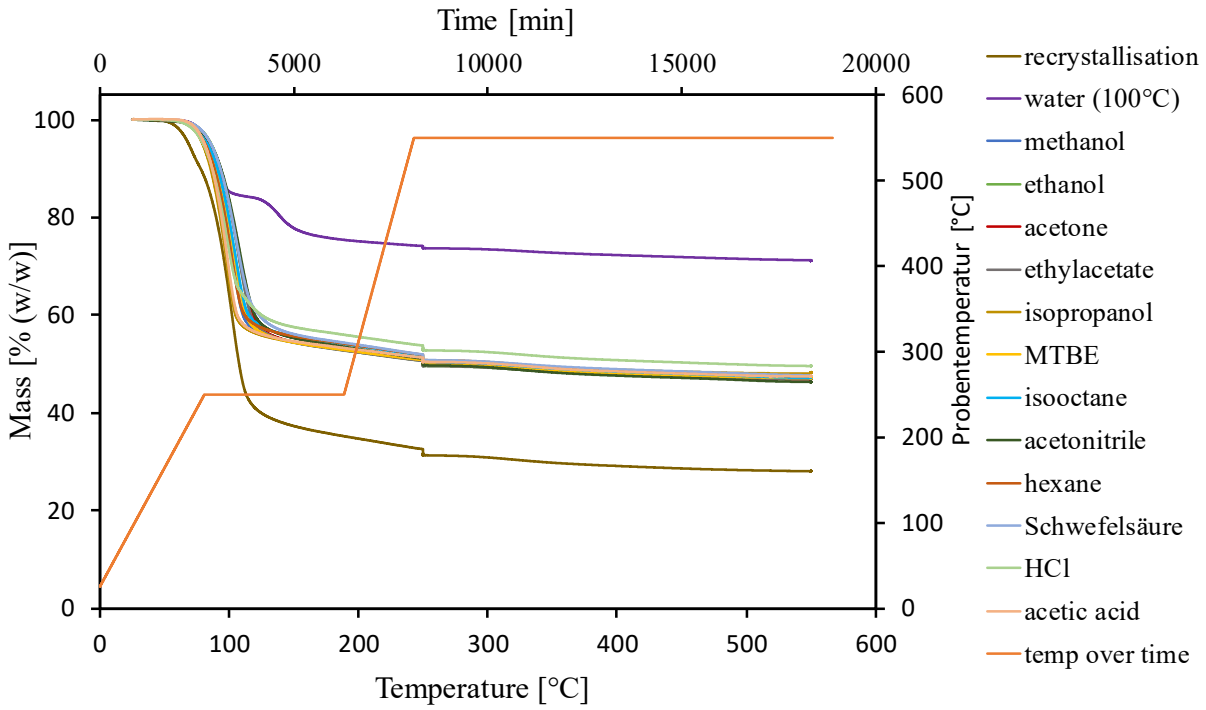

Figure B.18: Thermogravimetric analysis after struvite purification using different solvents and recrystallization.

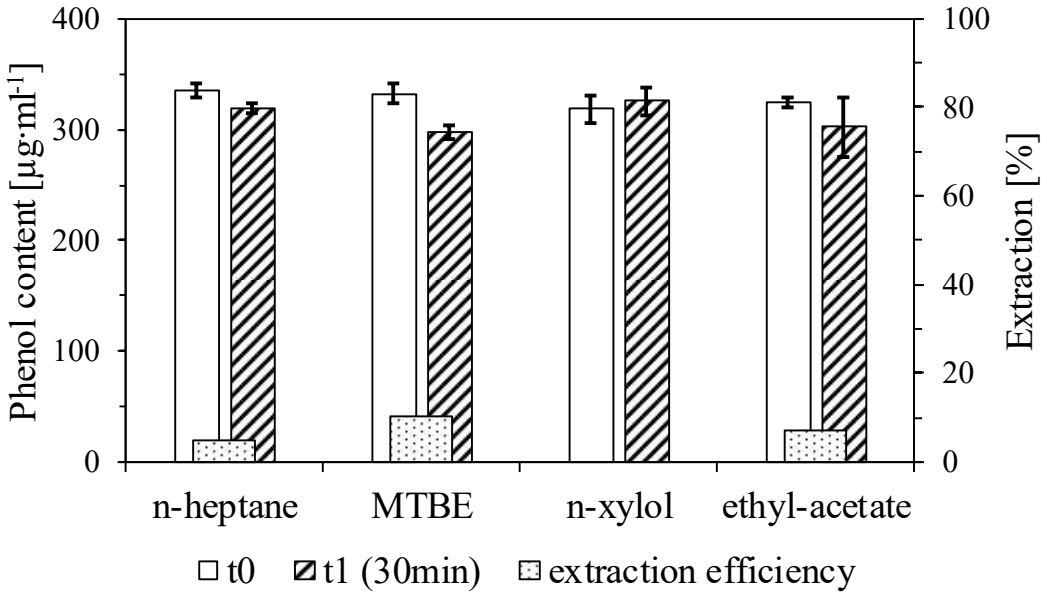

Figure B.19: Liquid-liquid extraction for the recovery of phenolic compounds from the process wastewater. The solvents were incubated and shaken overnight at room temperature in a one to one volume ration with the process wastewater.

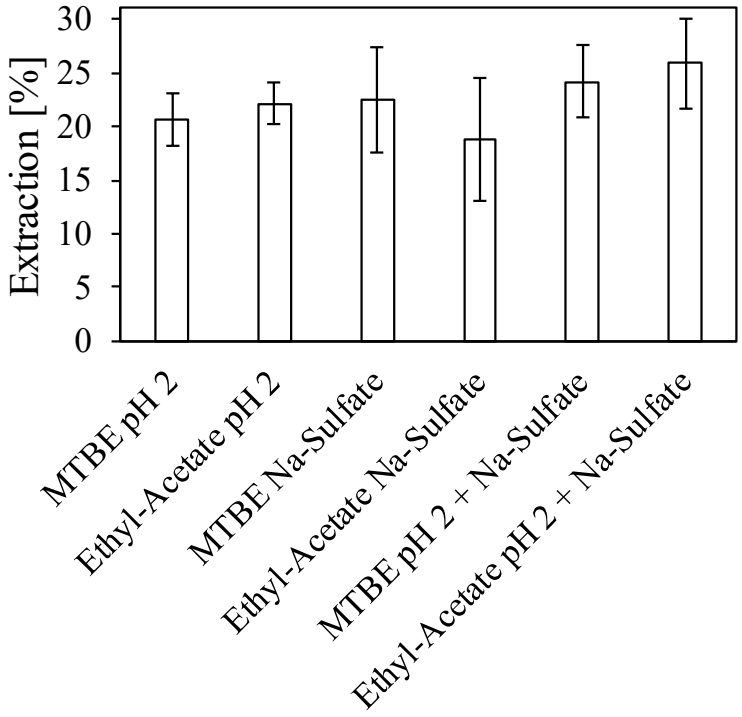

Figure B.20: Extraction efficiency of liquid-liquid extraction for MTBE and ethyl acetate including salting out and pH titration of the process wastewater. The solvents were incubated and shaken overnight at room temperature in a one to one volume ration with the process wastewater.

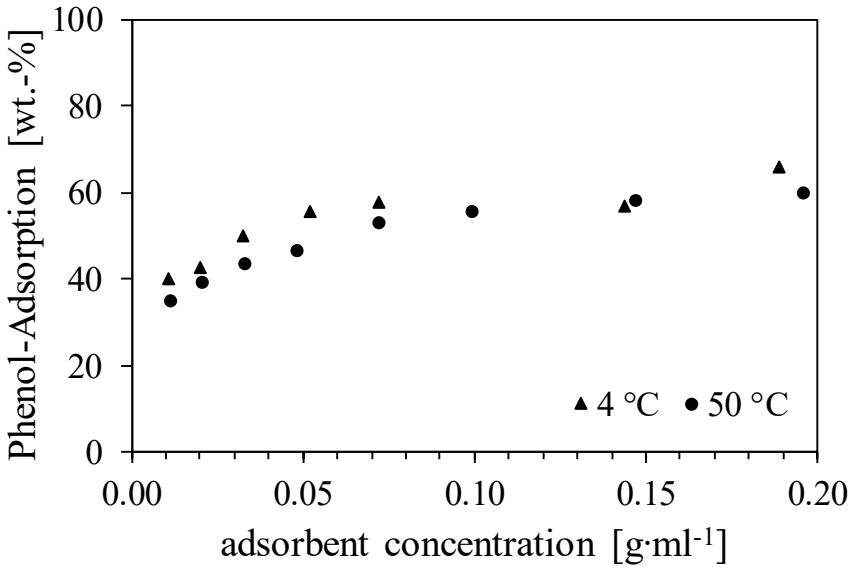

Figure B.21: Adsorption efficiency for XAD 16 at different temperatures and adsorbent concentrations. Shaken overnight.

Table B.1: Experimental design for maximizing inositol phosphorus degradation. Conditions: 15 to 60 °C (hard to change factor), pH 2 to 8, water content 30 to 1000% /v/w), 30 to360 min. Experimental design created with Design Expert® 12.

Group	Run	Temperature [°C]	pH	Ratio [% (v/w)]	Time [min]	Degradation [$g \cdot 100 g_{bran}^{-1}$]
1	1	48.1	4.4	1000.00	30	0.44
1	2	48.1	8.0	30.0	30	0.00
1	3	48.1	8.0	536.1	360	0.42
1	4	48.1	20.	30.0	247	0.02
2	5	15.0	5.2	631.4	228	0.14
2	6	15.0	2.0	30.0	360	-[a]
2	7	15.0	5.4	30.0	30	0.00
2	8	15.0	8.0	1000.0	30	0.08
3	9	60.0	2.0	1000.0	351	0.00
3	10	60.0	5.5	30.0	360	0.05
3	11	60.0	8.0	903.0	178	0.02
3	12	60.0	2.9	369.5	30	0.41
4	13	37.5	5.0	515.0	195	0.49
4	14	37.5	5.0	515.0	195	0.50
5	15	25.0	8.0	1000.0	310	0.50
5	16	25.0	8.0	553.8	30	0.22
5	17	25.0	5.6	30.0	168	0.09
5	18	25.0	2.0	381.8	360	0.61
6	19	41.2	2.0	660.5	142	0.11
6	20	41.2	5.3	456.8	195	0.48
6	21	41.2	8.0	1000.0	30	0.42
6	22	41.2	5.0	1000.0	360	0.54
7	23	25.0	2.0	1000.0	96	0.31
7	24	25.0	5.2	597.5	219	0.50
7	25	25.0	2.0	30.0	30	0.36
7	26	25.0	8.0	30.0	360	0.15

Table B.2: Struvit solubility products at different pH and 20°C.

	K_{sp}	pK_{sp}
pH 8	$1.11 \cdot 10^{-10}$	9.96
pH 9	$3.87 \cdot 10^{-12}$	11.41
pH 10	$7.84 \cdot 10^{-11}$	10.11
pH 11	$7.10 \cdot 10^{-11}$	10.15
pH 12	$4.65 \cdot 10^{-11}$	10.33

Table B.3: Struvite solubility products at different temperature and pH 9.

	K_{sp}	pK_{sp}
20 °C	$1.43 \cdot 10^{-10}$	9.84
25 °C	$8.04 \cdot 10^{-11}$	10.09
30 °C	$1.09 \cdot 10^{-10}$	9.96
35 °C	$9.53 \cdot 10^{-10}$	9.02
40 °C	$5.50 \cdot 10^{-7}$	6.26

Table B.4: Struvite solubility products at pH 9, 20 °C, and different Mg^{2+} input ratio**.**

	K_{sp}	pK_{sp}
1:0.9:1	$6.87 \cdot 10^{-12}$	11.16
1:1:1	$3.87 \cdot 10^{-12}$	11.41
1:1.1:1	$9.07 \cdot 10^{-12}$	11.04
1:1.2:1	$1.65 \cdot 10^{-11}$	10.78
1:1.3:1	$1.44 \cdot 10^{-11}$	10.84

Table B.5: Struvit solubility products at pH 9, 20 °C, and different NaOH concentrations.

	K_{sp}	pK_{sp}
32 % NaOH undiluted	$3.87 \cdot 10^{-12}$	11.41
32 % NaOH diluted	$1.05 \cdot 10^{-10}$	9.98
1 M NaOH undiluted	$5.98 \cdot 10^{-11}$	10.22
1 M NaOH diluted	$6.74 \cdot 10^{-12}$	11.17

Table B.6: Struvite solubility products at pH 9, 20 °C, and different nucleation conditions.

	K_{sp}	pK_{sp}
Without convection	$9.22 \cdot 10^{-8}$	7.04
Seed crystals	$1.36 \cdot 10^{-8}$	7.87
60 min stirring	$3.87 \cdot 10^{-12}$	11.41

Table B.7: Struvite solubility products at pH 9, 20 °C, and different stirring times.

	K_{sp}	pK_{sp}
10 min	$9.47 \cdot 10^{-13}$	12.02
20 min	$2.69 \cdot 10^{-11}$	10.57
30 min	$1.06 \cdot 10^{-11}$	10.98
45 min	$1.46 \cdot 10^{-11}$	10.84
60 min	$1.06 \cdot 10^{-10}$	9.98
90 min	$1.71 \cdot 10^{-11}$	10.77
120 min	$1.32 \cdot 10^{-9}$	8.88

Table B.8: Composition of struvite precipitates resulting from the scale-up experiment. Quantification of constitutent ions by ICP-OES.

	Mg [g·kg^{-1}]	P [g·kg^{-1}]	Na [g·kg^{-1}]	H [g·kg^{-1}]	K [g·kg^{-1}]	O (calculated) [g·kg^{-1}]	$NH_4MgPO_4 \cdot 6H_2O$
KL32 SK 13 05	97.6	125.3	45.0	62.0	14.6		
Scale-41 Struvite 11 08	95.0	122.0	47.0	64.0	16.5	655.4	
Molar mass [g·mol^{-1}]	24.3	31.0	14.0	1.0	39.1	16.0	245.4
Stoichiometry	1	1	1	16		10	
Index value	99.0	126.2	57.1	65.2	0.0	651.9	1000.0

BLDpharm

BLD Pharmatech GmbH
sales-eu@bldpharm.com

Certificate of Analysis

Compound Information

Product Name	Dipotassium phytate
Catalog No.	BD134707
CAS No.	129832-03-7
Formula	C6H18K2O24P6
Molecular Weight	738.23

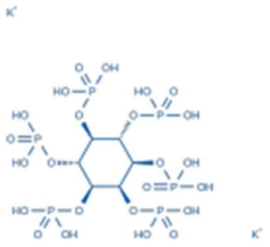

Batch Information

Lot No.	AGY557
Storage	Inert atmosphere,2-8°C
Mfg. Date	05/31/2019
Report Date	06/03/2019
Retest Date	07/30/2021

QC Test Information

Test Items	Test Result
Appearance	Off white solid
Structure	Conforms to Structure
Purity	91.46%

Analyst: Ada Li

Ada Li

Date: 08/09/2020

Approved: Monica Zhang

Monica Zhang

Date: 08/09/2020

Tel:+49-6303-208-2088 Email:sales-eu@bldpharm.com Web:www.bldpharm.com
Address: Trippstadter Str. 110, D-67663 Kaiserslautern, Germany.

SIGMA-ALDRICH®

3050 Spruce Street, Saint Louis, MO 63103 USA
Email USA: techserv@sial.com Outside USA: eurtechserv@sial.com

Certificate of Analysis

Product Name:	Phytic acid sodium salt hydrate rice Yes
Product Number:	P8810
Batch Number:	BCCC6842
Brand:	Sigma
CAS Number:	14306-25-3
Formula:	$C_6H_{18}O_{24}P_6$ * xNa+ * yH_2O
Formula Weight:	660.04
Quality Release Date:	27 JAN 2020

TEST	SPECIFICATION	RESULT
APPEARANCE (COLOR)	WHITE TO OFF WHITE	WHITE
APPEARANCE (FORM)	POWDER	POWDER
SOLUBILITY (COLOR)	COLORLESS TO FAINT YELLOW	COLORLESS
SOLUBILITY (TURBIDITY)	CLEAR TO VERY SLIGHTLY HAZY	CLEAR
SOLUBILITY (METHOD)	50MG/ML IN WATER	50MG/ML IN WATER
LOSS ON DRYING	REPORT RESULT	5.7 %
PROTON NMR SPECTRUM	CONFORMS TO STRUCTURE	CONFORMS
CARBON 13 NMR SPECTRUM	CONFORMS TO STRUCTURE	CONFORMS
METAL TRACE ANALYSIS (ICP)	CALCIUM NMT 2 % (DRIED BASIS)	PASSED
ASSAY (ICP)	SODIUM MIN. 5 MOLES/MOLE; PHOSPHORUS 19.0 - 25.0 % (DRIED BASIS)	SODIUM 5 MOLES/MOLE; PHOSPHORUS 22.2 % (DRIED BASIS)

Dr. Reinhold Schwenninger
Quality Assurance
Buchs, Switzerland

C LIST OF ABBREVIATIONS

ATR	Attenuated total reflection
CAS	Chemical Abstracts Service
CCD	Central-Composite-Design
DM	Dry matter
DoE	Statistical Design of Experiments
E. coli	*Escherichia coli*
EC	Enzyme Commission
FT-IR	Fourier-Transform Infrared Spectroscopy
FT-MIR	Fourier-Transform Mid-Infrared Spectroscopy
GfE	Gesellschaft für Ernährungsphysiologie
HPIC	High Performance Ion Chromatography
HPLC	High Performance Liquid Chromatography
inositol-P	Inositol phosphorus; amount of P bound to inositol phosphate
InsP	Inositol-monophosphate
$InsP_2$	Inositol-bisphosphat
$InsP_3$	Inositol-trisphosphate
$InsP_4$	Inositol-tetrakisphosphate
$Insp_5$	Inositol-pentakisphosphate
$InsP_6$	Inositol-hexakisphosphate
IEX	Ion Exchange Chromatography
LCA	Life Cycle Assessment
ME_{pig}	Metabolizable energy for pigs
MIR	Mid infrared
NIR	Near infrared
NMR	Nuclear Magnetic Resonance Spectroscopy
PAT	Process Analytical Technology
P	Phosphorus

P_I	Inorganic phosphorus
PCA	Principal Component Analysis
PLSR	Partial Least Squares Regression
rpm	Rounds per minute [min^{-1}]
RMSECV	Root Mean Square Error of Cross Validation
RMSEP	Root Mean Square Error of Prediction
SGDs	Sustainable Development Goals
STR	Stirred Tank Reactor
TBAH	Tetrabutylammonium hydroxide
TEA	Techno-Economic Analysis
TOM-complex	Translocase of the outer mitochondrial membrane
WHC	Water Holding Capacity
wt.-%	Weight percentage
X_{10}	10^{th} percentile
X_{50}	50^{th} percentile
X_{90}	90^{th} percentile

D LIST OF SYMBOLS

ΔE_{bio}	Error originating from biological fluctuations
ΔE_{cal}	Error of calibration
ΔE_{IEX}	Error originating from Ion Exchange Chromatography
ΔE_{total}	Total error
A	Matrix A
A_{DH}	Debye-Hückel constant
A_i	Peak Area of compound i
A_{total}	Total peak area
ß	Model parameter
c_i	Concentration of species i
$C_{f,i}$	Conversion factor for i^{th} degree of phosphorylation
d	Outer diameter of the impeller
$d_{2,3\ dry}$	Sauter mean diameter
ε	Residual vector
E	Enzyme
ES	Enzyme-Substrate-Complex
F_{swell}	Average swelling factor
γ_i	Activity coefficient
I	Ionic strength
k_1, k_2, k_{-1}	Rate constants
k_i	Model constant or concentration of species i
K_M	Michaelis-Menten constant
K_{sp}	Solubility product
M	Molar mass
m_i	Mass of species i
$m_{i,bran}$	Mass of species i in bran
$m_{i,liquid}$	Mass of species I in liquid phase
n	Count of elements, number of items

Ne	Newton number
P	Product
$Q_{2,3}$	Volume specific particle size distribution
Re	Reynolds number
ρ	Density
S	Substrate
SE	Standard error
S_V	Volume specific surface area
σ	Standard deviation
u_i	Input Factor
v	Reaction velocity
v_0	Initial rate
v_{max}	Maximum reaction velocity
ν	Kinematic visosity
$V_{2,3\ dry}$	Mean volume of dry particles
$V_{2,3\ soaked}$	Mean volume of soaked particles
Ψ	Sphericity
X	Independent variable
Y	Dependent variable
$\hat{Y}$	Predicted value
Z	Ion charge

E LIST OF FIGURES

F LIST OF TABLES

G REFERENCES

1. Thornton, P.K. Livestock production: recent trends, future prospects. *Philos. Trans. R. Soc. Lond. ,. B,. Biol. Sci.* **2010**, *365*, 2853–2867, doi:10.1098/rstb.2010.0134.
2. Hannah, R.; Max, R. Meat and Dairy Production. Available online: https://ourworldindata.org/ (accessed on 26 November 2021).
3. Herrmann, K.R.; Ruff, A.J.; Schwaneberg, U. Phytase-based phosphorus recovery process for 20 distinct press cakes. *Sustainable Chemistry & Engineering* **2020**, 3913–3921, doi:10.1021/acssuschemeng.9b07433.
4. Reta, G.; Dong, X.; Li, Z.; Su, B.; Hu, X.; Bo, H.; Yu, D.; Wan, H.; Liu, J.; Li, Y.; et al. Environmental impact of phosphate mining and beneficiation: review. *IJH* **2018**, *2*, doi:10.15406/ijh.2018.02.00106.
5. Blengini, G.A.; El Latunussa, C.; Eynard, U.; Torres de Matos, C.; Wittmer, D.M.A.G.; Georgitzikis, K.; Pavel, C.C.; Carrara, S.; Mancini, L.; Unguru, M.; et al. *Study on the EU's list of critical raw materials (2020)*: *Final report;* Publications Office of the European Union: Luxembourg, 2020, ISBN 9789276210498.
6. Schipanski, M.E.; Bennett, E.M. The Influence of Agricultural Trade and Livestock Production on the Global Phosphorus Cycle. *Ecosystems* **2012**, *15*, 256–268, doi:10.1007/s10021-011-9507-x.
7. Yuan, Z.; Jiang, S.; Sheng, H.; Liu, X.; Hua, H.; Liu, X.; Zhang, Y. Human Perturbation of the Global Phosphorus Cycle: Changes and Consequences. *Environ. Sci. Technol.* **2018**, *52*, 2438–2450, doi:10.1021/acs.est.7b03910.
8. Widderich, N.; Mayer, N.; Ruff, A.J.; Reckels, B.; Lohkamp, F.; Visscher, C.; Schwaneberg, U.; Kaltschmitt, M.; Liese, A.; Bubenheim, P. Conditioning of Feed Material Prior to Feeding: Approaches for a Sustainable Phosphorus Utilization. *Sustainability* **2022**, *14*, 3998, doi:10.3390/su14073998.
9. Herrmann, K.R.; Ruff, A.J.; Infanzón, B.; Schwaneberg, U. Engineered phytases for emerging biotechnological applications beyond animal feeding. *Appl. Microbiol. Biotechnol.* **2019**, *103*, 6435–6448, doi:10.1007/s00253-019-09962-1.
10. Hirvonen, J.; Liljavirta, J.; Saarinen, M.T.; Lehtinen, M.J.; Ahonen, I.; Nurminen, P. Effect of Phytase on in Vitro Hydrolysis of Phytate and the Formation of myo-Inositol Phosphate Esters in Various Feed Materials. *J. Agric. Food Chem.* **2019**, *67*, 11396–11402, doi:10.1021/acs.jafc.9b03919.
11. Sun, M.; He, Z.; Jaisi, D.P. Role of metal complexation on the solubility and enzymatic hydrolysis of phytate. *PLoS One* **2021**, *16*, 1-16, doi:10.1371/journal.pone.0255787.
12. Rutherfurd, S.M.; Chung, T.K.; Moughan, P.J. Effect of microbial phytase on phytate P degradation and apparent digestibility of total P and Ca throughout the gastrointestinal tract of the growing pig. *J. Anim. Sci.* **2014**, *92*, 189–197, doi:10.2527/jas.2013-6923.
13. Khan, F.A.; Ansari, A.A. Eutrophication: An Ecological Vision. *Bot. Rev* **2005**, *71*, 449–482, doi:10.1663/0006-8101(2005)071[0449:EAEV]2.0.CO;2.

14. Blume, H.-P.; Welp, G.; Thiele-Bruhn, S.; Brümmer, G.W.; Horn, R.; Tippkötter, R.; Kandeler, E.; Kögel-Knabner, I.; Kretzschmar, R.; Stahr, K.; et al. *Scheffer/Schachtschabel: Lehrbuch der Bodenkunde*, 16. 16th ed. 2010; Springer Berlin Heidelberg: Berlin, Heidelberg, 2016, ISBN 9783662499603.
15. Emsley, J.; Schleitzer, A. *Phosphor-ein Element auf Leben und Tod*, 2001.
16. Weihrauch, C. *Phosphor-Dynamiken in Böden*. Dissertation; Springer Fachmedien Wiesbaden: Wiesbaden, 2017, ISBN 9783658223472.
17. Jupp, A.R.; Beijer, S.; Narain, G.C.; Schipper, W.; Slootweg, J.C. Phosphorus recovery and recycling - closing the loop. *Chem. Soc. Rev.* **2021**, *50*, 87–101, doi:10.1039/d0cs01150a.
18. *World fertilizer trends and outlook to 2022;* Food & Agriculture Organization of United Nations: Rome, 2019, ISBN 9789251318942.
19. Humer, E.; Schwarz, C.; Schedle, K. Phytate in pig and poultry nutrition. *J. Anim. Physiol. Anim. Nutr. (Berl)* **2015**, *99*, 605–625, doi:10.1111/jpn.12258.
20. Düngemittelverordnung: Verordnung über die Anwendung von Düngemitteln, Bodenhilfsstoffen, Kultursubstraten und Pflanzenhilfsmitteln nach den Grundsätzen der guten fachlichen Praxis: DüV vom 26. Mai 2017 (BGBl. I S. 1305), geändert durch Artikel 1 der Verordnung vom 28. April 2020 (BGBl. I S. 846). **2017**.
21. Berücksichtigung N- und P-reduzierter Fütterungsverfahren bei den Nährstoffausscheidungen von Masthähnchen, Jung- und Legehennen.: DLG-Merkblatt 457, DLG e. V., Frankfurt am Main., *2021*.
22. TAUBE, F.; BACH, M.; Breuer, L.; EWERT, F.; FOHRER, N.; Leineweber, P.; MÜLLER, T.; WIGGERING, H. Novellierung der Stoffstrombilanzverordnung Stickstoff- und Phosphor-Überschüsse nachhaltig begrenzen. Fachliche Stellungnahme zur Novellierung der Stoffstrombilanzverordnung. **2020**.
23. Leitfaden zur nachvollziehbaren Umsetzung stark N-/P-reduzierter Fütterungsverfahren bei Schweinen: DLG Merkblatt 418 **2019**.
24. Sommerfeld, V.; Rodehutscord, M. *Phosphoreffizienz in der Nutztierernährung*, 52nd ed.; agrar spectrum, 2019.
25. Greiner, R.; Konietzny, U. Phytase for Food Application. *Food Technol. Biotechnol* **2006**, 125-140.
26. US Department of Agriculture. World Agricultural Production **2023**, 1–41.
27. Bundesverband Deutscher Pflanzenzüchter e.V. Getreide. Available online: https://www.bdp-online.de/de/Search/?start=0&quant=10&search=getreide (accessed on 7 November 2023).
28. Rimbach, G.; Möhring, J.; Erbersdobler, H.F. *Lebensmittel-Warenkunde für Einsteiger;* Springer Berlin Heidelberg: Berlin, Heidelberg, 2010, ISBN 978-3-642-04485-4.
29. Kamal-Eldin, A.; Lærke, H.N.; Knudsen, K.-E.B.; Lampi, A.-M.; Piironen, V.; Adlercreutz, H.; Katina, K.; Poutanen, K.; Man, P. Physical, microscopic and chemical

characterisation of industrial rye and wheat brans from the Nordic countries. *Food Nutr. Res.* **2009**, *53*, doi:10.3402/fnr.v53i0.1912.

30. Nilsson, M.; Åman, P.; Härkönen, H.; Hallmans, G.; Knudsen, K.E.B.; Mazur, W.; Adlercreutz, H. Content of Nutrients and Lignans in Roller Milled Fractions of Rye. *J. Sci. Food Agric.* **1997**, *73*, 143–148, doi:10.1002/(SICI)1097-0010(199702)73:2<143:AID-JSFA698>3.0.CO;2-H.
31. Nordlund, E.; Katina, K.; Aura, A.-M.; Poutanen, K. Changes in bran structure by bioprocessing with enzymes and yeast modifies the in vitro digestibility and fermentability of bran protein and dietary fibre complex. *Journal of Cereal Science* **2013**, *58*, 200–208, doi:10.1016/j.jcs.2013.05.006.
32. Roye, C.; Bulckaen, K.; Bondt, Y. de; Liberloo, I.; van de Walle, D.; Dewettinck, K.; Courtin, C.M. Side-by-side comparison of composition and structural properties of wheat, rye, oat, and maize bran and their impact on in vitro fermentability. *Cereal Chem* **2020**, *97*, 20–33, doi:10.1002/cche.10213.
33. Nyström, L.; Lampi, A.-M.; Rita, H.; Aura, A.-M.; Oksman-Caldentey, K.-M.; Piironen, V. Effects of processing on availability of total plant sterols, steryl ferulates and steryl glycosides from wheat and rye bran. *J. Agric. Food Chem.* **2007**, *55*, 9059–9065, doi:10.1021/jf071579o.
34. Curtis, T.Y.; Powers, S.J.; Balagiannis, D.; Elmore, J.S.; Mottram, D.S.; Parry, M.A.J.; Rakszegi, M.; Bedö, Z.; Shewry, P.R.; Halford, N.G. Free amino acids and sugars in rye grain: implications for acrylamide formation. *J. Agric. Food Chem.* **2010**, *58*, 1959–1969, doi:10.1021/jf903577b.
35. Kapreliants, L.; Zhurlova, O. Technology of wheat and rye bran biotransformation into functional ingredients. *International Fodd Research Journal* **2017**, 1975–1979.
36. Zykin, P.A.; Andreeva, E.A.; Lykholay, A.N.; Tsvetkova, N.V.; Voylokov, A.V. Anthocyanin Composition and Content in Rye Plants with Different Grain Color. *Molecules* **2018**, *23*, 948, doi:10.3390/molecules23040948.
37. Fretzdorff, B.; Weipert, D. Phytinsäure in Getreide und Getreideerzeugnissen. Mitteilung I: Phytinsäure und Phytase in Roggen und Roggenprodukten. *Z. Lebensm. Unters. Forsch.* **1986**, *182*, 287–293, doi:10.1007/BF01027626.
38. Frank, A.W. *Chemistry of plant phosphorus compounds;* Elsevier: Amsterdam, Boston, 2013, ISBN 9780124071940.
39. *Tierernährung für Tierärzte*: *Im Focus: Gesundheit und Leistung des Nutzgeflügels unter dem Einfluss von Futter und Fütterung ; Hannover, 8. April 2011;* Kamphues, J.; Wolf, P., Eds.; Inst. für Tierernährung: Hannover, 2011, ISBN 9783000338694.
40. Mikulski, D.; Kłosowski, G. Phytic acid concentration in selected raw materials and analysis of its hydrolysis rate with the use of microbial phytases during the mashing process. *J. Inst. Brew.* **2015**, *121*, 213–218, doi:10.1002/jib.221.

41. Xin gen Lei; Jesus M. Porres; Edward J. Mullaney; Henrik Brinch-Pedersen. Phytase: Source, Structure and Application. *Industrial Enzymes* **2007**, 505–529.
42. Lutz Hilterhaus; Andreas Liese; Udo Kragl. Biotransformation, Process Optimization, Kinetics and Engineering Aspects. *Encyclopedia of Industrial Biotechnology*; John Wiley & Sons, Ltd, 2010; pp 1–14.
43. Liese, A.; Seelbach, K.; Wandrey, C. *Industrial biotransformations*, 2., completely rev. and extended ed.; WILEY-VCH: Weinheim, 2006, ISBN 9783527310012.
44. THE 17 GOALS | Sustainable Development. Available online: https://sdgs.un.org/goals (accessed on 7 November 2023).
45. *Einführung in die Enzymtechnologie;* Jaeger, K.-E.; Liese, A.; Syldatk, C.; Ansorge-Schumacher, M., Eds.; Springer Spektrum: Berlin, Heidelberg, 2018, ISBN 978-3-662-57619-9.
46. Bedford, M.R.; Partridge, G.G. *Enzymes in farm animal nutrition*, 2nd ed.; CABI Pub: Wallingford Oxfordshire UK, Cambridge MA, 2010, ISBN 1845936744.
47. Global Feed Enzymes Market Report and Forecast 2024-2032. Available online: https://www.expertmarketresearch.com/reports/feed-enzymes (accessed on 8 November 2023).
48. Global Market Insights Inc. Animal Feed Enzymes Market Size | Growth Report, 2023 – 2032. Available online: https://www.gminsights.com/industry-analysis/animal-feed-enzymes-market (accessed on 8 November 2023).
49. Research, S. Animal Feed Phytase Market Size is projected to reach USD 760.79 million by 2031, growing at a CAGR of 5.7%: Straits Research. *Straits Research [Online]*. Available online: https://www.globenewswire.com/en/news-release/2023/06/14/2688227/0/en/Animal-Feed-Phytase-Market-Size-is-projected-to-reach-USD-760-79-million-by-2031-growing-at-a-CAGR-of-5-7-Straits-Research.html (accessed on 8 November 2023).
50. Pal, R.S.; Bhartiya, A.; Yadav, P.; Kant, L.; Mishra, K.K.; Aditya, J.P.; Pattanayak, A. Effect of dehulling, germination and cooking on nutrients, anti-nutrients, fatty acid composition and antioxidant properties in lentil (Lens culinaris). *J. Food Sci. Technol.* **2017**, *54*, 909–920, doi:10.1007/s13197-016-2351-4.
51. Greiner, R.; Alminger, M.L. Purification and characterization of a phytate-degrading enzyme from germinated oat (Avena sativa). *Journal of the Science of Food and Agriculture* **1999**, 1453–1460, doi:10.1002/(SICI)1097-0010(199908)79:11<1453:AID-JSFA386>3.0.CO;2-R.
52. Pakfetrat, S.; Amiri, S.; Radi, M.; Abedi, E.; Torri, L. Reduction of phytic acid, aflatoxins and other mycotoxins in wheat during germination. *J. Sci. Food Agric.* **2019**, *99*, 4695–4701, doi:10.1002/jsfa.9710.

53. Reddy, N.R.; Sathe, S.K.; Salunkhe, D.K. Phytates in Legumes and Cereals. In *Phytates in Legumes and Cereals*; Advances in Food Research, Ed.; Elsevier, 1982; pp 1–92, ISBN 9780120164288.
54. Infanzón, B.; Herrmann, K.R.; Hofmann, I.; Willbold, S.; Ruff, A.J.; Schwaneberg, U. Phytase blends for enhanced phosphorous mobilization of deoiled seeds. *Enzyme Microb. Technol.* **2022**, *153*, 109953, doi:10.1016/j.enzmictec.2021.109953.
55. Herrmann, K.R.; Fees, J.; Christ, J.J.; Hofmann, I.; Block, C.; Herzberg, D.; Bröring, S.; Reckels, B.; Visscher, C.; Blank, L.M.; et al. Biotechnological production of food-grade polyphosphate from deoiled seeds and bran. *EFB Bioeconomy Journal* **2023**, *3*, 100048, doi:10.1016/j.bioeco.2023.100048.
56. Nielsen, P.H.; McIlroy, S.J.; Albertsen, M.; Nierychlo, M. Re-evaluating the microbiology of the enhanced biological phosphorus removal process. *Curr. Opin. Biotechnol.* **2019**, *57*, 111–118, doi:10.1016/j.copbio.2019.03.008.
57. Kwapinski, W.; Kolinovic, I.; Leahy, J.J. Sewage Sludge Thermal Treatment Technologies with a Focus on Phosphorus Recovery: A Review. *Waste Biomass Valor* **2021**, *12*, 5837–5852, doi:10.1007/s12649-020-01280-2.
58. Morse,G.,K.; Brett, S.,W.; Guys, J.,Al; Lester J., N. Review: Phosphorus removal and recovery technologies. *Sci. Total Environ.* **1997**, 69–81.
59. Jupp, A.R.; Beijer, S.; Narain, G.C.; Schipper, W.; Slootweg, J.C. Phosphorus recovery and recycling - closing the loop. *Chem. Soc. Rev.* **2021**, *50*, 87–101, doi:10.1039/d0cs01150a.
60. González-Morales, C.; Fernández, B.; Molina, F.J.; Naranjo-Fernández, D.; Matamoros-Veloza, A.; Camargo-Valero, M.A. Influence of pH and Temperature on Struvite Purity and Recovery from Anaerobic Digestate. *Sustainability* **2021**, *13*, 10730, doi:10.3390/su131910730.
61. S. Kara. *Online Monitoring of Biocatalytic 2-Hydroxy Ketone Synthesis under Ambient and High Pressure*. Dissertation; MBV Berlin, 2012, ISBN 9783863871048.
62. Bro, R.; Smilde, A.K. Principal component analysis. *Anal. Methods* **2014**, *6*, 2812–2831, doi:10.1039/C3AY41907J.
63. Kessler, W. *Multivariate Datenanalyse für die Pharma-, Bio- und Prozessanalytik*: *Ein Lehrbuch;* WILEY-VCH: Weinheim, 2006, ISBN 9783527312627.
64. Kara, S.; Müller, J.,J.; Liese, A. Online analysis methods for monitoring of bioprocesses. *Chemistry Today* **2011**, 38–41.
65. van de Waterbeemd, H. *Chemometric methods in molecular design;* VCH: Weinheim, Ger, New York, 1995, ISBN 9783527615452.
66. Widderich, N.; Bubenheim, P.; Liese, A. Online monitoring of phytate content in plant residuals during wet-treatment. *Sci Rep* **2024**, *14*, doi:10.1038/s41598-023-49950-0.
67. Siebertz, K.; van Bebber, D.; Hochkirchen, T. *Statistische Versuchsplanung*: *Design of Experiments (DoE);* Springer: Berlin, Heidelberg, 2010, ISBN 9783642054921.

68. Töpfer, S. Statistische Versuchsplanung. In *Modellgestützte Steuerung, Regelung und Diagnose von Verbrennungsmotoren*; Isermann, R., Ed.; Springer: Berlin, Heidelberg, 2003; pp 121–130, ISBN 978-3-642-55698-2.
69. *Das ist gar kein Modell!;* Bandow, G., Ed.; Springer Fachmedien: Wiesbaden, 2010, ISBN 9783834918420.
70. *Design and analysis of experiments;* Dean, A.M.; Voss, D., Eds.; Springer: New York, Heidelberg, 1999, ISBN 0387985611.
71. Lee, R. Statistical Design of Experiments for Screening and Optimization. *Chemie Ingenieur Technik* **2019**, *91*, 191–200, doi:10.1002/cite.201800100.
72. Jones, B.; Goos, P. I-Optimal Versus D-Optimal Split-Plot Response Surface Designs. *Journal of Quality Technology* **2012**, *44*, 85–101, doi:10.1080/00224065.2012.11917886.
73. Ohlinger, K., N.; Young, T.,M.; Schroeder, E.,D. Predicting struvite formation in digestion. *Water Res.* **1998**, 3607-314, doi:10.1016/S0043-1354(98)00123-7.
74. Le Corre, K.S.; Valsami-Jones, E.; Hobbs, P.; Parsons, S.A. Phosphorus Recovery from Wastewater by Struvite Crystallization: A Review. *Critical Reviews in Environmental Science and Technology* **2009**, *39*, 433–477, doi:10.1080/10643380701640573.
75. Struvite formation, control and recovery. Doyle, J.,D.; Parson, S., A. *Water Res.* **2002**, 3925–3940, doi:10.1016/S0043-1354(02)00126-4.
76. Ferraris, G.; Fuess, H.; Joswig, W. Neutron diffraction study of MgNH 4 PO 4 .6H 2 O (struvite) and survey of water molecules donating short hydrogen bonds. *Acta Cryst B* **1986**, *42*, 253–258, doi:10.1107/S0108768186098269.
77. Whitaker, A.; Jeffery, J.W. The crystal structure of struvite, MgNH 4 PO 4 .6H 2 O. *Acta Cryst B* **1970**, *26*, 1429–1440, doi:10.1107/S0567740870004284.
78. Dieckmann, C. Kristallisation von Magnesium-Ammonium-Phosphat-Hydraten während der Aufbereitung von Fermentationsrückständen : Identifikation, Analyse und Vorhersage: Kristallisation von Magnesium-Ammonium-Phosphat-Hydraten während der Aufbereitung von Fermentationsrückständen : Identifikation, Analyse und Vorhersage; Dr. Kovač.
79. Rahaman, M.S.; Mavinic, D.S.; Bhuiyan, M.I.H.; Koch, F.A. Exploring the determination of struvite solubility product from analytical results. *Environ. Technol.* **2006**, *27*, 951–961, doi:10.1080/09593332708618707.
80. Abbona, F.; Madsen, H.; Boistelle, R. The initial phases of calcium and magnesium phosphates precipitated from solutions of high to medium concentrations. *Journal of Crystal Growth* **1986**, *74*, 581–590, doi:10.1016/0022-0248(86)90205-8.
81. Babić-Ivančić, V.; Kontrec, J.; Kralj, D.; Brečević, L. Precipitation Diagrams of Struvite and Dissolution Kinetics of Different Struvite Morphologies. *Croatica Chemica Acta* **2002**, *75*, 89–106.
82. Crutchik, D.; Garrido, J.M. Kinetics of the reversible reaction of struvite crystallisation. *Chemosphere* **2016**, *154*, 567–572, doi:10.1016/j.chemosphere.2016.03.134.

83. Bube, K. Über Magnesiumammoniumphosphat. *Fresenius, Zeitschrift f. anal. Chemie* **1910**, *49*, 525–596, doi:10.1007/bf01306233.
84. Zeitoun, R.; Biswas, A. Review—Potentiometric Determination of Phosphate Using Cobalt: A Review. *J. Electrochem. Soc.* **2020**, *167*, 127507, doi:10.1149/1945-7111/abad6c.
85. www.dfg.de. Good Research Practice. Available online: https://www.dfg.de/en/research_funding/principles_dfg_funding/good_scientific_practice/ (accessed on 13 November 2023).
86. Fiske, C.H.; Subbarow, Y. The Colorimetric Determination of Phosphorus. *Journal of Biological Chemistry* **1925**, *66*, 375–400, doi:10.1016/s0021-9258(18)84756-1.
87. Heinonen, J.K.; Lahti, R.J. A new and convenient colorimetric determination of inorganic orthophosphate and its application to the assay of inorganic pyrophosphatase. *Analytical Biochemistry* **1981**, *113*, 313–317, doi:10.1016/0003-2697(81)90082-8.
88. Eeckhout, W.; Paepe, M. de. Total phosphorus, phytate-phosphorus and phytase activity in plant feedstuffs. *Animal Feed Science and Technology* **1994**, 19–29, doi:10.1016/0377-8401(94)90156-2.
89. Jacob Lehrfeld. High-performance liquid chromatography analysis of phytic acid on a pH-stable, macroporous polymer column. *Cereal Chemistry* **1989**, 510–515.
90. Bullock, J.I.; Duffin, P.A.; Nolan, K.B. In vitro hydrolysis of phytate at 95°C and the influence of metal ion on the rate. *J. Sci. Food Agric.* **1993**, *63*, 261–263, doi:10.1002/jsfa.2740630214.
91. Graf; Dintzis. High-performance Liquid Chromatographie Method for the Determination of Phytate. *Anal. Biochem.* **1982**, 413–417.
92. Ionenaustauscher ROTI®Change 1 x 8, 250 g, online bestellen⮞ carlroth.com. Available online: https://www.carlroth.com/de/de/anionentauscherharze/ionenaustauscher-rotichange-1-x-8/p/6852.2 (accessed on 14 November 2023).
93. Marolt, G.; Kolar, M. Analytical Methods for Determination of Phytic Acid and Other Inositol Phosphates: A Review. *Molecules* **2020**, *26*, doi:10.3390/molecules26010174.
94. Sandberg; Ahderinne. HPLC Method for Determination of inositol Tri-, Tetra-, Penta-, and Hexaphosphates in Foods and Intestinal Contents. *Journal of food science* **1986**, 547-550.
95. Tangendjaja, B.; Buckle, K.A.; Wootton, M. Analysis of phytic acid by high-performance liquid chromatography. *Journal of Chromatography A* **1980**, *197*, 274–277, doi:10.1016/s0021-9673(00)81249-2.
96. KNUCKLES, B.E.; KUZMICKY, D.D.; BETSCHART, A.A. HPLC Analysis of Phytic Acid in Selected Foods and Biological Samples. *J Food Science* **1982**, *47*, 1257–1258, doi:10.1111/j.1365-2621.1982.tb07660.x.

97. LEE, K.E.; ABENDROTH, J.A. High Performance Liquid Chromatographic Determination of Phytic Acid in Foods. *J Food Science* **1983**, *48*, 1344–1345, doi:10.1111/j.1365-2621.1983.tb09226.x.
98. Madsen, C.K.; Brearley, C.A.; Brinch-Pedersen, H. Lab-scale preparation and QC of phytase assay substrate from rice bran. *Anal. Biochem.* **2019**, *578*, 7–12, doi:10.1016/j.ab.2019.04.021.
99. Phytinsäure Natriumsalz Hydrat from rice | Sigma-Aldrich. Available online: https://www.sigmaaldrich.com/DE/de/product/sigma/p8810?%20region=DE, (accessed on 16 December 2020).
100. Lehrfeld, J. HPLC Separation and Quantitation of Phytic Acid and Some Inositol Phosphates in Foods: Problems and Solutions. *J. Agric. Food Chem.* **1994**, *42*, 2726–2731, doi:10.1021/jf00048a015.
101. Karunakaran, C.; Vijayan, P.; Stobbs, J.; Bamrah, R.K.; Arganosa, G.; Warkentin, T.D. High throughput nutritional profiling of pea seeds using Fourier transform mid-infrared spectroscopy. *Food Chem.* **2020**, *309*, doi:10.1016/j.foodchem.2019.125585.
102. W. Frølich; T. Drakenberg; N.-G. Asp. Enzymic degradation of phytate (myo-inositol Hexaphosphate) in whole grain flour suspension and dough. A comparison between 31P NMR spectroscopy and a ferric ion method. *Journal of Cereal Science*, 325–334.
103. Tse, R.S.; Wong, S.C.; Yuen, C. Determination of deuterium/hydrogen ratios in natural waters by Fourier transform nuclear magnetic resonance spectrometry. *Anal. Chem.* **1980**, 2445.
104. Marty. Composition and Structure of Phytic Acid Derivates from Rice Bran. *BioResources* **2018**, 3411–3419.
105. Turner, B.L.; Mahieu, N.; Condron, L.M. QUANTIFICATION OF MYO-INOSITOL HEXAKISPHOSPHATE IN ALKALINE SOIL EXTRACTS BY SOLUTION 31P NMR SPECTROSCOPY AND SPECTRAL DECONVOLUTION. *Soil Science* **2003**, *168*, 469–478, doi:10.1097/01.ss.0000080332.10341.ed.
106. Carbas, B.; Machado, N.; Oppolzer, D.; Ferreira, L.; Brites, C.; Rosa, E.A.S.; Barros, A.I.R.N.A. Comparison of near-infrared (NIR) and mid-infrared (MIR) spectroscopy for the determination of nutritional and antinutritional parameters in common beans. *Food Chem.* **2020**, *306*, 125509, doi:10.1016/j.foodchem.2019.125509.
107. Pande, R.; Mishra, H.N. Fourier Transform Near-Infrared Spectroscopy for rapid and simple determination of phytic acid content in green gram seeds (Vigna radiata). *Food Chem.* **2015**, *172*, 880–884, doi:10.1016/j.foodchem.2014.09.049.
108. Chen, J.-B.; Sun, S.-Q.; Zhou, Q. Chemical morphology of Areca nut characterized directly by Fourier transform near-infrared and mid-infrared microspectroscopic imaging in reflection modes. *Food Chem.* **2016**, *212*, 469–475, doi:10.1016/j.foodchem.2016.05.168.

109. Türker-Kaya, S.; Huck, C.W. A Review of Mid-Infrared and Near-Infrared Imaging: Principles, Concepts and Applications in Plant Tissue Analysis. *Molecules* **2017**, *22*, doi:10.3390/molecules22010168.
110. Barron, C. Prediction of relative tissue proportions in wheat mill streams by fourier transform mid-infrared spectroscopy. *J. Agric. Food Chem.* **2011**, *59*, 10442–10447, doi:10.1021/jf201886c.
111. He, Z.; Honeycutt, C.W.; Zhang, T.; Bertsch, P.M. Preparation and FT-IR characterization of metal phytate compounds. *J. Environ. Qual.* **2006**, *35*, 1319–1328, doi:10.2134/jeq2006.0008.
112. Guan, X.-H.; Shang, C.; Zhu, J.; Chen, G.-H. ATR-FTIR investigation on the complexation of myo-inositol hexaphosphate with aluminum hydroxide. *J. Colloid Interface Sci.* **2006**, *293*, 296–302, doi:10.1016/j.jcis.2005.06.070.
113. Kazarian, S.G.; Chan, K.L.A. ATR-FTIR spectroscopic imaging: recent advances and applications to biological systems. *Analyst* **2013**, *138*, 1940–1951, doi:10.1039/c3an36865c.
114. Morisset, P.-O.; Gagnon, J.; Tremblay, R.; Deschênes, J.-S. Development and validation of an in situ and real-time quantification method for bicarbonate, carbonate and orthophosphate ions by ATR FT-IR spectroscopy in aqueous solutions. *Analyst* **2018**, *143*, 4387–4393, doi:10.1039/c8an00687c.
115. Gowen, A.A.; Downey, G.; Esquerre, C.; O'Donnell, C.P. Preventing over-fitting in PLS calibration models of near-infrared (NIR) spectroscopy data using regression coefficients. *Journal of Chemometrics* **2011**, *25*, 375–381, doi:10.1002/cem.1349.
116. Petersson, K.; Nordlund, E.; Tornberg, E.; Eliasson, A.-C.; Buchert, J. Impact of cell wall-degrading enzymes on water-holding capacity and solubility of dietary fibre in rye and wheat bran. *Journal of the Science of Food and Agriculture* **2013**, *93*, 882–889, doi:10.1002/jsfa.5816.
117. Mayer, N.; Widderich, N.; Scherzinger, M.; Bubenheim, P.; Kaltschmitt, M. Comparison of Phosphorus and Phytase Activity Distribution in Wheat, Rye, Barley and Oats and Their Impact on a Potential Phytate Separation. *Food Bioprocess Technol* **2023**, *16*, 1076–1088, doi:10.1007/s11947-022-02981-3.
118. PEERS, F.G. The phytase of wheat. *Biochem. J.* **1953**, *53*, 102–110, doi:10.1042/bj0530102.
119. Steiner, T.; Mosenthin, R.; Zimmermann, B.; Greiner, R.; Roth, S. Distribution of phytase activity, total phosphorus and phytate phosphorus in legume seeds, cereals and cereal by-products as influenced by harvest year and cultivar. *Animal Feed Science and Technology* **2007**, *133*, 320–334, doi:10.1016/j.anifeedsci.2006.04.007.
120. Viveros, A.; Centeno, C.; Brenes, A.; Canales, R.; Lozano, A. Phytase and acid phosphatase activities in plant feedstuffs. *J. Agric. Food Chem.* **2000**, *48*, 4009–4013, doi:10.1021/jf991126m.

121. Gegenbach, H.; Spreu, A.; Kolb; E., Bombien,M. Getreide sicher lagern: dlg-merkblatt_425 **2018**.
122. Greiner, R.; Konietzny, U. Endogenous phytate-degrading enzymes are responsible for phytate reduction while preparing beans. *Journal of Food Processing and Preservation* **1998**, *22*, 321–331, doi:10.1111/j.1745-4549.1998.tb00353.x.
123. Bickel, S. Brotgetreide. *Biologie in unserer Zeit* **2015**, *45*, 168–175, doi:10.1002/biuz.201510566.
124. Egli; Davidson; Juillerat; Barclay; Hurrell. Phytic Acid Degradation in Complementary Foods Using Phytase Naturally Occurring in Whole Grain Cereals. *Journal of food science* **2003**, 1855–1859.
125. Ursula Konietzny; Ralf Greiner. Molecular and catalytic properties of phytate-degrading enzymes (phytases). *International Journal of Food Science and Technology* **2002**, 791–812.
126. Elzagheid, M. *Water Chemistry, Analysis and Treatment*: *Pollutants, Microbial Contaminants, Water and Wastewater Treatment;* De Gruyter: Berlin, Boston, 2024, ISBN 9783111332468.
127. Xu, J.M.; Tang, C.; Chen, Z.L. The role of plant residues in pH change of acid soils differing in initial pH. *Soil Biology and Biochemistry* **2006**, *38*, 709–719, doi:10.1016/j.soilbio.2005.06.022.
128. Irgens, F. *Rheology and Non-Newtonian Fluids;* Springer International Publishing: Cham, 2014, ISBN 978-3-319-01052-6.
129. Mezger, T.G. *The Rheology Handbook*: *4th Edition;* Vincentz Network: Hannover, 2012, ISBN 9783748600367.
130. Feizollahi, E.; Mirmahdi, R.S.; Zoghi, A.; Zijlstra, R.T.; Roopesh, M.S.; Vasanthan, T. Review of the beneficial and anti-nutritional qualities of phytic acid, and procedures for removing it from food products. *Food Res. Int.* **2021**, *143*, 110284, doi:10.1016/j.foodres.2021.110284.
131. Daugan, S.; Talini, L.; Herzhaft, B.; Peysson, Y.; Allain, C. Sedimentation of Suspensions in Shear-Thinning Fluids. *Oil & Gas Science and Technology - Rev. IFP* **2004**, *59*, 71–80, doi:10.2516/ogst:2004007.
132. Tan, H.; Wu, X.; Xie, L.; Huang, Z.; Peng, W.; Gan, B. Identification and characterization of a mesophilic phytase highly resilient to high-temperatures from a fungus-garden associated metagenome. *Appl Microbiol Biotechnol* **2016**, *100*, 2225–2241, doi:10.1007/s00253-015-7097-9.
133. Ragon, M.; Aumelas, A.; Chemardin, P.; Galvez, S.; Moulin, G.; Boze, H. Complete hydrolysis of myo-inositol hexakisphosphate by a novel phytase from Debaryomyces castellii CBS 2923. *Appl. Microbiol. Biotechnol.* **2008**, *78*, 47–53, doi:10.1007/s00253-007-1275-3.

134. Herrmann, K. *Phytase engineering for efficient phosphate recovery from press cakes*. Doctoral dissertation, 1st ed., 2021.
135. Widderich, N.; Stotz, J.; Lohkamp, F.; Visscher, C.; Schwaneberg, U.; Liese, A.; Bubenheim, P.; Ruff, A.J. An up-scaled biotechnological approach for phosphorus-depleted rye bran as animal feed. *Bioresour. Bioprocess.* **2024**, *11*, 49, doi:10.1186/s40643-024-00765-5.
136. Albarracín, M.; José González, R.; Drago, S.R. Soaking and extrusion effects on physicochemical parameters, phytic acid, nutrient content and mineral bio-accessibility of whole rice grain. *Int. J. Food Sci. Nutr.* **2015**, *66*, 210–215, doi:10.3109/09637486.2014.986070.
137. Calson, D.; Poulsen, H.D. Phytate degradation in soaked and fermented liquid feed—effect of diet, time of soaking, heat treatment, phytase activity, pH and temperature. *Animal Feed Science and Technology*, *2003*, 141–154.
138. Ertas, N. Dephytinization processes of some legume seeds and cereal grains with ultrasound and microwave applications. *Legume Research - An International Journal* **2013**, *36*, 414–421.
139. Mohammadi, F.; Marti, A.; Nayebzadeh, K.; Hosseini, S.M.; Tajdar-Oranj, B.; Jazaeri, S. Effect of washing, soaking and pH in combination with ultrasound on enzymatic rancidity, phytic acid, heavy metals and coliforms of rice bran. *Food Chem.* **2021**, *334*, 127583, doi:10.1016/j.foodchem.2020.127583.
140. Figueroa-Espinoza, M.-C.; Poulsen, C.; Borch Søe, J.; Zargahi, M.R.; Rouau, X. Enzymatic solubilization of arabinoxylans from native, extruded, and high-shear-treated rye bran by different endo-xylanases and other hydrolyzing enzymes. *J. Agric. Food Chem.* **2004**, *52*, 4240–4249, doi:10.1021/jf034809h.
141. Falck, P.; Aronsson, A.; Grey, C.; Stålbrand, H.; Nordberg Karlsson, E.; Adlercreutz, P. Production of arabinoxylan-oligosaccharide mixtures of varying composition from rye bran by a combination of process conditions and type of xylanase. *Bioresour. Technol.* **2014**, *174*, 118–125, doi:10.1016/j.biortech.2014.09.139.
142. Berrin, J.-G.; Juge, N. Factors affecting xylanase functionality in the degradation of arabinoxylans. *Biotechnol. Lett.* **2008**, *30*, 1139–1150, doi:10.1007/s10529-008-9669-6.
143. Arte, E.; Katina, K.; Holopainen-Mantila, U.; Nordlund, E. Effect of Hydrolyzing Enzymes on Wheat Bran Cell Wall Integrity and Protein Solubility. *Cereal Chemistry Journal* **2016**, *93*, 162–171, doi:10.1094/CCHEM-03-15-0060-R.
144. Nyombaire, G.; Ng, P.K. Physicochemical Properties of Washed Wheat Bran. *AJFST* **2022**, *10*, 89–94, doi:10.12691/ajfst-10-2-5.
145. Brijs, K.; Bleukx, W.; Delcour, J.A. Proteolytic activities in dormant rye (Secale cereale L.) grain. *J. Agric. Food Chem.* **1999**, *47*, 3572–3578, doi:10.1021/jf990070t.

146. Loponen, J.; Mikola, M.; Katina, K.; Sontag-Strohm, T.; Salovaara, H. Degradation of HMW Glutenins During Wheat Sourdough Fermentations. *Cereal Chem* **2004**, *81*, 87–93, doi:10.1094/CCHEM.2004.81.1.87.
147. Katina, K.; Laitila, A.; Juvonen, R.; Liukkonen, K.-H.; Kariluoto, S.; Piironen, V.; Landberg, R.; Aman, P.; Poutanen, K. Bran fermentation as a means to enhance technological properties and bioactivity of rye. *Food Microbiology* **2007**, *24*, 175–186, doi:10.1016/j.fm.2006.07.012.
148. Roberts, P.J.; Simmonds, D.H.; Wootton, M.; Wrigley, C.W. Extraction of protein and solids from wheat bran. *J. Sci. Food Agric.* **1985**, *36*, 5–10, doi:10.1002/jsfa.2740360103.
149. Gesellschaft für Ernährungsphysiologie. *Empfehlungen zur Energie-und Nährstoffversorgung beim Schwein. Ausschuss für Bedarfsnormen der Gesellschaft für Ernährungsphysiologie*, 2006.
150. Staudacher, W.; Potthast, V. *DLG-Futterwerttabellen-Schweine*: *Deutsche Landwirtschaftliche-Gesellschaft;* DLG-Verlag, 2014.
151. Laurikainen, T.; Härkönen, H.; Autio, K.; Poutanen, K. Effects of enzymes in fibre-enriched baking. *J. Sci. Food Agric.* **1998**, *76*, 239–249, doi:10.1002/(SICI)1097-0010(199802)76:2<239:AID-JSFA942>3.0.CO;2-L.
152. Bayuseno, A.P.; Schmahl, W.W. Thermal decomposition of struvite in water: qualitative and quantitative mineralogy analysis. *Environ. Technol.* **2020**, *41*, 3591–3597, doi:10.1080/09593330.2019.1615558.
153. Abbona, F.; Lundager, M.H.; Boistell, R. Crystallisation of two magnesium phosphates, struvite and newberyite: Effects of pH and concentration. *Journal of Crystal Growth* **1982**, 6–14.
154. Chimenos, J.M.; Fernández, A.I.; Villalba, G.; Segarra, M.; Urruticoechea, A.; Artaza, B.; Espiell, F. Removal of ammonium and phosphates from wastewater resulting from the process of cochineal extraction using MgO-containing by-product. *Water Research* **2003**, *37*, 1601–1607, doi:10.1016/s0043-1354(02)00526-2.
155. Suzuki, K.; Tanaka, Y.; Kuroda, K.; Hanajima, D.; Fukumoto, Y.; Yasuda, T.; Waki, M. Removal and recovery of phosphorous from swine wastewater by demonstration crystallization reactor and struvite accumulation device. *Bioresour. Technol.* **2007**, *98*, 1573–1578, doi:10.1016/j.biortech.2006.06.008.
156. Cusick, R.D.; Ullery, M.L.; Dempsey, B.A.; Logan, B.E. Electrochemical struvite precipitation from digestate with a fluidized bed cathode microbial electrolysis cell. *Water Res.* **2014**, *54*, 297–306, doi:10.1016/j.watres.2014.01.051.
157. Ohlinger, K.N.; Young, T.M.; Schroeder, E.D. Postdigestion Struvite Precipitation Using a Fluidized Bed Reactor. *J. Environ. Eng.* **2000**, *126*, 361–368, doi:10.1061/(ASCE)0733-9372(2000)126:4(361).

158. Kataki, S.; West, H.; Clarke, M.; Baruah, D.C. Phosphorus recovery as struvite from farm, municipal and industrial waste: Feedstock suitability, methods and pre-treatments. *Waste Manag.* **2016**, *49*, 437–454, doi:10.1016/j.wasman.2016.01.003.
159. Tünay, O.; Kabdasli, I.; Orhon, D.; Kolçak, S. Ammonia removal by magnesium ammonium phosphate precipitation in industrial wastewaters. *Water Science and Technology* **1997**, *36*, 225–228, doi:10.2166/wst.1997.0524.
160. Hao, X.; Wang, C.; van Loosdrecht, M.C.M.; Hu, Y. Looking beyond struvite for P-recovery. *Environ. Sci. Technol.* **2013**, *47*, 4965–4966, doi:10.1021/es401140s.
161. Huang, H.; Zhang, D.; Li, J.; Guo, G.; Tang, S. Phosphate recovery from swine wastewater using plant ash in chemical crystallization. *Journal of Cleaner Production* **2017**, *168*, 338–345, doi:10.1016/j.jclepro.2017.09.042.
162. Quintana, M.; Colmenarejo, M.F.; Barrera, J.; García, G.; García, E.; Bustos, A. Use of a byproduct of magnesium oxide production to precipitate phosphorus and nitrogen as struvite from wastewater treatment liquors. *J. Agric. Food Chem.* **2004**, *52*, 294–299, doi:10.1021/jf0303870.
163. Shin, H.S.; Lee, S.M. Removal of Nutrients in Wastewater by using Magnesium Salts. *Environ. Technol.* **1998**, *19*, 283–290, doi:10.1080/09593331908616682.
164. Di Iaconi, C.; Pagano, M.; Ramadori, R.; Lopez, A. Nitrogen recovery from a stabilized municipal landfill leachate. *Bioresour. Technol.* **2010**, *101*, 1732–1736, doi:10.1016/j.biortech.2009.10.013.
165. Bhuiyan, M.I.H.; Mavinic, D.S.; Beckie, R.D. A solubility and thermodynamic study of struvite. *Environ. Technol.* **2007**, *28*, 1015–1026, doi:10.1080/09593332808618857.
166. Aage, H.K.; Andersen, B.L.; Blom, A.; Jensen, I. The solubility of struvite. *J Radioanal Nucl Chem* **1997**, *223*, 213–215, doi:10.1007/bf02223387.
167. Ben Moussa, S.; Tlili, M.M.; Batis, N.; Amor, M.B. Influence of tempereature on Struvite precipitation by CO 2 -deagassing method. *Cryst. Res. Technol.* **2011**, *46*, 255–260, doi:10.1002/crat.201000571.
168. Kofina, A.N.; Koutsoukos, P.G. Spontaneous Precipitation of Struvite from Synthetic Wastewater Solutions. *Crystal Growth & Design* **2005**, *5*, 489–496, doi:10.1021/cg049803e.
169. Siciliano, A.; Limonti, C.; Curcio, G.M.; Molinari, R. Advances in Struvite Precipitation Technologies for Nutrients Removal and Recovery from Aqueous Waste and Wastewater. *Sustainability* **2020**, *12*, 7538, doi:10.3390/su12187538.
170. Kim, D.; Ryu, H.-D.; Kim, M.-S.; Kim, J.; Lee, S.-I. Enhancing struvite precipitation potential for ammonia nitrogen removal in municipal landfill leachate. *Journal of Hazardous Materials* **2007**, *146*, 81–85, doi:10.1016/j.jhazmat.2006.11.054.
171. Hutnik, N.; Kozik, A.; Mazienczuk, A.; Piotrowski, K.; Wierzbowska, B.; Matynia, A. Phosphates (V) recovery from phosphorus mineral fertilizers industry wastewater by

continuous struvite reaction crystallization process. *Water Res.* **2013**, *47*, 3635–3643, doi:10.1016/j.watres.2013.04.026.

172. Ren, W.; Zhou, Z.; Wan, L.; Hu, D.; Jiang, L.-M.; Wang, L. Optimization of phosphorus removal from reject water of sludge thickening and dewatering process through struvite precipitation. *Desalination and Water Treatment* **2016**, *57*, 15515–15523, doi:10.1080/19443994.2015.1072059.
173. Marques, M.P.C.; Cabral, J.M.S.; Fernandes, P. Bioprocess scale-up: quest for the parameters to be used as criterion to move from microreactors to lab-scale. *J of Chemical Tech & Biotech* **2010**, *85*, 1184–1198, doi:10.1002/jctb.2387.
174. Ohlinger, K.N.; E, P.; Young, T.M.; Schroeder, E.D. Kinetics Effects on Preferential Struvite Accumulation in Wastewater. *J. Environ. Eng.* **1999**, *125*, 730–737, doi:10.1061/(ASCE)0733-9372(1999)125:8(730).
175. Paul, I.; Varghese, G.; Ittyachen, M.A. Thermal decomposition studies of struvites. *0975-1041* **2002**.
176. Georgé, S.; Brat, P.; Alter, P.; Amiot, M.J. Rapid determination of polyphenols and vitamin C in plant-derived products. *J. Agric. Food Chem.* **2005**, *53*, 1370–1373, doi:10.1021/jf048396b.
177. Senturk, H.B.; Ozdes, D.; Gundogdu, A.; Duran, C.; Soylak, M. Removal of phenol from aqueous solutions by adsorption onto organomodified Tirebolu bentonite: equilibrium, kinetic and thermodynamic study. *Journal of Hazardous Materials* **2009**, *172*, 353–362, doi:10.1016/j.jhazmat.2009.07.019.
178. Alfano, S.; Berruti, F.; Denis, N.; Santagostino, A. The future of second-generation biomass. *McKinsey & Company [Online],* November 18, 2016. Available online: https://www.mckinsey.com/capabilities/sustainability/our-insights/the-future-of-second-generation-biomass (accessed on 5 July 2024).
179. Srivastava, S.; Sharma, M.; Usmani, Z.; Dubey, S.; Yadav, G.K.; Singh, N.P.; Bhargava, A. Plant cell wall degrading enzymes in biomass bioprocessing to biorefineries: a review. *Recent Developments in Bioenergy Research*; Elsevier, 2020; pp 415–432, ISBN 9780128195970.
180. Shokri, N.; Stevens, B.; Madani, K.; Grabe, J.; Schlüter, M.; Smirnova, I. Climate Informed Engineering: An Essential Pillar of Industry 4.0 Transformation. *ACS Eng. Au* **2023**, *3*, 3–6, doi:10.1021/acsengineeringau.2c00037.
181. Singh, B.; Satyanarayana, T. Fungal phytases: characteristics and amelioration of nutritional quality and growth of non-ruminants. *J. Anim. Physiol. Anim. Nutr. (Berl)* **2015**, *99*, 646–660, doi:10.1111/jpn.12236.
182. Paul, P.E.V.; Sangeetha, V.; Deepika, R.G. Emerging Trends in the Industrial Production of Chemical Products by Microorganisms. *Recent Developments in Applied Microbiology and Biochemistry*; Elsevier, 2019; pp 107–125, ISBN 9780128163283.

183. Singleton, V.L.; Rossi, J.A. Colorimetry of Total Phenolics with Phosphomolybdic-Phosphotungstic Acid Reagents. *Am J Enol Vitic.* **1965**, *16*, 144–158, doi:10.5344/ajev.1965.16.3.144.
184. Matissek, R.; Schnepel, F.-M.; Steiner, G. *Lebensmittelanalytik*: *Grundzüge, Methoden, Anwendungen*, 2., korr. Aufl.; Springer: Berlin, Heidelberg, 1992, ISBN 0387138358.
185. Pulliainen; Wallin. Determination of Total Phosphorus in Foods by Colorimetry: Summary of NMKL' Collaborative Study. *Journal of AOAC International* **1996**, 1408–1410, doi:10.1093/jaoac/79.6.1408.